Synthesis and Characterization of Oligo(thiophene carboxamide)s

Dissertation

zur Erlangung des Grades

„Doktor der Naturwissenschaften“

im Promotionsfach Chemie

Am Fachbereich Chemie, Pharmazie und Geowissenschaften der

Johannes Gutenberg-Universität Mainz

Johannes Klos

geboren in Neunkirchen/Saar

Mainz 2010

Dekan:

Prodekan:

1. Berichterstatter:

2. Berichterstatter:

Tag der mündlichen Prüfung: 12.10.2010

Hiermit versichere ich gemäß § 10 Abs. 3d der Promotionsordnung vom 24.07.2007, dass ich die als Dissertation vorgelegte Arbeit selbst angefertigt und alle benutzten Hilfsmittel (Literatur, Apparaturen, Material) in der Arbeit angegeben habe.

Die vorliegende Arbeit wurde in der Zeit von Oktober 2006 bis Juli 2009 am Institut für Organische und Makromolekulare Chemie der Johannes Gutenberg Universität Mainz im Arbeitskreis von [redacted] angefertigt.

Für meine Eltern

Table of Contents

Chapter 1. Abstracts and aim of this work

1.1. Abstract

The work consists of two parts: In the first section the self aggregation of poly(ethylene oxide)-*block*-oligo-(*p*-benzamide) block copolymers was analyzed in detail. By varying the precipitation conditions for the block copolymer, different supramolecular structures were obtained. The dissolved polymer was drop wise added to chloroform, a selective solvent for poly(ethylene oxide). From hollow spheres with diameters in the micrometer regime to small rods with dimensions of several hundred nanometers in length and ten nanometers in width were observed.

The main part of the thesis deals with the synthesis and characterization of a novel conjugated oligomer: oligo(thiophene carboxamide)s. The needed monomer, a 2-aminothiophene-5-carboxylic acid, was made by the *Gewald*-Reaction, which is a multi-component, ring-closure reaction. This method generally allows the synthesis of tetra-substituted thiophenes, whereas the 3- and 4-position usually carries alkyl chains or esters. The so obtained material can be directly used in step-wise synthesis of well-defined oligomers, which exhibit interesting absorption and fluorescence phenomena. In dichloromethane, a bathochromic shift, depending on the oligomers length, was observed. The absorption energy of the pentamer is similar to that of the poly(thiphene carboxamide), revealing that the maximum effective conjugation length is achieved. In contrast to chloroform, aggregation of the oligomer, beginning with the trimer, was observed in *N*,*N*-dimethylformamide. A charge transfer band was observed, which vanished with increased concentrations. A possible hypsochromic shift of that band, suggested the formation of *H*-aggregates. Fluorescence spectroscopy as well as time-resolved fluorescence showed the expected trends for fully conjugated oligomers. Conjugation along the amide bond was also proven by quantum mechanical calculations.

1.2. Zusammenfassung

Die vorliegende Arbeit besteht aus zwei Teilen: Im ersten Teil der Arbeit werden supramolekulare Strukturen betrachtet, die durch unterschiedliche Fällungsbedingungen von Polyethylenoxid-*block*-oligo-*p*-benzamid-copolymeren erhalten wurden. Durch tropfenweise Zugabe des gelösten Polymers zu Chloroform, ein für Polyethylenoxid selektives Lösemittel, konnten verschiedenste Aggregate hergestellt werden. Von großen Hohlkugel mit einem Durchmesser von mehreren Mikrometern, bis zu kleinen Stäbchen mit den Abmessungen von zehn Nanometern in der Breite und einigen hundert Nanometern Länge, konnten beobachtet werden.

Der Hauptteil der Arbeit handelt von der Synthese und Charakterisierung eines neuen, konjugierten Oligomers: Oligothiophencarbonsäureamid. Das hierfür nötige Monomer, eine 2-Aminothiophen-5-carbonsäure konnte mittels *Gewald*-Synthese, eine multikomponenten Ringschlussreaktion dargestellt werden. Diese Methode erlaubt die Herstellung von vierfach substituierten Thiophenen, wobei 3- und 4-Position meist Alkylketten und Ester sind. Das so hergestellte Material konnte in der stufenweise Synthese von Oligothiophencarbonsäureamiden genutzt werden. Die neuen Oligomere zeigten interessante Absorptions- und Fluoreszenzeigenschaften. In Dichlormethan wurde eine bathochrome Verschiebung der Absorptionsbande in Abhängigkeit der Oligomerlänge beobachtet. Das Pentamer erreichte eine Absorptionsenergie, die der Bande des Polythiophencarbonsäureamids entspricht, was bedeutetet, dass die effektive Konjugationslänge erreicht wurde. Im Gegensatz zu den Messungen in Dichlormethan, zeigten die Oligomere Aggregationstendenzen ab dem Trimer in *N*,*N*-Dimethylformamid. Die auftretende *Charge-Transfer* Bande verschwand mit steigenden Konzentrationen. Eine mögliche hypsochrome Verschiebung dieser Bande, deutet auf eine Bildung von *H*-Aggregaten hin. Fluoreszenz und zeitaufgelöste Fluoreszenzmessungen ergaben die für konjugierte Systeme zu erwartenden Effekte. Die Konjugation entlang des Amids konnte ebenfalls mittels quantenmechanischer Berechnung nachgewiesen werden.

1.3. Aim of this work

The aim of this work is to develop a new set of conjugated oligomers: oligo(thiophene carboxamide)s. The backbone of the new material should by fully conjugated and carrying amides. Knowing from the oligo(*p*-benzamide)s (OPBAs) this conjugation is possible, however the observed bathochromic shifts of the absorptions bands are small. Replacing the benzene rings by thiophene, might increase the electron density und thus larger bathochromic shifts are possible. Pure oligo(thiophene)s are known for their conjugation and they are used in optoelectronic devices such as solar cells, organic light emitting diodes and field effect transistors. The new structure, consisting of thiophenes, which are linked through amides, will be synthesized beginning from a 2-aminothiophene-5-carboxylic acid. The synthetic strategy for the monomer as well as the oligomers will be part of this work. The subsequently characterization, like absorption and fluorescence spectra, will also be discussed.

Chapter 2. Studies of the aggregation behavior of oligo(*p*-benzamide)s

2.1. Introduction

2.1.1. Block copolymers

Since the first discovery and characterization of polymers large effort has been put into the research of macromolecules. A large variety of polymers is known with diverse properties. Since most polymers consist of one monomer, the repeating unit, changing the polymer properties can be obtained by using various monomers. Instead of using one monomer, two or even more monomers can be used in the polymerization reaction to form copolymers. In the case of two different repeating units, the following set of polymers can be achieved: statistical copolymer, alternating copolymer, block copolymers and graft copolymers (Figure 2.1).

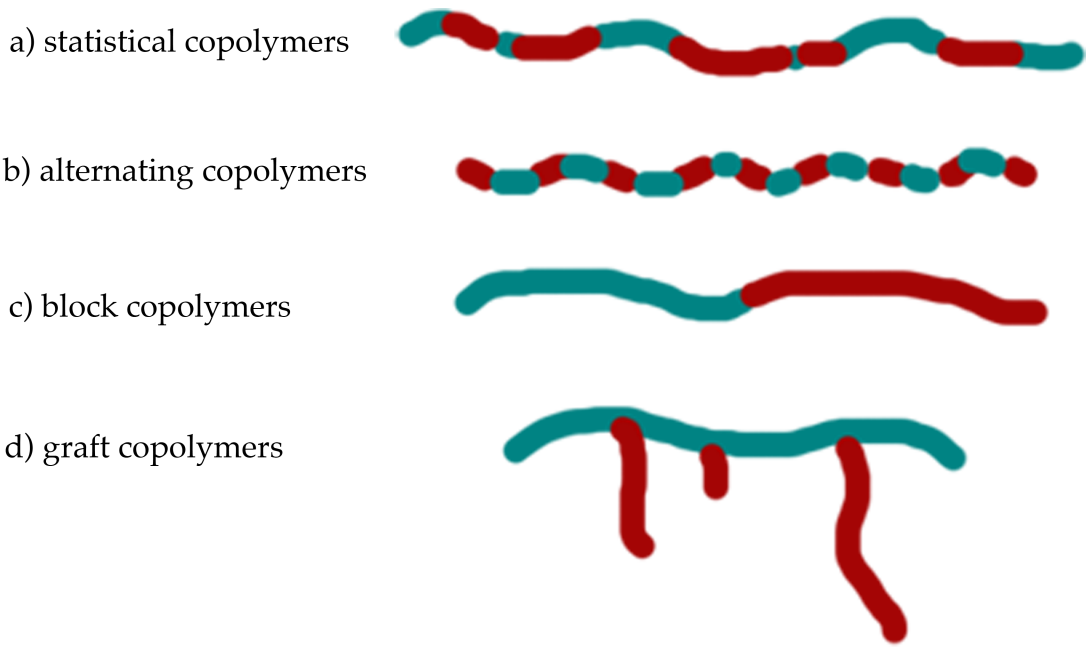

Figure 2.1: Block copolymer architectures.

One of the first block copolymers was poly(styrene)-*block*-poly(isoprene) and it is a coil-coil block copolymer, because each segment exists of a flexible block (Figure 2.2 a). A block, has one segment with a stiff and shape persistent block, for example a poly(ethylene oxide)-*block* oligo-(*p*-benzamide) copolymer, is a rod-coil block copolymer (Figure 2.2 b).

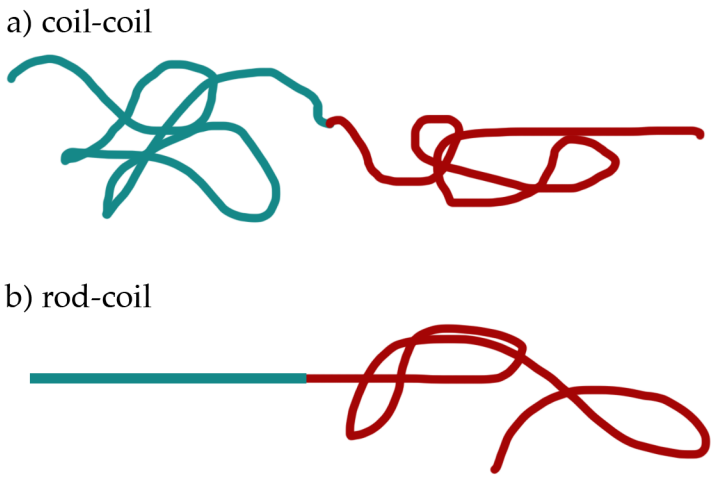

Figure 2.2: Schematic figure of a) coil-coil block copolymer and b) a rod-coil block copolymer.

2.1.2. Supramolecular Chemistry

In the last decades supramolecular chemistry became more and more important and is still a fast growing science, which connects lots of different research areas, aiming the development of highly complex and functional chemical systems through noncovalent intermolecular forces. Supramolecular preorganization is achieved through a numerous types of interactions like hydrogen bonds, metal coordination or weaker van der Waals forces and π–π-interactions. With all of these different interactions, those molecules and supramolecular architectures are capable of information storage at molecular level through molecular recognition and self-organization.

Jean-Marie Lehn, who was honored with the Nobel Prize for chemistry in 1987 together with Donald J. Cram and Charles J. Pederson, first introduced supramolecular chemistry in 1978. Since then the discipline of supramolecular chemistry is growing and has evolved a large variety and numerous developments at the interface between biology, physics and chemistry.

Nature uses supramolecular chemistry in proteins, enzymes and DNA. Without the self-organization from the nanometer to the micrometer scale, the outstanding properties of such biological ensembles would not be possible. One example of self-assembly in nature is the tobacco mosaic virus (Figure 2.3). Its transmission electron micrograph (TEM) shows stiff, rod like structures with 300 nm in length and 18 nm in width. A closer look at the virus will show that the structure is formed by proteins surrounding the central RNA. Beside the interesting structure, the virus shows an interesting behavior. Once the virus is decomposed and left under physiological conditions it is exactly self-assembled into its

well-defined structure and it regains full functionality. All this is possible with just a tiny amount of genetic information.

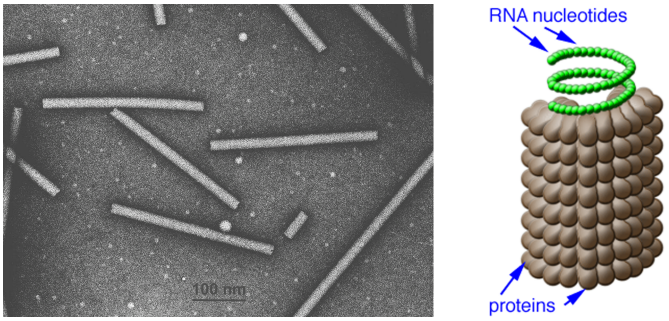

Figure 2.3: Tobacco mosaic virus: transmission electron micrograph image (*left*) and schematic representation (*right*).[1,2]

Due to the knowledge that self-assembly is important for nature; lots of scientist put a large effort in supramolecular chemistry in order to understand the mechanism of those processes. Better understanding will help to mimic biological systems like enzymes, which are well known for their excellent molecular recognition. Model systems using noncovalent bonding mechanisms are synthesized in order to improve the understanding of the self-assembly process. Typically, polymers use metal coordination, hydrogen bonding or π-π-interactions to build up supramolecular architectures. Examples of each type are shown in Figure 2.4.

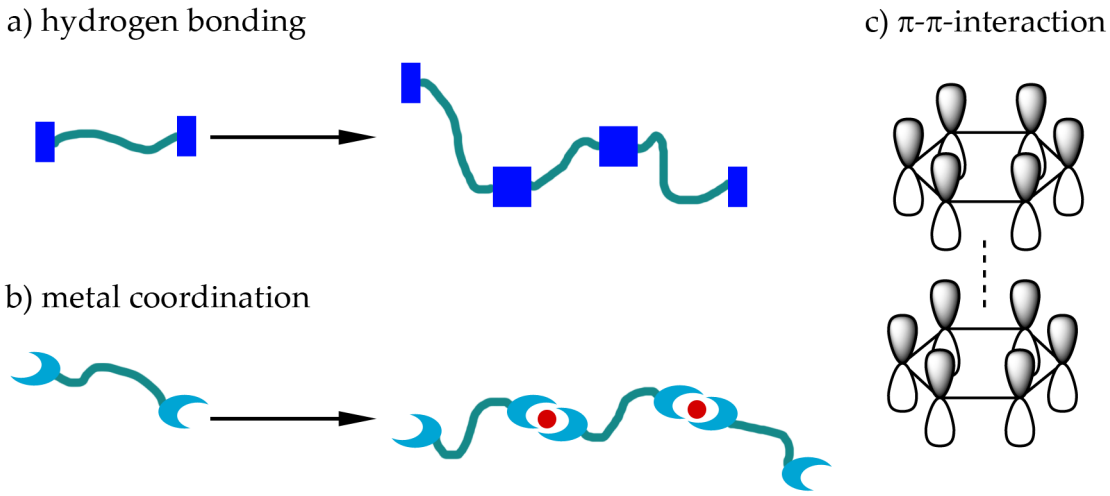

Figure 2.4: Schematic illustration of a) hydrogen bonding b) metal coordination and c) π-π-interaction.

An example of molecular recognition using hydrogen bonds is demonstrated by Tang et al.[3] He used a system consisting of A-B and C-D block copolymers, where B is a hydrogen donor block, and C is the hydrogen acceptor (Structures shown in Figure 2.5 *left*). The two diblock copolymers **2.1** and **2.2** were synthesized, whereas 4-vinylpyridine (C) as a

hydrogen-bonding acceptor and 4-hydroxystyrene block (B) as a hydrogen-bonding donor are incorporated into the polystyrene blocks. Molecular recognition is shown when a 1:1 molar ration between the hydrogen acceptors and donors are reached. Those mixtures are spin coated on a silicon wafer and further processed (Figure 2.5 *right*). The corresponding exhibited only square arrays with an extremely high degree of in-plane order. If the numbers of hydrogen donors and acceptors differ from each other, hexagonal or square packing was observed. The self-assembly to square arrays is very important for the compatibility to semiconducting integrated circuit designs, since those set-ups are usually built in a rectangular draft and not in a hexagonal one.[4]

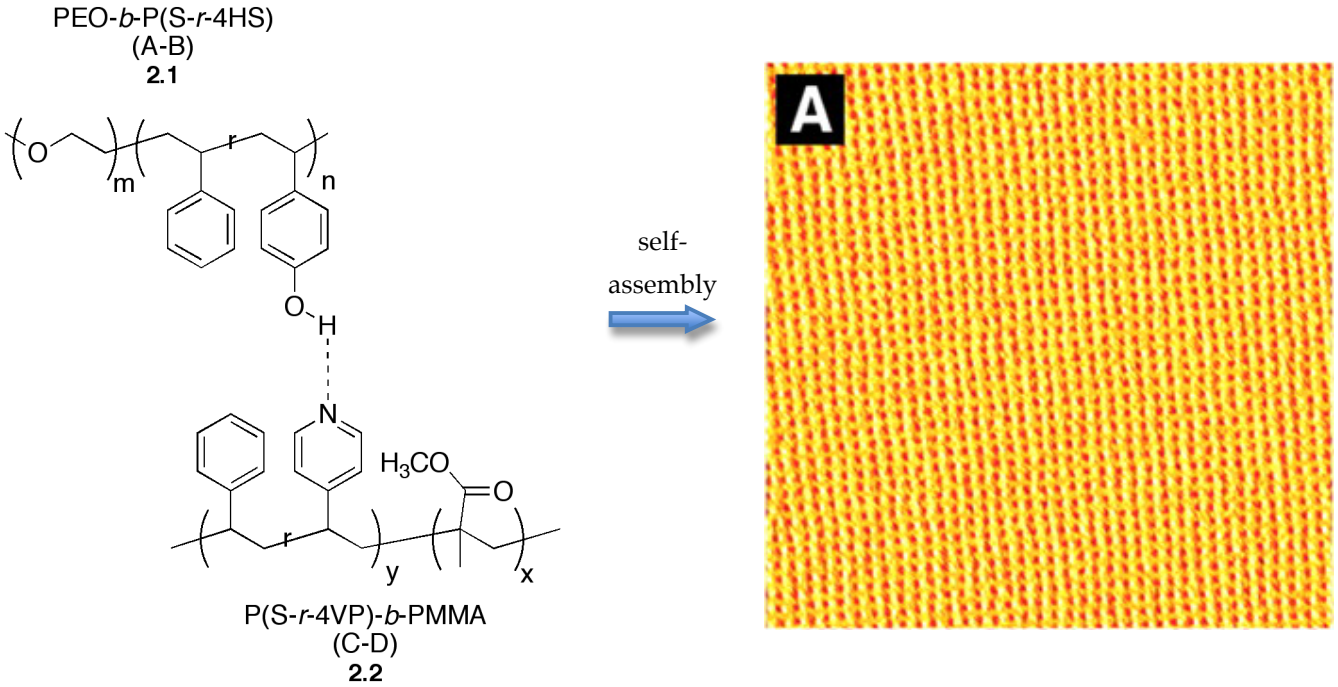

Figure 2.5: Self-assembly of A-B and C-D diblock copolymer blends on a silicon wafer. The AFM images show well-ordered square arrays which will only form when equal numbers of hydrogen-bonding donors and acceptors are present in the two block copolymers.[3]

2.1.3. Self-assembly of rod-coil block copolymers

In contrast to coil-coil block copolymers, rod-coil polymers have a stiff, shape persistent block. The rod-block can consist of various stiff structures: an aromatic rod, a helical rod or a β-sheet rod (Figure 2.6).[5]

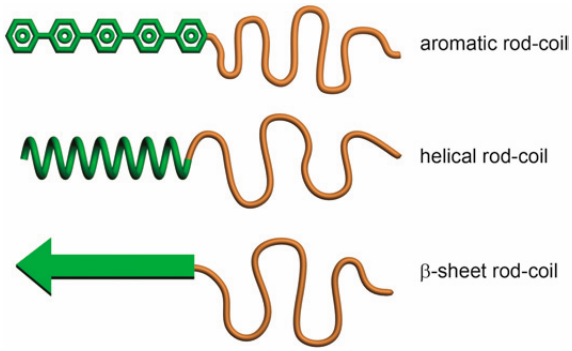

Figure 2.6: Schematic illustrations of an aromatic rod-coil, a helical rod-coil and a β-sheet rod-coil.[5]

Aromatic rod-coil block copolymers are usually based on a rigid moiety (mesogens), because their synthesis is well known, and they are monodisperse, so the structural variation in the rod block is easy to control. Lee and co-workers designed carbohydrate conjugated aromatic rod-coils, where the coil block is PEO. By varying the length of the coil block or the number of the rods, different structures from vesicles, to spherical micelles to cylindrical micelles could be shown (Figure 2.7).[5,6] A block copolymer consisting of tetra(*p*–phenylene) as the rod-block and a short poly(ethylene oxide) block (12 repeating units) forms vesicles with a diameter of 40 nm. Increasing the chain length of the poly(ethylene block) to 23 units will end in a different supramolecular structure. Spherical micelles with a diameter of 20 nm are created. By doubling the amount of rod block per coil polymer a different structure is subsequently observed. Cylindrical micelles with a diameter of 20 nm are found.

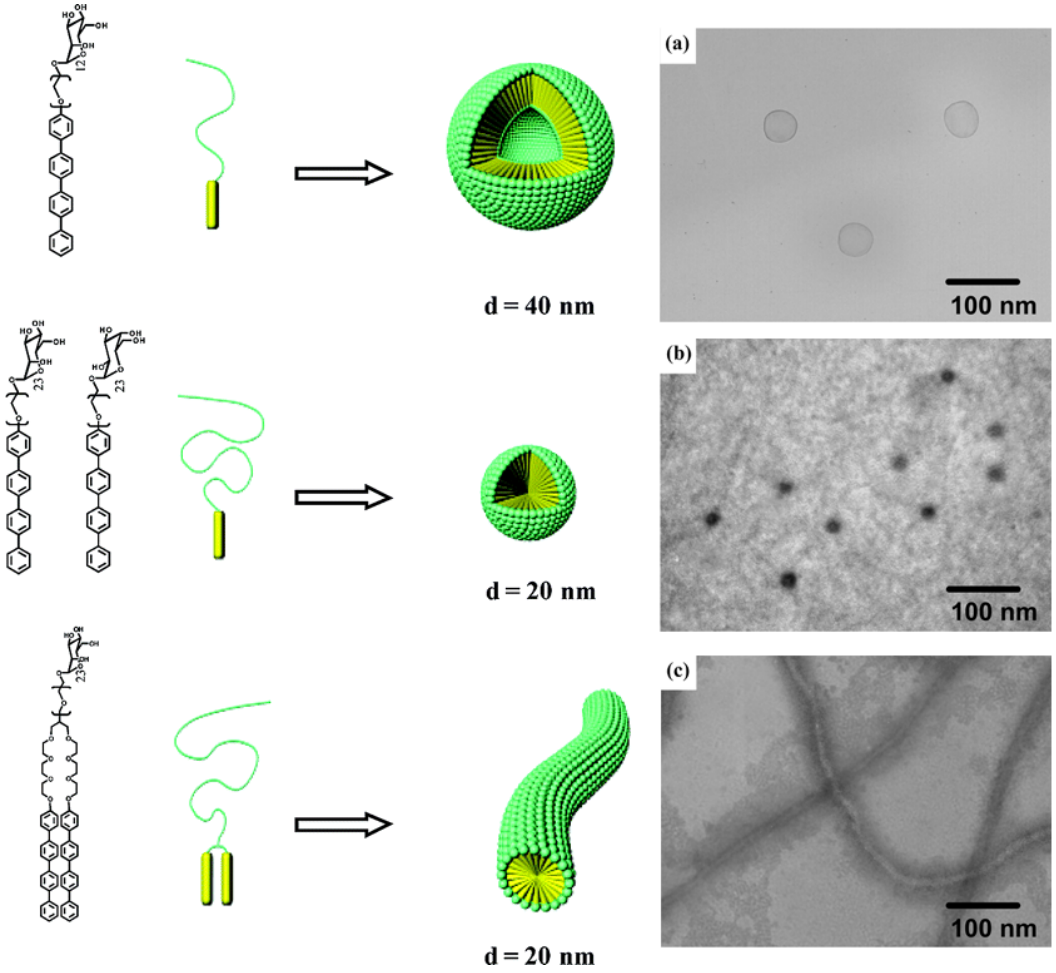

Figure 2.7: Model structures and TEM images of aromatic rod-coils self assembled into a) vesicle, b) spherical micelle or c) cylindrical micelle.[5,6]

2.1.4. Oligo(*p*-benzamide)s: structure and properties

The following part of this dissertation is focused on linear rod-coil block-copolymers. The first block is either poly(styrene) or poly(ethylene oxide), whereas the second part consists of oligo(*p*-benzamide)s. They consist of *p*-amino benzoic acid as a repeating unit and each unit is connected via an amide bond to the next monomer. Due to the fact that the electrons along the amide bond are partially delocated the benzene rings cannot rotate around the bond and therefore those oligomers are stiff and shape persistent (Figure 2.6 a). Beside that fact, each amide bond consists of a hydrogen bond acceptor and donor (Figure 2.6 b). This way each oligomer can form bonds to different oligomers, and therefore supramolecular architectures can be created.

a) partially delocated electrons b) hydrogen bonds

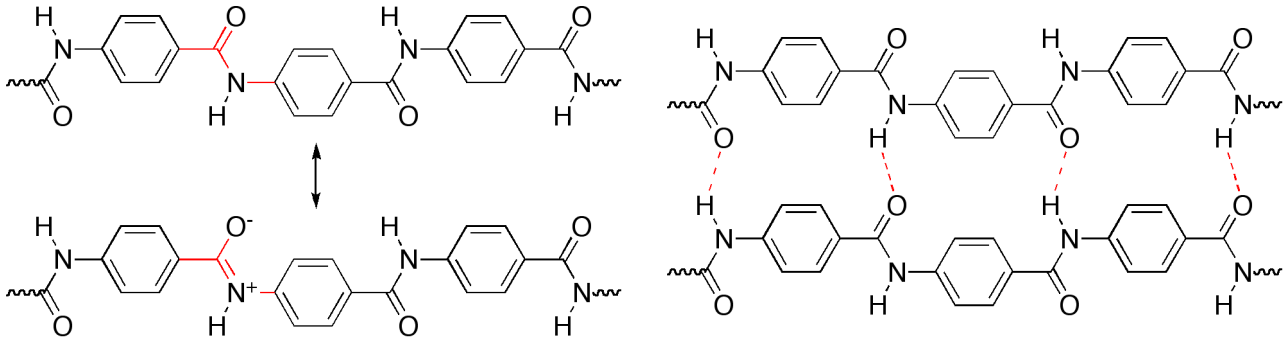

Figure 2.8: a) partially delocated electrons and b) hydrogen bonding of oligo-(*p*-benzamide).

2.1.5. Synthesis of well-defined oligo(*p*-benzamide) containing block copolymers

Several synthetic routes to β-sheet mimicking oligo(*p*-benzamide) (OPBA) have already been developed. Solution based methods, as well as solid supported syntheses are available[7-17] and produce block copolymers consisting of a precisely defined oligomeric rod-block and a flexible coil-block. Due to the used syntheses, the amounts of these very precisely defined materials are typically limited to the multi-milligram regime. In recent years, many groups have synthesized ever more complex and precisely defined polymeric materials using the tools of classical organic chemistry.[18] While this approach provides a high level of structural confidence, multi-step organic syntheses can severely hamper the preparation of larger quantities of materials. In order to be able to evaluate materials properties especially in the bulk, synthetic routes are required that give access to the 10-100 g scale without the need for laborious multi-step syntheses and wasteful purification procedures. Such a synthetic procedure, which is fully automated, can be run on a 100 g scale, and still produced well-defines supramolecular OPBA rod-coil copolymers. Two different types of polymers (PS and PEG) showed the proof of concept. On these polymers octa(*p*-benzamide) was condensed to get PEO-OPBA **(2.3)** and PS-OPBA **(2.4)** (Figure 2.9).[8]

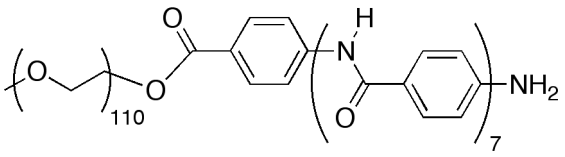

PEG-OPBA
2.3

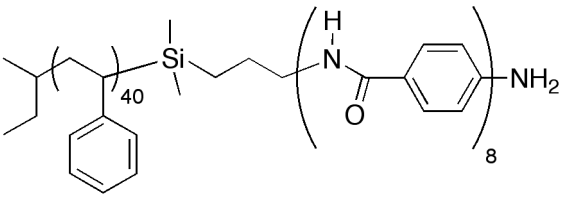

PS-OPBA
2.4

Figure 2.9: Oligo(*p*-benzamide) (OPBA) copolymers with poly(ethylene glycol) (PEG) **(2.3)** (*top*) and poly(styrene) (PS) **(2.4)** (*bottom*) coil block as prepared via the automated reaction cycle shown in Figure 2.11.

Before the large-scale synthesis of well-defined OPBAs is described, synthetic routes to mono disperse OPBAs will be shown briefly. Abbel et al. showed a synthetic pathway to soluble trimers and tetramers (Figure 2.10).[16] Similar approaches were used to synthesize longer oligomers (up to the octamer) on poly(ethylene oxide) (Figure 2.11).[14,16] In both cases a stepwise addition lead to the desires oligomers or block-copolymers. The longest soluble oligomer exists of four aromatic units **(2.13)**. This can be used, as well as the trimer **(2.11)**, to get block-copolymers, whereas one block consists of poly(ethylene oxide).

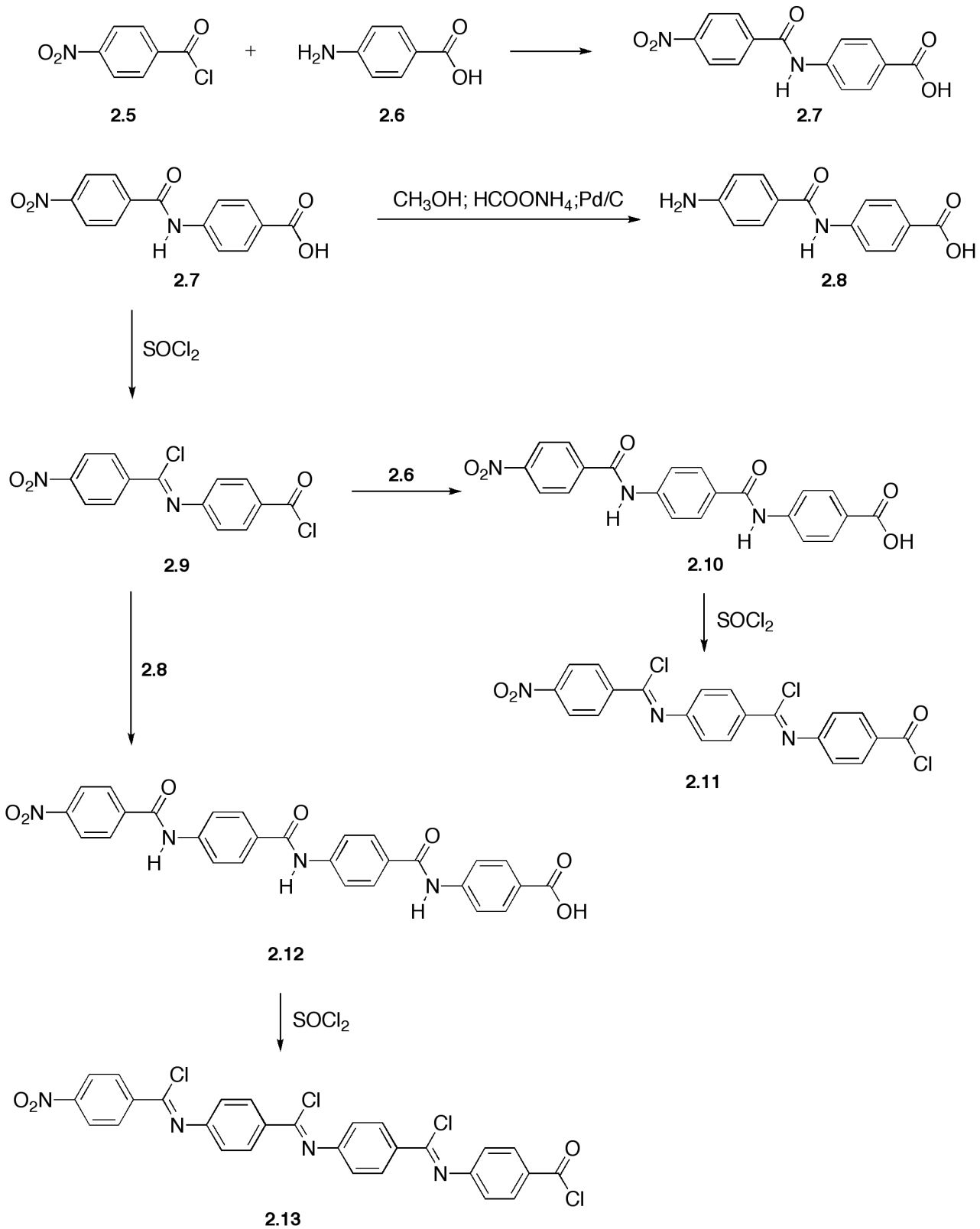

Figure 2.10: Synthesis of the trimer and tetramer by Abbel et al.[16]

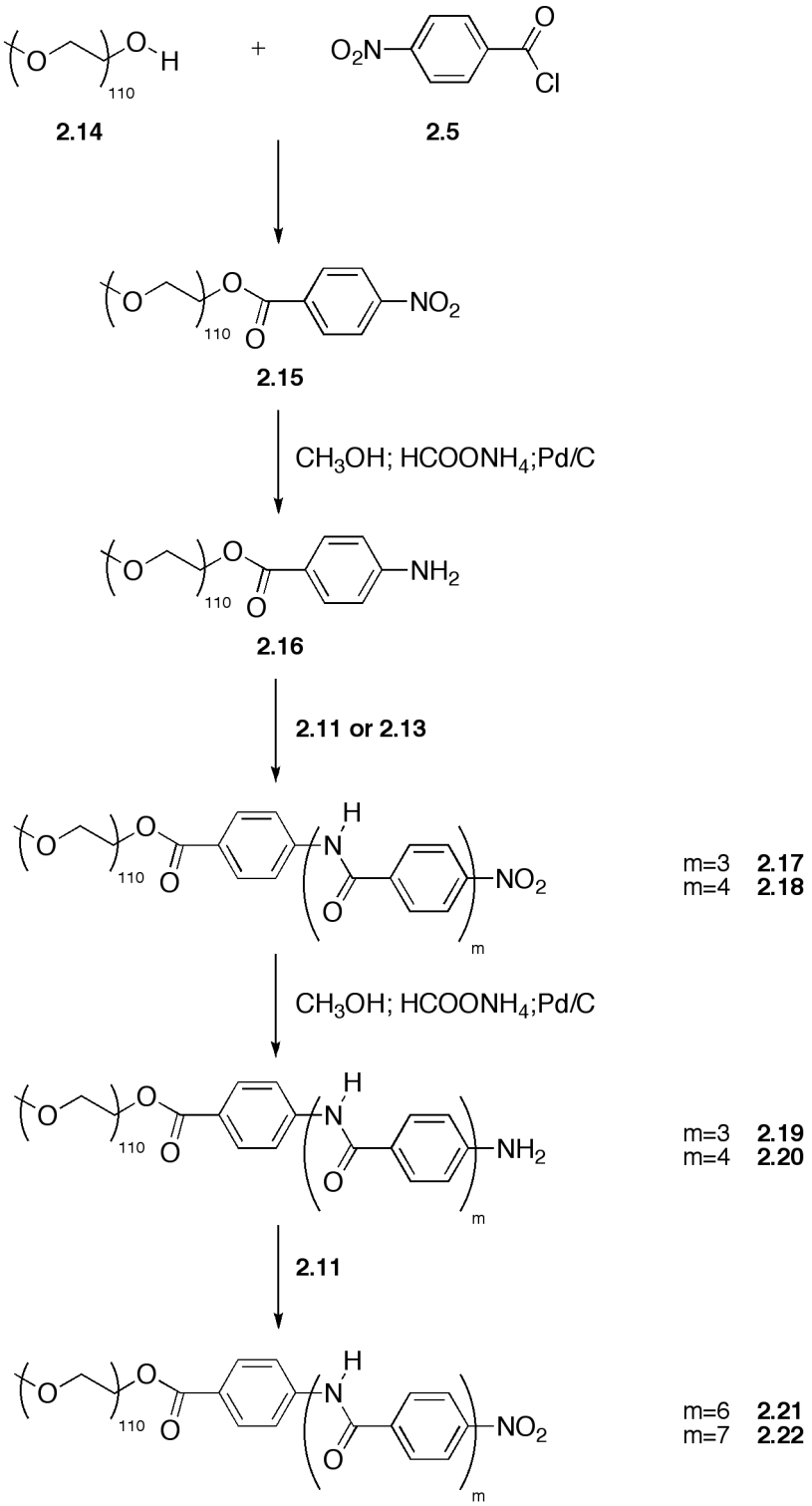

Figure 2.11: Synthesis of MPEG-OPBA.[14,16]

2.1.5.1. Synthesis of 4-*N*-sulfinylaminobenzoyl chloride and its polycondensation

One of the established routes to prepare poly(*p*-benzamide) employs 4-*N*-sulfinylaminobenzoyl chloride **(2.5)**, which is readily prepared from *p*-aminobenzoic acid and thionyl chloride (Figure 2.12).[19,20]

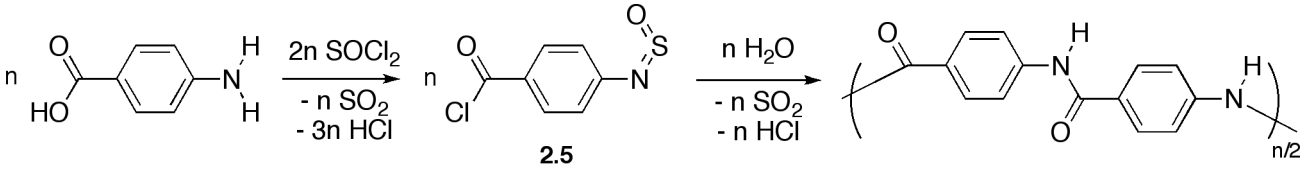

Figure 2.12: Preparation of 4-*N*-sulfinylaminobenzoyl chloride **(2.5)** from *p*-aminobenzoic acid.

2.1.5.2. Synthetic route to well-defines oligo(*p*-benzamide)s

Polymerization is typically initiated by adding water to a solution of **2.5**, which results in the formation of SO_2 and a primary amine which immediately reacts with the acid chloride to form a dimer, which can undergo further reactions to get the polymer (Figure 2.10).[19] Intrigued by the somewhat unusual reactivity of the sulfinylamine group, **2.5** was employed in a controlled step-wise condensation to produce oligo(*p*-benzamide)s. In the proposed reaction scheme, the sulfinylamine group acts as an amine protective group that can be removed quantitatively without accumulation of either the cleavage reagent (water) or cleaved-off protective group (SO_2).[21-23] Such a requirement in not easily met by most of the well-known protective groups. Compound **2.5** was therefore the ideal candidate for the construction of a reaction cycle in which a polymer carrying a primary amine was alternating reacted with **2.5** and water (Figure 2.13).

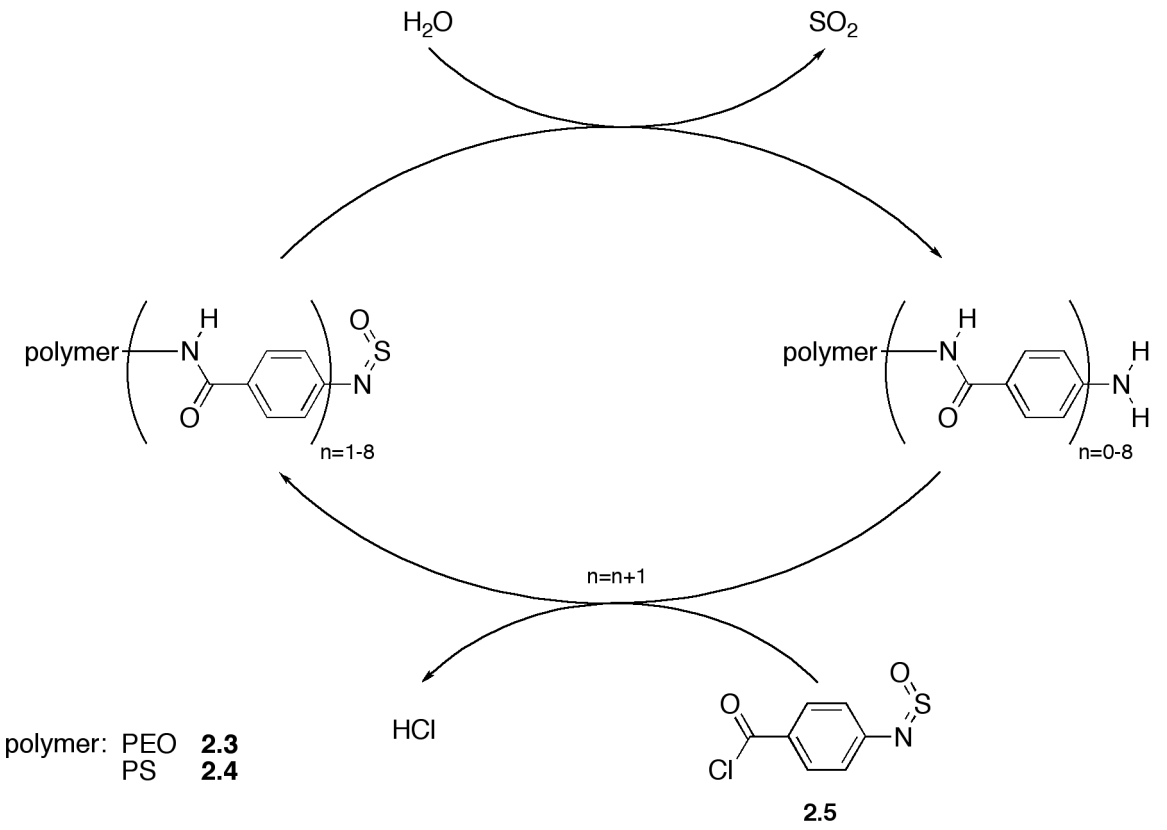

Figure 2.13: Reaction cycle in which a polymer carrying a terminal primary amine (Polymer-NH_2) is reacted alternating with **2.5** and water.

Initially, **2.5** is added to the polymer that carries a terminal amine forming an amide. The sulfinylamine is now situated at the chain end of the polymer. Addition of water cleaves off SO_2 and releases the terminal primary amine, which can continue to react in the next reaction cycle.

The reaction cycle is therefore situated at the boundary between classical organic synthesis and polymer synthesis. In multi-step organic synthesis, protective groups would be used to ensure complete control over the oligomer growth process. Work-up and purification procedures would follow each synthetic transformation, ensuring full control over the reaction. The polymer approach on the other hand, would not require any protective groups at the expense of exact control over the molecular weight and the molecular weight distribution. In this approach, no work-up procedure is carried out after the monomer addition. The protective groups (sulfinylamines) merely serve as a means of controlling the oligomerization kinetics in a "stop-and-go" fashion. The condensation of the oligomer thereby follows a pseudo-chain growth, which should allow for high levels of control over the molecular weight. In order to evaluate the feasibility of this synthetic cycle

and to figure out the best reaction parameters, several studies on the non-polymeric model compound, aniline, were carried out and can be found in ref.[8]

2.1.5.3. Synthesis of oligo(*p*-benzamide) based block copolymers

Poly(ethylene oxide) was chosen as the coil block for the initial investigations in order to compare the obtained block copolymers with the ones already prepared and analyzed by solution or solid supported syntheses.[10-12,14-16] PEG mono methyl ether (M_n = 5000 g mol^{-1}) was reacted with *p*-nitrobenzoyl chloride to form the corresponding ester. The nitro group was subsequently reduced to a primary amine.

The amine-terminated PEG (20 g) was dissolved in NMP/pyridine mixture (v:v = 50:50) at 50 °C. Monomer **2.5** and water were added in an alternating fashion in 5 h intervals while stirring the reaction mixture mechanically at 50 °C. Samples were taken after each reaction cycle (just prior to adding monomer **2.5**). After seven reaction cycles the reaction was stopped and the polymer recovered by precipitation into diethyl ether to give a PEG-OPBA **(2.3)** rod coil copolymer (Figure 2.9 *top*).

The samples taken after each reaction cycle were analyzed by GPC in DMF and chloroform and ^{1}H-NMR spectroscopy. The GPC data in DMF showed the molecularly dissolved copolymer as well as traces of oligomers that were not attached to PEG.

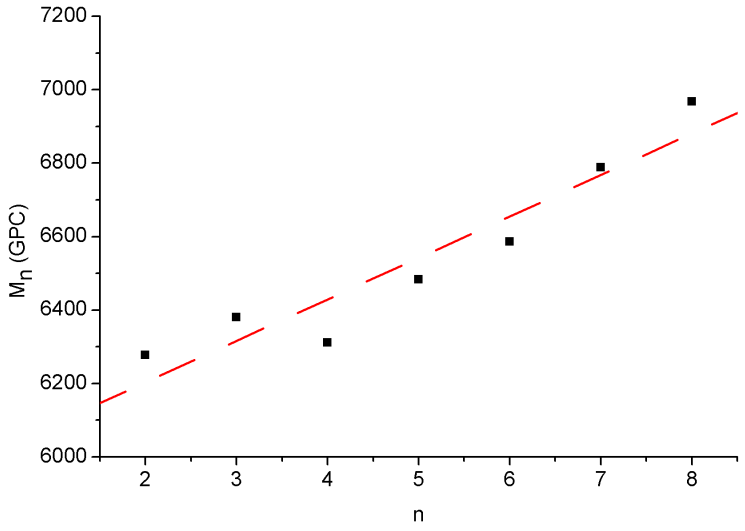

Figure 2.14: Plot of the apparent number average molecular weight (M_n) of poly(ethylene glycol)-*block*-oligo(*p*-benzamide) (PEG-OPBA) determined by gel permeation chromatography (GPC) in *N*,*N*-dimethylformamide (DMF) against the number of reaction cycles n (linear fit shown as a dashed red line).

Interestingly, plotting the apparent molecular weights of the PEG-copolymer samples, determined by GPC in DMF, against the number of reaction cycles gave a remarkably linear relationship (Figure 2.14). The molecular weight (M_n) shifts systematically towards higher molecular weights with increasing number of reaction cycles. This clearly shows that a very high level of control over the molecular weight of the growing OPBA is achieved via this automated step-wise synthesis.

In order to further demonstrate the versatility of this new automated synthetic approach an amine functionalized polystyrene (M_n = 2950 g mol^{-1}) was prepared via anionic polymerization. The living carbanion was quenched with dimethylchlorosilane and subsequently hydrosilylated onto allylamine. The presence of an amine functionality directly attached to the PS allowed the introduction of the polymer into the reaction cycle without further functionalization. After eight reaction cycles under identical conditions to those of the PEG copolymer prepared before, the polymer was precipitated into methanol to give a PS-OPBA block copolymer (Figure 2.9 *bottom*). When chloroform was added to solid PS-OPBA, a turbid solution was obtained. Filtration of this PS-OPBA solution through a 0.45 μm syringe filter resulted in a particularly high back pressure which is an indication for very high molecular weight polymers or aggregates.

2.1.5.4. TEM images of oligo(*p*-benzamide) based block copolymers

To unambiguously show the existence of high molecular weight aggregates, transmission electron microscopy (TEM) images were recorded from chloroform solutions of PEG-OPBA and PS-OPBA drop cast onto carbon coated copper grids.[10,11]

The TEM images of PEG-OPBA show extremely rigid rod-like micelles with a uniform width of ca. 9 nm (Figure 2.15). The images obtained are strikingly similar to those observed for the precisely defined polymers prepared via laborious solution syntheses.

The PS-OPBA copolymer solution was also investigated by TEM before and after filtration (0.45 μm syringe filter). Bundles of fiber-like aggregates could be seen (Figure 2.16 left) for the solution that was not passed though a syringe filter. The size of these bundles of fibers exceeds the pore size of the syringe filter used for filtration. As expected, the images of the filtered solution did not show large aggregated bundles but revealed individual fiber-like structures (Figure 2.16 right). Association of the aggregates into bundles of high molecular weight is therefore most likely the reason for the high back pressure observed during the syringe filtration of the sample. The individual PS-OPBA

aggregates (Figure 2.16 right) do not appear to form micelles that are as rigid as the ones observed for PEG-OPBA. However, micellar aggregates can be seen with a perfectly uniform width of ca. 10 nm.

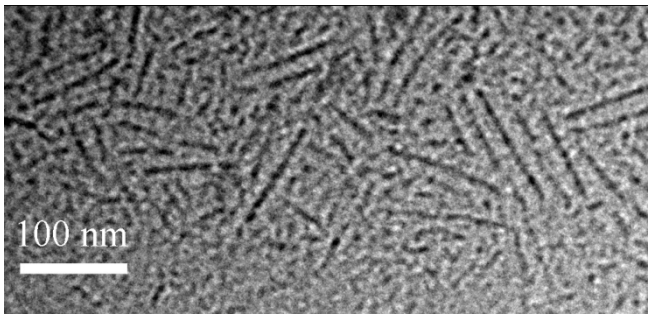

Figure 2.15: Transmission electron microscopy (TEM) image (unstained) of poly(ethylene glycol)-*block*-oligo(*p*-benzamide) copolymer (PEG-OPBA, **2.3**, Figure 2.9 *top*) drop cast from chloroform solution onto carbon coated copper grids.

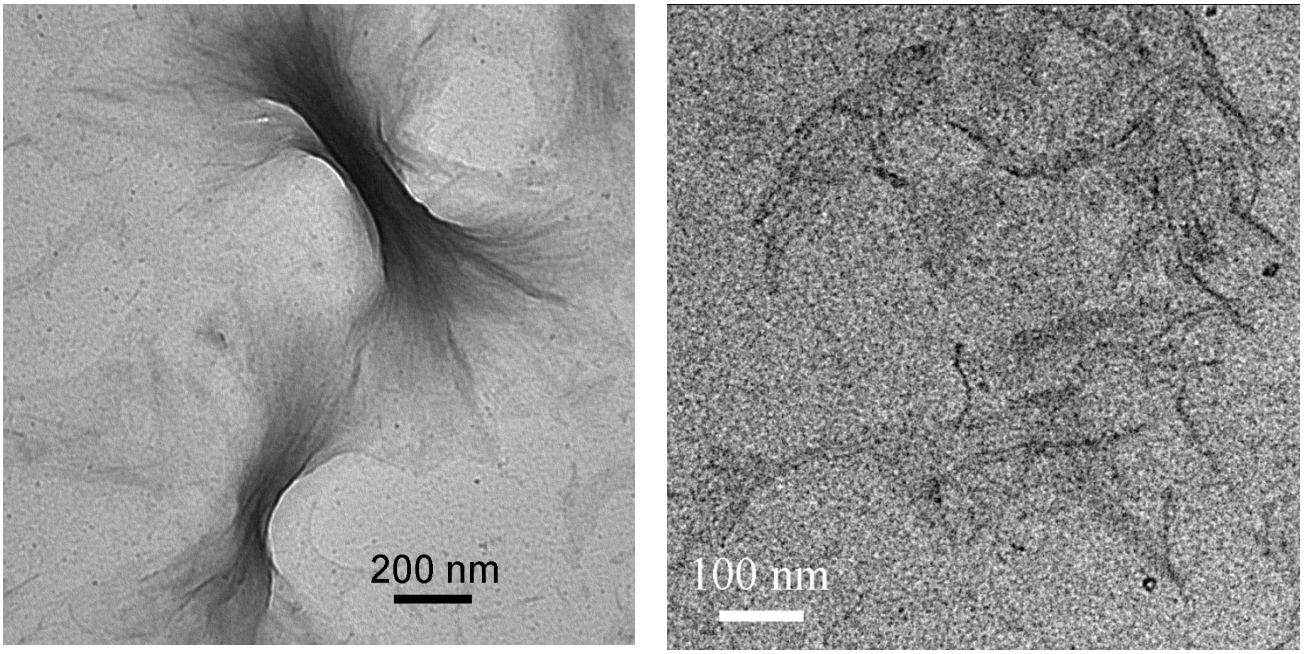

Figure 2.16: Transmission electron microscopy (TEM) images (unstained) of poly(styrene)-*block*-oligo(*p*-benzamide) (PS-OPBA, **2.4**, Figure 2.9 *bottom*) drop cast from chloroform solution onto carbon coated copper grids. *Left*: without syringe filtration. *Right*: after syringe filtration.

The reason why the PS-OPBA copolymer forms bundles of fibers whereas the PEG-OPBA shows well defined and separated linear aggregates is unknown at present.

It is necessary to emphasize at this point that the block copolymers forming such outstandingly well-defined aggregation structures were synthesized in large quantities via an automated reaction cycle. The data presented here clearly shows that the step-wise addition of 4-*N*-sulfinylaminobenzoyl chloride and water to amine-terminated polymers results in well-defined rod-coil block copolymers. However, any multi-step reaction that is carried out without work-up after each reaction step will eventually accumulate side-products, give faulty sequences and result in a molecular weight distribution. Even though the amount of residual oligomers is small, it has to be assumed that the polymer bound oligomers also show a certain molecular weight distribution. In this case it is even more astonishing that the copolymers form such extremely well defined aggregates as observed by TEM. It appears that small deviations in the oligomer length of the rod-coil copolymer can be averaged out such that the aggregate presents itself similarly to those of the precisely defined monodisperse copolymers.

2.2. Sample Preparation

Analysis of the supramolecular structures desire standardized sample preparation conditions. Thus always the same conditions have been applied and only a small set of parameters where changed to see whether they have an effect on the aggregation behavior. In the first instance, the sample preparation is described before the different conditions are discussed. The constant amount (1 nmol; 5.9 mg) of polymer (PEO-OPBA, **2.3**, Figure 2.9 *top*) was dissolved in *N*,*N*-dimethylformamide (1 mL), which is a good solvent for both blocks of the polymer. The mixture is treated with ultrasonic at 40 °C for 30 minutes in order to dissolve the polymer completely. This step is necessary, because the oligo(*p*-benzamide) block is strongly aggregating and therefore gets dissolved very slowly. The ultrasonic radiation disrupts the intermolecular hydrogen bonds and thus erases all existing structures, which may have been existent in the solid state of the polymer. To this solution different salts may be added prior to ultrasonic treatment. The precipitation took place in a given amount of selective solvent for the poly(ethylene oxide) block. In some cases a co-solvent or salts where added to this liquid. The polymer solution was then slowly dropped to the precipitation solution using a syringe pump with a speed of 0.2 mL/min. The different effect between shaking and stirring was also analyzed. Table 2.1 summarizes different sample preparation conditions.

Table 2.1: Samples

No	Polymer solution	Precipitation			
		Precipitation solvent			Condition
	Added salt	Solvent	Volume / mL	Added salt	
1		chloroform	5		shaking
2		chloroform	10		shaking
3		chloroform	20		shaking
4		chloroform	40		shaking
5		chloroform	60		shaking
6	1 mg LiCl	chloroform	20		shaking
7		chloroform	20	1 mg LiCl	shaking
8	5 mg CsBr	chloroform	20		shaking
9		chloroform	20	5 mg CsBr	shaking
10		chloroform:DMF	20:0		shaking
11		chloroform:DMF	16:4		shaking
12		chloroform:DMF	12:8		shaking
13		chloroform	20	1 mg LiCl	stirring

2.3. Results and Discussion

The carried out sample preparations can be classified into different sets of condition variations:

- Variation of the good solvent to the selective solvent ratio.
- Addition of salts to the polymer solution respectively to the selective solvent.
- Time dependency of the formed supramolecular structures.
- Precipitation in solvent mixtures.
- Shaking versus stirring while adding the polymer solution.

2.3.1. Ratio variation of the good solvent to the selective solvent

The first discussed results are the different solvent rations. While leaving the amount of good solvent constant, with a constant polymer concentration, the amount of selective solvent for the PEO block was increased. Whereas 1 mL PEO-OPBA solution in DMF was kept constant, the amount of chloroform was chosen from 5 mL to 60 mL. The samples where shaken after the polymer solution was added to the chloroform. Figure 2.18 illustrates the different formed structures. The first sample (Sample 1, Figure 2.16 a) shows round and filled spheres with a diameter of around 200 nm. Beginning from the second sample (Sample 2, Figure 2.18 b), hollow spheres are obtained with different dimensions. The second sample (10 mL chloroform) forms spheres with a diameter of 3 μm and a wall thickness of 45 nm. If the polymer was drop wise added to 20 ml chloroform (Sample 3, Figure 2.18 d), the thickness of the wall increases and a darker and lighter region are visible. The darker region is around 180 nm thick, where as the lighter one is around 500 nm thick. The spheres have a diameter of 9 μm. The higher diluted samples show smaller sphere: around 1.8 μm to 5.2 μm in the case of 40 mL chloroform (Sample 4, Figure 2.18 d), or 1.4 μm to 3.0 μm for 60 mL chloroform (Sample 5, Figure 2.18 e). The wall thicknesses are 30 nm (40 mL chloroform), and 20 nm (60 mL chloroform). With increasing chloroform to DMF ratio the wall thickness decreases down to 20 nm (Sample 5, Figure 2.18 d), which is in the range of the double length of on one oligo(*p*-benzamide) block. This indicates that two OPBA blocks are face-to-face orientated, meaning that both end-groups (amino groups) are located facing each other. Comparing this width to the *bilayer hockey-puck micelle* model[12] it is still double the thickness. The model claims 10 nm for a face-to-face orientation of two oligo-(*p*-benzamide) blocks (Figure 2.17). A possible explanation for the double thickness is the weak contrast of the sample, which does not

allow an accurate measurement. Sample 3 (Figure 2.18 c) shows small micelles, which have a diameter around 90 nm. It looks like, that those small structures fuse together, to create a larger spherical hollow micelle.

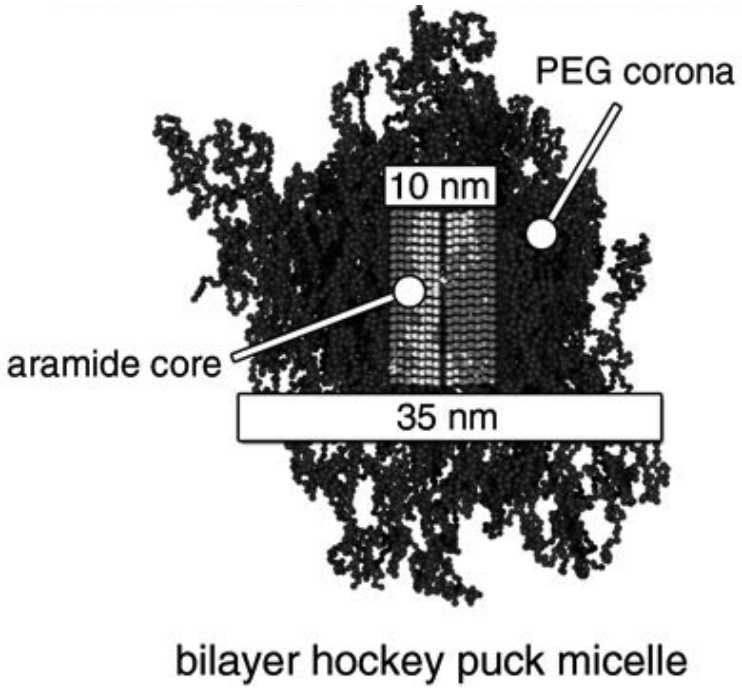

Figure 2.17: Bilayer hockey-puck micelle claimed by T.W. Schleuss.[12]

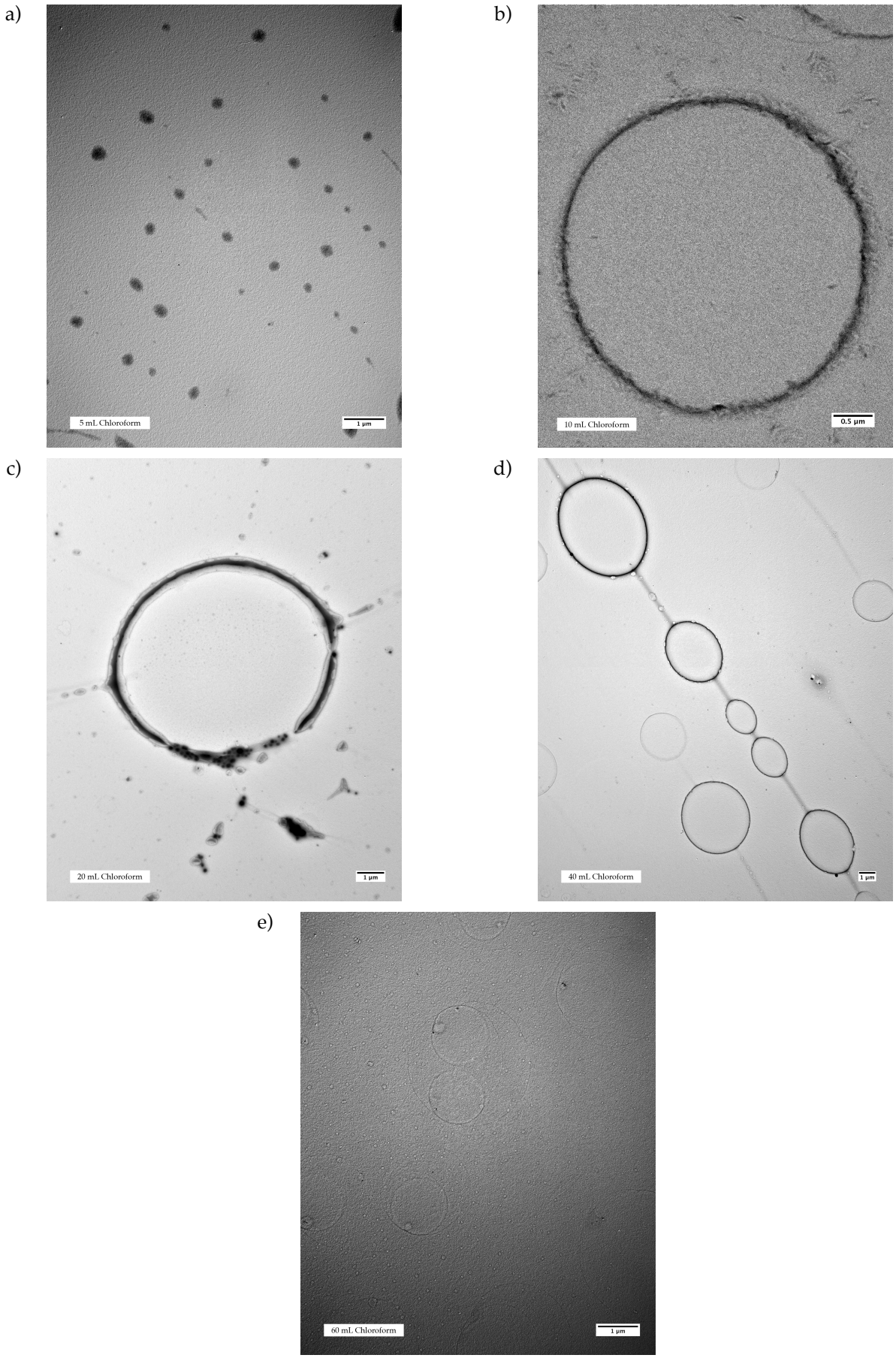

Figure 2.18: Supramolecular structures of a) sample 1, b) sample 2, c) sample 3, d) sample 4 and e) sample 5.

2.3.2. Addition of salts to the polymer solution respectively to the selective solvent

Lithium chloride is known to interrupt hydrogen bonds, and in this case, this may lead to less stronger aggregation and is analyzed in the following part. Since the lithium ion is very small, a larger counter part, cesium bromide, will be used, too. The salt can be added to the polymer containing solution (DMF) as well as to the selective solvent in which the polymer solution is drop wise added. Sample 6 (Figure 2.19) is prepared with 1 mg lithium chloride. The salt was added to the polymer solution and then slowly given to chloroform. The result are two supramolecular structures: large spherical micelles with varying diameter (100 nm to 350 nm) and smaller elongated aggregates with dimension of 9 nm in width and around 100 nm in length.

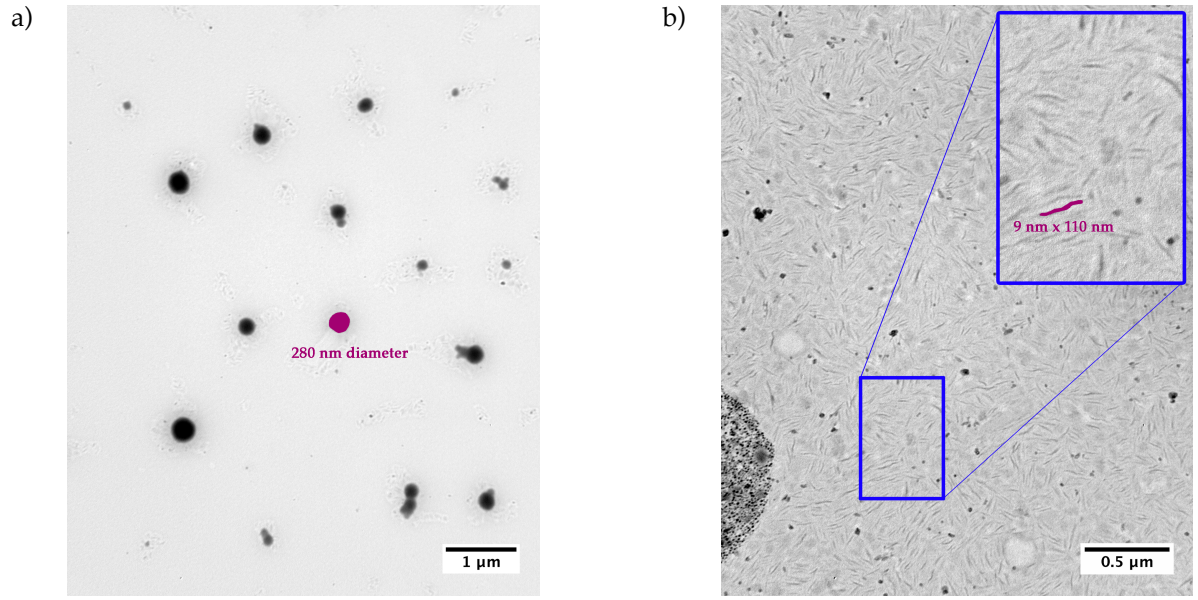

Figure 2.19: TEM images of sample 6: 1 mg lithium chloride in the polymer solution.

In contrast, adding lithium chloride to the chloroform and not to the polymer solution, the large spherical micelles are not observed anymore (Sample 7, Figure 2.20). The small long structures are still visible and have similar dimensions.

a) b)

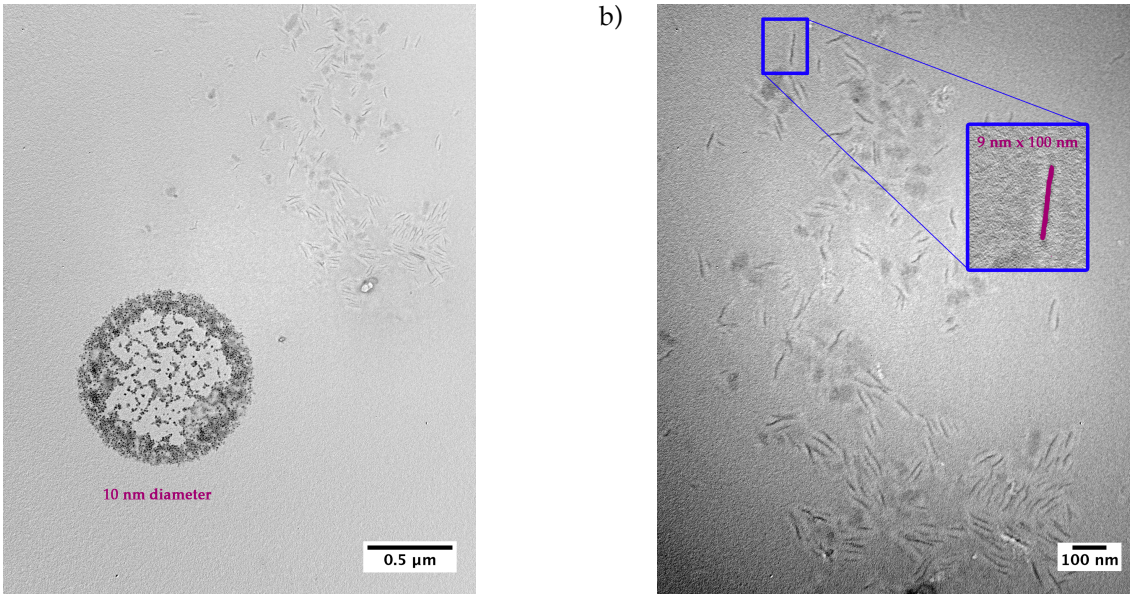

Figure 2.20: TEM images of sample 7: 1 mg lithium chloride in chloroform.

Adding the larger cesium bromide will induce different structures. For both cases (Sample 8 and 9, Figure 2.21 and 2.22), the salt is added to the polymer solution or to the chloroform, spherical micelles, with a varying diameter (150 nm to 300 nm), are observed. For sample 8 (Figure 2.21), beside the large micelles, small micelles with a diameter of 8 nm appear. Long micelles with a length of 500 nm and a width of 35 nm are visible beside the large spherical micelles in sample 9 (Figure 2.22).

a) b)

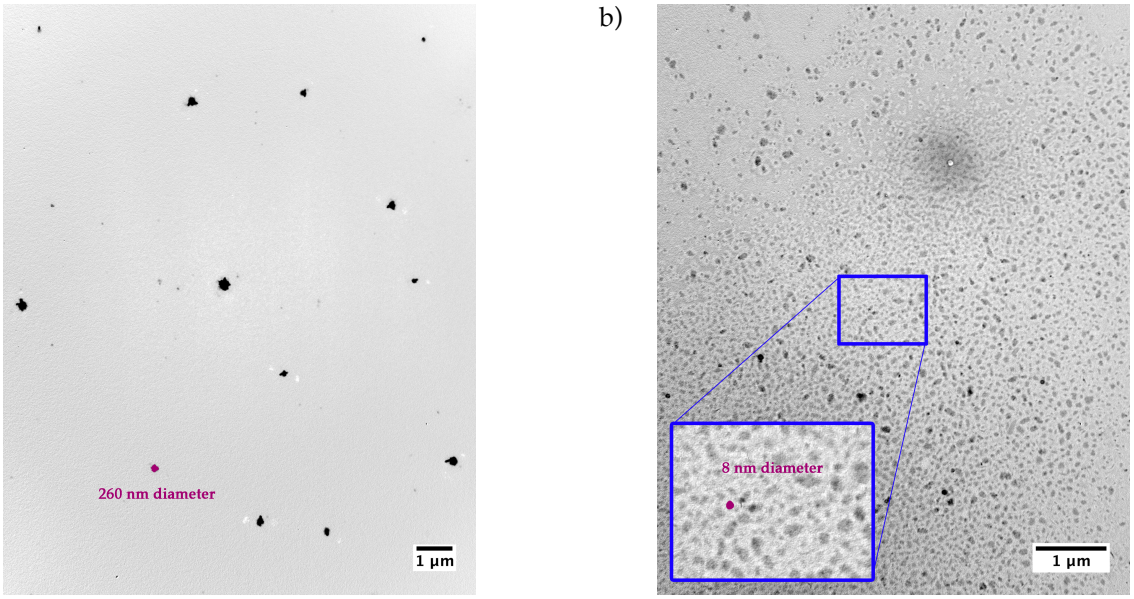

Figure 2.21: TEM images of sample 8: 5 mg cesium bromide in the polymer solution.

a) b)

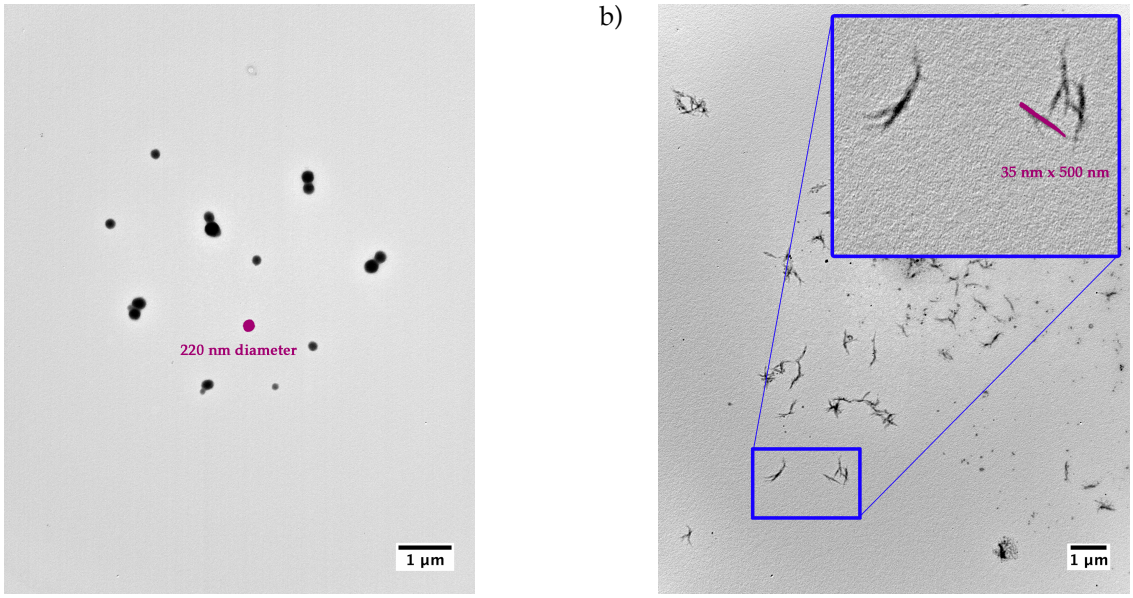

Figure 2.22: TEM images of sample 9: 5 mg cesium bromide in chloroform.

2.3.3. Time dependency of the formed supramolecular structures

The interesting effect, which is observed in the presence of cations, is further observed in the process of time. The samples where left for 5 and 10 days before they where drop casted on the TEM grid and analyzed. Figure 2.23 shows the pictures for sample 6 (Figure 2.23 *left*) and sample 7 (Figure 2.23 *right*) directly after mixing (2 hours) and after 5 and 10 days of resting the solution. In both cases, small linear micelles with a length of 100 nm and a width of around 8 nm are observed. Beside these structures, small spherical supramolecular aggregates with diameters of about 10 nm are also visible. Both samples show a total different picture after 5 days. The small linear structures, as well as the small spherical micelles are vanished. For sample 6 spherical micelles with diameters of 150 to 250 nm are observed, which are statistically spread over the grid. Sample 7 shows a similar picture with spherical micelles having diameters between 80 and 180 nm. In contrast to sample 6, the structures are not dispensed over the grid, but gathered in a larger oval structure with diameters of 1.3 μm respectively 1.7 μm. After another 5 days, both samples show no further difference.

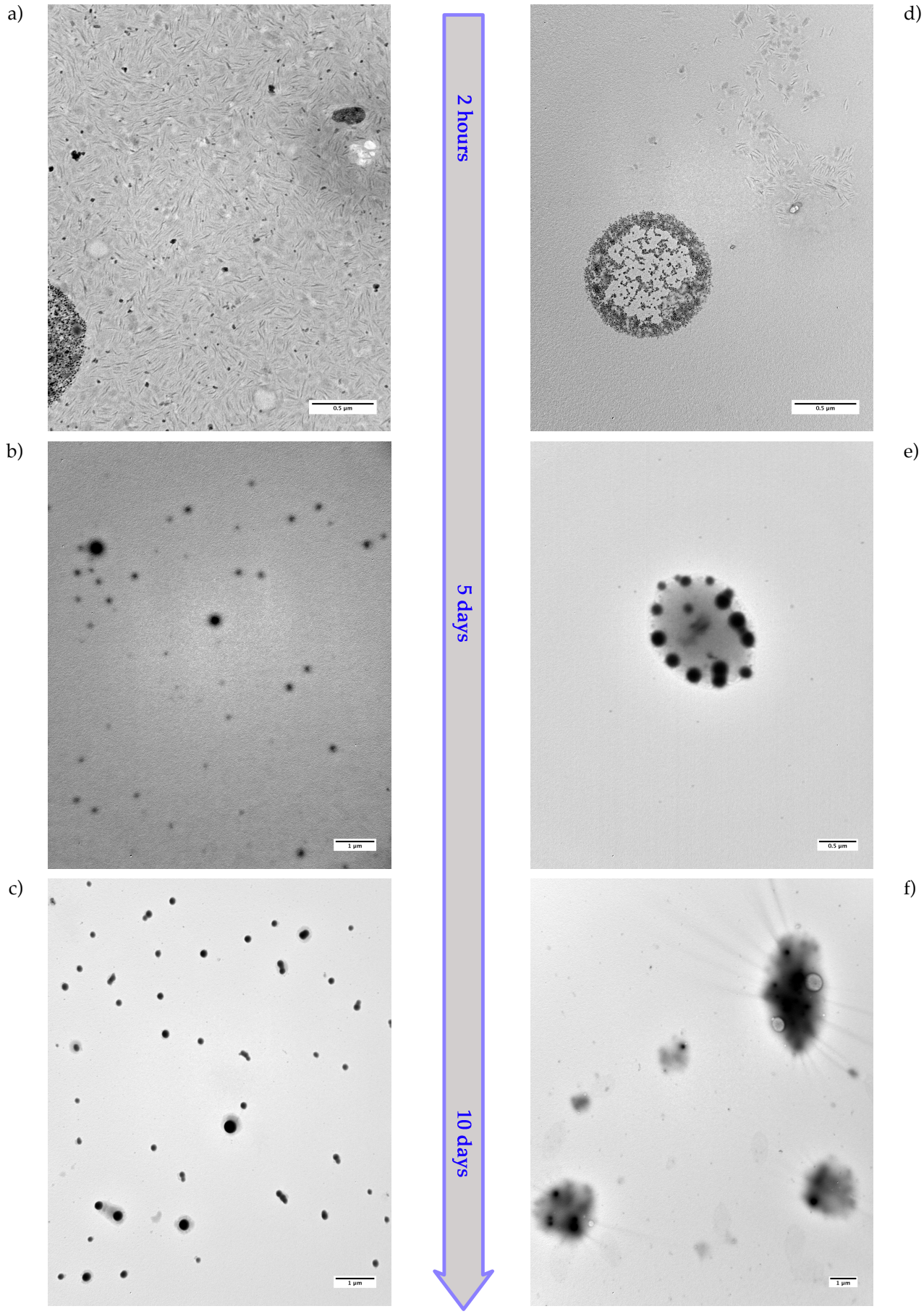

Figure 2.23: TEM images of sample 6 (*left*) and 7 (*right*) after 2 hours, 5 days and 10 days.

2.3.4. Precipitation in solvent mixtures

Chloroform is a selective solvent for the PEO block. It does not dissolve the OPBA block. Adding a given amount of DMF to the chloroform before addition of the polymer solution (in DMF) changes the form of the supramolecular structures and these where analyzed (Figure 2.24). The total amount of precipitation was 20 mL. In sample 10 no DMF was added, thus 20 mL chloroform where used. The probes where shaken during the addition of the polymer solution. Spherical micelles, with a large diameter distribution (between 100 nm and 600 nm), were found to be the dominant structure. Increasing the amount of DMF to 4 mL (and leaving 16 mL chloroform), ends in the decrease of the found aggregates. They are still spherical, but only have a diameter between 80 nm and 150 nm. Adding another 4 mL DMF to the chloroform will further decrease the aggregates' size: 35 nm to 50 nm small spherical micelles were found next to elongated aggregates, which are 75 nm in width and 240 nm in length.

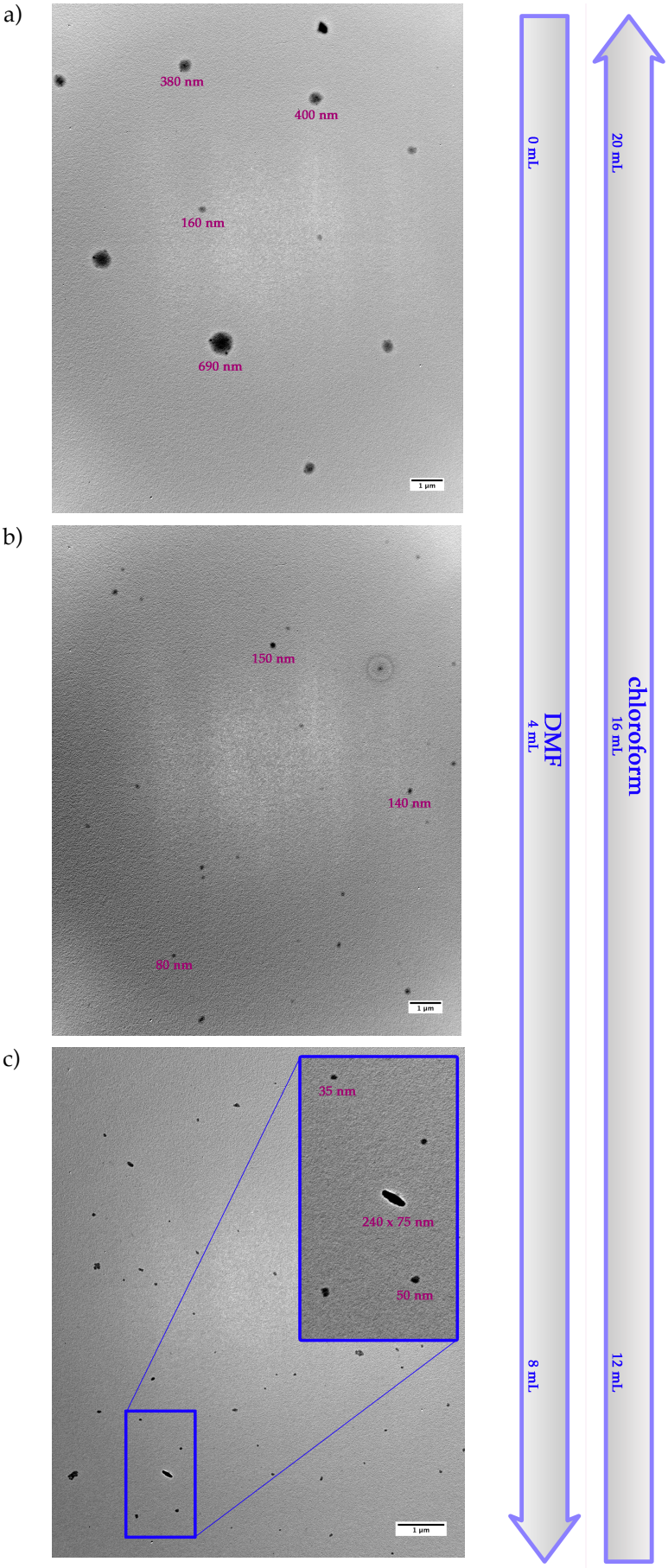

Figure 2.24: TEM images of a) sample 10, b) sample 11 and c) sample 12.

2.3.5. Shaking versus stirring while adding the polymer solution

The last set of experiments show the difference of shaking and stirring while the polymer solution is added to chloroform. Stirring is much harsher and thus is capable of destroying less stable aggregates. So shaking should leave them intact. Figure 2.25 shows sample 7, which was shaken, and sample 13, which was stirred. Sample 7 shows the already discussed spherical micelles (diameter around 10 nm) and long structures (8 nm x 70 nm). In contrast, in the shaken sample larger spherical aggregates (diameter around 120 nm) and long structures (45 nm in width and 370 nm in length) are observed.

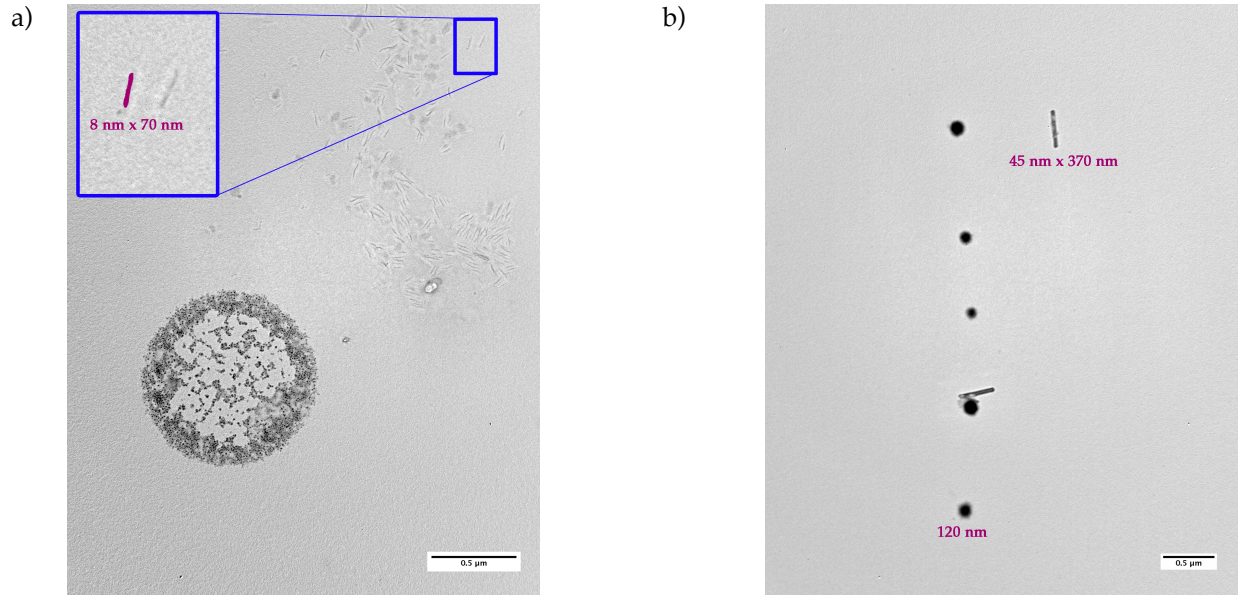

Figure 2.25: TEM images of a) sample 7 and b) sample 13.

2.4. Conclusion

The rod-coil block copolymer PEO-OPBA is capable of forming different supramolecular structures when it is dissolved in a good solvent for both blocks and subsequently given to a selective solvent for one block. In here, DMF dissolves both blocks, whereas chloroform only dissolves the poly(ethylene oxide) block. The first experiment deals with different DMF to chloroform ratio. Using more chloroform ends in larger structures. Except the first sample, all other samples (2-5) shows spherical hollow micelles and with increasing amount of chloroform, the wall thickness decreases, until it is only about 20 nm wide. This size correlates to the double width of the proposed bilayer hockey-puck micelle (Figure 2.16). If lithium chloride is now added to either the polymer containing solution or to the chloroform, elongated structures are observed with a width of 9 nm and a length of 100 nm. In the case of being lithium chloride in the polymer solution, large spherical micelles with a diameter of 280 nm are observed. If the salt is dissolved in chloroform, the observed spherical micelles are smaller and have a diameter of 10 nm. Similar results are found to be the case, when cesium bromide is added to the liquids. In both cases (salt in the polymer solution, respectively in chloroform) spherical micelles with a diameter of around 250 nm are visible. If cesium bromide is added to the polymer solution, small round structures with a diameter of 8 nm are found. In the case, where cesium bromide is dissolved in chloroform, longish structures where proved. Compared to the ones obtained with lithium chloride, these are longer (500 nm) and wider (35 nm). Besides adding salts to the solutions, DMF can also be added to chloroform. This will increase the solubility of both blocks. The result is the formation of smaller spherical micelles with an increasing ratio of DMF to chloroform. Beginning from large structures (up to 700 nm) down to small micelles (35 nm) can be created.

The stability of aggregates has also been analyzed in two ways. In the first case, the aggregates where left for a longer time period (5 and 10 days) and in the second case, the samples where stirred and not shaken. The structures observed after 2 hours, are totally vanished after 5 days. The small longish aggregates are fused to create larger spherical micelles. After 10 days no difference is visible compared to the samples state after 5 days. The same effect is observed in the case of stirring. Larger spherical micelles are obtained beside some linear aggregates, which are also bigger.

By varying the sample preparation, a large variety of supramolecular structures can be created. Simple droppings of the polymer solution to a changeable amount of chloroform, spherical hollow micelles with different sizes are obtained. More interesting is

the fact, that adding salts to the solution, long and thin structures are observed. Especially in the case of lithium chloride, these structures seem to be bilayer hockey-puck micelles. Small spherical micelles are obtained, when DMF is added to the chloroform.

Rod-coil block copolymer are capable of forming a variety of supramolecular architectures, such as vesicles, spherical or cylindrical micelles (Figure 2.7). All these potential aggregates can be formed by simply one polymer, the PEO-OPBA, just depending on the way of preparation. The hockey-puck micelles may also be worm-like architectures. The difference is now easy visible with standard TEM techniques. Adding salts or DMF may increase the solubility of the block co-polymer. Whereas DMF will definitely increase the solubility of the OPBA block, salts, like lithium chloride, will interrupt hydrogen bonds. Both methods slow done the aggregation process, and therefore help to more stable structures. If the plain polymer is given to chloroform, it will readily precipitates and form the observed structures. Since no interruption of hydrogen bonds can occur, nor solubilization of the OPBA block, it is difficult for the polymer to aggregate into different structures. This circumstance can be easily overcome by adding lithium chloride or DMF to the system and thereby opening a large variety of different supramolecular structures.

2.5. References

1. Blamire, J. http://www.brooklyn.cuny.edu/bc/ahp/LAD/C4b/C4b_assembly.html (17.06.2009),
2. Milne, R. http://www.ncbi.nlm.nih.gov/ICTVdb/Images/Milne/tobamo1.htm (17.06.2009),
3. Tang, C.; Lennon, E. M.; Fredrickson, G. H.; Kramer, E. J.; Hawker, C. J. *Science* **2008,** 322, (5900), 429-432.
4. Lim, Y.; Lee, M. *Angew. Chem. Int. Edit.* **2009,** 48, (19), 3394-3396.
5. Lim, Y.; Moon, K.; Lee, M. *J. Mater. Chem.* **2008,** 18, (25), 2909-2918.
6. Kim, B.-S.; Hong, D.-J.; Bae, J.; Lee, M. *J. Am. Chem. Soc* **2005,** 127, (46), 16333-16337.
7. Klos, J.; Wurm, F.; Kilbinger, A. F. M. *Abstracts of Papers, 235th ACS National Meeting, New Orleans, LA, United States, April 6-10, 2008* **2008**, PMSE-493.
8. Klos, J.; Wurm, F.; König, H. M.; Kilbinger, A. F. M. *Macromolecules* **2007,** 40, (22), 7827-7833.
9. König, H. M.; Kilbinger, A. F. M. *Angew. Chem. Int. Edit.* **2007,** 46, (44), 8334-8340.
10. Seyler, H.; Berger-Nicoletti, E.; Kilbinger, A. F. M. *J. Mater. Chem.* **2007,** 17, (19), 1954-1957.
11. König, H. M.; Gorelik, T.; Kolb, U.; Kilbinger, A. F. M. *J. Am. Chem. Soc.* **2007,** 129, (3), 704-708.
12. Schleuss, T. W.; Abbel, R.; Gross, M.; Schollmeyer, D.; Frey, H.; Maskos, M.; Berger, R.; Kilbinger, A. F. M. *Angew. Chem. Int. Edit.* **2006,** 45, (18), 2969-2975.
13. König, H. M.; Abbel, R.; Schollmeyer, D.; Kilbinger, A. F. M. *Org. Lett.* **2006,** 8, (9), 1819-1822.
14. Abbel, R.; Schleuss, T. W.; Frey, H.; Kilbinger, A. F. M. *Macromol. Chem. Physic.* **2005,** 206, (20), 2067-2074.
15. Abbel, R.; Schleuss, T. W.; Frey, H.; Berger, R.; Rietzler, U.; Kilbinger, A. F. M. *Abstr Pap Am Chem S* **2005,** 229, U916-U917.
16. Abbel, R.; Frey, H.; Schollmeyer, D.; Kilbinger, A. F. M. *Chem. Eur. J.* **2005,** 11, 2170-2176.
17. Kilbinger, A. F. M.; Feast, W. J. *J. Mater. Chem.* **2000,** 10, (8), 1777-1784.
18. Hawker, C. J.; Wooley, K. L. *Science* **2005,** 309, 1200-1205.
19. Kwolek, S. L.; Morgan, P. W.; Schaefgen, J. R.; Gulrich, L. W. *Macromolecules* **1977,** 10, 1390-1396.
20. Taylor, E. C.; Fletcher, S. R.; Sabb, A. L. *Synth. Commun.* **1984,** 14, (10), 921-924.
21. Dawson, T. L. Ph.D. thesis, University of Kentucky, 1960.
22. Ivanova, E. V.; Muchall, H. M. *Can. J. Chem.* **2005,** 83, 1588-1596.
23. Miranova, D. F.; Konoplya, O. Y. *Ukr. Khim. Zh. (Russ. Ed.)* **1976**, (42), 374-378.

Chapter 3. Synthesis and characterization of oligo- and poly(thiophene carboxamide)s

3.1. Introduction

In the late 1970s, conjugated polymers were first discovered and proclaimed as a new class of materials leading to a new generation of electronic and optical devices. Nowadays, for example, the discovery of polymer light emitting diodes (PLEDs) and organic transistors that new technology is eminent.[1,2]

Poly(thiophene)s play an important role in the class of conjugated polymers, because they form some of the most environmentally and thermally stable materials. Taking this into account, they can be used as electrical conductors, non-linear optical devices, polymer LEDs, transistors, batteries, nanoswitches, nanoelectronic-, optical-, memory-devices, solar cells, electrochromic and smart windows, photo resists, antistatic coatings, sensors, nanoswitches, imaging materials, optical modulators and valves.[3,4] Modifications of the parent compounds, giving rise to new molecular designs and development strategies for new poly(thiophene)s, have lead to an increasing performance in certain devices.

Since the structure plays a dominant role in determining the physical properties of conducting polymers, more research has been focused on directing the structure and functionalization of these materials. Synthesis permits the variation of the π-overlap along the backbone and eliminate structural defects (Figure 3.1),[5] whereas materials assembly and processing determines interchain overlap and dimensionality. For examples, planarization and π-π stacking along the backbone lead to improved materials and device performance in almost every perspective ranging from stability to electrical conductivity.

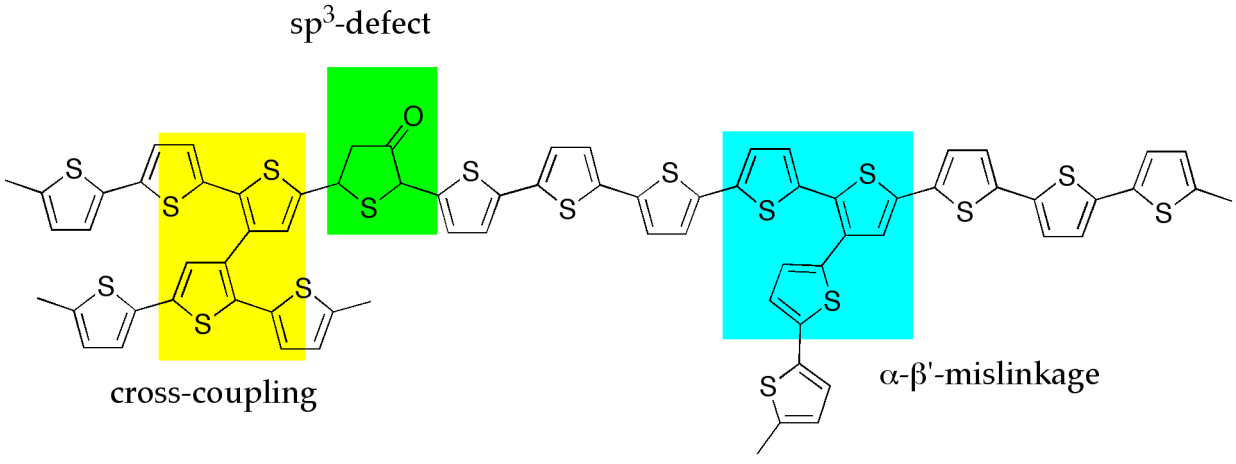

Figure 3.1: Defect structures of poly(thiophene).

Even though the polymer properties can be influenced and modified by alteration of the monomer building blocks, precise predictions concerning the structure-property relationships are not possible; the physical properties of the poly(thiophene)s cannot be

directly associated to there structure which are depending on the used synthetic pathways. Statistical variations in chain lengths, disruption of the conjugated chain by mislinkages and other defects, which are typical for all polymers, makes it impossible to achieve a direct structure-property relationship. Thus creating a library of well-defined, monodisperse oligo(thiophene)s is important to understand those relationships and to gain insight into the structural and electronic properties of the corresponding polymers. Using well-understood organic reactions as well as mono- and oligomers, a step-by-step synthesis can build up those needed well-define structures, where the conjugation length is well controlled and strictly defined.[6] Besides the usage of defined structures as model compounds, they also serve as building blocks in molecular electronics[7-10] and optical devices.[11] Due to their well-defined structure they even surpassed the properties of the polymers.

Since the backbone system of the poly- and oligo(thiophene)s **(3.1)** is fixed due to its conjugation, the only variation is possible at the three and four position of the thiophene rings. Introducing side-chains will adept and trigger properties. By including the structural amid bond from the oligo-(*p*-benzamide)s (OPBAs) **(3.2)** into the poly- and oligo(thiophene)s a new class of photoactive and conjugated oligo- and polymer **(3.3)** is created (Figure 3.2): the poly(thiophene carboxamide). The added hydrogen bond acceptor and donor will help the self-aggregation process, and still keeps the conjugated system in tact.

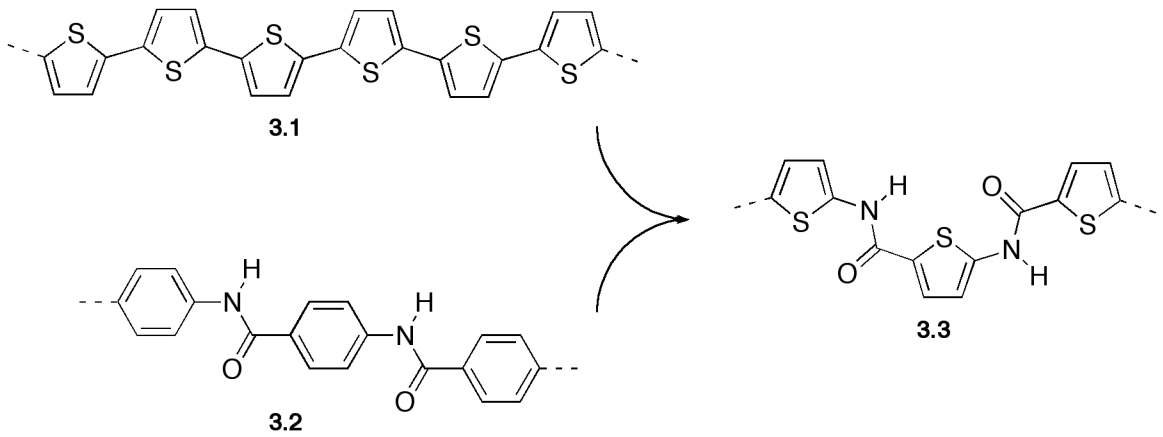

Figure 3.2: Mixing of oligo-(*p*-benzamide) and poly(thiophene): poly(thiophene carboxamide).

3.1.1. Poly(thiophene)s: Synthesis

3.1.1.1. Chemical synthesis of unsubstituted poly(thiophene)s (PTs)

Unsubstituted poly(thiophene)s can be easily synthesized by a variety of different reactions. The first polycondensation reactions where published by two groups: The Yamamato group[12] and the group of Lin and Dudek.[13] They both used a metal catalyzed polycondensation reaction with 2,5-dibromothiophene **(3.4)**. Yamamoto et al. first treated the starting compound with Magnesium to get 2-bromo-5-magnesiobromothiophene which is then self coupled with a Ni(2,2′-bipyridene)Cl_2 (bipy = 2,2′-bipyridine) catalyst (Figure 3.3 a) (*Kumada* cross coupling reaction). Lin and Dudek found similar results beginning from the same *Grignard* compound (2-bromo-5-magnesiobromothiophene) by using different metal catalysts: Pd(acetylacetonate)$_2$, Ni(acac)$_2$, Co(acac)$_2$ or Fe(acac)$_3$ (acac = acetylacetonate) (Figure 3.3 b).

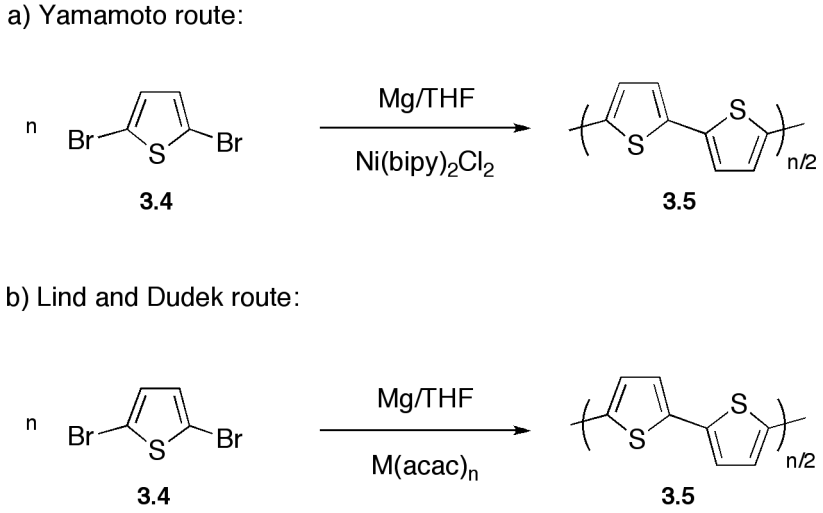

Figure 3.3: First polycondensations to obtain poly(thiophene): a) Yamamoto route,[12] b) Lin and Dudek route.[13]

Instead of using Ni(bipy)Cl_2, a different Ni(II) catalyst has also been used and extensively studied: Ni(1,3-bis(diphenylphosphino)propane)Cl_2 (dppp = 1,3-bis(diphenylphosphino)propane) (Figure 3.4).[14-21]

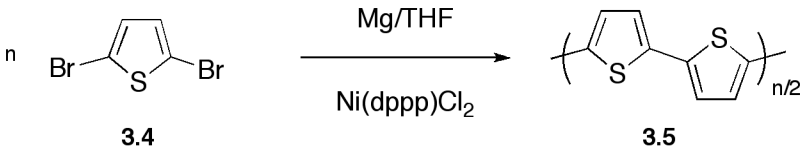

Figure 3.4: Polycondensation of 2,5-dibromothiophene using Ni(dppp)Cl_2.

Polymerization reactions can be achieved by treating the generated bromo-*Grignard*-species of thiophene with a nickel (II) catalyst like Ni(dppp)Cl_2 or the 2,5-dihalothiophene **(3.4)** can directly be polymerized by a dehalogenation reaction with nickel(0)-species such as Ni(cod)$_2$ (Figure 3.5).[16]

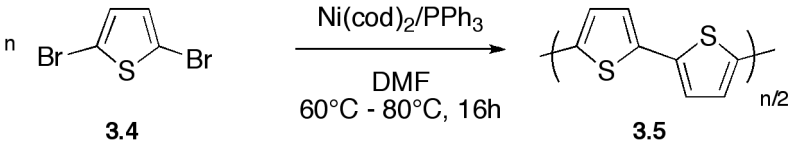

3.4 **3.5**

Figure 3.5: Dehalogenation polymerization with Ni(cod)$_2$.

Even though the above methods have been generally used to prepare poly(thiophene) in high quality, other methods have been reported: The first acid (sulfuric acid) induced polymerization was reported in 1883 by V. Meyer,[22] but produced tetrahydrothiophene units (defects shown in Figure 3.1). In 1989 Julia et al. showed a polymerization of thiophene using trifluoroacetic acid in the presence of thallium (III) trifluoroacetate.[23] Treating thiophene with butyl lithium gives 2,5-dilithiothiophene which can be polymerized with $CuCl_2$.[24] Sugimoto reported the synthesis of poly(thiophene) **(3.5)** by treating thiophene **(3.6)** with $FeCl_3$ in chloroform (Figure 3.6).[25]

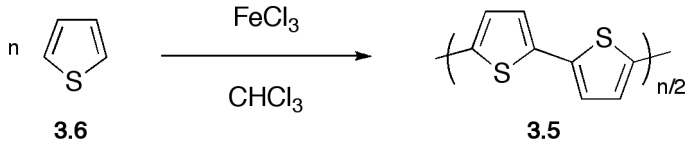

3.6 **3.5**

Figure 3.6: Polymerization of thiophene by Sugimoto and Yoshino.[25]

The poor solubility of those unsubstituted poly(thiophene)s made it nearly impossible to gain polymers with a molecular weight above 3000 g/mol.[16]

3.1.1.2. Chemical synthesis of regioirregular poly(alkylthiophene)s (PATs)

In order to increase the poor solubility of PTs, substituted thiophenes have been used, where as in most of the cases an alkyl chain in the β-position was introduced. In 1985 Elsenbaumer reported the first chemical synthesis of an environmentally stable and soluble poly(alkylthiophene) (PAT).[26-28] PATs, where the alkyl chains are longer than butyl, can be solution- or melt-processed into films. After oxidation, those films show high electrical conductivity in the rage of 1-5 S cm^{-1} due to the doping effect of partially oxidized poly(thiophene).[25-30]

The first synthesis of PATs where similar to those of unsubstituted poly(thiophene)s. Elsenbaumer prepared them via *Kumada* cross-coupling (Figure 3.7 a).[26-28] 2,5-Diiodo-3-alkylthiophene **(3.7)** is treated with one equivalent of magnesium in THF in order to generate a mixture of *Grignard* species. The halo-*Grignard* coupling reaction is then started by adding a catalytic amount of $Ni(dppp)Cl_2$ to obtain the polymer. First reports showed that the polymers have only low molecular weight (M_n = 3-8K, PDI=2), but later S.A. Chen et al. reported higher molecular weights by improving the reaction conditions.[31] ^{1}H-NMR of those polymers showed only 2,5-linkages and random regioselectivity. Homopolymers where the side chains equal to butyl or greater are soluble in common organic solvents like THF, chloroform, toluene etc. From any of those solvents thin films of PATs can be casted. Yoshino and Sugimoto also applied their route to PATs (Figure 3.7 b). 3-Alkylthiophene **(3.9)** is dissolved in chloroform and $FeCl_3$ is than added, which gives PAT by an oxidative polymerization. Those prepared polymers show molecular weights of M_n = 30-300 kg/mol with polydispersities ranging from 1.3 to 5.[32,33] This method does not appear to create 2,4-couplings.

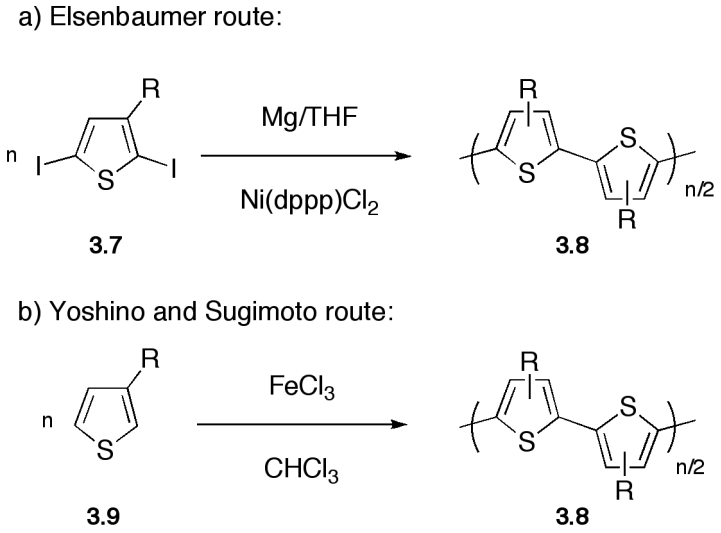

Figure 3.7: Synthesis of poly(alkylthiophene): a) Elsenbaumer route, b) Yoshino and Sugimoto route.

In analogy to the syntheses of PT, the alkylthiophenes can be polymerized using $Ni(cod)_2$ in DMF (Figure 3.8), however higher reaction temperatures and longer reactions times are necessary. Diiodoalkylthiophenes are found to be more active monomers than the corresponding dibromo derivates. This organometallic coupling polymerization proceeds with predominantly 5- 5'-types (head-to-head, HH) of combination, resulting in a polymer with mainly head-to-head and tail-to-tail (2-2', TT) couplings (Figure 3.9).[16] An explanation for that fact is the selective oxidation addition of nickel to the less sterically hindered 5-position on the alkylthiophene, which is furthest away from the bulky alkyl group. The

molecular masses of those polymers have been reported to be $M_n = 7.4\ kg/mol$, $M_w = 30\ kg/mol$, PDI = 4 (light scattering).

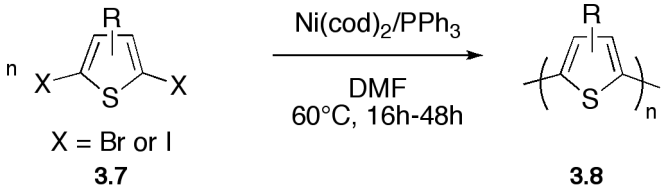

Figure 3.8: Synthesis of PATs using $Ni(cod)_2$.

3.1.1.3. Chemical synthesis of regioregular poly(3-alkylthiophene)s (P3ATs)

While the above-mentioned methods lack the regiochemical control over head-to-tail (HT) couplings between two alkylthiophenes, different synthetic strategies have been developed to overcome this disadvantage. Having a closer look at the possible relative coupling reactions (head-to-head (HH); tail-to-tail (TT) and head-to-tail (HT); Figure 3.9) one can recognize that four chemical distinct triad regioisomers are employed when 3-alkylthiophene are used (Figure 3.10).[34,35]

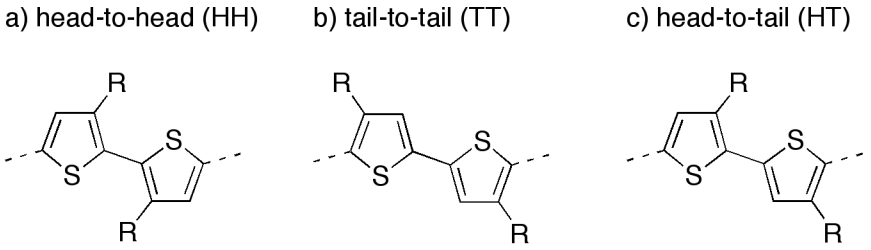

Figure 3.9: Coupling possibilities between two alkylthiophenes: a) head-to-head, b) tail-to-tail and c) head-to-tail.

These structurally irregular polymers have disadvantages compared to the favored HT-P3AT. Head-to-head coupled polymers, for example, are twisted because of the sterically hindrance of both alkyl chains, leading to an interruption of the conjugated system. In contrast to that, pure head-to-tail (HT) poly(3-alkylthiophene) can easily access a low energy planar conformation, which lead to a highly conjugated polymer. By increasing the torsion angle between two thiophene rings, the band gab grows, which consequent destructs the high conductivity.

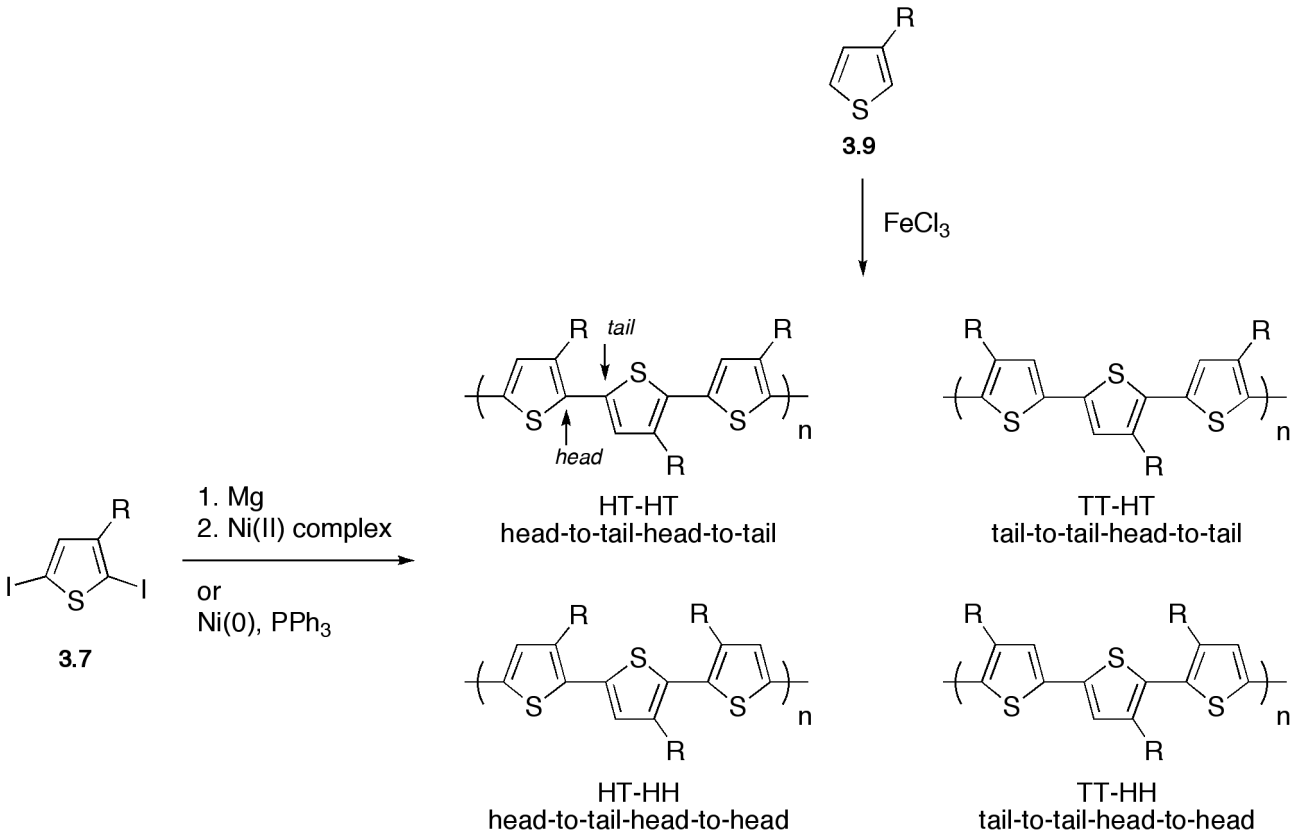

Figure 3.10: Possible triad regioisomers of poly(alkylthiophene).[36]

Elsenbaumer et al. showed in 1987 the importance of pure HT couplings. He used a 3-butylthiophene-3'-methylthiphene dimer and polymerized it to get a 63:37 mixture of HT:HH couplings, leading to a threefold increase in electrical conductivity compared to a random copolymerization of 3-butylthiophene and 3-methylthiophene (50:50).[37] Consequently, an increase in HT coupling leads to a higher conducting P3AT.

McCullough published the first regioregular head-to-tail coupled poly(3-alkylthiophene)s in 1992.[38] The so synthesized P3ATs contain nearly 100% HT-HT couplings. The first step is to synthesis 2-bromo-3-alkylthiophene **(3.11)**, before 2-bromo-5-(bromomagnesio)-3-alkylthiophene is generated by treating **3.11** with lithium diisopropylamide (LDA) and $MgBr_2$. The polymerization is then induced by adding a catalytic amount of $Ni(dppp)Cl_2$ using *Kumada* cross-coupling methods (Figure 3.11).[39-42] This way P3ATs can be synthesized in a one-port, multistep synthesis with yields between 44% and 69%. The key step is the selective metallation with LDA.[43,44] That compound is stable at -78 °C and does not undergo any metal exchange reactions. In addition, thienyl lithium structures are poor organo lithium reagents and therefore do not undergo metal-halogen exchange reactions with 2-bromo-3-alkylthiophene. This intermediate is reacted

with $MgBr_2 \bullet Et_2O$ to obtain 2-bromo-5-(bromomagnesio)-3-alkylthiophene, which is even stable at elevated temperatures, and can than be polymerized with $Ni(dppp)Cl_2$.

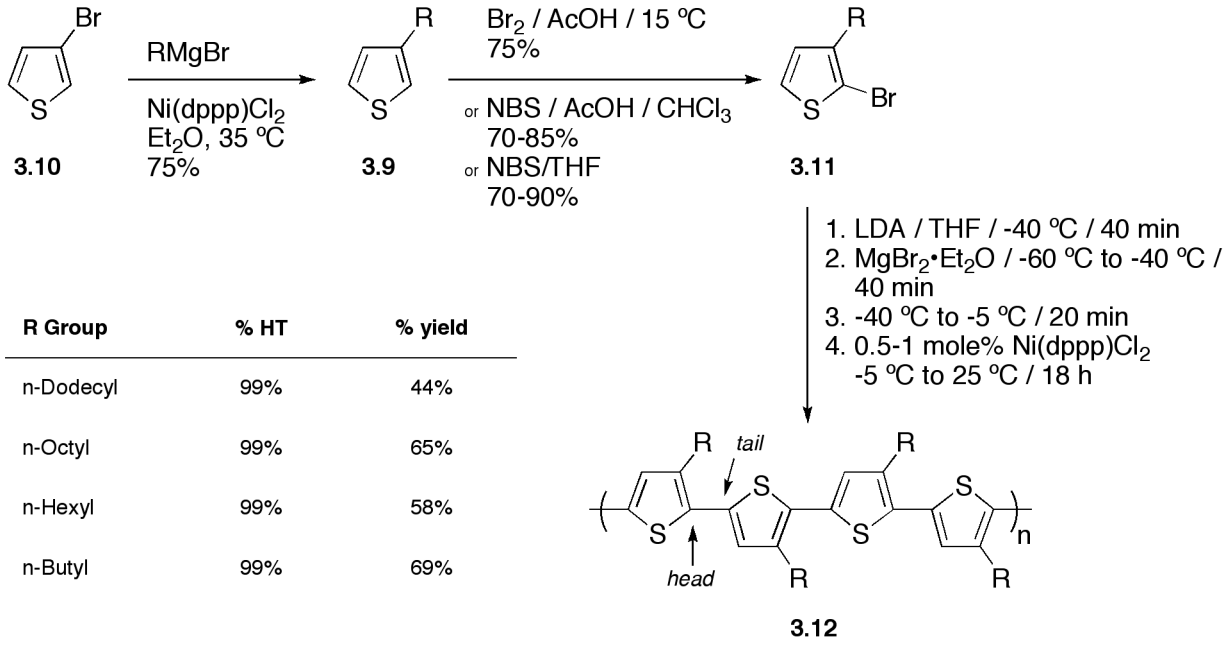

R Group	% HT	% yield
n-Dodecyl	99%	44%
n-Octyl	99%	65%
n-Hexyl	99%	58%
n-Butyl	99%	69%

Figure 3.11: McCullough method for regioregular synthesis of PATs with 100% HT couplings.

Some years later, McCullough et al. adopted the method.[45,46] He started from 2,5-dibromo-3-alkylthiophene **(3.13)** and applied a *Grignard* reagent solution. By *Grignard metathesis* (GRIM) they received a mixture of 2-(bromomagnesio)-5-bromo-3-alkylthiophene **(3.14a)** and 2-bromo-5-(bromomagnesio)-3-alkylthiophene **(3.14b)** (Figure 3.12 a). This mixture can then be readily polymerized with $Ni(dppp)Cl_2$ to yield analytically pure and highly regioregular PATs **(3.12)**. Since this reaction can be done at room temperature or in refluxing THF, no cryogenic setup is needed. By applying the GRIM-method the reaction setup and polymerizations are easy, quick and cost effective (no cryogenic conditions, cheaper materials). Further investigations on the reaction revealed a much faster reaction to form TT- and HT-Dimers, compared to HH- and HT-Dimers (Figure 3.12 b). Interestingly the formation of HT-Dimers can be observed with two different reaction speeds, depending on which side the *Grignard*-species is formed (Figure 3.12 c).[45]

a)

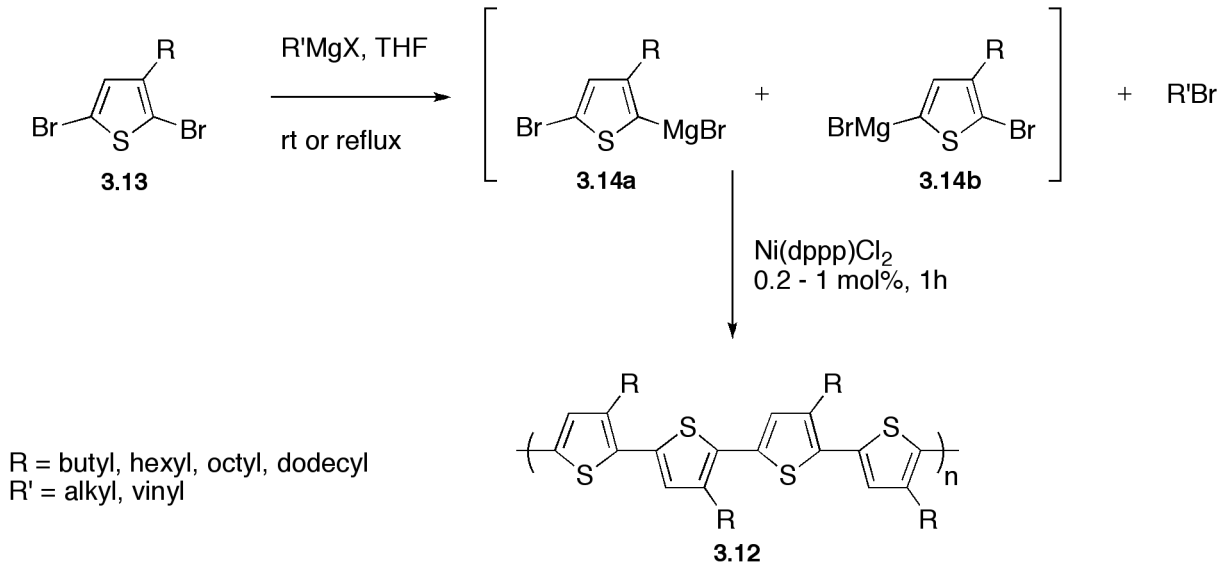

b)

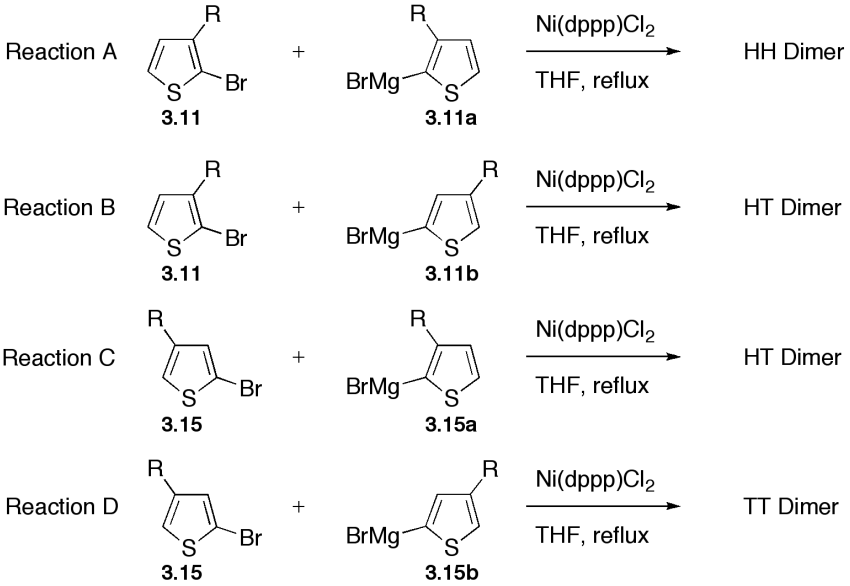

c)

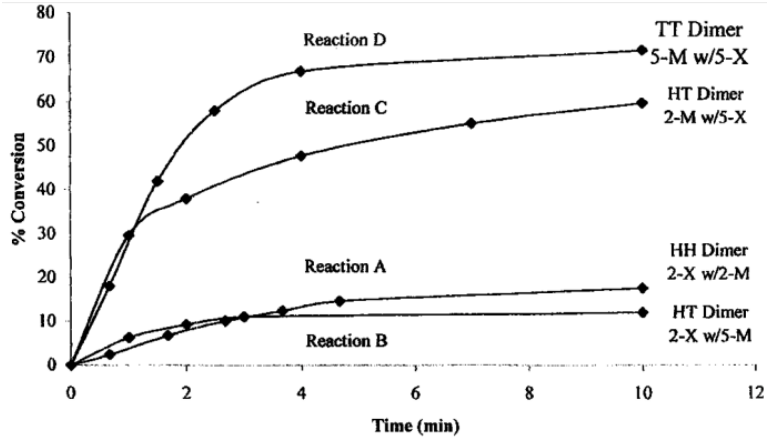

Figure 3.12: a) GRIM-Method to get HT-PATs by McCullough, b) four model reactions for dimer formation c) plot of percent dimer formation.[45]

A closer look at the mechanism revealed a chain growth polymerization, leading to molecular masses of M_n = 5.6 – 11.2 kg/mol with a low polydispersity index of 1.2 to 1.4.[47,48] The polymerization starts with an oxidative addition of the Ni(dppp)Cl_2 complex to two thiophene monomers under elimination of two MgBrCl. The first coupling of two thiophenes takes place afterwards leaving an associated pair of Ni(0)(dppp) **(3.17)** and a tail-to-tail coupled thiophene dimer **(3.18;** n=1**)** . After oxidative addition of the nickel (0) catalyst into the bromine-thiophene-dimer bond and substitution of the bromine through a new monomer, a new reductive elimination occurs, leaving a new associated pair **(3.18;** n=2**)**, now with a ternary thiophene structure with each one HT- and TT-coupling. The polymerization now takes place with repetition of oxidative additions followed by reductive eliminations (Figure 3.13).

In situ end-group functionalization is now possible by adding a new *Grignard*-compound to the reaction mixture when the monomer is consumed. Figure 3.14 demonstrated the termination step using vinyl-magnesium-bromide. The drawback of that termination procedure is the possibility of di-capped polymers, since both ends carry bromine. Vinyl-, allyl-, and ethnyl-magnesium compounds result in a very high mono-capped yield. The reason for that might be the addition of the nickel(0) complex to the double or triple bond, consequently it is impossible for the catalyst to react at the second end of the polymer.[48,49] Table 3.1 shows different end-capping reagents and the ratio between mono- and di-capped polymers.

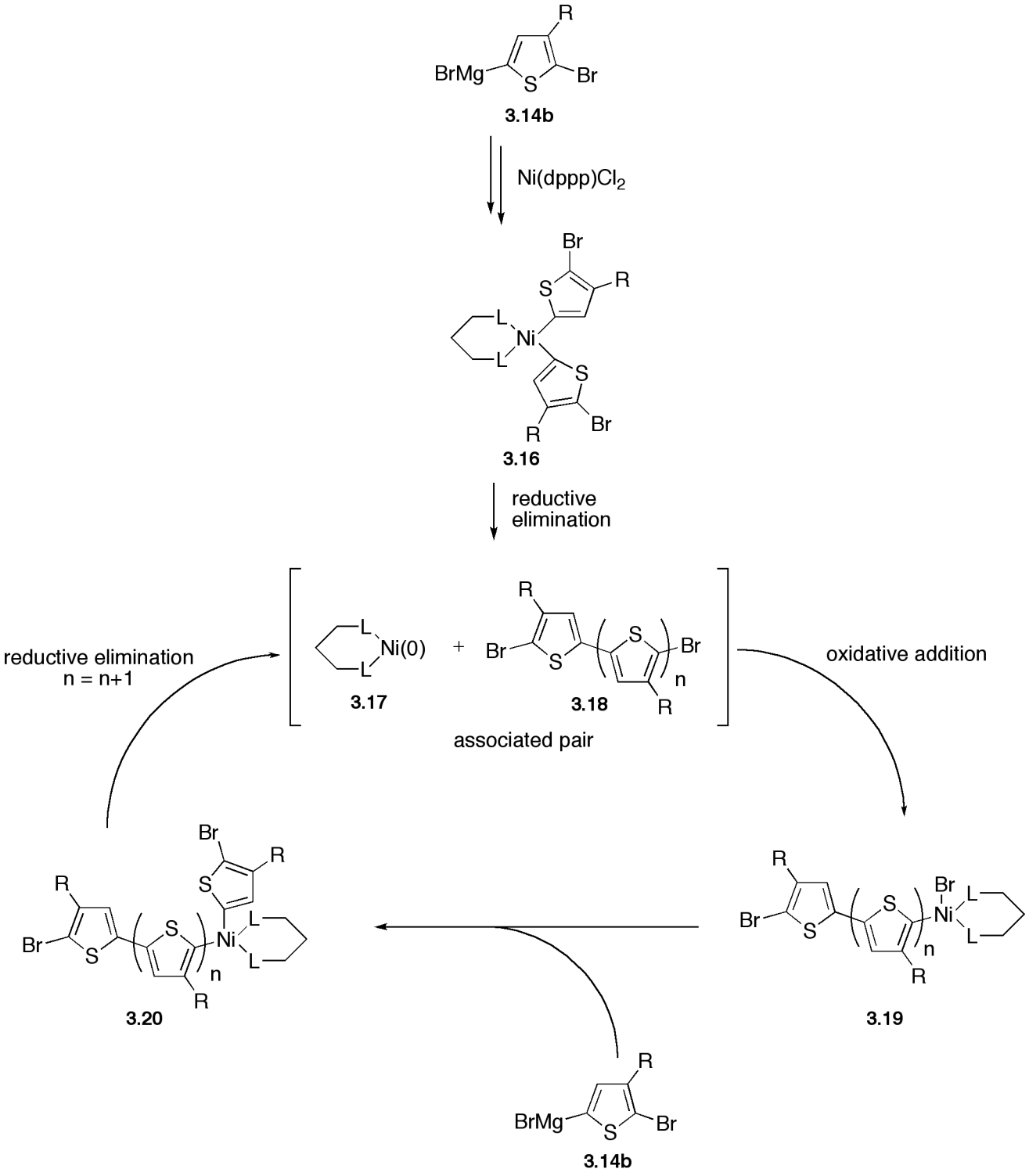

Figure 3.13: Proposed mechanism for the nickel-initiated cross-coupling polymerization.

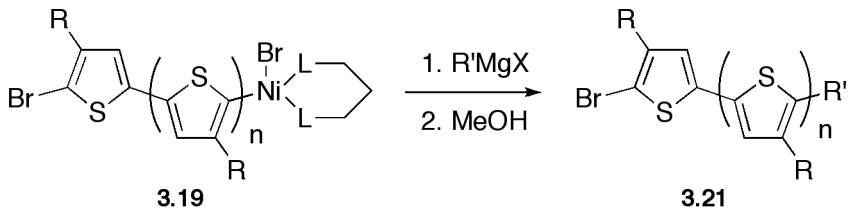

Figure 3.14: Mono-capping of the growing polymer chain using R'MgX.

Table 3.1: End-Capping reagents[48]

Grignard reagent	End group	Di-capped[a]	Mono-capped[a]
VinylMgBr		0%	91%
AllylMgBr	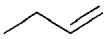	0%	87%
EthnylMgBr		14%	86%
PhenylMgBr	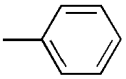	76%	24%
TolylMgBr	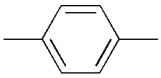	80%	20%
BenzylMgBr	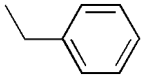	80%	20%
p-OTHP-PhenylMgBr[b]	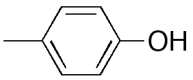	75%	12%
MethylMgBr		76%	24%
ButylMgBr		67%	21%
tert-Butyl-MgBr		no reaction	

[a]Where the sum is not equal to 100%, the remaining polymer is uncapped. [b]THP = tetrahydropyranyl

Chen and Rieke published a similar approach to that of McCullough (Figure 3.15).[50-54] The primary difference is the synthesis of the asymmetric organometallic intermediate. 2,5-dibromo-3-alkylthiophene **(3.13)** is treated with "*Rieke-Zinc*" (a highly reactive Zinc; Zn*), which reacts quantitatively to a mixture of isomers, namely 2-(bromozincio)-5-bromo-3-alkylthiophene **(3.14c)** and 2-bromo-5-(bromozincio)-3-alkylthiophene **(3.14d)**, where as the ratio between both is mostly dependent on the temperature and less on the steric influence of the alkyl chain. Adding $Pd(PPh_3)_4$ as a metal cross-coupling catalyst results in a completely regiorandom PAT **(3.8)**. In contrast to that, adding $Ni(dppe)Cl_2$ (dppe = 1,2-bis(diphenylphosphino)ethane), as a more bulky catalyst, only regioregular HT-P3AT **(3.12)** is synthesized. Instead of using the dibromo compound, 2-bromo-3-alkyl-5-iodothiophene **(3.22)**, will only result in one product: 2-bromo-3-alkyl-5-(iodozincio)thiophene **(3.23)**. However the polymerization result are similar to that of **3.12**. Depending on the choice of catalyst, regioregular HT-P3AT or regiorandom PAT is synthesized. Polymers prepared by the *Rieke*-method typically have a molecular weight of $M_n = 24 - 34$ kg/mol with a PDI of 1.4. The advantage of the *Rieke*-method compared to the *McCullough*-method is that the *Rieke-Zinc* affords a functional group tolerant synthesis. Both methods are applicable to thiophenes implying a tolerance towards organo lithium, *Grignard* reagents or zinc reagents. Polymers synthesized in both ways are comparable materials and show no distinct spectroscopy difference.

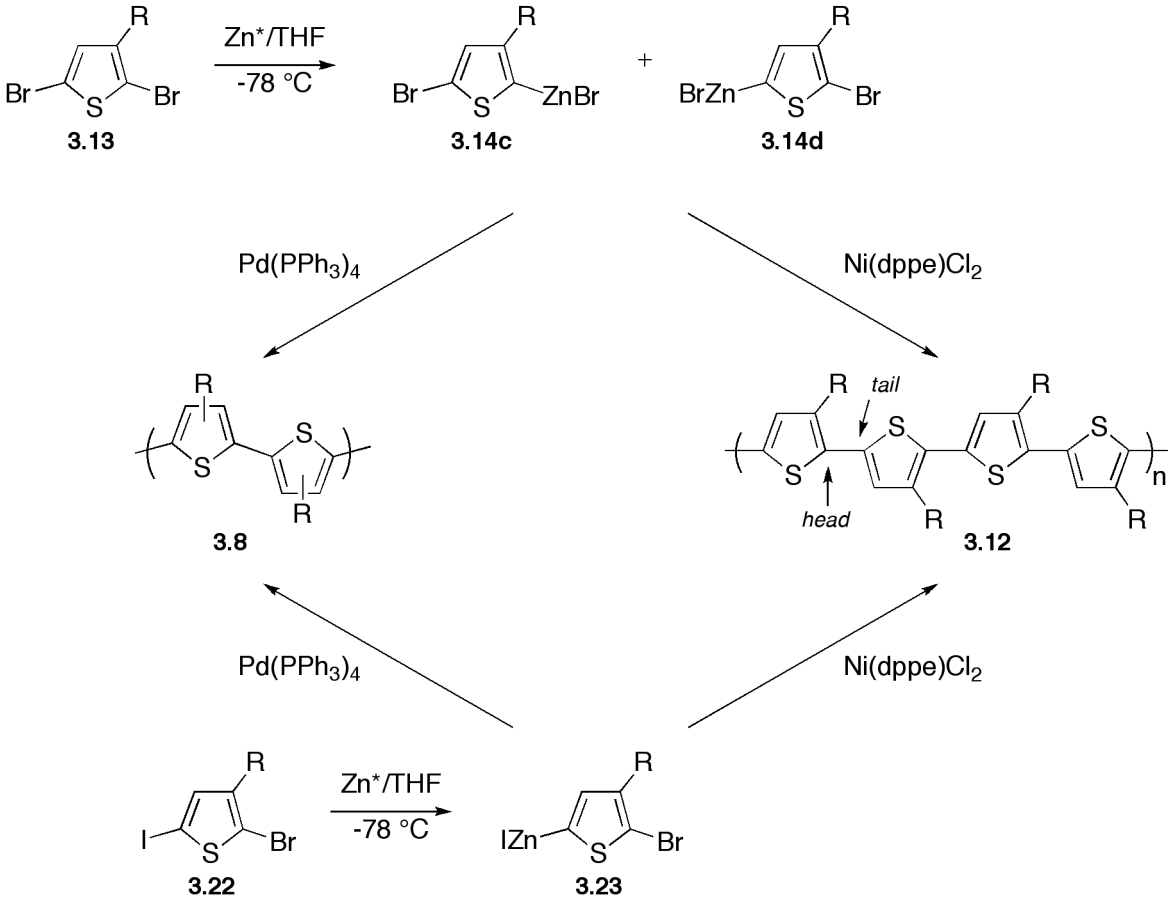

Figure 3.15: HT-PATs synthesized by the Rieke method.

3.1.2. Poly(thiophene): Properties

3.1.2.1. NMR-Characterization of HT-PAT

Because of the good solubility in common organic solvents of poly(3-alkylthiophenes) ^{1}H- and ^{13}C-NMR characterization is possible. Due to the fact that those PATs have only one aromatic proton, assignments of the different proton shifts in different triads are feasible.[26,27,32,34,35,38,50,55-59] Barbarella and co-workers synthesized the four possible triads (HT-HT, TT-HT, HT-HH and TT-HH) and assigned the four different signals to the four corresponding triads (Table 3.2).[58] A relative integration of the HT-HT peak compared to the other non-HT peaks, results in a quantitative amount of HT-HT couplings. Looking at the NMR data of regioregular PATs, these polymers contain ≈100% HT-HT couplings. Polymers prepared by the $FeCl_3$-method have 50-70% HT-HT couplings, in general.[38,57]

Table 3.2: Relative chemical shifts of triads.[36]

Configuration	Structure	Chemical shift δ / ppm
HT-HT	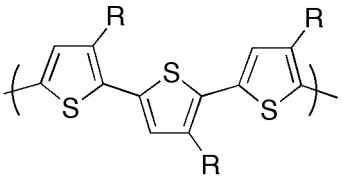	6.98
TT-HT	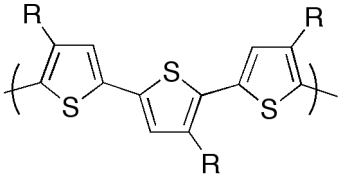	7.00
HT-HH	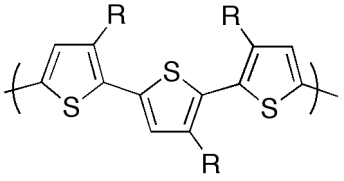	7.02
TT-HH	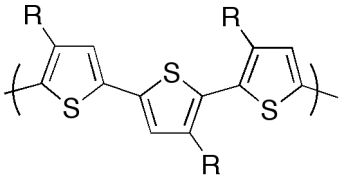	7.05

Using MALDI-ToF-MS and NMR characterization, end groups of HT-PATs have also been characterized.[53,60]

^{13}C-NMR characterization leads to the same apparent structural regularity information: only four resonances are visible in the aromatic region. Those four signals (e.g. poly(hexyl thiophene) (PHT), δ = 128.5, 130.5, 134.0 and 140.0 ppm) can be clearly assigned to the four protons of HT-PAT, whereas regioirregular PHT lack the resonances in the region from 125-144 ppm.[36]

3.1.2.2. IR and UV/vis

Measurements of the conjugation lengths can be both done by IR and UV/vis spectroscopy. If the conjugation length increases, the intensity ratio of the asymmetric band at 1510 cm^{-1} C=C ring stretches to the symmetric IR band at 1460 cm^{-1} increases, too. For regiorandom PATs this ratio is about 15-20, where as the value for regioregular HT-PATs is 6-9, only around half of that for irregular PATs.[53]

A more detailed look into the conjugation length can be observed with the help of UV-Vis spectroscopy. A read shift of the maximum absorption is observed for the increase

of conjugation length, thus meaning the π-π* transition is an indicator for the conjugation length. Comparing regioirregular PATs with regioregular HT-P3ATs a red shift is observed for the HT-PATs.[38,50,53,57,59,61] Table 3.3 shows the different λ_{max} values for different PATs in solution.

Table 3.3: Red shift λ_{max} for PATs in solution.

3-substituent	λ_{max} / nm (in solution)			
	Random[62] 50% HT	$FeCl_3$[63] 70% HT	Rieke[62] 98-99% HT	McCullough[63] 98%-99% HT
butyl	428	436	449	450
hexyl	428	436	456	442
octyl	428	436	451	446
dodecyl	428	436	453	460

Solid state UV/vis of regioirregular PAT revealed little structure and broad π-π* transition, where as HT-P3AT may show a fine structure beginning from shoulders to define peaks, which is depending on the thickness of the film and the processing conditions. Another difference between regioirregular and regioregular PAT is that the HT-PAT is red-shifted compared to the regioirregular PAT. The λ_{max} absorption is depending on the film thickness: thicker films show a maximum at 530 nm whereas thinner films have their absorption maximum around 562 nm.[36]

3.1.2.3. Self assembly to supramolecular structures

One major difference between regioirregular PAT and regioregular HT-P3ATs is the behavior in self-assembly. Whereas regioirregular PAT does not show any distinct supramolecular ordering, HT-P3AT clearly self assembles into well defines superstructures. Those phenomena where first discovered by McCullough.[61,64-66] A variety of analytical methods like solution light scattering[67] and X-ray[57,68] on thin films, shows the macromolecular self-assembly of those polymers (Figure 3.16).[69]

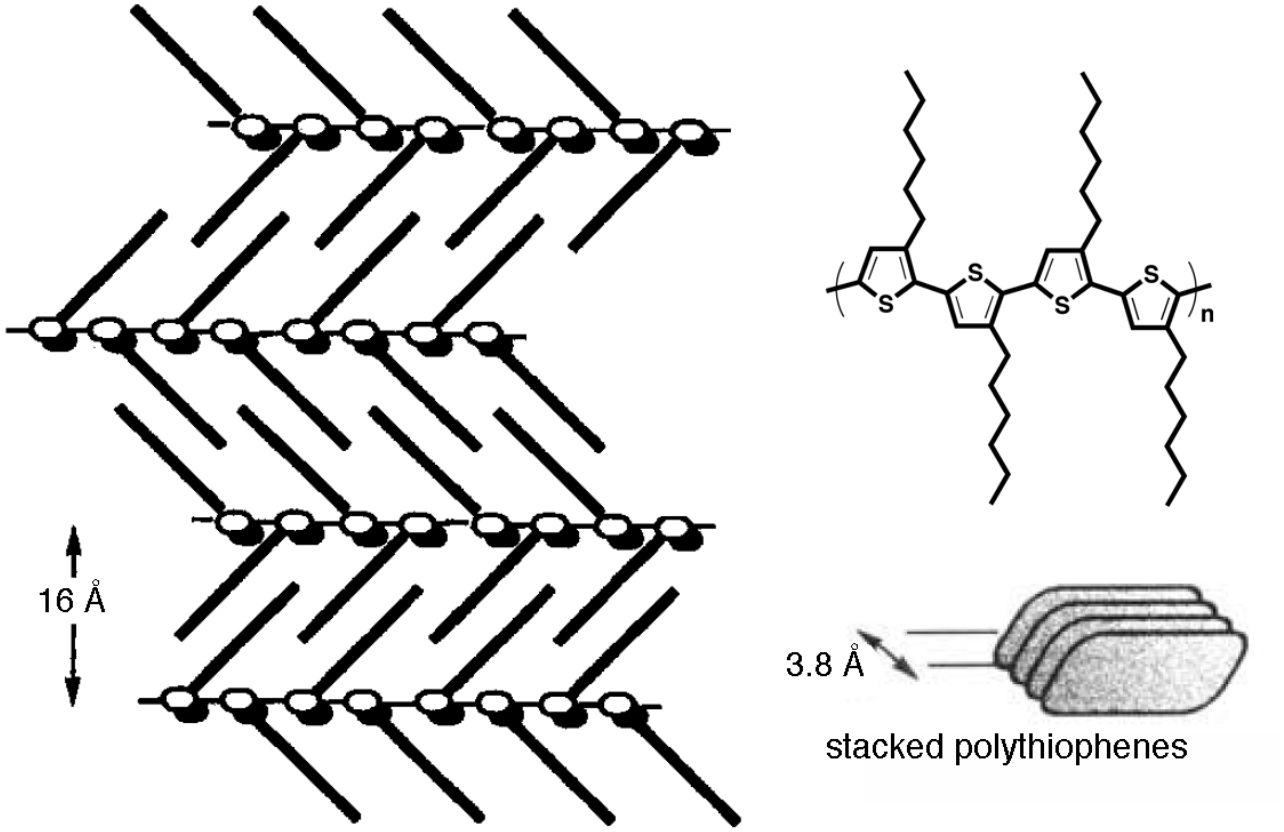

Figure 3.16: Suprastructure of self-assembled conducting regioregular HT-PAT.[36]

Self-assembled structures of HT-P3AT show a large increase in electrical conductivity relative to irregular PATs, while the measured conductivities of HT-P3AT vary from 100 to 2000 S/cm[38,51,53,57,61] regioirregular PATs only show have a conductivity around 0.1 to 20 S/cm.[36]

3.1.3. Oligo(thiophene)s: Synthesis

The first mono-disperse and well-defined oligo(thiophene)s have already been synthesized in the late 1930s by Steinkopf.[70] By applying *Ullmann's* biaryl synthesis using 2-iodothiophene **(3.24)** and copper-bronze the hole series beginning from α-bithiophene to the α-septithiophene could be obtained in very small amounts (Figure 3.17). By characterization the different oligomers with their melting point, absorption maxima and the qualitative assessments of fluorescence the first correlation between their structures and properties were done.

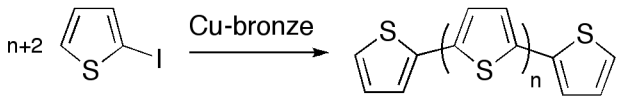

3.24 **3.25**

Figure 3.17: Oligo(thiophene)-synthesis by Steinkopf in the 1930s.[70]

In the late 1980s, 60 years later, those structures are very important for organic light emitting devices,[71] and therefore new way of synthesis, a more detailed characterization and new structures based on oligo(thiophene)s are more important than ever. In 1960, Gronowith et al. published a new synthetic way to α-bithiophene using lithiated thiophene **(3.26)** coupling those with $CuCl_2$ (Figure 3.18).[72] This synthetic breakthrough gave rise to a vast amount of synthetic work.[43,44,73] Looking at the poly(thiophene) systems it is easy understandable that those defined oligomers gain high importance as models for the polymers. The use of α-sexithiophene use in *all*-organic electronic devices has started a new beginning of interest and intensive research work around oligo(thiophene)s, their structures and properties.

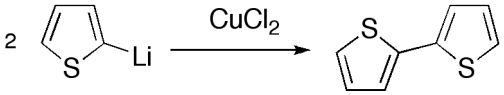

3.26 **3.27**

Figure 3.18: Synthesis of α-bithiophene by Gronowitz.[72]

Unsubstituted oligo(thiophene)s exhibit the same solubility problems than their polydisperse and longer matches, thus making it nearly impossible to synthesize longer oligomers. Synthetic approaches for unsubstituted oligo(thiophene)s are similar to those for substituted oligo(thiophene)s. Different coupling methods have been reported: arene/arene-coupling methods by oxidative coupling, transition metal catalyzed coupling method and ring closure reactions.

3.1.3.1. Arene/arene coupling methods

The oxidative coupling of lithiated thiophenes was first demonstrated by Gronowitz in 1960 (Figure 3.18).[72] This coupling method is more effective than the first used *Ullmann* coupling, thus leading to higher yields of the desired oligomers. Lithiating can be easy achieved by simple deprotonation or by metal-halogen exchange reaction. Adding one equivalent of buthyl lithium to thiophene and afterwards adding one equivalent of $CuCl_2$ lead to 54% yield, whereas adding two equivalents of $CuCl_2$ already lead to 85% yield,

demonstrating that the effect of the salt is more than catalytic.[74] But not only dimers can be synthesized using this methods, also higher oligomers can be synthesized (Figure 3.19 a).

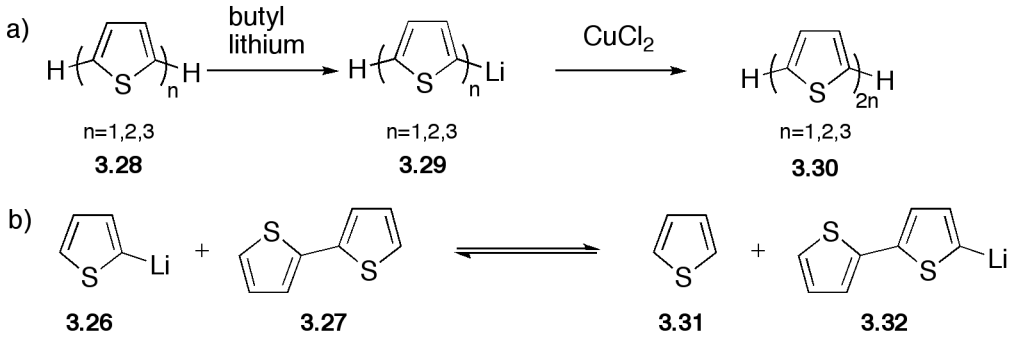

Figure 3.19: a) Synthesis of higher oligomers using $CuCl_2$. b) Equilibrium between lithiated and non-lithiated thiophene/oligo(thiophene).

The drawback of that reaction is that equilibrium between the lithiated and non-lithiated thiophene respectively oligo(thiophene) (Figure 3.19 b). Experiments have shown that the lithiated bithiophene is more favorable than the lithiated thiophene. Consequently, α-protons of oligo(thiophene)s are more acidic compared to those of thiophene.[5] However, longer oligomers, like α-sexithiophene, are accessibly be coupling shorter ones, e.g. trimers to obtain the sexithiophene.[9,75] On the other hand, coupling two α-quarterthiophenes in order to obtain α-octithiophene is not possible.[5]

3.1.3.2. Transition metal catalyzed coupling methods

Besides the already mentioned *Ullmann* coupling, three more coupling reactions are widely used in the synthesis of well-defined oligo(thiophenes): *Kumada-*, *Stille-* and *Suzuki-*reaction. All four of them will be briefly described here.

Ullmann-reaction

Already being described early, the *Ullmann* reaction was the first coupling used to prepare oligo(thiophene)s (Figure 3.17).[70] However, improvements to the reaction conditions have been made (using DMF as solvent to avoid the formation of higher oligomers;[76] using copper acetate instead of copper;[77] using directly organocopper derivates[75,78]) the yields are still low and the tedious workup procedure to remove undesired side products made it necessary to use different reactions. Besides that fact, this reaction is still the best one to couple acceptor substituted with electron deficient arenes.[79]

Kumada-reaction

Being aware of the fact, that the *Ullmann* reaction only results in low yields (42% for the α-bithiophene)[79], it is a very expensive synthetic route to higher oligomers, due to the low yields and high costs for the copper catalyst. An advance in the synthesis of those oligomers was achieved, when very effective transition metal catalyzed cross coupling reactions were used. In 1972, the groups of Kumada[39] and Corriu[80] independently published the coupling of aryl and alkenyl C_{sp^2}-halides using phosphine-nickel complexes (Figure 3.20).

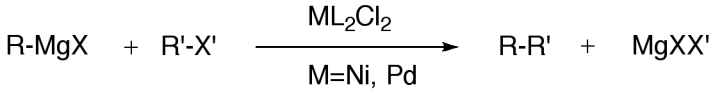

Figure 3.20: *Kumada* cross coupling reaction.

Later in the beginning of the 1980s, where conductive polymers already gained more interest, Kumada published cross-coupling reactions including heterocyclic compounds like pyridine and thiophene.[40] The easiness and high effectiveness of the *Kumada-reaction* made it to the most frequently used method for the preparation of oligo(thiophene)s.[41,81] Since this coupling method is the most important one its mechanism will be discussed briefly here. The mechanisms for all other transition metal catalyzed cross-coupling reactions are similar. Figure 3.22 shows the mechanism, which basically consists of five separated steps, on the example of *ethyl*- and *allyl*-groups.

1. NiL_2X_2 reacts with two equivalents of *Grignard* reagent to form NiL_2*(ethyl)*$_2$. During this step, the insoluble catalyst is dissolved.
2. In this step, *allyl*-halide reacts with NiL_2 *ethyl*$_2$ to form the actually active catalytic compound NiL_2*(allyl)*X′ and the homo-coupling compound *butane*.
3. The halogen X′ is now replaced with another organic group ethyl from one equivalent of *Grignard* reagent, thereby releasing MgXX′.
4. A second organic halide *allyl*-halide is taken up to form the fivefold coordinated intermediate NiL_2(···*(allyl)*X′)*(ethyl)(allyl)*R′.
5. During the last step *pent-1-en* is released from the catalytic center and the active species NiL_2*(allyl)*X′ is recycled.

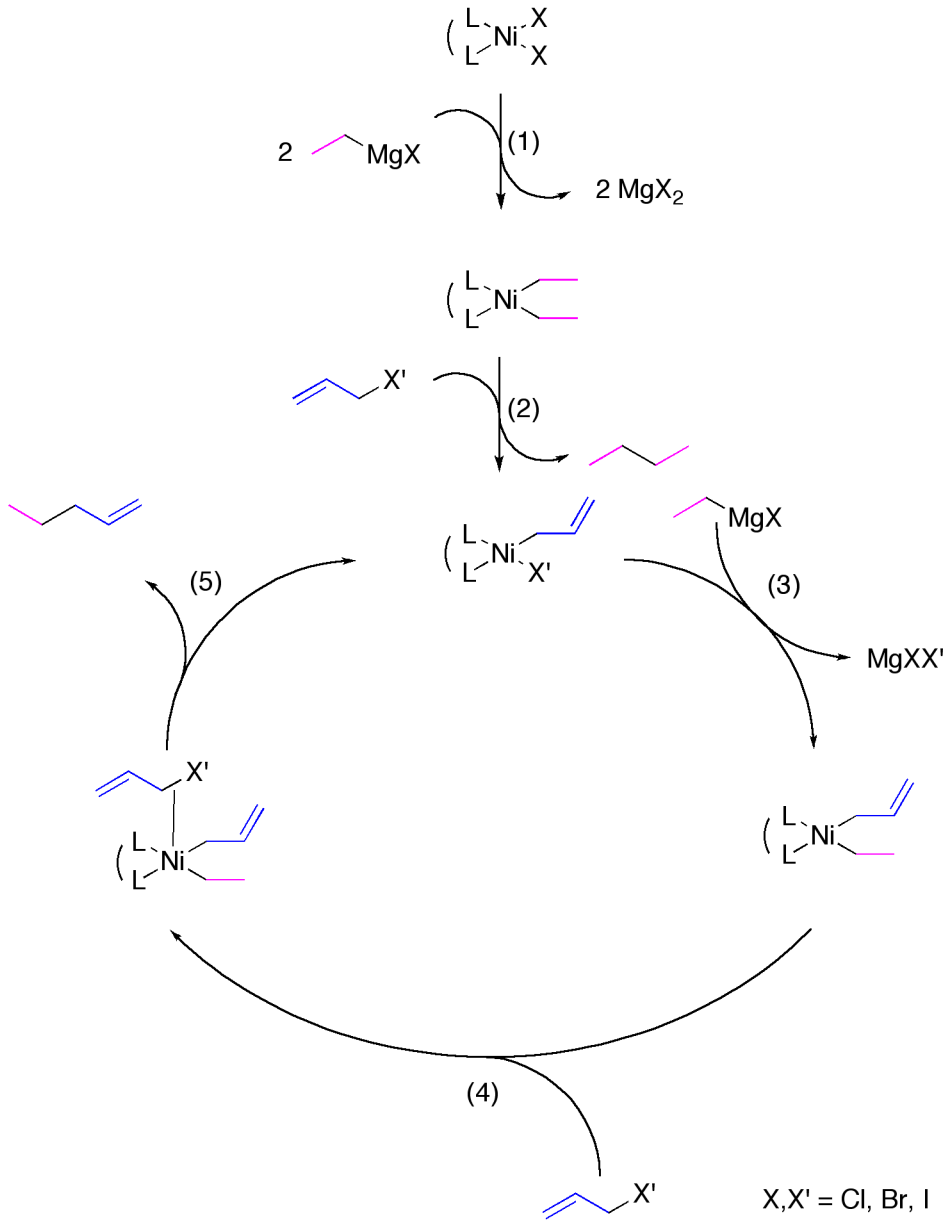

Figure 3.21: Mechanism of the *Kumada-reaction*.[5]

Figure 3.22 illustrates the synthesis of terthiophene using the *Kumada-reaction*. The 2-(bromomagnesio)-thiophene **(3.33)** can be readily synthesized by treating 2-bromothiophene with one equivalent magnesium or a different *Grignard* reagent (e.g. bromomagnesio-methane). By adding 2,5-dibromothiophene **(3.4)** and a nickel catalyst (e.g. Ni(dppp)Cl_2) to the freshly made *Grignard* compound terthiophene **(3.34)** is obtained in 80% yield.[82]

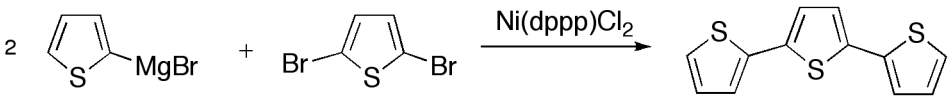

3.33 **3.4** **3.34**

Figure 3.22: Synthesis of terthiophene by *Kumada-reaction*.

Stille-reaction

A different coupling method is the *Stille-reaction*. Treating organotin compounds (R'-SnR''_3) and organic halides (R-X) with a palladium catalyst, the coupling occurs resulting in R-R' (Figure 3.23). The benefits of the *Stille-reaction* are the mild reaction conditions, the regioselectivity and the tolerance of many functional groups (e.g. NO_2, CHO, OH, CN, CO_2R). Generally aspects of the reaction are reviewed[62] and with respect to heterocyclic compounds the literature is summed up to 1991.[83]

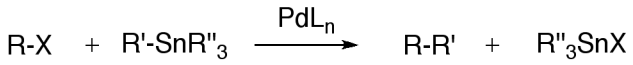

Figure 3.23: *Stille-reaction*.

The organotin compound can be easily synthesized from the lithiated thiophene and a trialkylstannyl chloride or by reaction of organic halides with hexaalkyldistanne.[84,85] As catalyst a large variety of palladium based complexes have been used (e.g. $Pd(PPh_3)_4$, $Pd(PPh_3)_2Cl_2$, $Pd(dppp)Cl_2$, Pd(1,1'-bis(diphenylphosphino)ferrocene)Cl_2, $Pd(OAc)_2$/ P(*o*-tolyl)$_3$, $Pd_2(dba)_3$) (dppf = 1,1'-bis(diphenylphosphino)ferrocene; dba = dibenzylidene-acetone). Since the mechanism is similar to that of the *Kumada-reaction* it will not be discussed in detail here, but can be looked up in ref [5]. This reaction has mostly been used substituted thiophenes, however Crisp describes the synthesis of α-bithiophene and α,α-terthiophene.[86] The terthiophene was synthesized by coupling 2,5-diiodothiophene **(3.36)** and tributyl(2-thienyl)tin **(3.35)** and $Pd(PPh_3)_2Cl_2$ as catalyst (Figure 3.24). The yields of the *Stille-reaction* are slightly lower (59% for the terthiophene)[87] compared to that of the product obtained by *Kumada-reaction* (80%).[82]

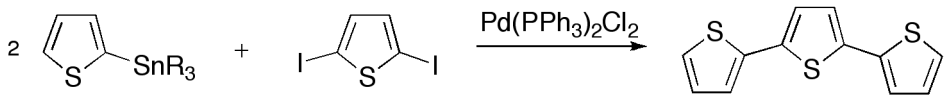

3.35 **3.36** **3.34**

Figure 3.24: Synthesis of terthiophene from Chrisp.[86]

Suzuki-reaction

Suzuki[88] and Miller[89] have both published a palladium-catalyzed cross coupling reaction of benzene boronic acid and various bromobenzenes. This coupling method is also useable in sterically demanding positions. Gronowitz et al. modified the *Suzuki-coupling* so that it became useful for heteroaromatic cycles.[90] Tolerating a large variety of function groups, like the *Stille-coupling* does, this method is mostly applied in substituted

oligo(thiophene) synthesis. The mechanism of the reaction is similar to that of the *Kumada-reaction* and will not be discussed in detail here. The starting material, thiophene boronic acid **(3.37)** , can be readily synthesized by reaction of lithiated thiophene **(3.26)** with boronic acid trimethylester. Treating this compound and 2,5-dibromothiophene **(3.4)** with a palladium catalyst, such as $Pd(PPh_3)_4$, the terthiophene **(3.34)** can be obtained in 40% yields (Figure 3.25).[5] This reaction even proceeds without any necessary precautions against oxygen, in a mixture of dimethyl ether (DME) and aqueous sodium bicarbonate.

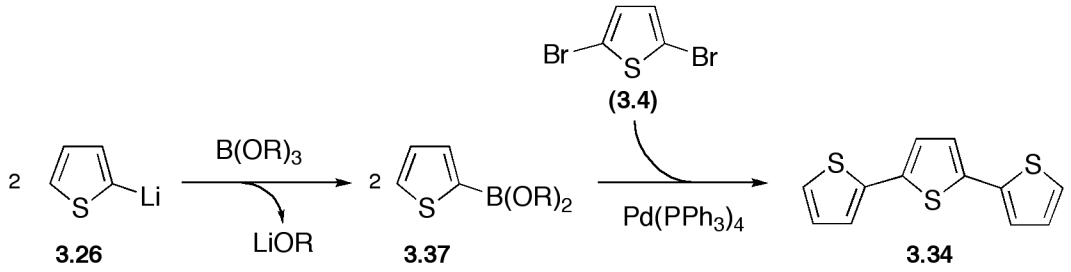

Figure 3.25: Synthesis of terthiophene via *Suzuki-coupling*.

Optimizing the reaction can be done, by adding a 20% excess of boronic acid compound in order to reduce mono coupling. Gronowitz observed deboronation as a side reaction if using electron rich heteroaromatics.[91]

3.1.4. Oligo(thiophene)s: Properties

3.1.4.1. Oxidation potentials

The oxidation potentials for unsubstituted oligo(thiophene)s have all been measured.[92] By increasing the chain length, the oxidation potential decreases (Table 3.4). This can be explained by the larger electronic system. The larger that system is, the easier it is to remove one electron from the backbone.

Table 3.4: Oxidation Potentials of unsubstituted oligo(thiophene)s.[5]

Oligo(thiophene)	Melting point / °C	Oxidation potentials[a] / V
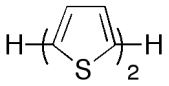	33	1.28
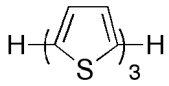	95-96	1.05
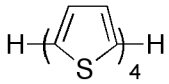	215-216	0.97
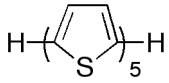	258-259	0.70
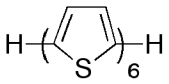	307-309	0.46
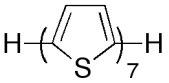	328	-

[a]Irreversible oxidation potentials, differential pulse voltammetry in $CH_3CN/TBABF_4$ vs. Ag/AgCl

3.1.4.2. Absorption and fluorescence spectra

Similar to the trend in the oxidation potential a trend is clearly visible in the absorbance and fluorescence data. With increasing chain length, both maxima are moved towards higher wavelengths. The explanation is the larger electronic system; the electrons are dispensed over the whole molecule. All oligo(thiophene)s, except the bithiophene, exhibits two fluorescence maxima (Table 3.5).

Table 3.5: Absorbance and fluorescence bands of unsubstituted oligo(thiophene)s.[5]

Oligo(thiophen)e	Absorption[a] λ_{max}/nm	Extinction coefficient[a] lg e	Fluorescence[b] λ_{max} / nm
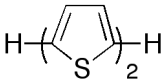	302	4.1	362
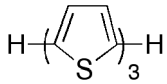	355	4.4	407, 426
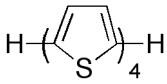	390	4.66	437, 478
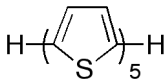	416	4.74	482, 514
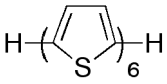	432	~4.78	510[d]
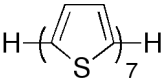	440[c]	-	522, 560

[a]Maximal absorbance and extinction coefficient in $CHCl_3$.[92] [b]fluorescence maxima in dioxane/acetonitrile at 298 K[93] [c]low solubility, thus not reliable [d]predicted value based on 1/n vs. E_{max} plot.

3.1.5. Optical Properties of oligo(*p*-benzamide)s

The different possible synthetic routes to well-defined or monodisperse oligo(*p*-benzamide)s have already been described in chapter *2.1.5.2*. On order to provide evidence of a conjugation along the amide bond, UV/vis spectra in dimethylacetamide (DMAc) of soluble oligo(*p*-benzamide)s (up to four repeating units) have been recorded and are shown in Figure 3.26.[94] Longer OPBAs are not soluble, so they have been synthesized onto a poly(ethylene oxide) block and subsequently their optical properties were studied in *N*,*N*-dimethylformamide, chloroform and water.[95] The amine-terminated polymers generally show higher fluorescence intensities than the nitro-terminated polymers. Both series of compounds exhibit generally the same trend. As expected, the absorption maximum of the amine terminated OPBA block copolymers in DMF increases with increasing OPBA length (Figure 3.27). A linear relationship is observed between the wavelength of the absorption maximum and the inverse of the oligomer length 1/n. This is an indication of molecular solvation of the OPBA rods and correlates well with the observations from SEC measurements in the same solvent. The increase in absorption

coefficient and decrease in fluorescence intensity with increasing oligomer length is typical for extended π-conjugated oligomers. In order to investigate whether the aggregation phenomena observed in chloroform affect the optical properties of the block copolymers, UV/vis and fluorescence spectra of the amine-terminated OPBA block copolymers MPEG-PBA_n-NH_2 (n = 2–5). in chloroform were recorded (Figure 3.28). The wavelength of the absorption maximum shifts to longer wavelengths with increasing OPBA length up to an oligomer length of n = 4. For n = 5 a blue shift of $\Delta\lambda = 25$ nm (from n = 4 to 5) is observed. This indicates parallel stacking of the OPBA chromophores (*H* aggregate).[96] This abrupt change in absorption maximum from OPBA oligomers matches exactly the onset of aggregation observed in chloroform GPC experiments. Compared to the spectra in DMF, the fluorescence spectra in chloroform are significantly reduced in intensity and two emission bands can be observed. The one at longer wavelength increases in intensity with increasing OPBA length up to n = 4. For n = 5, the emission band at longer wavelength is markedly reduced in intensity. The step from n = 4 to 5 is discribed as the onset of aggregation of OPBA chromophores.

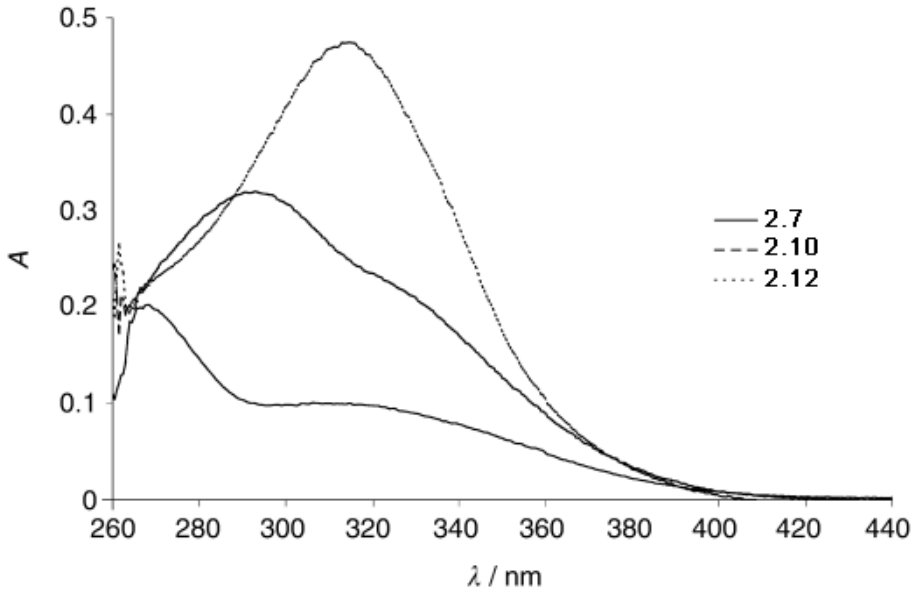

Figure 3.26: UV/vis spectra of compounds **2.7**, **2.10** and **2.12** (in DMAc+1 % LiCl, *c*=0.01 mM).

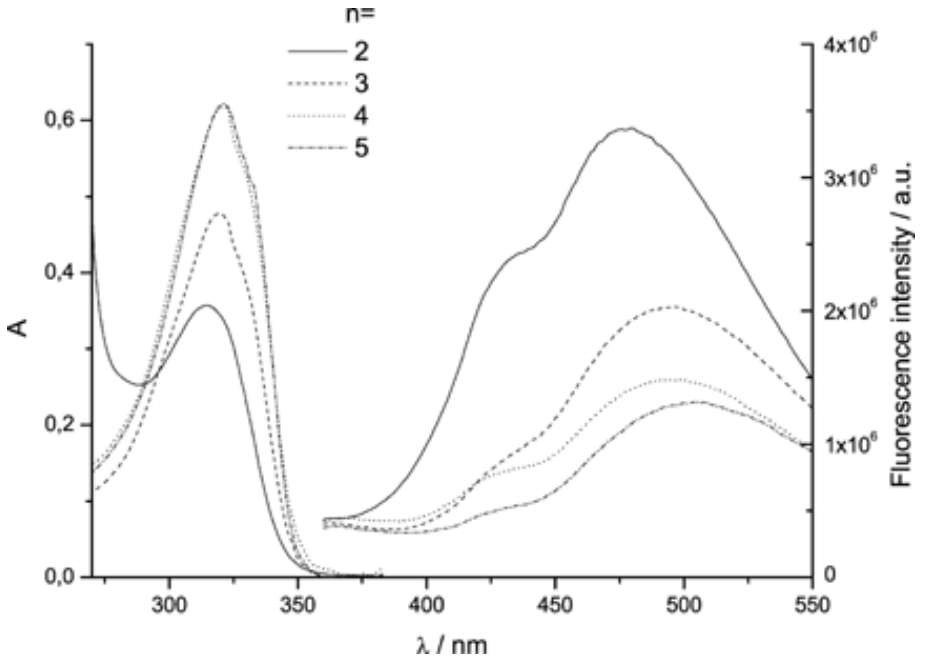

Figure 3.27: UV / vis and fluorescence spectra of MPEG-PBA$_n$-NH$_2$, n = 2–5 in DMF (7.8 x 10^{-6} mol L^{-1}): n = 2, n = 3 , n = 4 **(2.17)**, n = 5 **(2.20)**.

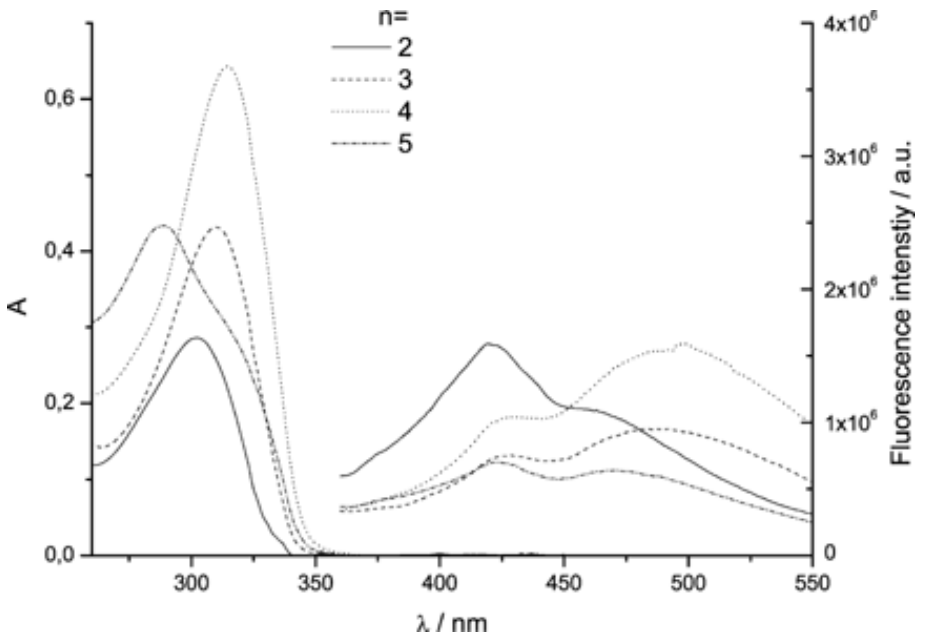

Figure 3.28: UV / vis and fluorescence spectra of MPEG-PBA$_n$-NH$_2$, n = 2–5 in chloroform (7.8 x 10^{-6} mol L^{-1}): n = 2, n = 3 , n = 4 **(2.17)**, n = 5 **(2.20)**.

3.1.6. Theoretically backgrounds on photoluminescence

Electromagnetic radiation (photons), which a substance re-radiates after absorption of photons, is called photoluminescence.[97,98] Depending on the way of excitation, different luminescence types are used. Would a chemical or biological reaction be the cause of luminescence, chemoluminescence respectively bioluminescence would happen. By using electrical fields for excitation, electro-luminescence occurs.

The process of photoluminescence begins with the absorption of a photon trough an atom or molecule. Through this absorption (A) an electron gets excited to a higher energy state, thus leaving its ground state S_0 to a singlet state S_1 or S_2. The molecule can afterwards relax in different ways, under radiation of a photon or without any radiation. The different ways are showed in the *Jablonski*-diagram (Figure 3.29).

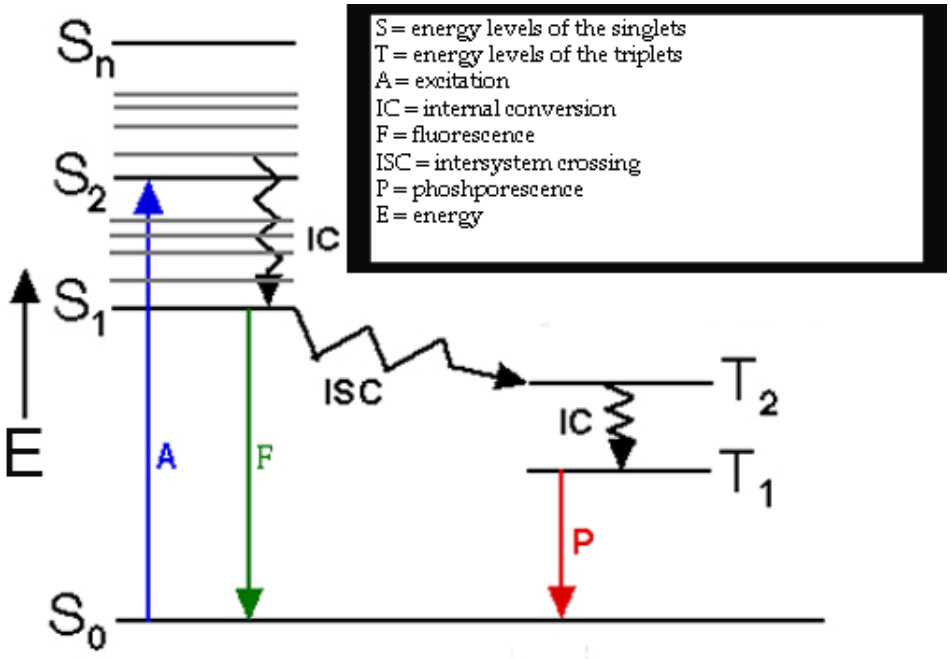

Figure 3.29: *Jablonski*-diagram.

Nonradiative transitions arise through vibrational energy relaxation (VR) internal conversion (IC) or intersystem crossing (ISC). VR means the relaxation of the excited state to its lowest vibrational level, whereas IC is the relaxation from one excited state to the next lowest excited state (e.g. $S_2 \rightarrow S_1$) respectively the ground state ($S_1 \rightarrow S_0$). The third type ISC is a spin-forbidden transition to state with higher spin multiplicity (e.g. $S_1 \rightarrow T_1$). Since this is quantum mechanically forbidden, this process takes longer and exhibits a longer lifetime.

All these processes involve the dissipation of energy to the surrounding of the molecule, such as solvent molecules.

Radiative transitions are the spin-allowed fluorescence (F) from an excited singlet state to the ground state (e.g. $S_1 \rightarrow S_0$) and the spin-forbidden phosphorescence (P) from a triplet state to the ground state (e.g. $T_1 \rightarrow S_0$). A third way of radiation is the resonant radiation in which a photon of a particular wavelength is absorbed and an equivalent photon of the same wavelength is emitted. In the fluorescence and phosphorescence the emitted wavelengths are longer than the absorbed one, thus meaning the emitted electron has less energy. The lifetime of the resonant radiation is around 10 ns, compared to the lifetime of fluorescence (0.5 – 20 ns), it is the same time scale. Only the lifetime of phosphorescence can be much longer (minutes to hours).

3.1.6.1. Solvatochromism

Solvatochromism describes the influence of the solvent on the position of the absorption- and emissions-bands.[99,100] These positions are depending on the nature of the transmission; where as the polarity of the solvent influences the level of the ground state as well as the levels of the excited states. The causes are direct intermolecular interactions like hydrogen bonds and dipole-dipole interactions. Both spectra (absorption and emission) may be changed due to the solvent effect.

Absorption

In the UV/Vis absorption the polarity of the solvents changes the $n \rightarrow \pi^*$ and $\pi \rightarrow \pi^*$ transmissions. Through the absorption of a photon, the dipole moment is changed, because the charge density in the molecule is distorted. In this case there are two different types:

- *Negative solvatochromism*
  In this case the excited state is less polar than the ground state, meaning that the energy level of the ground state is decreased the more polar the solvent is, whereas the level of the excited state nearly stays the same (Figure 3.30). This way the energy gap gets bigger and a hypsochromic shift is observed. In the UV-Spectra the absorption maxima is shifted to lower wavelengths.

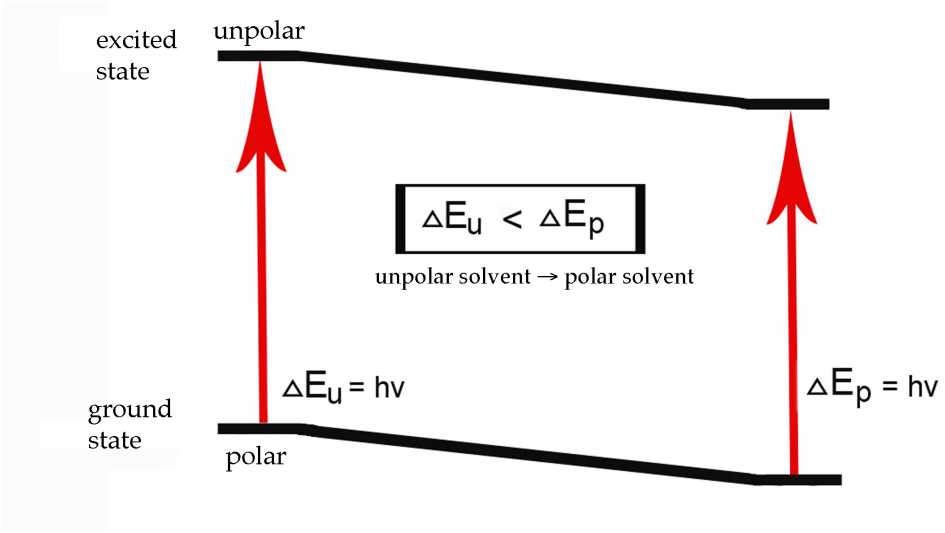

Figure 3.30: Negative solvatochromism.

- *Positive solvatochromism*

  If the excited state is now more polar than the ground state, the excited state gets more stabilized with an increase in solvent polarity, meaning that the energy difference between both states decreases (Figure 3.31). Thus the excitation energy decreases and a bathochromic shift is observed; the absorption maxima is moved to higher wavelengths.

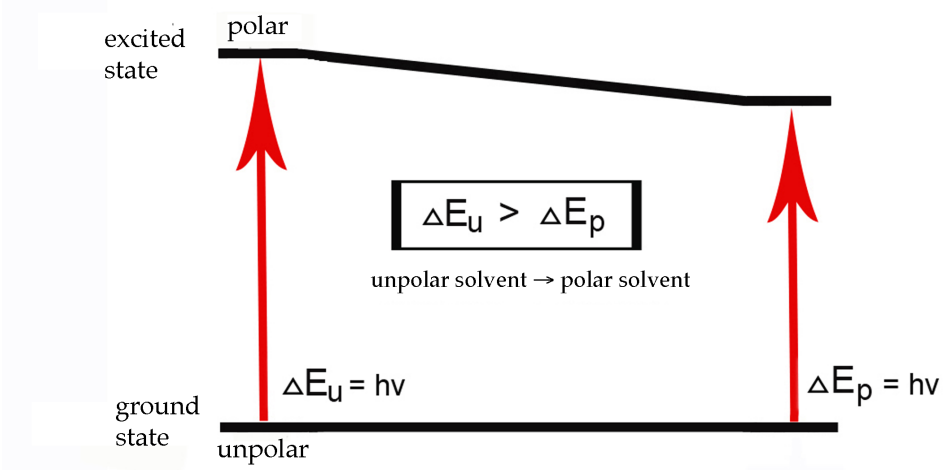

Figure 3.31: Positive solvatochromism.

Fluorescence

Solvent molecules can also have an effect on the fluorescence. They are ordered around the dissolved molecule depending on the dipole in its ground state (S_0) (Figure 3.32). If the dipole moment changes of the dye, the solvent molecules around it will stay and this will lead to a slightly higher excited state (S_1'). The relaxation of the solvent molecules lowers the excited state S_1' to the regular excited state S_1, whereas the solvent molecules now reoriented their dipole moment to fit that of the dye. If the photon is now emitted, the dye molecule is situated in the ground state again (S_0'). Due to the fact that the dipole of the dye is changed again, and the solvent molecules are not reoriented yet, this ground state is destabilized, meaning it has a higher energy than the regular ground state (S_0). By reorganization of the solvent molecules in order to fit the dipole moment of the dye, the ground state is stabilized, so the molecule is in the ground state (S_0) again.

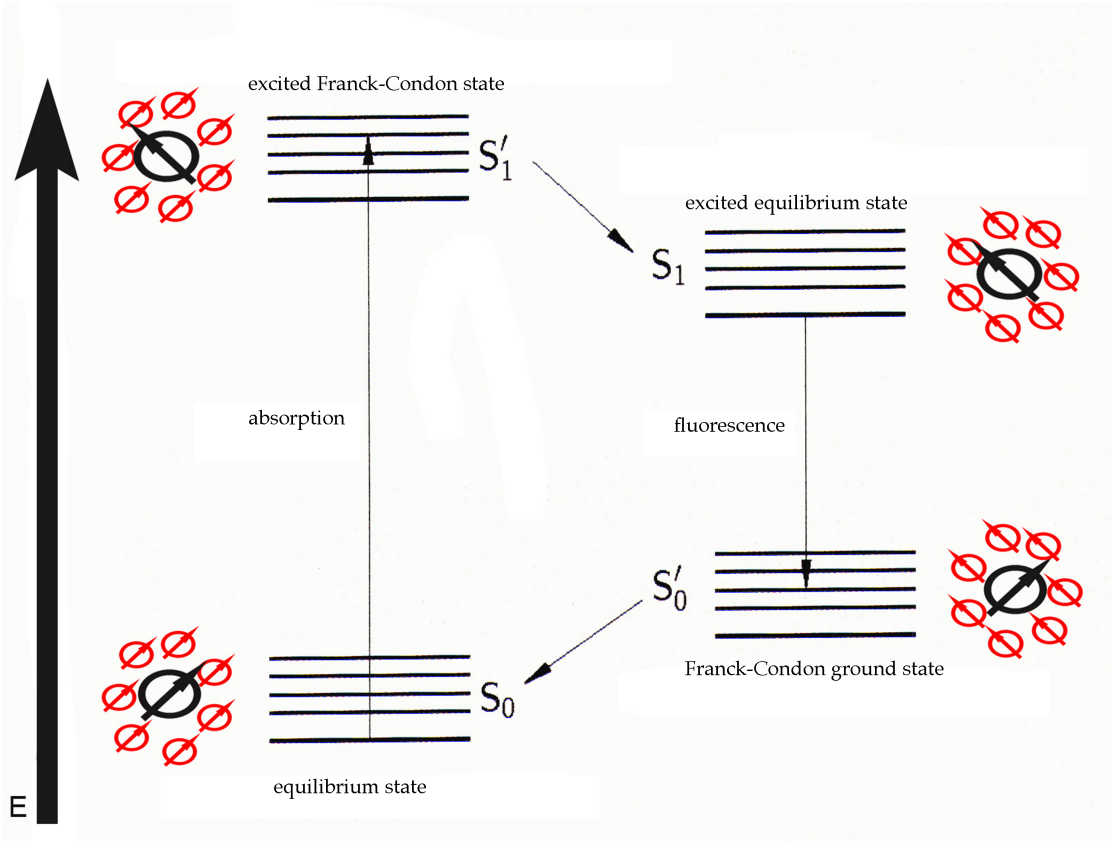

Figure 3.32: Illustration of the effect induced by solvent relaxation.

3.2. Synthesis of thiophene amino acid, oligo- and poly(thiophene carboxamide)s

Oligo(*p*-benzamide)s are well known for their structural stiffness as well as their well described supramolecular structures. In cases where the OPBA block does not carry any side chains, the onset of the aggregation in chloroform is well defined and takes place when the length of the OPBA block increases from four to five units (see chapter *3.15*). Beside the strong aggregation tendency, conjugation along the amide bond has also been observed and characterized. With increasing chain length of the OPBA block, its UV/vis absorption maximum is more red shifted. In chloroform, a selective solvent for the poly(ethylene oxide) block, a blue shift is observed when the length of the OPBA block increases from four to five, indicating a parallel stacking of the OPBAs (*H* aggregates). The observed red shifts in the UV/vis spectra indicate a conjugation along the amide, which is also responsible for the aggregation. Oligo(thiophene)s, on the other side, are well known for their optical properties, such as large red shifts with increasing chain lengths (see chapter *3.1.5*). These properties make them to ideal candidates for optoelectronic devices such as thin film transistors, organic solar cells and organic light emitting diodes.

Introducing an amide between two thiophene rings (instead of the benzene ring in the case of OPBAs) will lead to a new set of oligomers: Oligo(thiophene carboxamide)s. These chromophores will unite the high electron density of the thiophene ring with the amide. Conjugation along such an amide was already been proven, and therefore they will not split the electronic system between two thiophene rings. The amide bond is responsible for the strong self aggregation in the OPBAs and might function in this matter for the oligo(thiophene carboxamide)s.

The oligo(thiophene carboxamide)s are a logical evolution to the OPBAs in which the aromatic system is swapped to one with a higher electron density, but leaving the amide. Figure 3.33 a illustrates the new structure of this polymer and the repeating unit (cyan), thus a new monomer is needed: 2-aminothiophene-5-carboxylic acid **(3.39)** (Figure 3.33 b). After monomer synthesis, polymerizations through polycondensation or well-defined oligomers have been synthesized and characterized.

a)

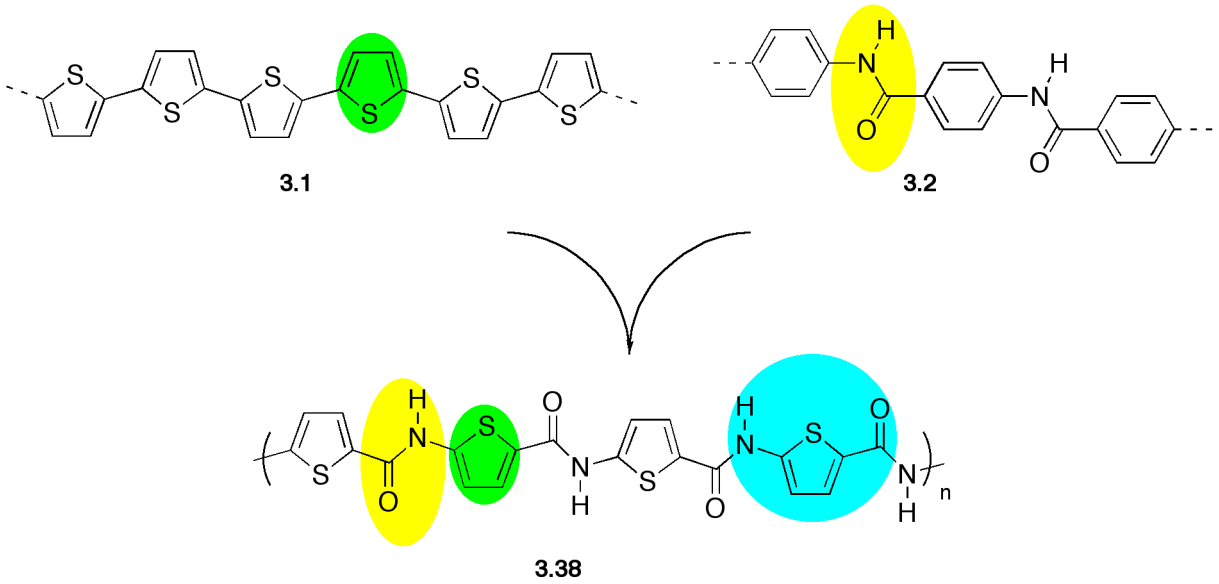

b)

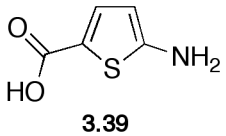

Figure 3.33: a) Poly(thiophene carboxamide); cyan illustrates the repeating unit.
b) 2-Aminothiophene-5-carboxylic acid **(3.39)**

3.2.1. 2-Aminothiophene-5-carboxylic acid: Synthetic Approaches

In order to synthesize 2-aminothiophene-5-carboxylic acids different synthetic methods where applied (Figure 3.34):

a) *Gewald*-synthesis.
b) Nitration of thiophene-2-carboxylic acids with following reduction.
c) *Curtius*-rearrangement to introduce the amine.

The *Gewald*-synthesis produces di-substituted thiophene amino acids, which are *tert*-butyl ester protected at the carboxylic acid. In contrast to this method, the other syntheses should be able to produce only unsubstituted thiophene amino acids.

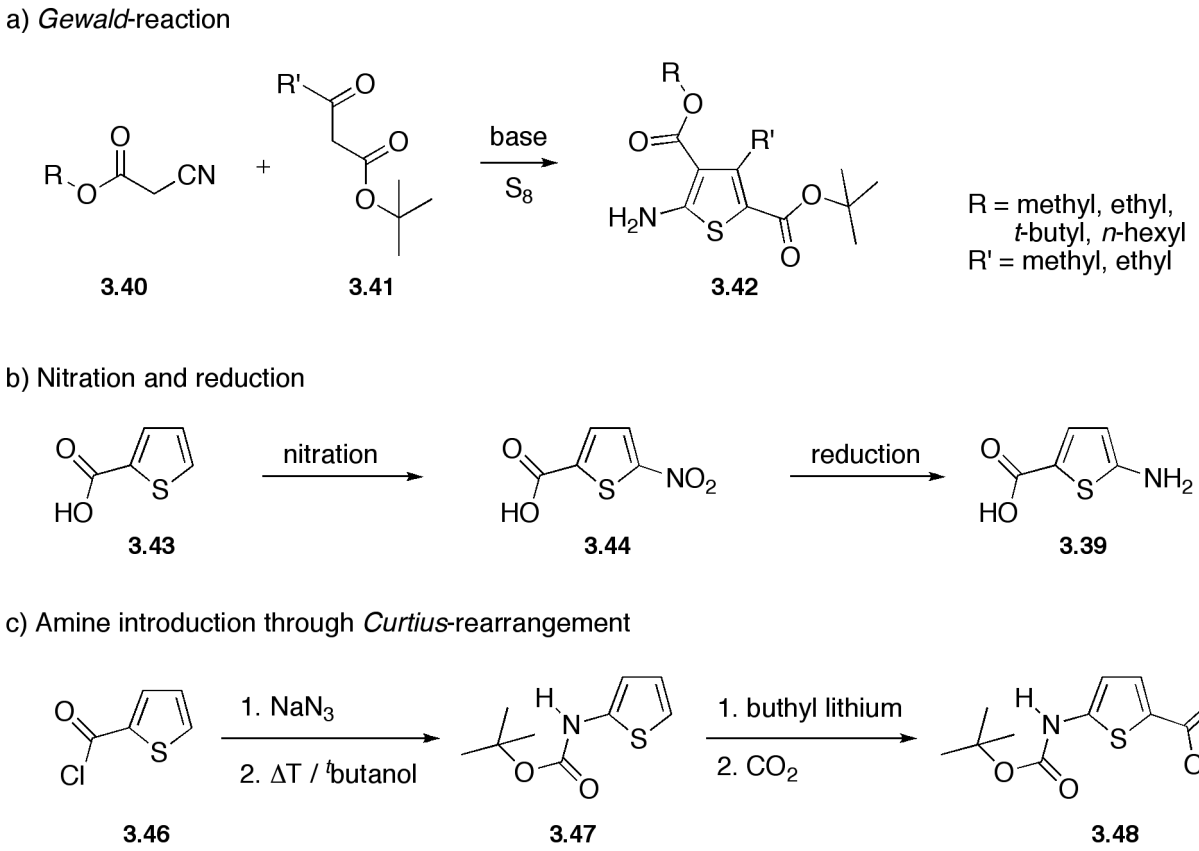

Figure 3.34: Schematic representation of synthetic approaches to 2-amino-5-carboxylic acids: a) *Gewald*-synthesis b) Nitration and reduction and c) *Curtius*-rearrangement.

3.2.1.1. *Gewald*-synthesis

The *Gewald*-synthesis is a multi component, ring closure reaction. The reaction of different esters of 3-oxo-butyric acid with esters of 2-cyano acetic acid and sulfur leads to a tetra-substituted thiophene **(3.50)**. Figure 3.35 shows an example of *tert*-butyl acetoacetate

(3.49) and an ester of 2-cyano acetic acid **(3.40)**. The *tert*-butyl ester can also be varied, but an easy cleavage of the ester makes it useful for later synthesis.

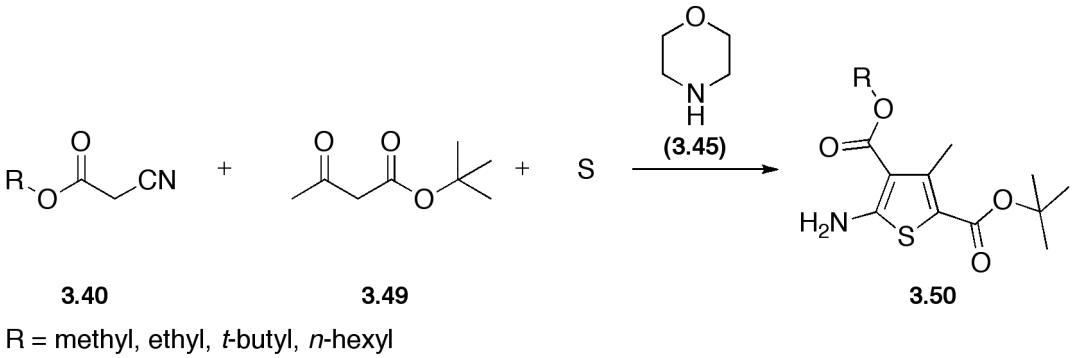

Figure 3.35: *Gewald*-reaction.

The mechanism of the reaction is not yet fully understood and analyzed. The proposed one is shown in Figure 3.36. The first step is an aldol addition between the 3-oxo-butyric acid and the 2-cyano acetic acid, where a single bond (Figure 3.36, *red* bond) is created, before water is eliminated leaving a double bond. After deprotonation of **3.51**, it attacks the sulfur, and a five membered heteroatomic ring is created. After reprotonation and a hydrogen shift, the twofold-substituted thiophene amino acid is formed **3.52**.[101-103]

The only drawback of the *Gewald*-reaction is that only tetrasubstituted thiophenes can be synthesized that way. On the other hand, the one-pot reaction and low-cost starting materials allow a synthesis of large amounts of the desired monomer.

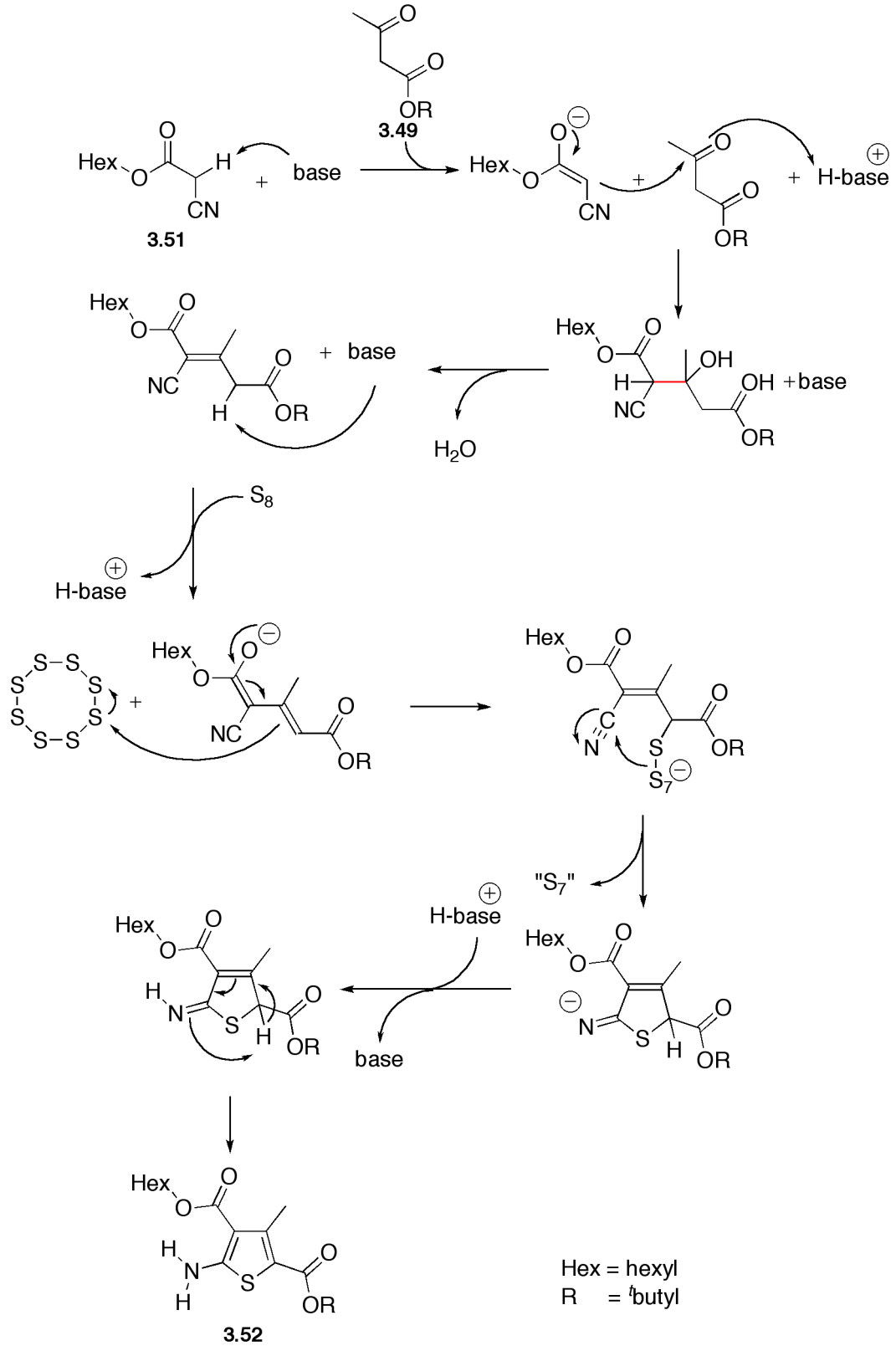

Figure 3.36: Proposed mechanism of *Gewald*-synthesis.

3.2.1.2. Nitration of thiophene-2-carboxylic acids with following reduction

Starting from thiophene, 3-hexylthiophene or 3,4-ethylendioxythiophene (EDOT), thiophene amino acids can be synthesized carrying zero, one or two side chains. After introducing the carboxylic acid by lithiation and carbon dioxide afterwards, nitration of the aromatic acid and following reduction would lead to the desired amino acid (Figure 3.37).

a) Using thiophene-2-carboxylic acid **(3.43)**, nitration by acetic acid and nitric acid leads to yield of 40% 5-nitrothiophene-2-carboxylic acid **(3.44)** after column chromatography (Figure 3.37a). The side product (3-nitrothiopene-2-carboxylic acid) **(3.53)** was not used in further syntheses.
b) 3-Hexylthiophene is lithiated by butyl lithium and subsequently carboxylated by carbon dioxide. Since the lithiation is not regioselective (both positions, the 2- and 5-position are lithiated) two products are obtained **3.55** and **3.56**. Using *tert*-butyl lithium instead of *n*-butyl lithium or lower temperatures (-100 °C instead of -78 °C) will also result in a mixture of both products. After column chromatography the desired 4-hexylthiophene-2-carboxylic acid **(3.56)** is obtained in 40% yield. Nitration is then done by treating the starting material with nitric acid in acetic acid (Figure 3.37 b).
c) 3,4-ethylendioxythiophene-2-carboxylic acid **(3.60)** is synthesized by treating EDOT with *n*-butyl lithium at -78°C in THF and subsequently with carbon dioxide. Nitration conditions need to be a little bit harsher in this case, and therefore nitric acid is used in acetic acid and acetic acid anhydride (Figure 3.37 c).

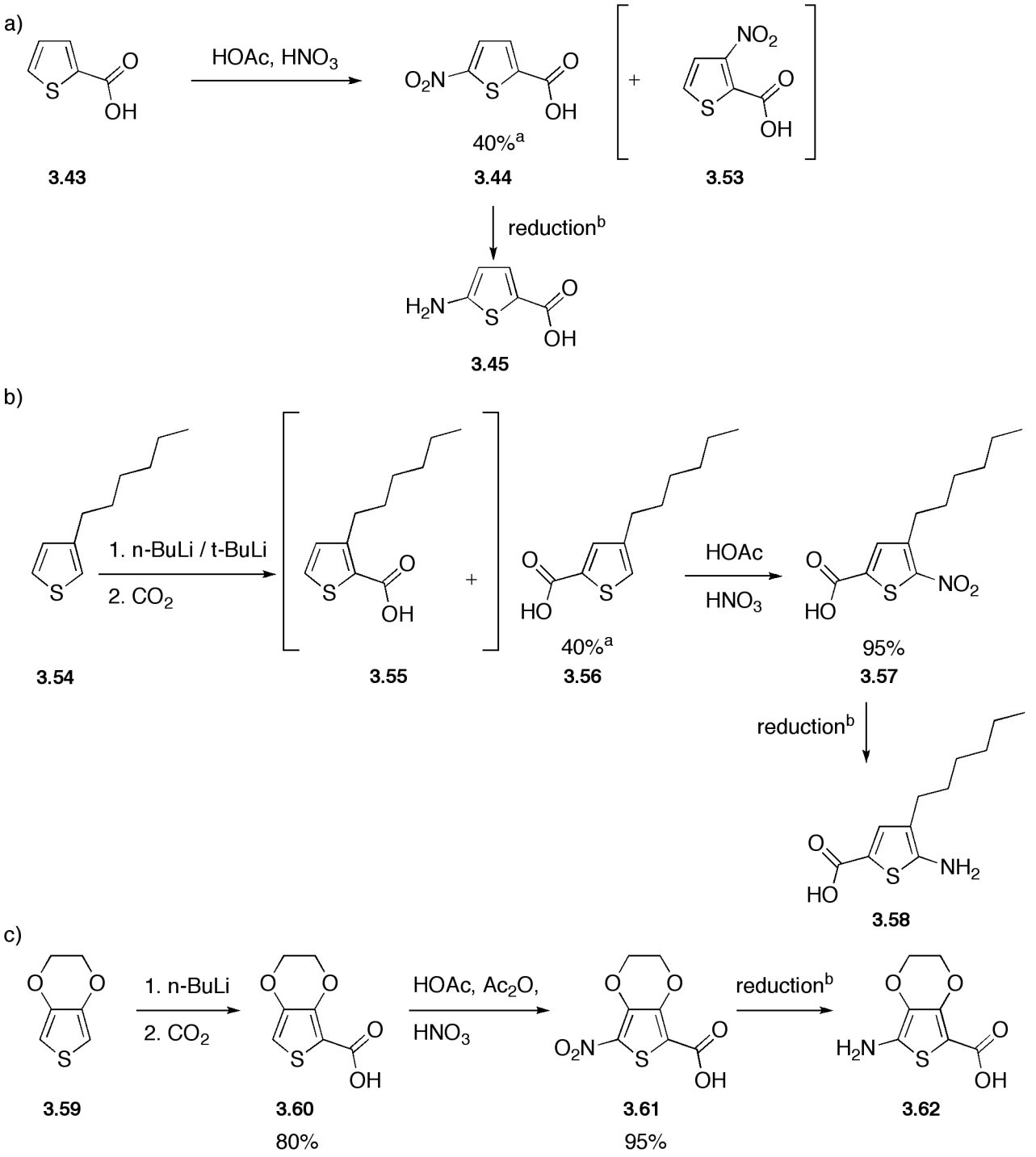

Figure 3.37: Synthesis of 2-aminothiophene-5-carboxylic acid via nitration and reduction.
[a]after column chromatography [b]several reductions have been dried.

Reductions

Beginning from the three synthesized thiophenes (5-nitrothiophene-2-carboxylic acid **(3.44)**, 4-hexyl-5-nitrothiophene-2-carboxlyic acid **(3.57)** and 3,4-diethylendioxy-5-nitrothiophene-2-carboxylic acid **(3.61)**) different reduction methods have been applied to synthesize the amino acid. None of the used reductions yielded in the preferred product.

Either the reduction potentials appear to low, because no reaction is observed, or they where too strong and hydrogenated the aromatic ring, thus leaving no aromatic signal in proton NMR spectra. Table 3.6 shows all tried reductions.

Table 3.6: Tried reactions to reduce the nitro group to an amine.

Thiophene compound	Catalyst	Reagent	Conditions
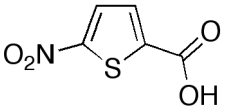	Sn	conc. HCl	room temperature
	Zn	conc. HCl	room temperature
	Fe	conc. HCl	room temperature
	$SnCl_2$	conc. HCl	room temperature
	$SnCl_2$	half conc. HCl	room temperature
	$ZnCl_2$	conc. HCl	room temperature
	$ZnCl_2$	half conc. HCl	room temperature
	Pd/C	H_2	2 bar, room temperature
	Pd/C	H_2	4 bar, room temperature
	Pd/C	H_2	8 bar, room temperature
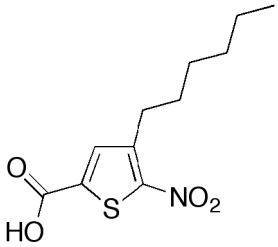	Sn	conc. HCl	room temperature
	Zn	conc. HCl	room temperature
	Fe	conc. HCl	room temperature
	$SnCl_2$	conc. HCl	room temperature
	$ZnCl_2$	conc. HCl	room temperature
	Pd/C	H_2	2 bar, room temperature
	Pd/C	H_2	4 bar, room temperature
	Pd/C	H_2	8 bar, room temperature
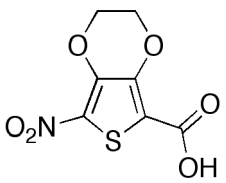	Sn	conc. HCl	room temperature
	Zn	conc. HCl	room temperature
	Fe	conc. HCl	room temperature
	$SnCl_2$	conc. HCl	room temperature
	$ZnCl_2$	conc. HCl	room temperature
	Pd/C	H_2	2 bar, room temperature
	Pd/C	H_2	4 bar, room temperature

This synthetic route does not return the thiophene amino acids and can therefore not be used. Reductions of nitro groups are not possible with the used thiophene carboxylic acids. The high electron density of the aromatic ring might be one explanation. This density would also increase if the nitro group has been reduced to the corresponding amine. The effect of that increased electron density would subsequently be an easier reduction of the aromatic system. Nonetheless, the possibility of introducing nitro groups to thiophene carboxylic acids could be important in the case where electron density need to be lowered in the conjugated system. This class of material could be a possible *pull*-end in so called *push-pull* systems, in which one end of a conjugated system pushes electrons into the system, whereas the other end pulls them out of it.

3.2.1.3. *Curtius*-rearrangement to introduce the amine

A further method to introduce an amine is the *Curtius*-reaction. In this case a thiophene-2-carbonyl chloride **(3.46)** reacts with sodium azide to obtain thiophene-2-carbonyl azide **(3.63)**, which rearranges to 2-isocyanatothiophene **(3.64)** under heat treatment (Figure 3.38).[103] The isocyanate compound reacts to 2-aminothiophene **(3.65)** with water, to *tert*-butyl thiophene-2-yl-carbamate **(3.47)** (^{t}Boc-2-aminothiophene; ^{t}Boc = *tert*-butyloxycarbonyl) with *tert*-butanol or to (9*H*-fluoren-9-yl)methyl thiophen-2-ylcarbamate **(3.66)** with 9-fluorene methanol (Fmoc-2-aminothiophene; Fmoc = fluorenylmethyloxy carbonyl).

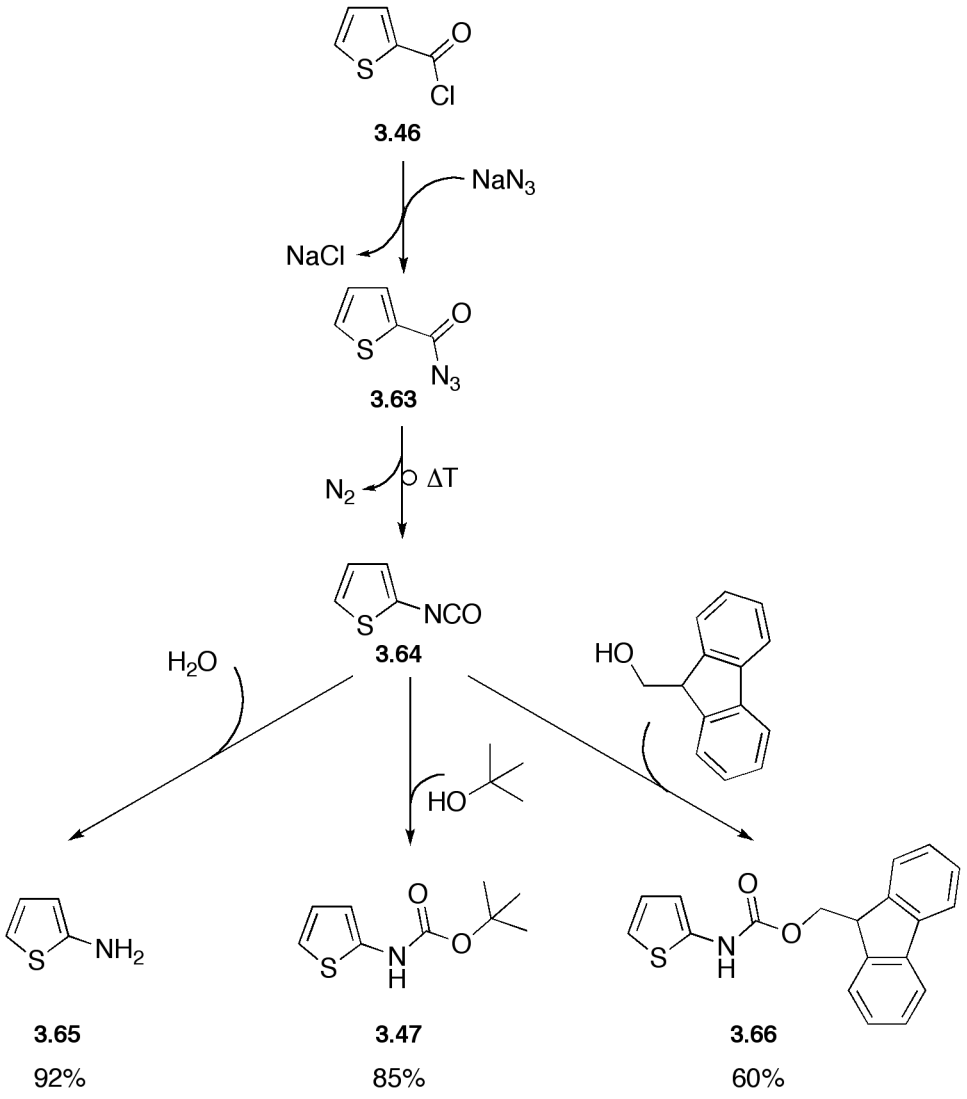

Figure 3.38: *Curtius*-rearrangement

The ^{t}Boc- and Fmoc-protected 2-aminothiophenes are good candidates for further synthesis. Whereas the ^{t}Boc group is acid labile, and thus stable under basic conditions, the Fmoc group is base labile and stable under acidic conditions. Because the next step is a

lithiation of the thiophene with a strong basic the ^{t}Boc-protected 2-aminothiophene is used (Figure 3.39). ^{t}Boc-2-aminothiophene **(3.47)** is treated with butyl lithium at -78°C or -100 °C and carbon dioxide is afterwards added to the reaction mixture (Figure 3.39). This reaction procedure does not lead to the desired thiophene amino acid. So in some cases the reaction mixture was refluxed before it was cooled to -78°C again and carbon dioxide was added. However, after workup of the reaction mixture, the desired thiophene-carboxylic acid was not obtained, instead the starting material was nearly quantitatively recovered. Table 3.7 shows the different tried reaction conditions. Neither *n*-butyl- nor *tert*-butyl-lithium, or the usage of two equivalents of base will result in the favored product. Treating ^{t}Boc-2-aminothiophene **(3.47)** with sodium hydride, in order to deprotonate the amide, and subsequently adding butyl lithium, will not lead to the desired carboxylic acid **(3.67)**.

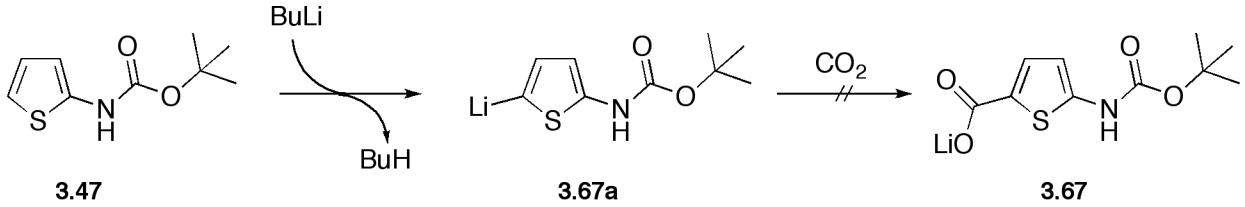

Figure 3.39: Introduction of the carboxylic acid group.

Table 3.7: Tried carboxylations.

Reactants	Solvent	Reaction temperature / °C	Reaction time / h
1 eq. *n*-BuLi	THF	-78	2
2 eq. *n*-BuLi	THF	-78	2
2 eq. *n*-BuLi	THF	-100	2
2 eq. *n*-BuLi	THF	-78 → reflux	4
2 eq. *n*-BuLi	CH; TMEDA[a]	-78 → reflux	4
1. 1 eq NaH 2. 1 eq. *n*-BuLi	THF	1. room temp. 2. -78	1. 2 2. 2
1 eq. *tert*-BuLi	THF	-78	2
2 eq. *tert*-BuLi	THF	-78	2
2 eq. *tert*-BuLi	THF	-100	2
2 eq. *tert*-BuLi	THF	-78 → reflux	4

[a]CH = cyclohexane; TMEDA = tetramethylethylenediamine

Since the starting material is recovered in every case, it is not possible to say whether the lithiation or the reaction with carbon dioxide does not work. To analyze the lithiation step, a halogen-metal exchange reaction was used. Therefore ^{t}Boc-2-aminothiophene **(3.47)** was brominated with *N*-bromosuccinimde (NBS) yielding 5-bromo-^{t}Boc-2-aminothiophene **(3.68)** (Figure 3.40). This compound can then undergo a halogen-metal exchange reaction

with butyl lithium to form butyl bromide and lithiated thiophene **(3.67a)**, which should now react with carbon dioxide forming the ^{t}Boc-5-aminothiophene-2-carboxylic acid **(3.67)**. Different equivalents of butyl lithium, *n*- or *tert*-butyl lithium as well as sodium hydride before butyl lithium was tried in the synthesis. Sodium hydride should deprotonate the amide but not exchange with the bromine.

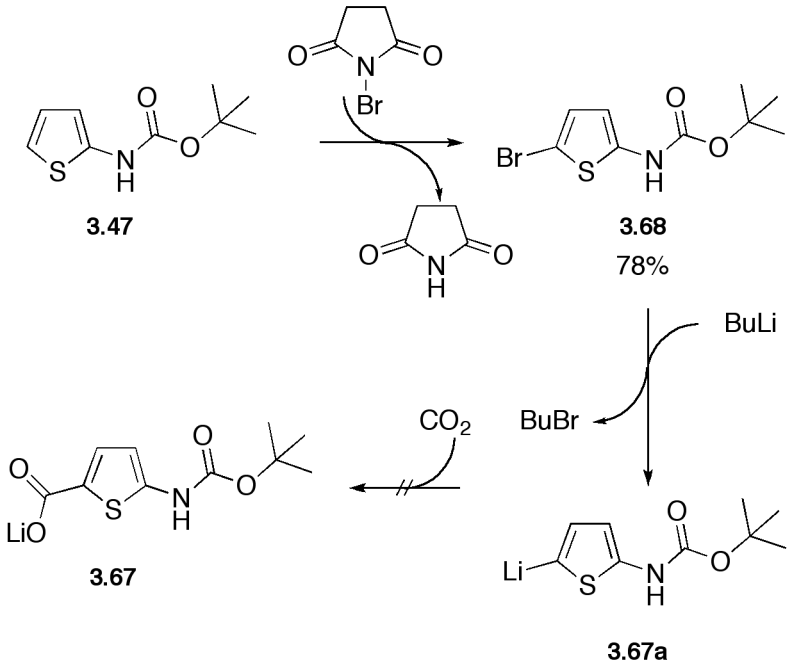

Figure 3.40: Introducing a carboxylic acid via a halogen-metal exchange reaction.

Table 3.8: Tried halogen-metal exchange reactions.

Reactants	Solvent	Reaction temperature / °C	Reaction time / h
1 eq. *n*-BuLi	THF	-78	2
2 eq. *n*-BuLi	THF	-78	2
1. 1 eq NaH 2. 1 eq. *n*-BuLi	THF	1. room temp. 2. -78	1. 2 2. 2
1 eq. *tert*-BuLi	THF	-78	2
2 eq. *tert*-BuLi	THF	-78	2

Neither of the above reaction conditions produced the desired carboxylic acid. In all cases the bromine was exchanged with lithium, but after adding carbon dioxide and workup the starting material ^{t}Boc-2-aminothiophene was obtained. Therefore the lithiated intermediate **3.67a** does not react with carbon dioxide. On this account, the lithiated thiophene species was reacted with boron trimethoxide, trimethyltin chloride or tributyltin chloride (Figure 3.41). None of those reaction resulted in the preferred monomer, instead ^{t}Boc-2-aminothiophene was obtained in all cases.

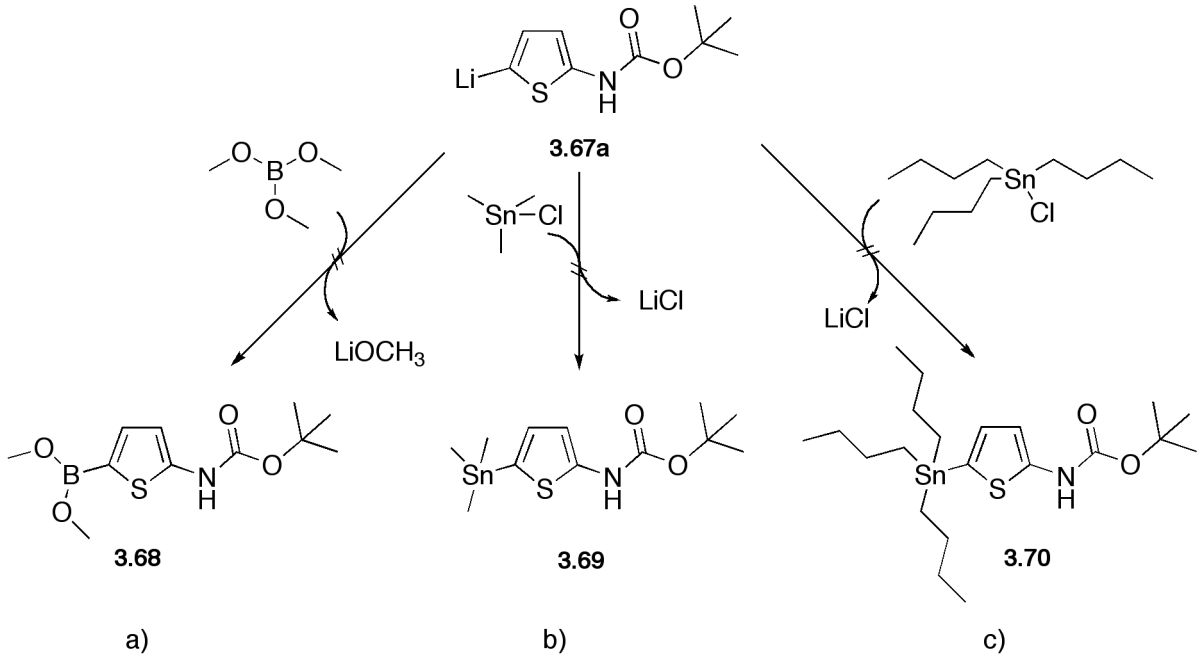

Figure 3.41: Reactions of lithiated ^{t}Boc-2-aminothiophene with a) boron trimethoxide, b) trimethyltin chloride or c) tributyltin chloride .

^{t}Boc- as well as Fmoc-protected amines could be introduced using the *Curtius*-rearrangement. The subsequent insertion of a carboxylic group was not possible. The lithiation step appears not to be the problematic step, since the halogen-metal exchange reaction results in the preferred lithiated thiophene. This species seems to be not reactive enough. Neither carbon dioxide, nor the boron or tin species reacted with the lithiated thiophene. Being aware of these results, these synthetic approaches cannot be used to synthesize thiophene amino acids. Nevertheless, this synthetic pathway allows access to thiophene carrying protected or unprotected amines. These aminothiophenes could then be used as the amine part in reactions with activated carboxylic acids to give amides. Substituted initiators or end-groups for oligo(thiophene carboxamide)s could be introduced using this synthetic route to aminothiophenes.

3.2.2. Synthesis of different protected 5-aminothiophene-2-carboxylic acids

The large range of tetrasubstituted thiophene amino acids, which can be synthesized by *Gewald*-reaction, can be further used. Both esters can be easily varied before the multi component ring closure reaction is used to synthesize the thiophene. Tert-butyl ester is used at the 2-position, since it is easy to cleave compared to methyl and ethyl esters. The ester next to the amine (4-position) can be modified in order to change the properties, like solubility, of the later synthesized polymers and oligomers. Figure 3.42 shows different possible thiophene amino acids.

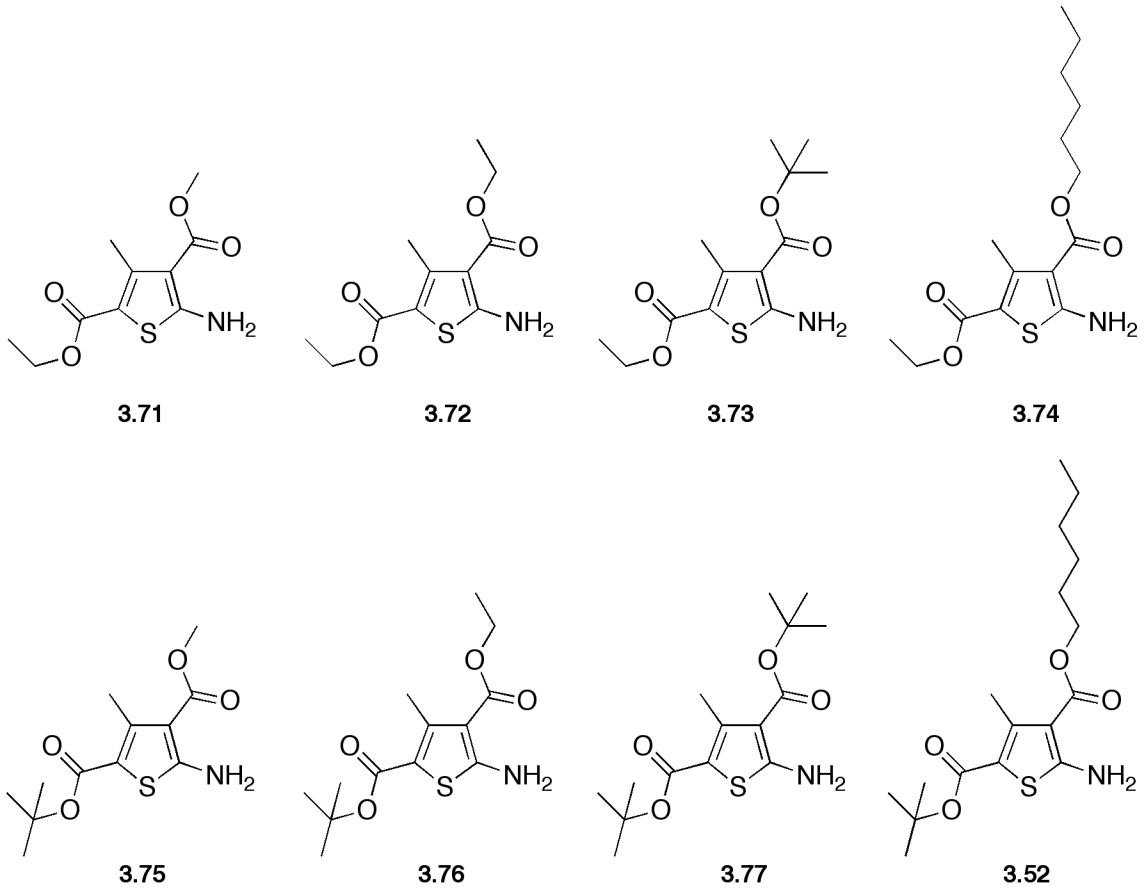

Figure 3.42: Different thiophene amino acids, synthesized by *Gewald*-reaction.

Fmoc-protected thiophene amino acid

The second row shows already *tert*-butyl ester protected acids with an unprotected amine. For use in common peptide synthesis, the amine should be protected instead of the carboxylic acid. This can be achieved in a two-step synthesis (Figure 3.43).

1.) Protecting the aminothiophene with fluorenylmethyloxycarbonyl chloride (Fmoc-Cl) or fluorenylmethyloxycarbonyl *O*-succinimide (Fmoc-*O*Su).

2.) Cleavage of the *tert*-butyl ester with trifluoroacetic acid (TFA).

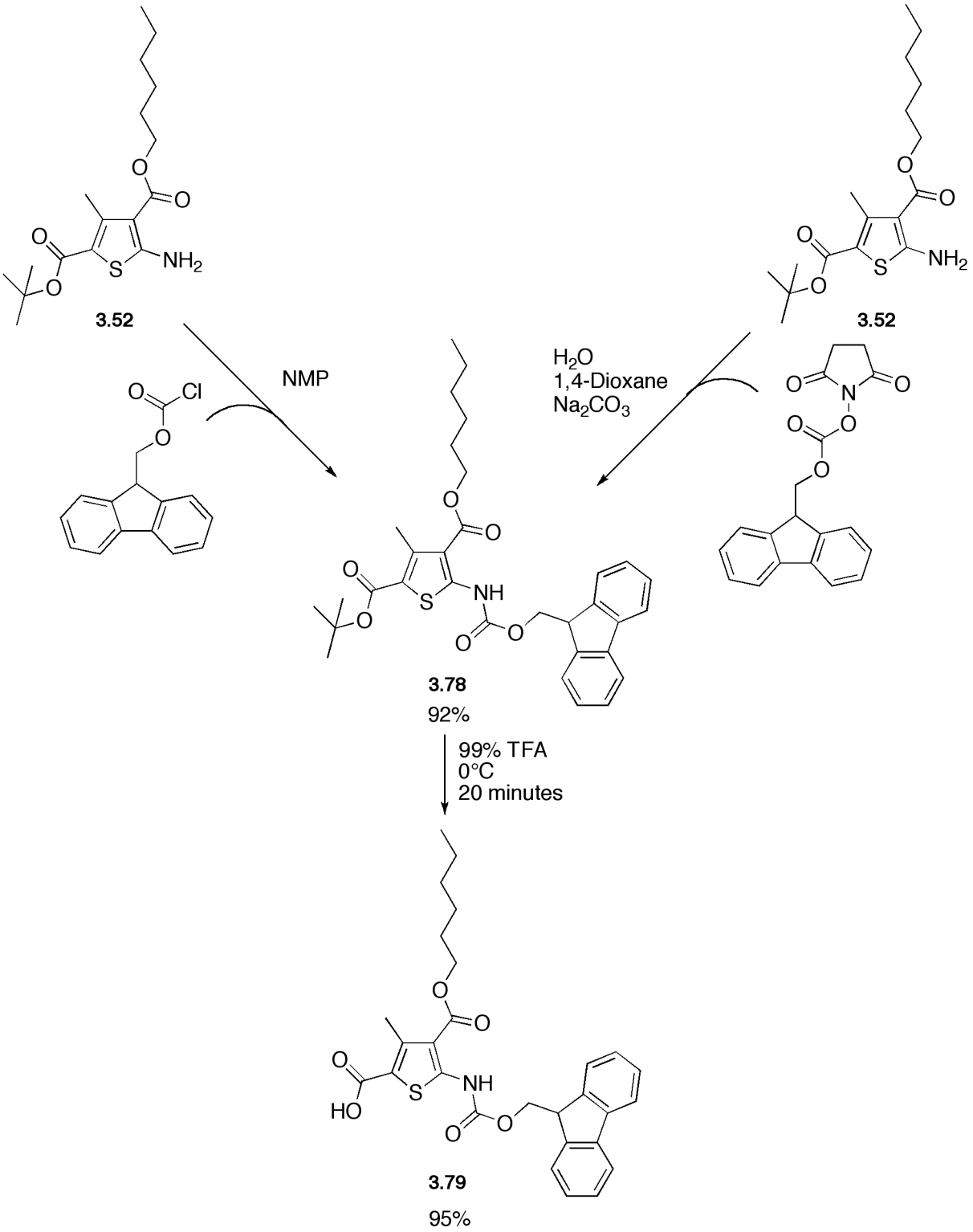

Figure 3.43: Synthesis of Fmoc-protected thiophene amino acid.

The protection with Fmoc can be done in two ways:

1) Fluorenylmethyloxycarbonyl chloride in *N*-methyl-2-pyrrolidone (NMP) is slowly added to a solution of the amine **3.52** in NMP. After precipitation the reaction mixture is filtered and the solid is washed with diethyl ether and dried, yielding about 90% of **3.78**.
2) Fluorenylmethyloxycarbonyl *O*-succinimide is dissolved in 1,4-dioxane and given to a solution of amine **3.52**, sodium carbonate in water and stirred for 24 hours. After removing the solvents, the crude material is extracted with water and chloroform. The organic phase is dried and the Fmoc-protected amine **3.78** is obtained in about 70%.

The thiophene amino acid **3.78** is now double protected. Since the Fmoc-group is acid stable, the *tert*-butyl ester can be cleaved under acidic conditions. Regular *tert*-butyl esters could be cleaved by 1 molar hydrochloric acid. This ester in contrast is stable enough, that it is not cleaved. Much harsher conditions are needed in this case: 99% aq. tetrafluoroacetic acid meets the requirements and the Fmoc-protected amino acid **3.79** is yielded in 95%.

Unprotected thiophene amino acid

The unprotected thiophene amino acid **3.80** is needed for polycondensation reactions und therefore needs to be synthesized from the *tert*-butyl ester protected amino acid **3.52** (Figure 3.44).

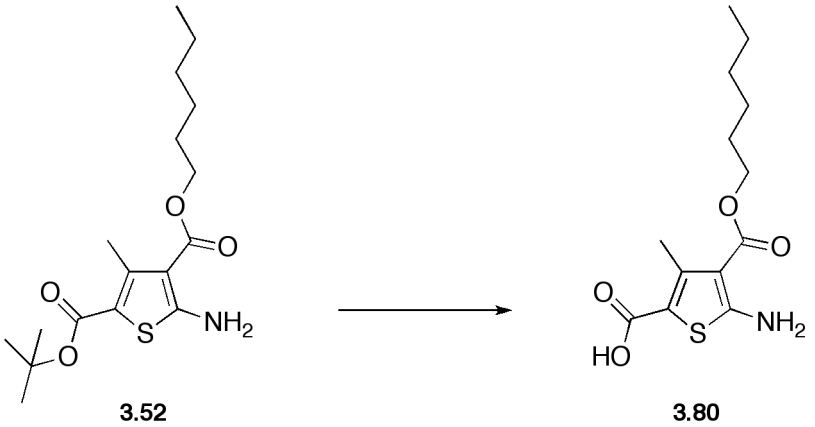

Figure 3.44: Synthesis of unprotected thiophene amino acid.

The deprotection of the ester in the case of the Fmoc-protected thiophene amino acid **3.78** works with trifluoroacetic acid in high yields. In the case of **3.52**, TFA does not work;

the ester is not cleaved and the starting material is recovered completely. Cleavage of the ester group by using 5 molar hydrochloric acid, does not lead to any reaction. On the other hand, using concentrated hydrochloric acid at 0 °C for 16 hours, does cleave the ester, but in most cases the product is decarboxylated, thus not leaving an acid group. Only very small amounts of the amino acid **3.80** (<1%) can be obtained from those reaction conditions after workup. Owing to those facts, other cleavage methods were tried. Titanium(IV) chloride in dichloromethylene is known to cleave *tert*-butyl ester selectively.[104] Adding titanium(IV) chloride to a solution of *tert*-butyl ester protected amino acid **3.52** at -10 °C and stirred for two hours, the thiophene is decarboxylated (Figure 3.45). Because of this, the method is not useful for this monomer.

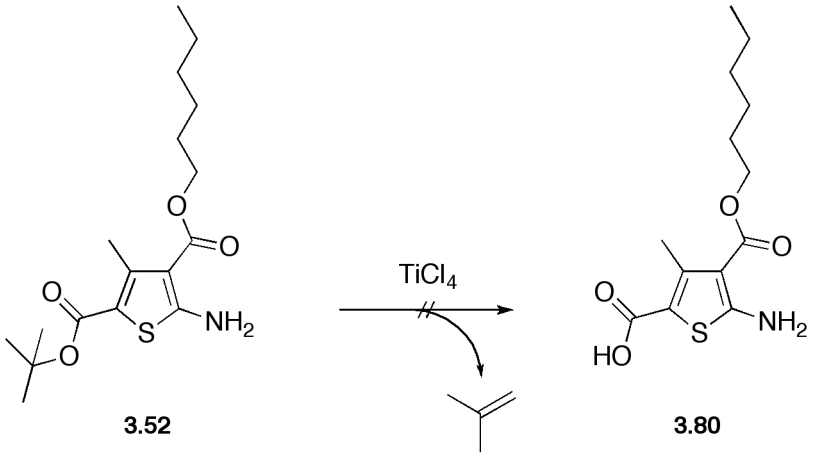

Figure 3.45: Deprotection of *tert*-butyl ester with titanium(IV) chloride.

A similar approach is the usage of cerium(III) chloride and sodium iodide in refluxing acetonitril.[105] The *tert*-butyl ester **3.52** is dissolved in this mixture and refluxed for three to five hours (Figure 3.46). The result is also decarboxylation of the amino acid und thus the method is not useful either.

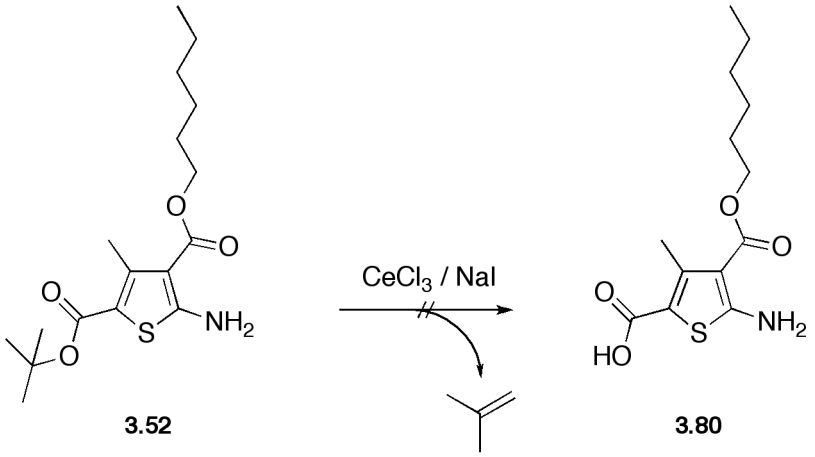

Figure 3.46: Deprotection of *tert*-butyl ester with cerium(III) chloride/sodium iodide.

Tert-butyl esters are also known to be cleaved under thermal conditions.[106,107] Heating **3.52** to 200 °C should cleave the ester and **3.80** should be obtained (Figure 3.47). However, any test did not result in the desired monomer. Thermogravimetric analysis showed a complete disappearance of **3.52** at 232 °C without any partial mass decrease before 232 °C, thus meaning, that the ester cannot be selectively removed by simply heating the monomer.

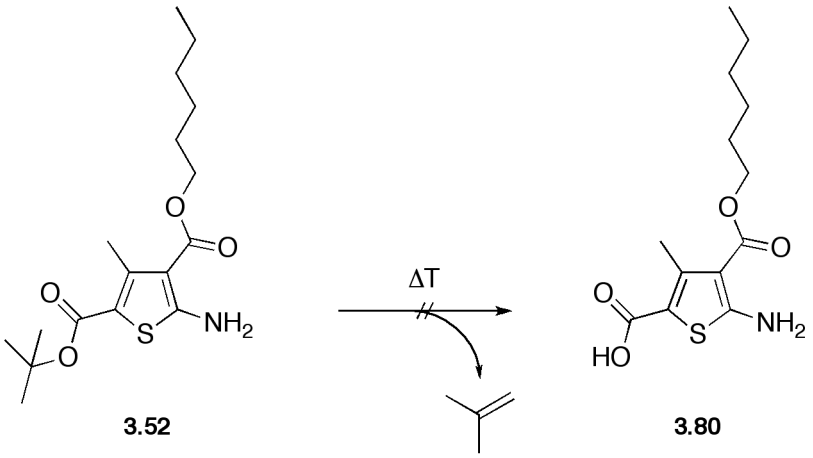

Figure 3.47: Deprotection of *tert*-butyl ester by heating to 200 °C.

All deprotections of 2-*tert*-butyl 4-hexyl 5-amino-3-methylthiophene-2,4-dicarboxylate **3.52** did not result in the amino acid **3.80**. Taking into account, that the deprotection of the ester does work at the Fmoc-protected amino acid **3.78,** the amine was protected with trifluoroacetic anhydride before the *tert*-butyl ester is cleaved (Figure 3.48).

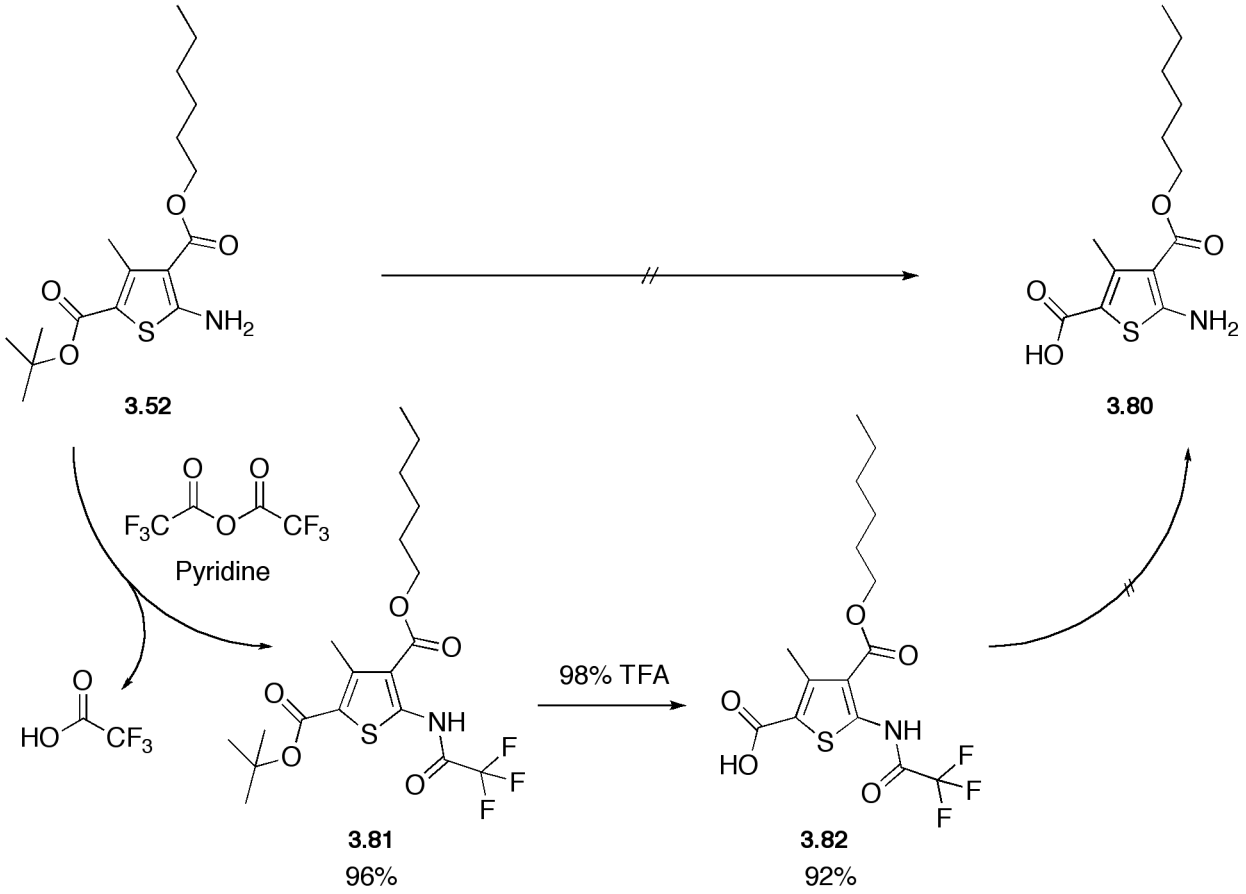

Figure 3.48: Synthesis of thiophene amino acid.

Adding trifluoroacetic anhydride to a solution of **3.78** in pyridine at 0 °C and stirring for 2 hours will yield after workup the desired double protected thiophene amino acid **3.81**.[108] Afterwards the treatment with 99% aq. trifluoroacetic acid and precipitating in water yields 4-(hexyloxycarbonyl)-3-methyl-5-(2,2,2-trifluoroacetamido)thiophene-2-carboxylic acid **(3.82)**. The later on removal of the trifluoroacetamide group is usually possible under mild basic condition. Three different methods have been tried, but none of them let to the preferred structure **3.80**. Table 3.9 summarizes the approached deprotection reactions.

Table 3.9: Deprotection reactions of **(3.82)**.

Reagent	Solvent	Reaction temperature	Reaction time	Comment
sodium carbonate[109-114]	methanol, water	room temperature	4 h	starting material not soluble
lithium hydroxide[115]	THF, methanol	room temperature	24 h	
potassium hydroxide[116]	water, dichloromethane	room temperature	1 h	triethyl benzyl ammonium bromide, phase transfer

Analysis of the data showed that under these mild basic conditions, the monomer is decarboxylated.

As a consequence, none of the shown reactions resulted in the desired monomer **3.80**. Only the treatment of **3.52** with concentrated hydrochloric acid yielded a very small amount of **3.80**. The so obtained monomer was then used in the following polymerization reactions and to synthesize oligomers.

3.2.3. Poly(thiophene carboxamide): Synthesis and Characterization

The first reaction with the new amino acid monomer **3.80** was a polycondensation, which returned poly(thiophene carboxamide)s. One of the standard protocols for condensations is a coupling reaction using *N*,*N*'-dicyclohexylcarbodiimide (DCC) and 4-dimethylaminopyridin (DMAP) in dichloromethane. The reaction was carried out at room temperature for a time period of four days to yield poly(thiophene carboxamide) **(3.83)**. Figure 3.49 illustrates the reaction scheme.

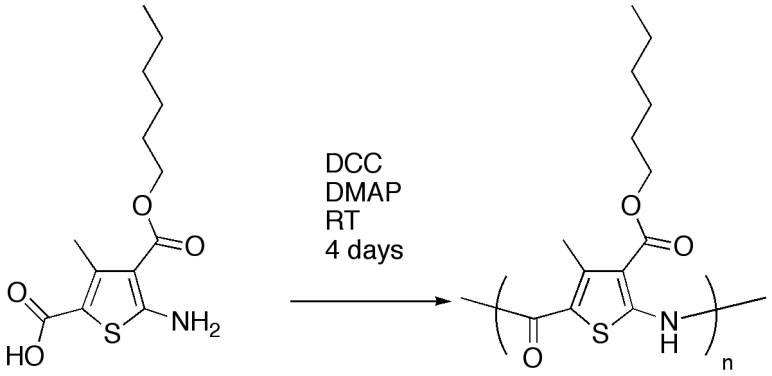

3.80 **3.83**

Figure 3.49: Polycondensation of **3.80.**

The first proof of fluorescence of the new structure was easily done by using the reaction mixture as ink to write on a piece of weighing paper. By illumination this piece of paper, the drawn image can be observed (Figure 3.50).

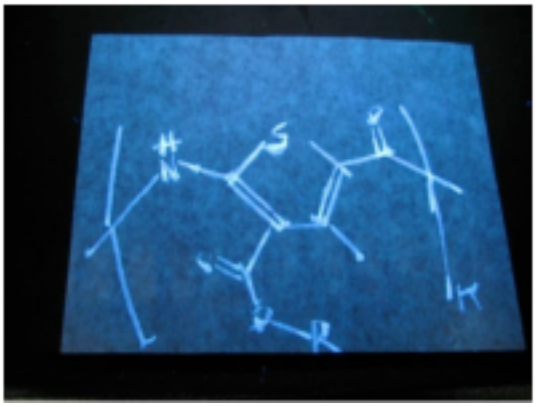

Figure 3.50: First proof of fluorescence of **3.83**.

Since this was only the first proof of fluorescence further analyses were done. After the polymerization the reaction mixture was analyzed by SEC and the crude reaction material was further separated by preparative SEC, whereas every 30 seconds a new fraction was taken. As expected these fractions represent polymers with more defined molar masses and narrow distributions than the original polymer (Figure 3.51; Table 3.10). Whereas the polymer shows a PDI around two, which was expected for a standard polycondensation, the different fractions of the preparative SEC show PDIs around 1.1 to 1.2. The SEC traces of the polymer and fractions 31 and 37 still show residual monomer. The fact, that monomer is still left after four days of reaction time, indicates that the condensation reaction is very slow und thus only low molecular weight polymers are obtained. Table 3.10 summarizes the SEC data of the different fractions. The highest molecular weight, which could be obtained, was 4800 g/mol, meaning a length of around 17 monomers for the polymer. The fractions with the lower molecular weight polymers show a separation of each different molecule. Fraction 31, for example, shows beside the monomer signal two more peaks for the dimer, respectively trimer. This fine structure is also observed in fraction 25 as well as in the SEC trace of the reaction mixture.

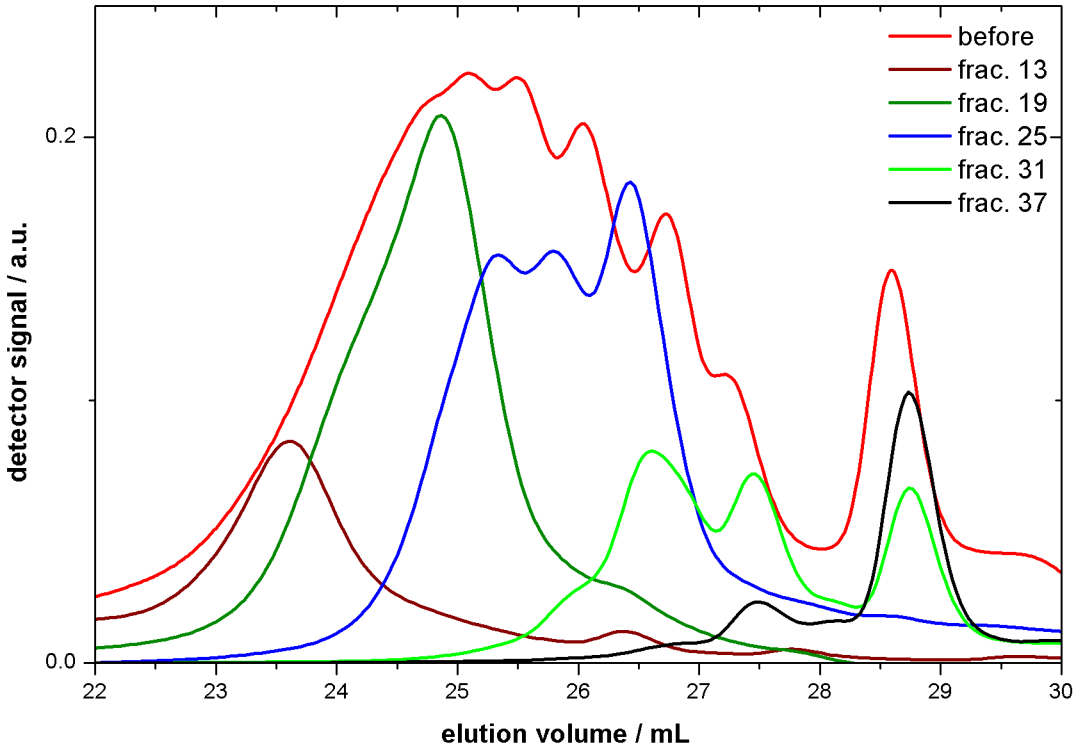

Figure 3.51: SEC of **3.83** and its fractions.

Table 3.10: SEC-data of **3.83** and its fractions.

Fraction	M_w / g/mol[1]	M_n / g/mol[1]	PDI	n
total	2000	1100	1.74	7.0
13	4800	3900	1.24	16.8
19	2800	2200	1.25	9.8
25	1500	1300	1.14	5.3
31	750	620	1.21	2.6
37	430	400	1.07	1.5

[1]Calibration was done using poly(styrene) standards.

Each fraction, representing a different molecular mass, shows a different degree of coloring. Where as the yellow color is the strongest for the 20th fraction, it turns lighter for the higher and lower fractions (Figure 3.52 top). The same trend is observed in the fluorescence of those fractions. In this case the lower fractions (with the higher molecular weights) show a light green fluorescence, whereas the lower molecular weights are blue fluorescing (Figure 3.52 bottom).

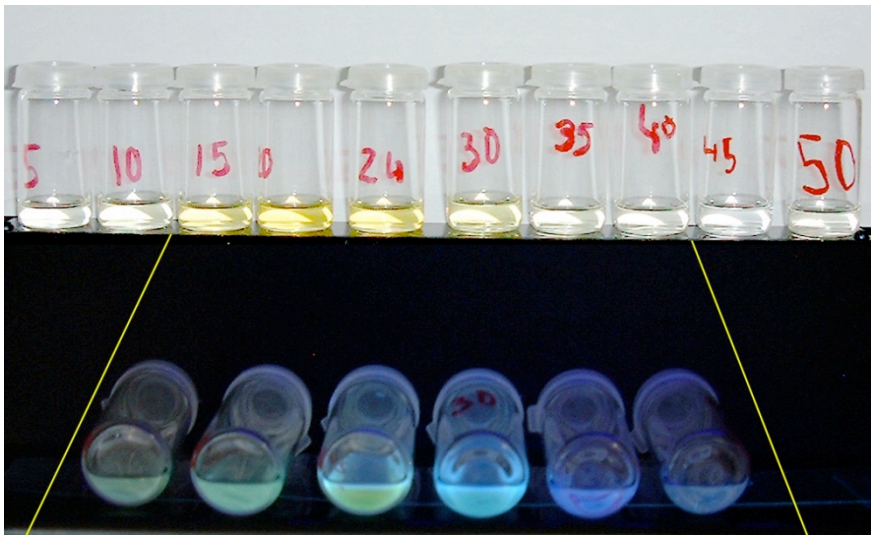

Figure 3.52: *top*: Picture of the different SEC-fractions of **3.83**.
bottom: Fluorescence of SEC-fractions of **3.83**.

Every fifth fraction beginning with the 5th to the 55th was analyzed by UV/vis spectroscopy, to reveal very interesting absorption phenomena, which are depending on the size of the polymer. Figure 1 shows the UV spectra of those SEC fractions. Very interesting is the fact that beginning from the 5th fraction to the 35th fraction the absorption at 365 nm is increasing, whereas from the 35th to the 55th fraction that maximum is again becoming smaller till it is nearly complete erased (Figure 3.53 a and 3.53 b). The highest absorption maximum at 365 nm is shown by fraction 35. In this case the relative absorption is even higher than the one at 300 nm. The concentration dependence measurements of fraction 35 show a small effect of the relative height of the two maxima at 305 nm and 365 nm. With decreasing concentration the absolute absorption at 305 nm decreases linear to the concentration (Figure 3.53 a) in contrast to the peak at 365 nm, which can be observed in the normalized spectra (Figure 3.53 d). In all cases the second maximum is higher than the first one, indicating that the relative height ratio is not strongly depending on the concentration, but more on the length of the polymer.

a)

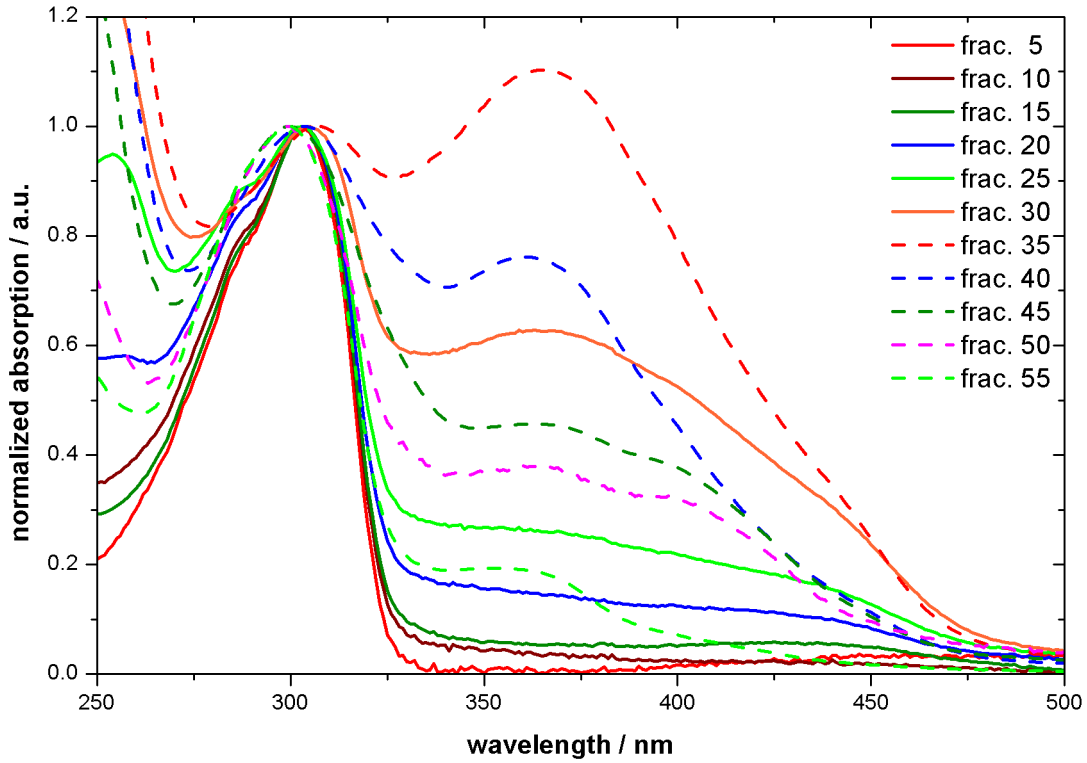
normalized absorption / a.u.
wavelength / nm
frac. 5
frac. 10
frac. 15
frac. 20
frac. 25
frac. 30
frac. 35
frac. 40
frac. 45
frac. 50
frac. 55

b)

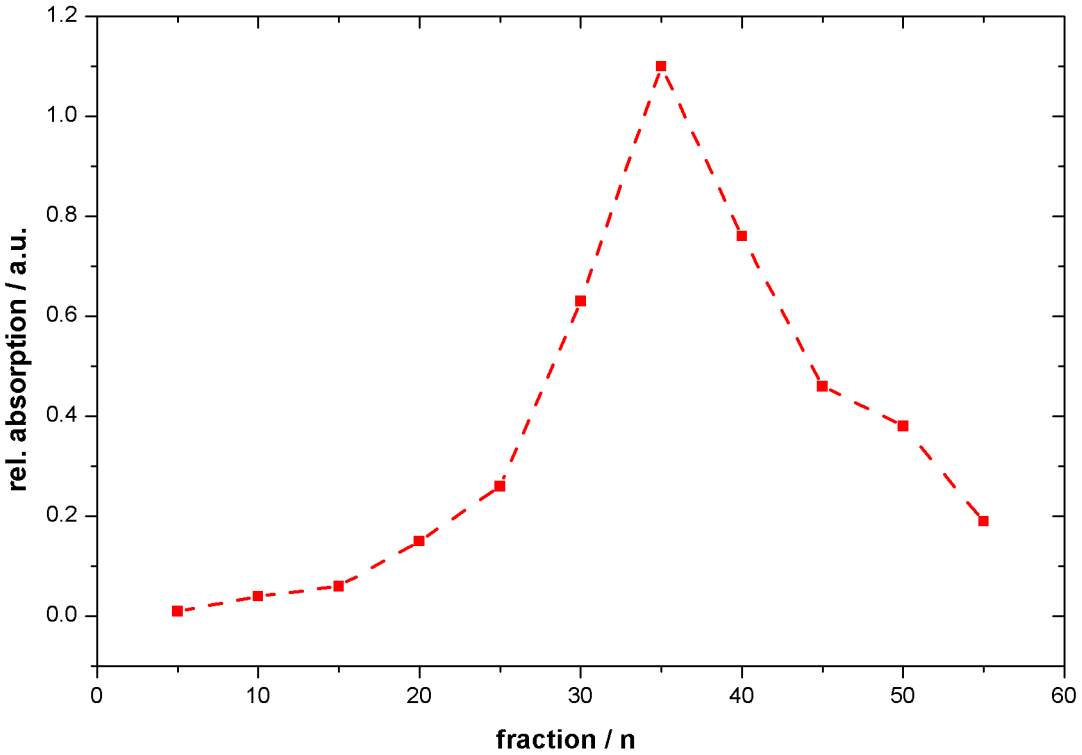
rel. absorption / a.u.
fraction / n

c)

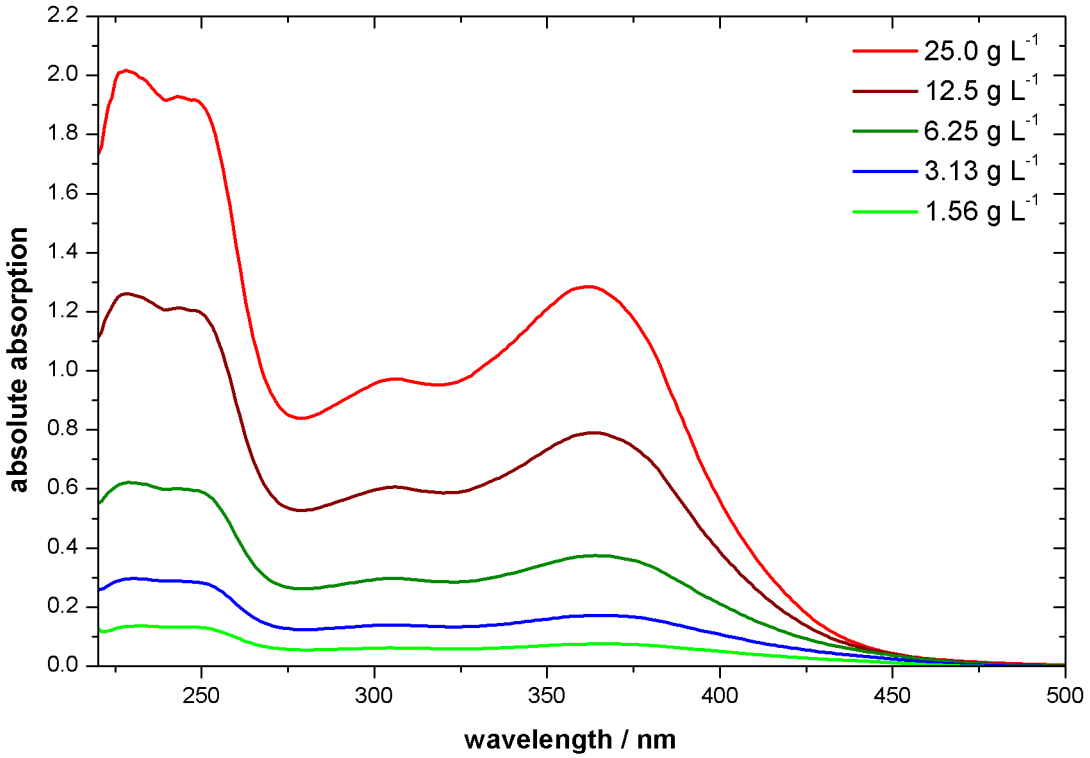

d)

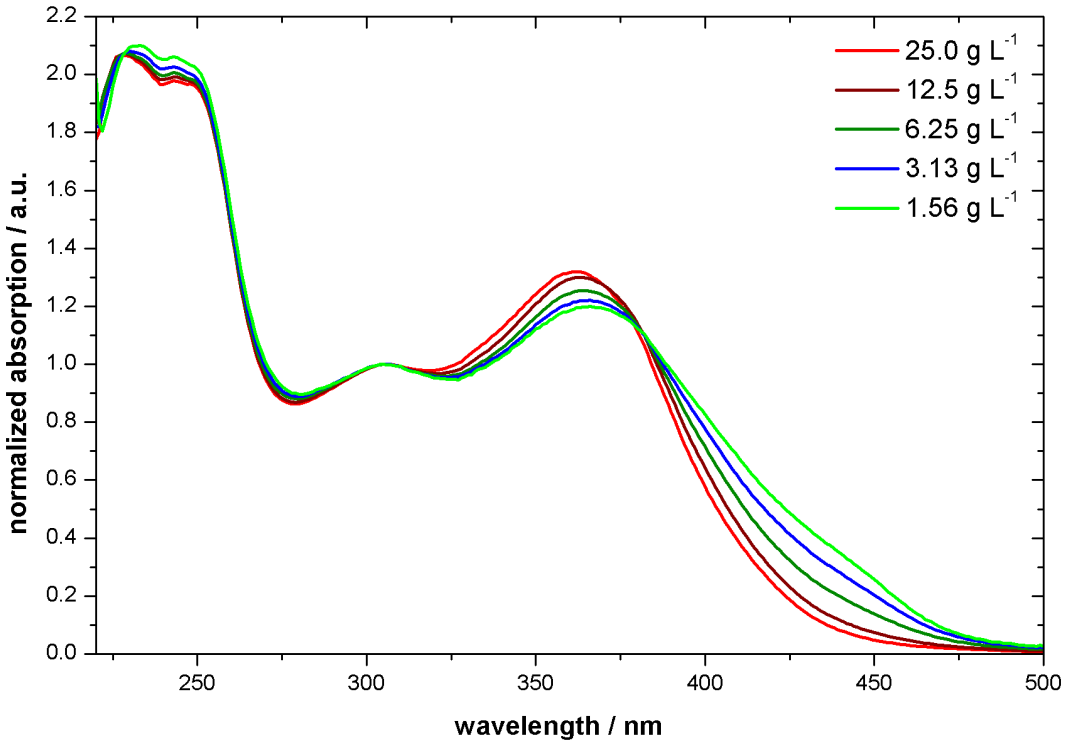

Figure 3.53: a) UV / vis spectra of SEC fractions of **3.83**, b) relative absorption at 365 nm of each 5th fraction of **3.83**, c) absolute and d) normalized absorption of different dilutions of fraction 35.

Photoluminescence spectroscopy at excitation wavelength of 365 nm of fraction 20 to 45 reveals a similar trend. Fraction 35 shows a maximum fluorescence at 465 nm whereas the others have a stepwise decrease at the peak compared to the peak around 430 nm (Figure 3.54 a and Figure 3.54 b). The maximum ratio of fraction 30 and 35 are nearly the same. In the case of fraction 30 it is only a little bit smaller. This effect is not observed in the UV/vis spectra, in where fraction 35 is clearly the maximum and the ration in the case of fraction 30 is nearly 50% smaller.

This new class of polymer exhibits very interesting effects in the UV/vis absorption and the photoluminescence. Depending on the size of the polymer the peak maximum at 365 nm in the absorption measurements increases from zero to a maximum value, which is higher than the normalized peak at 305 nm. After it reaches its maximum it will decrease again. The same tendency can be observed for the photoluminescence spectroscopy. Also here, the shoulder at 465 nm reaches its maximum in the 35th fraction, before it decreases again till it is superimposed by the tailing from the first peak at 435 nm. All these effects show a clear conjugation between the thiophene rings over the amide bonds, which makes the material interesting for optoelectronic devices. However the absorption phenomena have to be more intensively studied, including better polymerization techniques in order to get narrowly defined molecular weights and higher masses. A stepwise synthesis to monodisperse oligomers will help to understand these phenomena and will be addressed in the next chapter. By stepwise synthesis of well-defined oligomers each molecule can be fully characterized. Since the SEC data shows quite small oligomers (length from three to 19) it might by possible to synthesize those molecules and get detailed characteristics.

a)

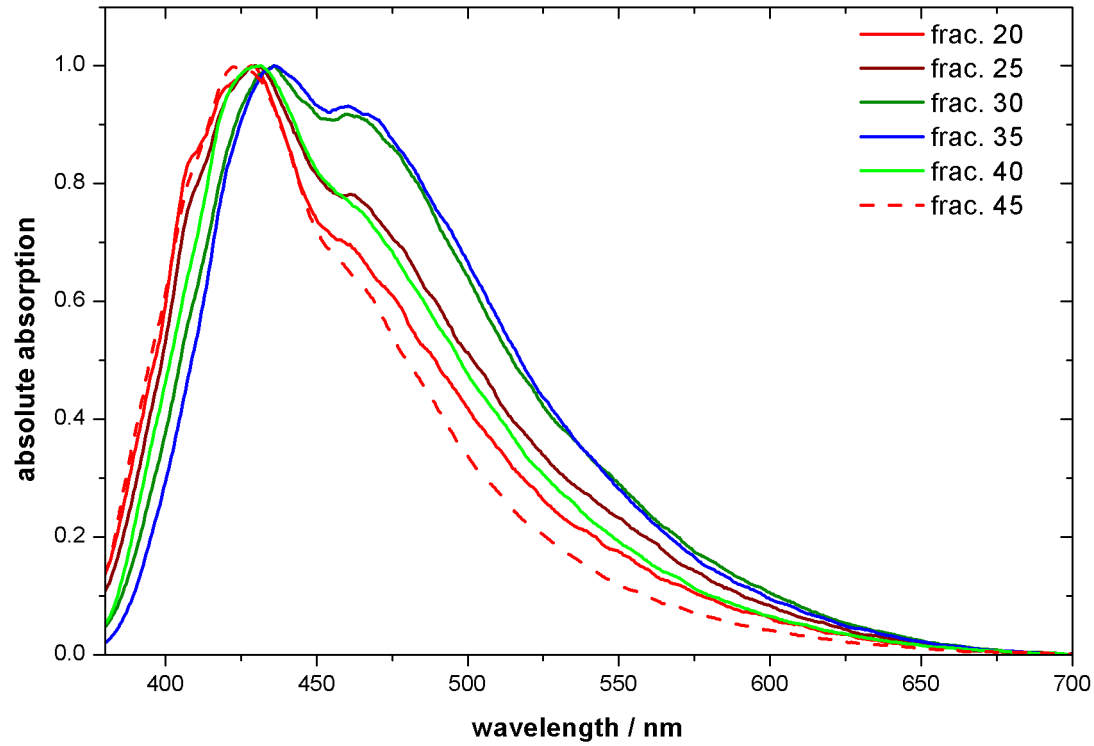

b)

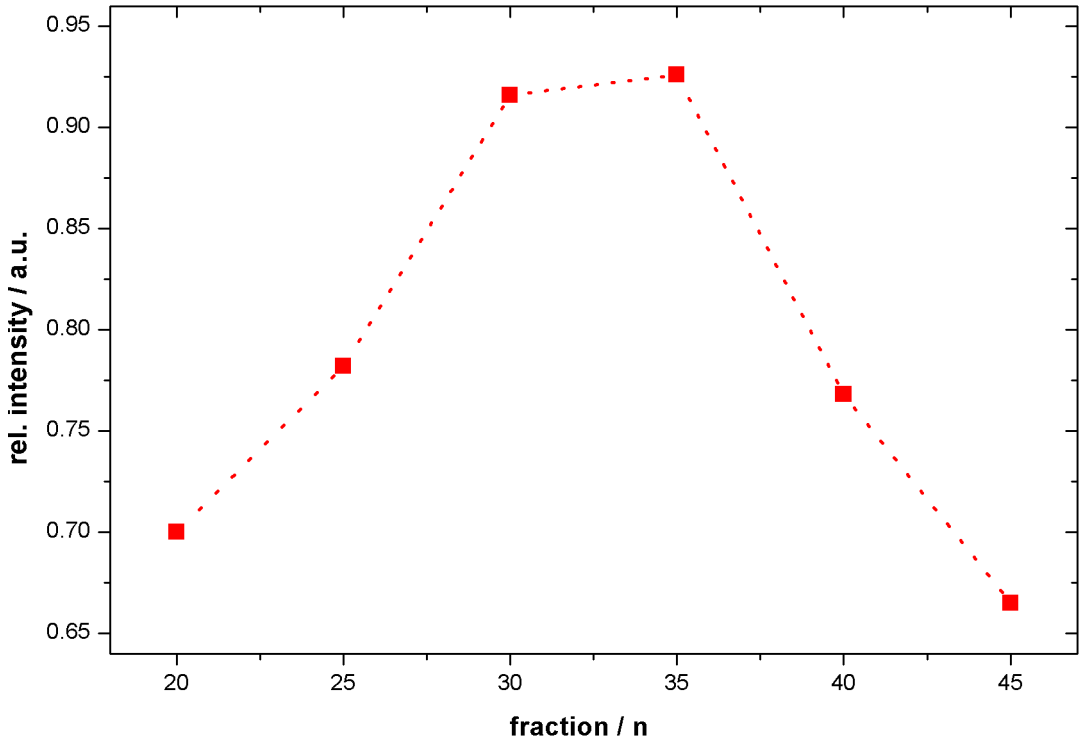

Figure 3.54: a) Photoluminescence spectra of SEC fractions of **3.83**, b) relative photoluminescence at 465 nm of SEC fractions of **3.83**.

3.2.4. Oligo(thiophene carboxamide)s: Synthesis

The poly(thiophene carboxamide)s show interesting effects in their UV/vis absorption and fluorescence spectra depending on the length of the polymer. By synthesizing defined oligomers it is possible to analyze those effects depending on the length of the oligomer. UV/vis absorption and fluorescence maxima shifts can be measured and beginning from those data for well-defined molecules, their corresponding polymer properties can be predicted.

For the synthesis of the well-defined oligomers, two approaches are possible:

a) Solid-phase supported synthesis.
b) Solution synthesis.

In the first case a peptide synthesizer is used and the oligomer is stepwise synthesized using standard protein protection and resin chemistry. In the second case, solution-synthesis, protective groups and their corresponding chemistry is also used. Compared to the resin-based synthesis, the workup procedures are more complex, on the other side; larger amounts of material can be readily synthesized in solution.

3.2.4.1. Solid-Phase Supported Synthesis

The synthesis of the 9-fluorenylmethyloxycarbonyl protected thiophene amino acid **3.79** (Figure 3.55) is already shown in chapter *3.2.2.* and can be done in multi gram dimensions in four steps.

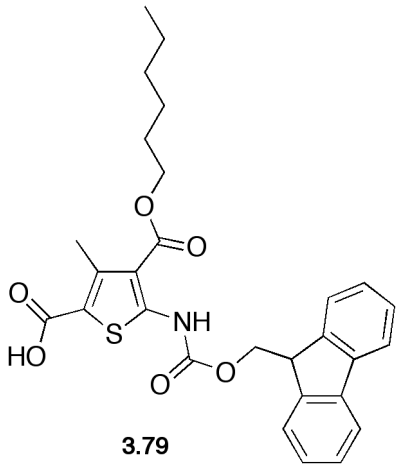

3.79

Figure 3.55: Fmoc-protected thiophene amino acid **3.79**.

The solid-supported synthesis of aromatic amino acids was already described early in the literature. Fmoc-protected *p*-aminobenzoic acid was stepwise added to a *Wang* resin

up to the octamer. The so synthesized oligo(*p*-benzamide)s (OPBAs) where analyzed in the meaning of UV/vis absorption and aggregation behavior. For the first synthesis of oligo(thiophene carboxamide)s the same protocols as for the OPBAs was used. The monomer **3.79** was activated using one equivalent of thionyl chloride in *N*-methyl-2-pyrrolidone (NMP) yielding the thiophene acid chloride monomer **3.84**, which can then be readily used in the peptide synthesizer. Figure 3.56 shows the synthetic scheme using a *Wang* resin. The first reaction is an ester synthesis with the hydroxyl groups of the *Wang* resin. The subsequent removal of the Fmoc protection group with piperidine is monitored by an UV/vis detector, which detects the amount of Fmoc being released from the resin-bound oligomer. The next addition of the monomer is induced by adding new thiophene acid chloride **3.84** yielding **3.85** with n=2. Removal of the protective group by piperidine is again monitored by the UV/vis detector. The Fmoc cleavage protocol shows addition of the first monomer to the alcohol of the resin but only 70% of the free functional groups reacted with the second monomer (Table 3.11 Reaction 1, Figure 3.54a). The reaction conditions in all coupling steps where four equivalents of monomer and a reaction time of one hour and 10 mol% DMAP in a NMP/DCM mixture. Beside the fact that only 70% of the free amine groups did react with the acid chloride, the signal of the first coupling is too low. Regular signal heights of the used amount of *Wang*-resin should have the double height, which was confirmed by flushing the UV-detector with the expected amount of dibenzofulvene (Figure 3.57). Comparing those signals to the one obtained from the first experiment, it is clearly visible that the first coupling was not sufficient. Therefore, the unreacted alcohol groups from the *Wang*-resin need to be end-capped, in order to prevent the reaction of the next monomeric unit with those groups. The end capping was done in all of the following experiments. *p*-Nitrobenzoyl chloride was added to the resin and was reacted before Fmoc was removed from the oligomers.

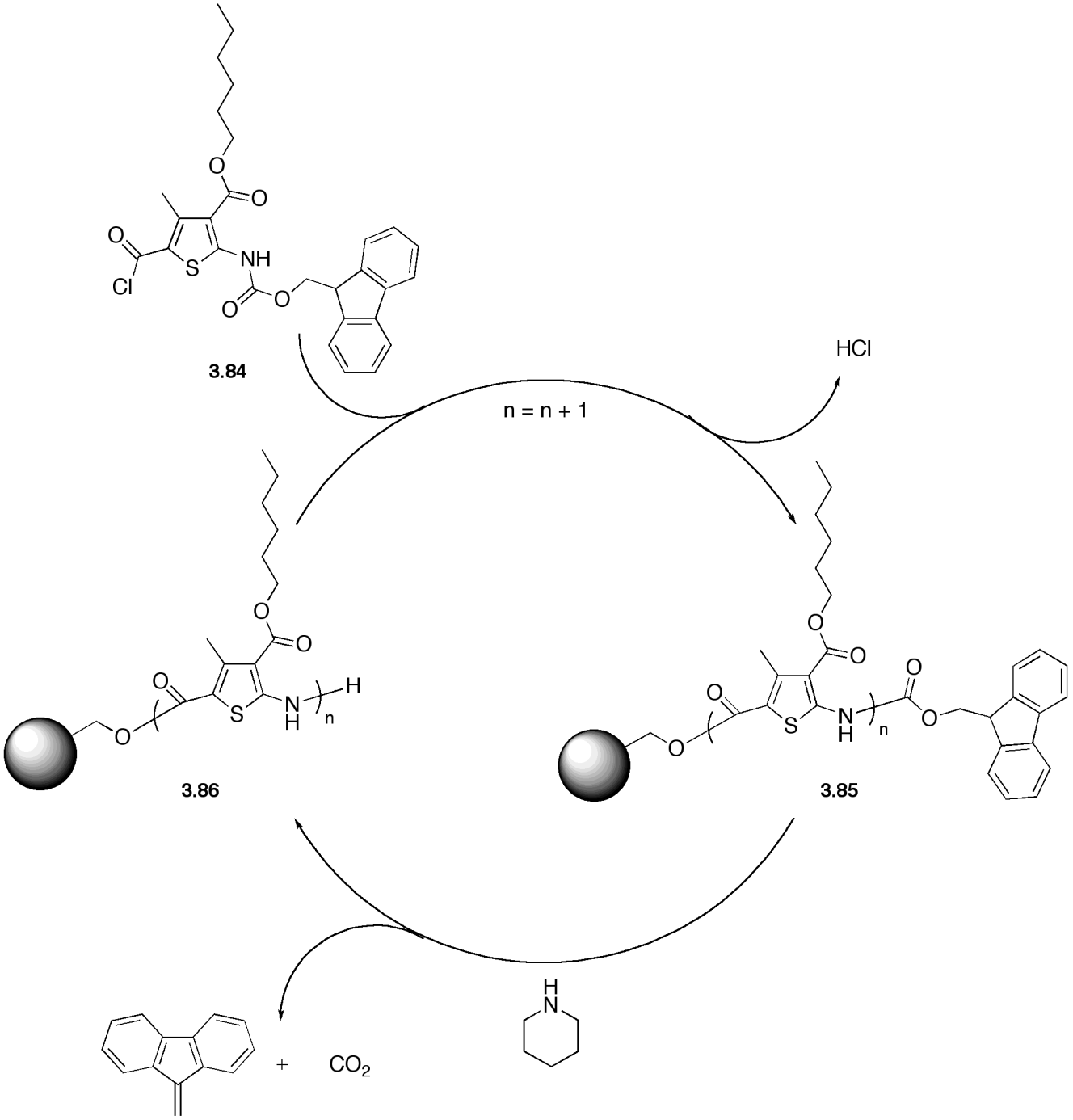

Figure 3.56: Oligo(thiophene carboxamide) synthesis by solid-supported method.

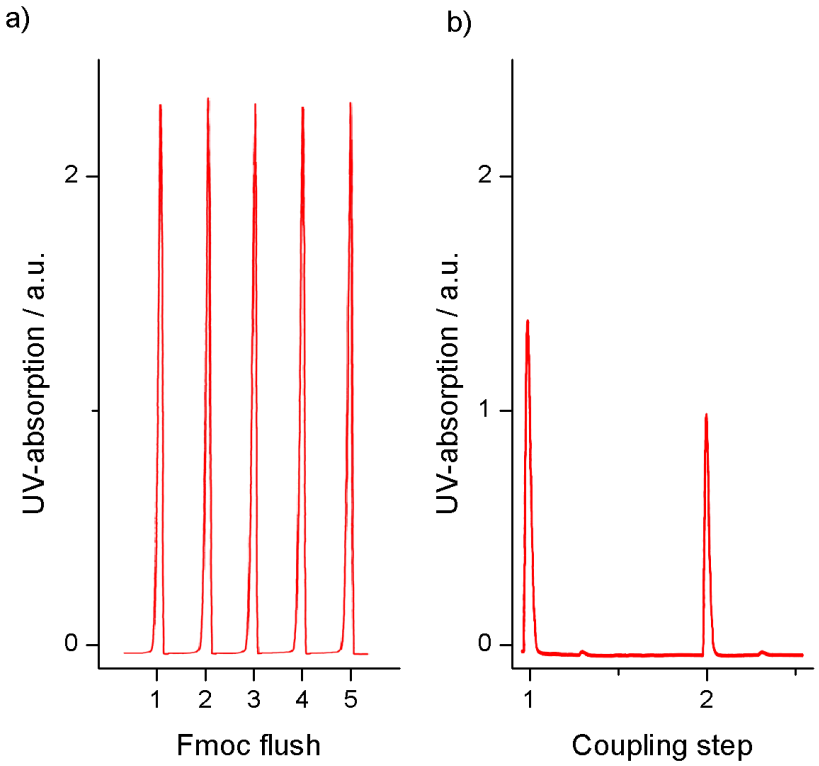

Figure 3.57: a) Protocol of Fmoc flushing. b) Coupling protocol of the first experiment

Taking the incomplete first and second coupling into account, different activations may help to overcome the partial couplings, so different synthesis of acid chlorides have been tried. Instead of using oxalyl chloride, thionyl chloride (Table 3.11 experiment 2) or phosphorous pentachloride (Table 3.11 experiment 3 and 4) have been used to generate the corresponding acid chloride of **3.79**. The coupling conditions (one hour reaction time and four equivalents of monomer) where the same in all examples. For the case of thionyl chloride 10 mol% DMAP have been applied, where as for phosphorous pentachloride one equivalent DMAP respectively two equivalents where added. Comparing the Fmoc cleavage signal of experiment 2 with the first one, the signal of the first coupling is smaller than for experiment 1. In view of the fact that the same amount of *Wang*-resin was used in all reactions, this signal should be the same size if the reaction would have the same efficiency. The smaller signal indicates that the so activated monomer is not as reactive as the one activated by oxalyl chloride. The signals in the cases of the phosphorous pentachloride activations are even smaller. A strong influence of the amount of DMAP on the signal strength is shown here. Adding one equivalent of DMAP to the coupling reaction, will only result in a signal of only 15% compared to the signal of experiment one, where as two equivalents of DMAP will result in about 45% of the signal size. Thus far, the activation through acid chlorides was not satisfying, anhydrides where synthesized and

used in the coupling steps. Figure 3.58 a shows the synthesized asymmetric anhydride **3.87** where as Figure 3.58 b shows the symmetric anhydride **3.88**.

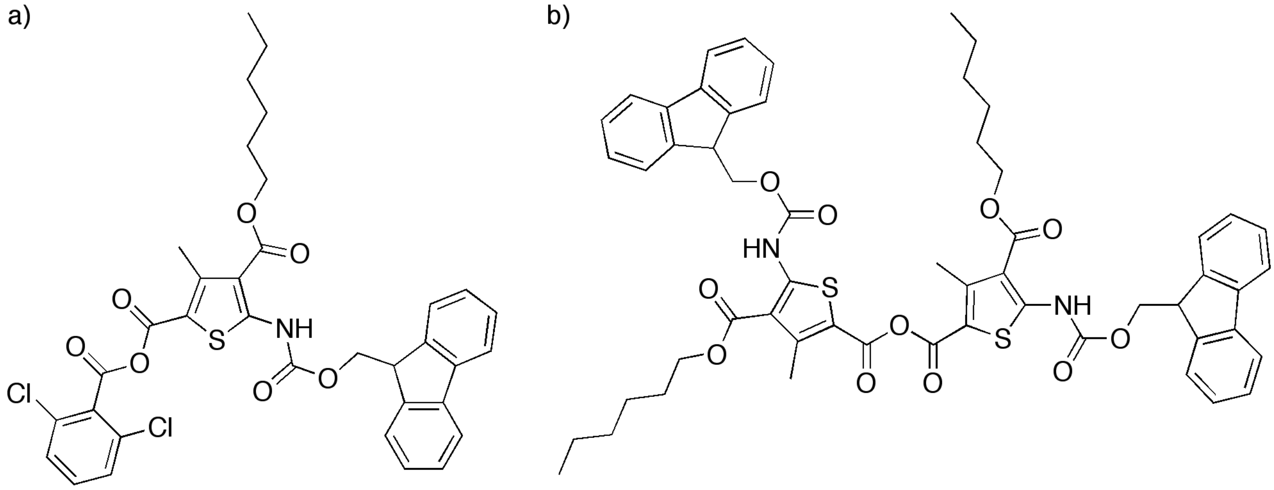

3.87 **3.88**

Figure 3.58: a) asymmetric **3.87** and b) symmetric anhydride **3.88** of **3.79**.

In the first reaction, the asymmetric anhydride was used (Table 3.11 experiment 5) under regular reaction conditions, meaning a coupling time of one hour and four equivalents of monomer. The Fmoc cleavage signal shows around 15% conversion of the coupling step. The result of the symmetric anhydride (Table 3.11 experiment 6; same reaction conditions) is even lower and only around 8% compared to the first experiment. No activation respectively coupling procedure resulted in the desired oligomer. The highest efficiency was obtained by the activation with oxalyl chloride, so the same reaction parameters where used, but the temperature was increased to 80°C and only have of the amount of *Wang*-resin was used. As this temperature cannot be applied in the peptide synthesizer, the coupling reaction was carried out in standard glass equipment. Only the deprotection was done in the synthesizer in order to record the amount of removed Fmoc. The first step shows nearly full coupling, as the signal height indicates, where as the second step shows only little conversion. So increasing temperature during the coupling reaction improves the reaction of the *Wang*-resins alcohol groups with the first monomer, but not the reaction with the free amine of the monomer with the next monomeric unit (Table 3.11 experiment 7). The eighth experiment was done applying a different resin: glycine modified *Wang*-resin. The resin carries an initial Fmoc group, which is removed before the first thiophene amino acid unit is added. By this way each addition can be compared to the first deprotection of the glycine. Being aware of the results from the first experiments, the coupling reaction was applied two times, before the removal of the protection group. The

first addition shows nearly 85% conversion, meaning, that the addition of the acid chloride to the glycine amine nearly works quantitative (Table 3.11 experiment 8). In contrast to the first addition, the second addition only shows about 15% conversion. This is a highest conversion observed in all experiments compared to other experiments. Only experiment one shows a higher conversion, but in this case, no end capping was applied, thus it cannot be compared to the last experiment, because free alcohol groups might have reacted besides the amines of the monomeric unit.

In summary, the Fmoc based coupling procedure using standard peptide chemistry does not lead to the desired oligomers. No experiment showed sufficient coupling results. Even the first addition to the plain resin does not work in high yields in most cases. Only the last two experiments could provide high coupling yields for the first step, but the second addition did not get higher conversions than 15%.

Based on these results a different synthetic strategy need to be found in order to synthesize the oligo(thiophene carboxamide)s. Therefore solution based syntheses was applied in order to obtain those structures. The monomer **3.52**, which is directly obtained from the *Gewald*-synthesis, can be readily used for this purpose.

Table 3.11: Fmoc cleavage protocols of various reactions.

Nr	Resin	Solvent	Activation	Coupling conditions	End-capping[1]	Fmoc cleavage protocol[2]
1	*Wang-OH*	DCM, NMP	excess oxalyl chloride	4 eq. monomer, 1 h, RT, 10 mol% DMAP	No	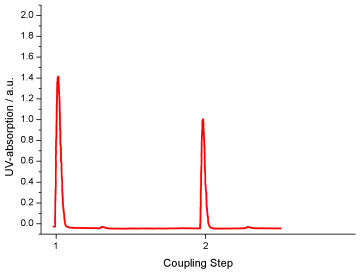
2	*Wang-OH*	DCM, NMP	1 eq. thionyl chloride in NMP	4 eq. monomer, 1 h, RT, 10 mol% DMAP	Yes	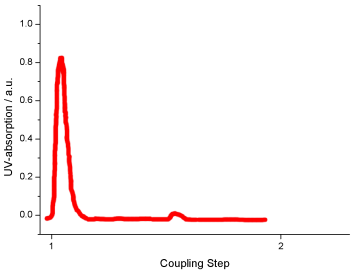
3	*Wang-OH*	DCM, NMP	1 eq phosphorus pentachloride	4 eq. monomer, 1h, RT, 1 eq DMAP	Yes	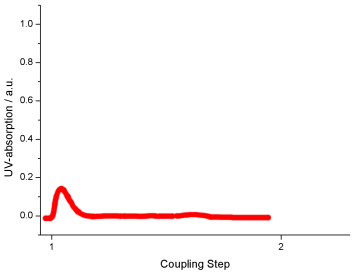
4	*Wang-OH*	DCM, NMP	1 eq phosphorus pentachloride	4 eq. monomer, 1 h, RT, 2 eq DMAP	Yes	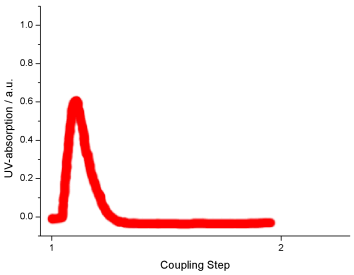
5	*Wang-OH*	DCM, NMP	Asymmetric anhydride **(3.87)** with DCB[3]	4 eq. monomer, 1 h, RT	Yes	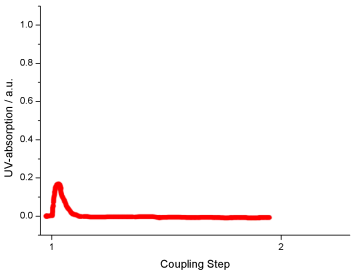

Nr	Resin	Solvent	Activation	Coupling conditions	End-capping[1]	Fmoc cleavage protocol[2]
6	*Wang*-*OH*	DCM, NMP	Symmetric anhydride **(3.88)**	4 eq. monomer, 1 h, RT,	Yes	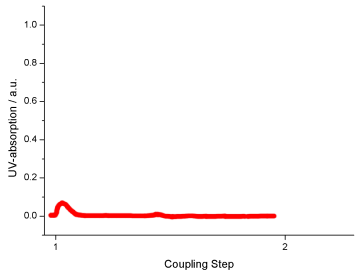
7	*Wang*-*OH*	NMP	excess oxalyl chloride	4 eq. monomer, 6 h, 80°C, 10 mol% DMAP	Yes	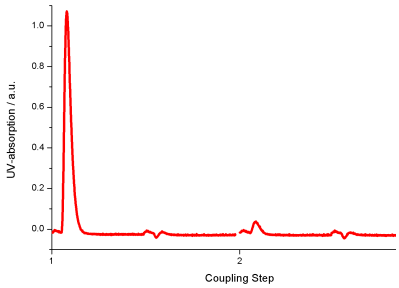
8	*Wang*-*Glycine* -NH_2	DCM, NMP	excess oxalyl chloride	2 couplings: 4 eq. monomer, 4 h, RT, 10 mol% DMAP	Yes	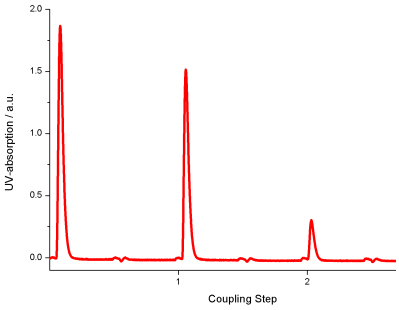

[1]End-capping was done with *p*-nitrobenzoyl chloride [2]Experiment 1-7 has been run with half the amount of *Wang*-resin. [3]DCB = 2,6-dichlorobenzoyl chloride

3.2.4.2. Solution-Synthesis

The previous chapter dealt with the solid-supported synthesis of oligo(thiophene carboxamide)s and as a result, it is not possible to synthesize those oligomers with the used monomer **3.79**. It was possible to add the first monomer nearly quantitatively to the *Wang*-resin, but the addition of the second monomer was not satisfying. Thus, a different strategy to the new oligomers was needed. In this chapter the synthesis of these molecules is described using a solution base method, with needed workup procedures for each step and as a consequence a better control over purity is accessible.

The free amino group of the used monomer **3.52** (Figure 3.59) led to a synthesis in which activated carboxylic acids reacted with this amine. After deprotection of the ester and subsequent activation the next addition of a new monomer is possible.

The dimer was synthesized by reaction of thiophene-(2)-carbonyl chloride with the *tert*-butyl ester protected thiophene amino acid **3.52** in THF/pyridine (3:1) for 24 hours at room temperature. After recrystallization in 1-hexanol **3.90a** is received in 80% yield. In contrast to the deprotection of the monomer **3.52**, the removal of the *tert*-butyl ester with 98% aq. trifluoroacetic acid (TFA) is possible and after recrystallization from 1-hexanol the dimer **3.91a** is yielded in 72% (Figure 3.59).

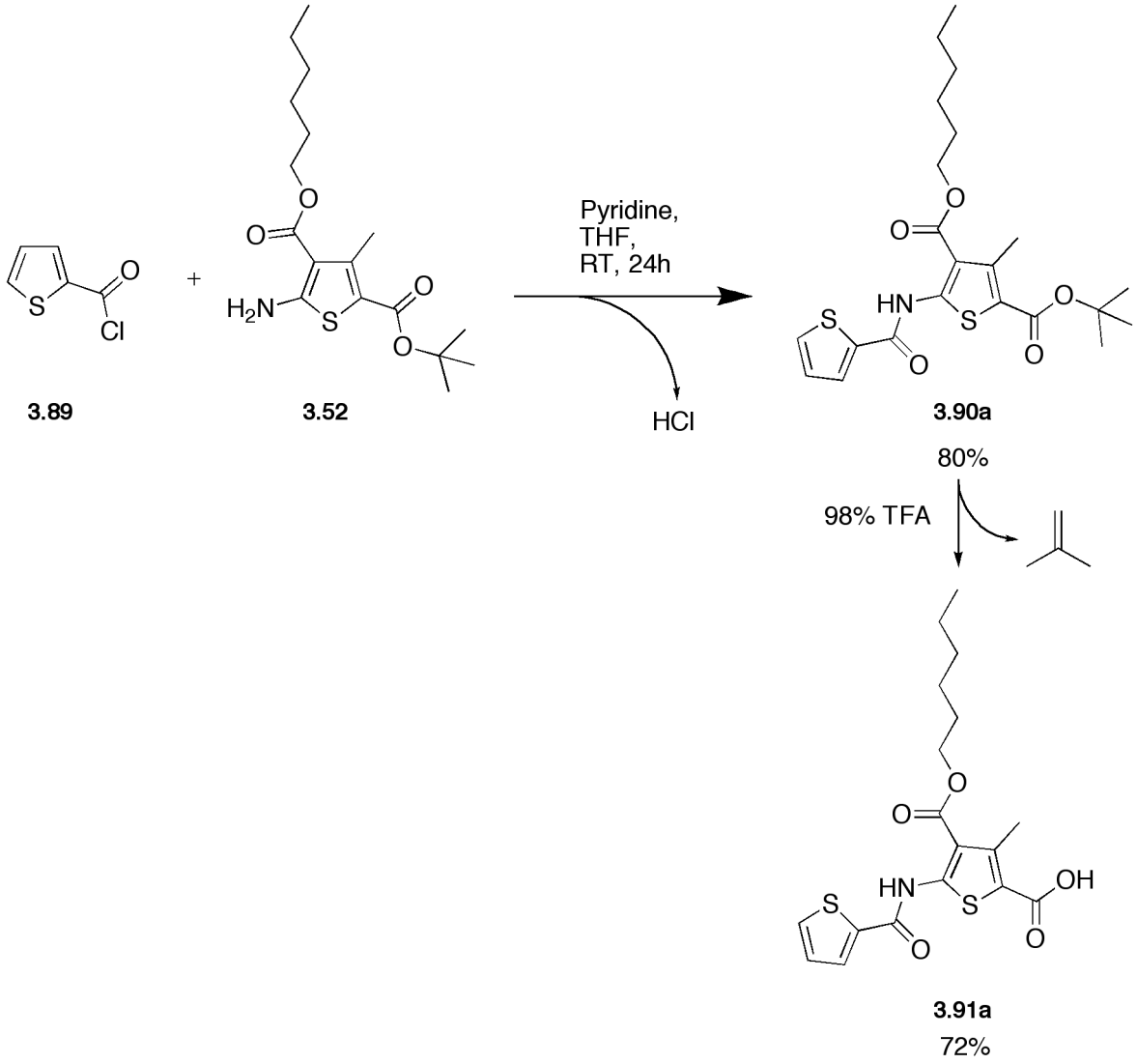

Figure 3.59: Synthesis of the dimer **3.91a.**

Activation of **3.91a** with oxalyl chloride and the following reaction of the resulting acid chloride with **3.52** in THF/pyridine (55:25) provided the trimer **3.90b**, which can also be recrystallized from 1-hexanol (Figure 3.60). The deprotection with 98% aq. TFA and recrystallization from 1-hexanol yields 85% of the trimer **3.91b**. Whereas the synthesis of the tetramer **3.90c** carrying the *tert*-butyl ester is possible using the above-mentioned conditions (activation with oxalyl chloride, THF/pyridine, room temperature) the cleavage of the ester is not quantitatively possible. The deprotection with 98% aq. TFA results mainly in decarboxylated tetramer **3.92** and not in the desired tetramer carboxylic acid **3.91c** (Figure 3.61). Since the decarboxylated product is not usable in further steps, the tetramer **3.91c** was synthesized from the unprotected thiophene amino acid **3.80**. The trimer acid **3.91b** was activated using oxalyl chloride and dissolved in THF and pyridine and a solution

of **3.80** in THF was added. As both tetramers cannot be recrystallized anymore, column chromatography was useful to purify the oligomers. Applying a mixture of chloroform and ethyl acetate (95:5) yielded 61% of **3.90c** and 59% of **3.91c** respectively. The pentamer carboxylic acid **3.91d** was synthesized with the same method, the shorter tetramer was (Figure 3.61). After activation of **3.91c** with oxalyl chloride, the acid chloride was dissolved in THF and pyridine and the resulting solution was reacted with **3.80** dissolved in THF. Again column chromatography in chloroform and ethyl acetate (90:10) yielded 54% of **3.91d**.

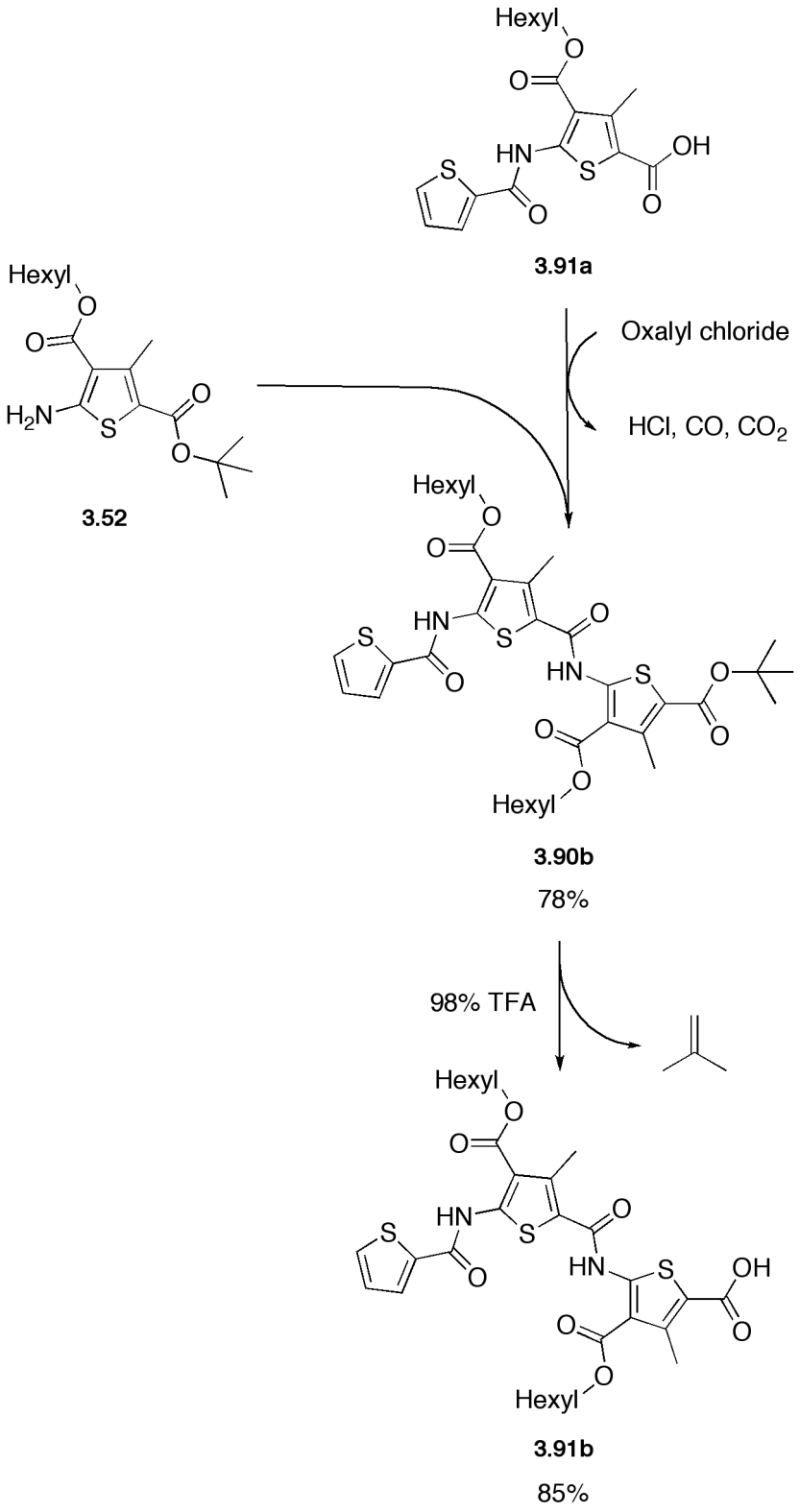

Figure 3.60: Synthesis of trimer **3.90b** and **3.91b**.

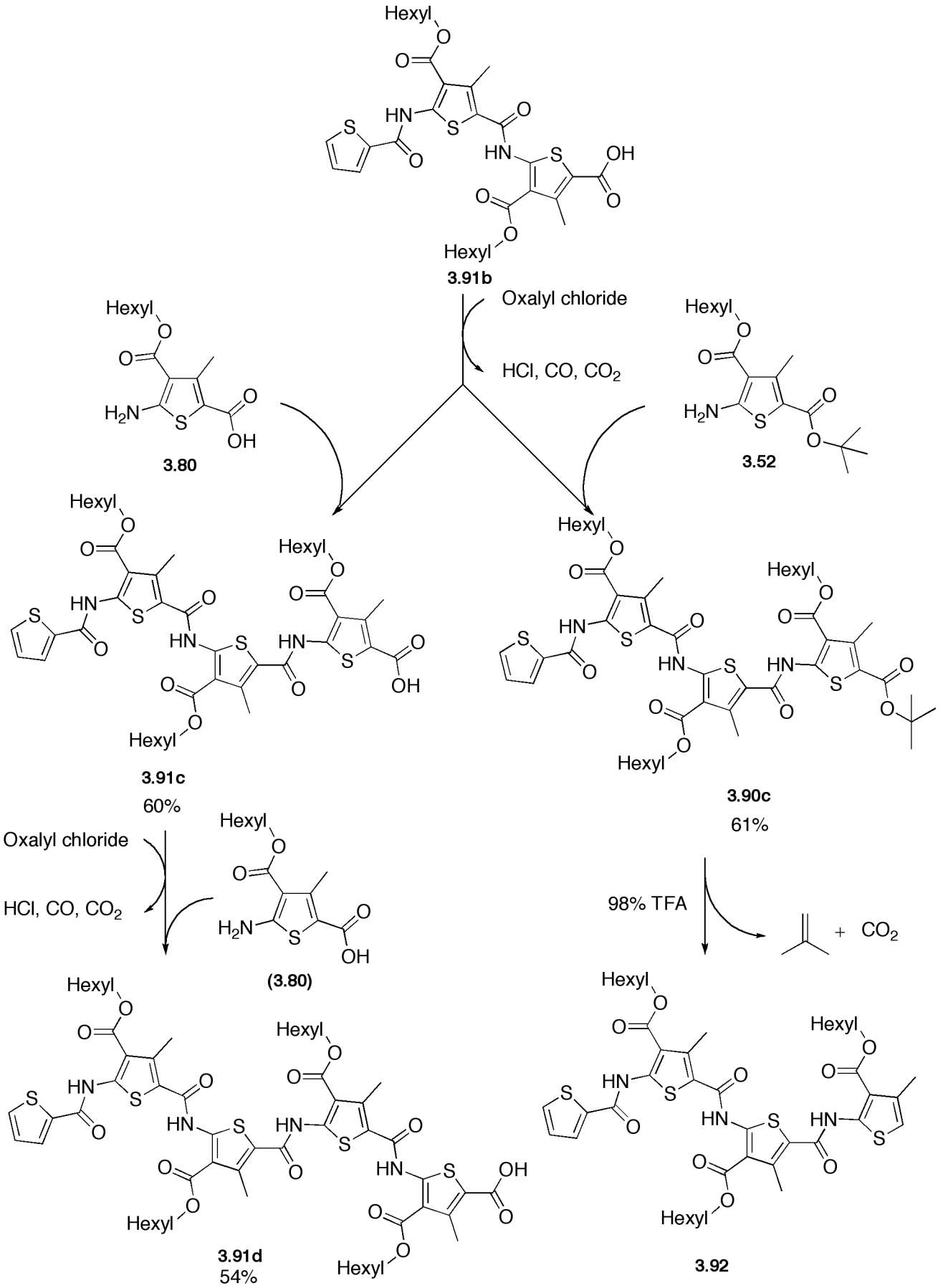

Figure 3.61: Synthesis of tetramers **3.90c** and **3.91c** and pentamer **3.91d**.

3.3. Results and Discussion

The oligo(thiophene carboxamide) up to the pentamer have been successfully synthesized. The absorption spectroscopy in dichloromethane of the different oligomers revealed a red shift depending on the degree of oligomerization (Figure 3.62). The monomer has an absorption maximum at 308 nm, whereas the pentamer has a maximum at 365 nm and a shoulder with higher wavelength at 374 nm so a continuous increase of λ_{max} with the growing chain length is observed. While the difference between the monomer and dimer is 24 nm, the step of λ_{max} between the tetramer and pentamer is negligible, but the difference between λ_{max} of the tetramer to the wavelength of the observed shoulder of the pentamer is 10 nm. As already known from oligo(thiophene)s[5,36] the difference between each step is decreasing. Plotting the energy against the inverse chain length, a linear dependence beginning with the dimer to the pentamer is observed. The linear regression[5,36] through the maximums of the dimer to tetramer reveals an absorption maximum of 406 nm for the polymer (Figure 3.63 *red line*). A more precise fit was published by Meier et al.[117] and is shown in equation 1. $E_{i,1}$ is the absorption energy of the parent compound, the monomer and $E_{i,\infty}$ are the limiting values for n → ∞. Solving this equation for $E_{i,\infty}$ lead to λ_{max} for the polymer and is shown as the *green* and *blue line* in Figure 3.63. Interpolation of the energy maximums from the monomer to the pentamer results in a to λ_{max} value of 375 nm or 391 nm for the poly(thiophene carboxamide). The different values are the result of the different interpretation of the pentamer's spectrum. If λ_{max} is used (Figure 3.63, *green* data), 375 nm are found and if the shoulder is used for the fitting (Figure 3.63, *blue* data), 391 nm is the predicted value for the polymer.

$$E_i(n) = E_{i,\infty} + (E_{i,1} - E_{i,\infty})e^{-a_i(n-1)} \qquad \text{(eq. 1)}$$

The molar extinction coefficients ε of the oligomers **3.91a-d** are to some extent higher than ε from the monomer **3.52**. The logarithmic value of ε for the monomer is 4.16, whereas the oligomers show values between 4.57 and 4.87. Comparing these coefficients to those of regular oligo(thiophene)s, one recognized that they are in the same order (lg ε: usually 4.4 to 4.8 for terthiophene to sexithiophene).[92]

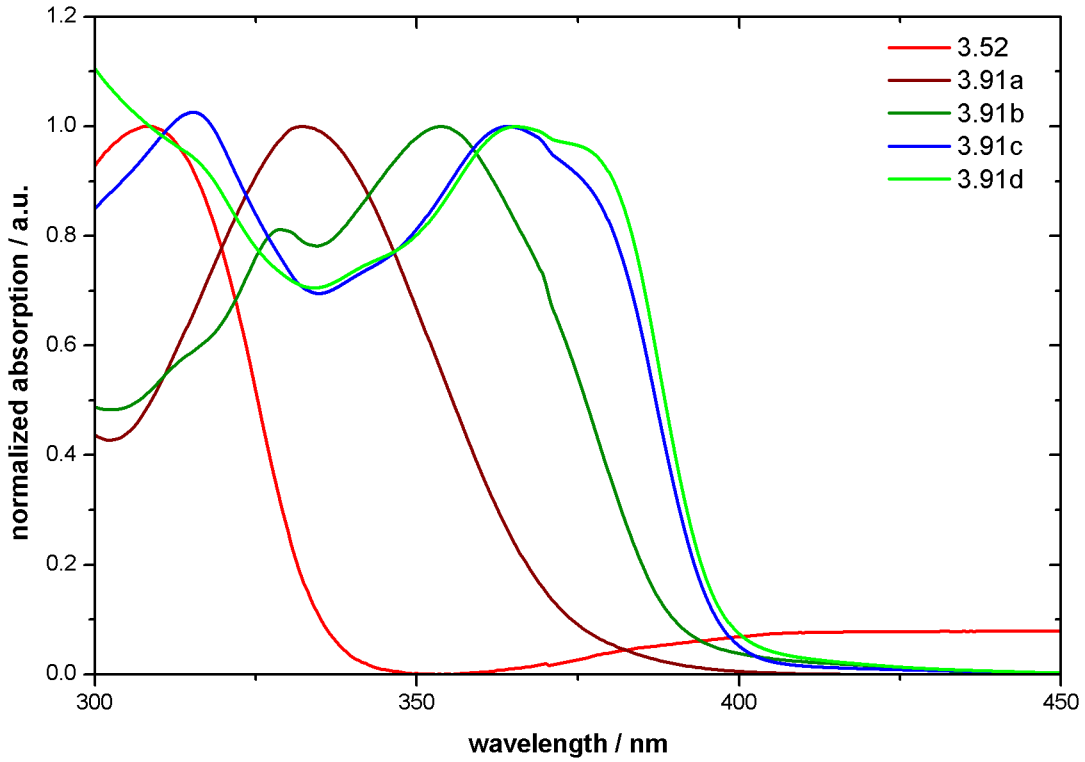

Figure 3.62: UV/vis absorption spectra of the oligomers in dichloromethane showing a red shift with increasing chain length (2 x 10^{-3} mg/mL).

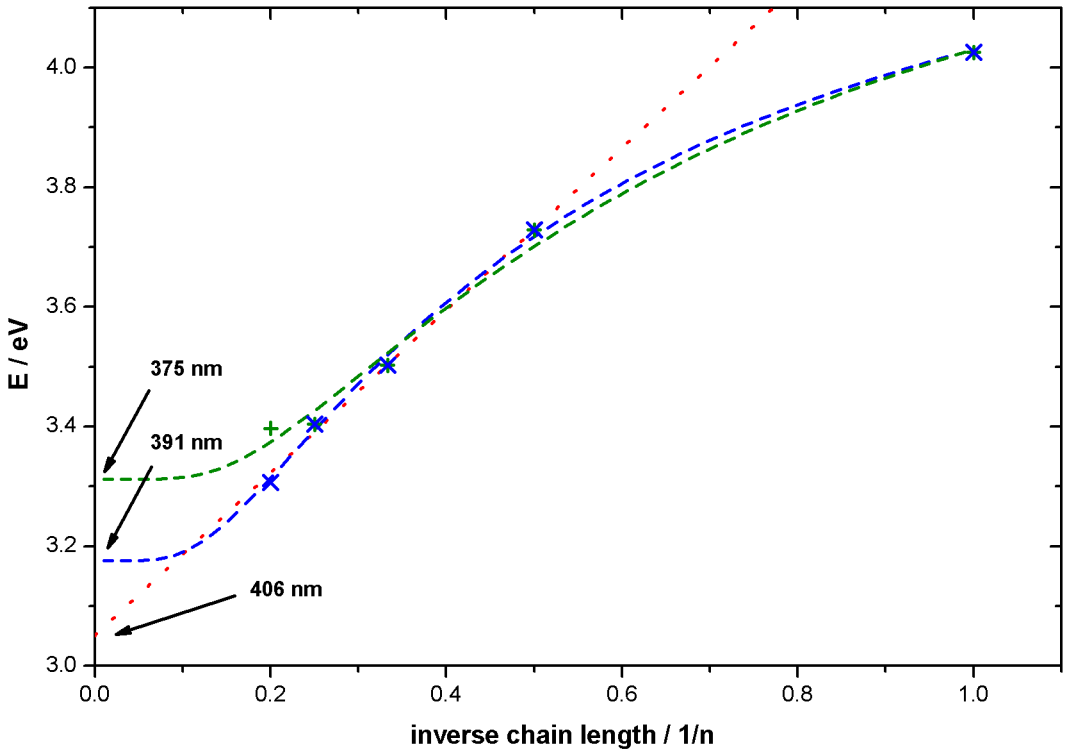

Figure 3.63: Plot of the absorption energy versus the inverse chain length: *red* linear regression *green* and *blue* fitted according to equation 1.

To analyze the effect of solvent polarity, *N*,*N*-dimethylformamide was chosen to measure the absorption spectra of the oligomers (Figure 3.64) in a more polar environment. In contrast to the spectra in dichloromethane, the first absorption maximum is not red-shifted in all cases. Only the mono-, di- and trimer show a bathochromic shift. For the tetra- and pentamer λ_{max} is hypsochromic. In contrast to the solutions in the nonpolar solvent, the oligomers in DMF show a strong second maximum, which appears for the tri-, tetra- and pentamer, whereas the dimer does not show this maximum. The wavelength of this absorption maximum is around 430 nm. Its appearance in the polar solvent DMF, indicate that it is a charge transfer band, which can result for molecules where a charge separation is possible, which is stabilized by the polar solvent molecules.

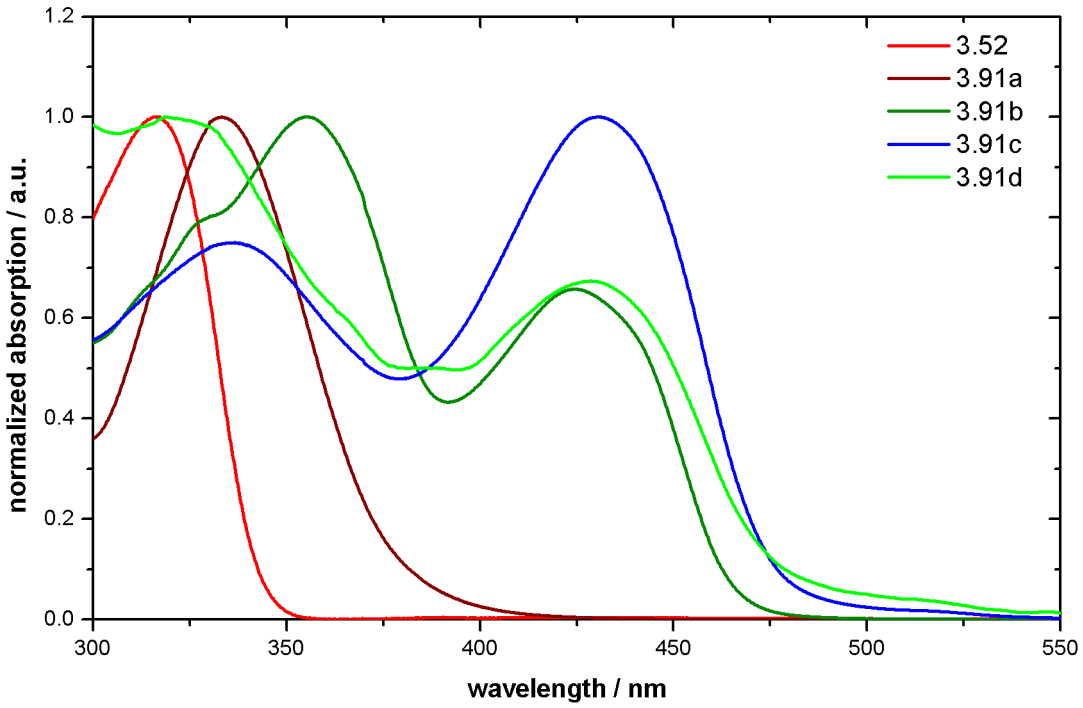

Figure 3.64: UV/vis spectra in DMF of the mono-, di- and trimer showing a red-shift of λ_{max}. The longer oligomers (trimer to pentamer) have a second absorption maximum located at 430 nm (2 x 10^{-3} mg/mL).

The fluorescence spectra in dichloromethane (Figure 3.65) also show a trend for λ^{F}_{max} for the oligomers: The fluorescence maxima are hypsochromically shifted, beginning from the dimer to the pentamer, whereas the monomer is not fluorescent. Two sets of fluorescence spectra of the oligomers in DMF with different excitation wavelengths have been measured (Figure 3.66 and 3.67): excited at the first absorption maximum of each oligomer (between 330 nm 360 nm) and with radiation into the charge transfer absorption maximum of the oligomer **3.91b-d**. A broad fluorescence is observed in all cases over the

complete wavelength range from 370 nm to 620 nm. A set of two to three fluorescence maxima appear for each oligomer, which probably indicates a vibrational fine structure.

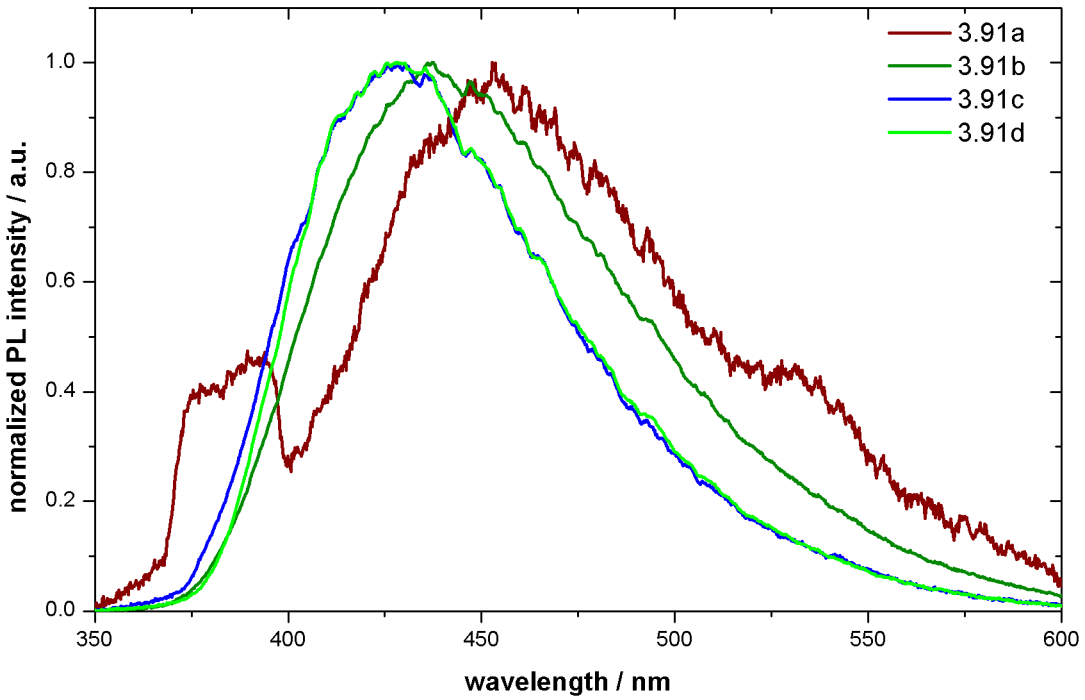

Figure 3.65: Fluorescence spectra of **3.91a-d** in dichloromethane (2 x 10^{-3} mg/mL).

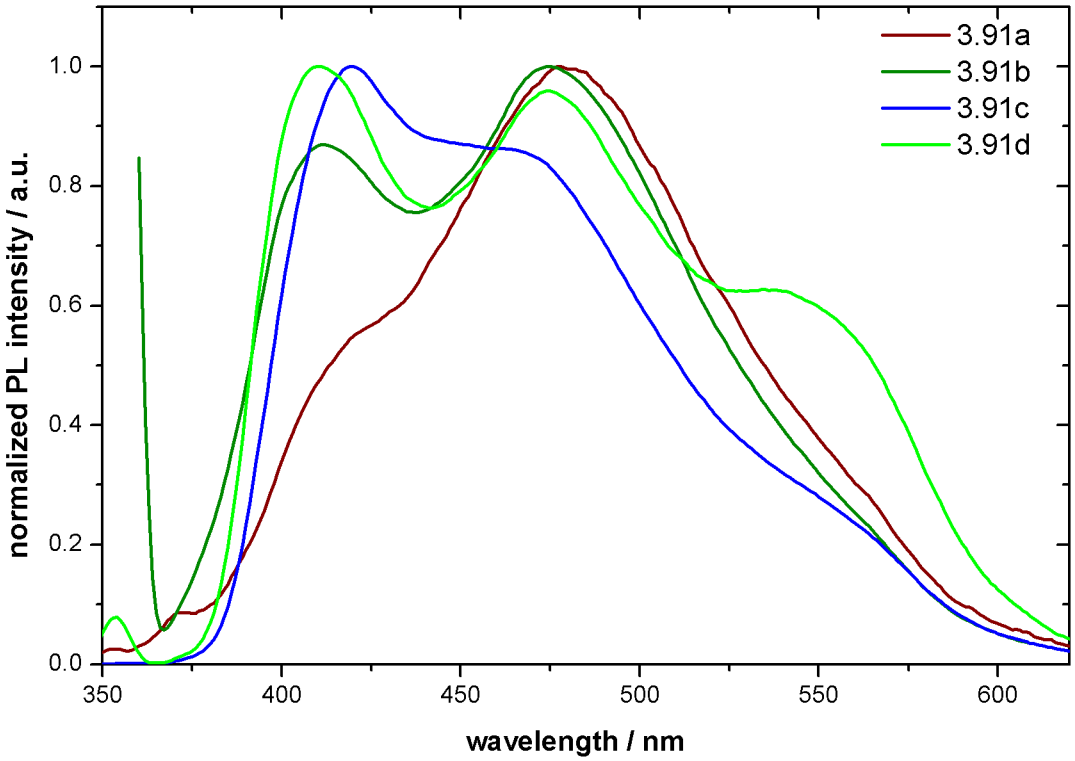

Figure 3.66: Fluorescence spectra of **3.91a-d** in *N*,*N*-dimethylformamide; excited at the absorption bands between 320 and 360 nm (2 x 10^{-3} mg/mL).

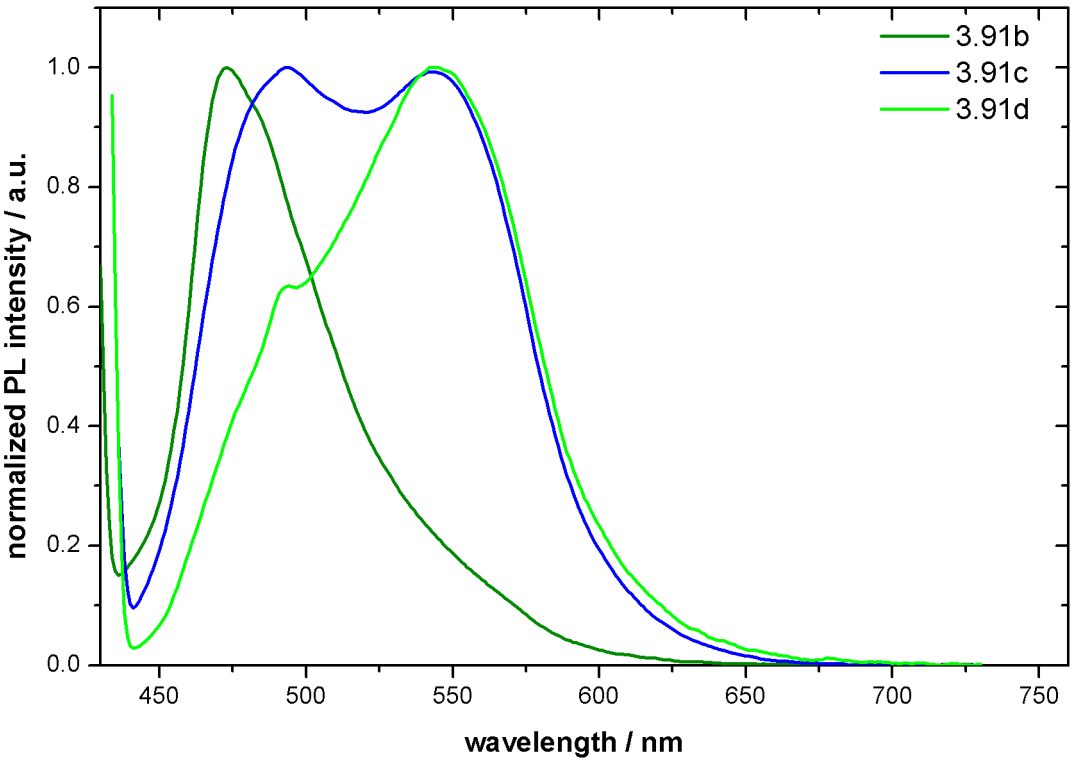

Figure 3.67: Fluorescence spectra of **3.91b-d** in *N*,*N*-dimethylformamide; radiated into the charge transfer bands (around 430 nm) (2 x 10^{-3} mg/mL).

In time resolved fluorescence spectroscopy in dichloromethane another trend is observed for the oligomers (Figure 3.68). This measurement reveals the lifetime for the oligomers. Whereas the excited dimer has the shortest lifetime with 515 ps, the trimer has a lifetime of 660 ps (ester terminated oligomer) and, respectively, 635 ps (carboxylic acid terminated oligomer). The lifetime of the tetramer is 580 ps, respectively 540 ps for the pentamer, thus showing a decrease of the lifetime with increasing chain length. The measurements in *N*,*N*-dimethylformamide of the oligomers **3.91b-d** reveal a non-mono exponential decay of the fluorescence intensity, indicating that several processes are possible, and thus di/multi exponential decays are observed (Figure 3.69).

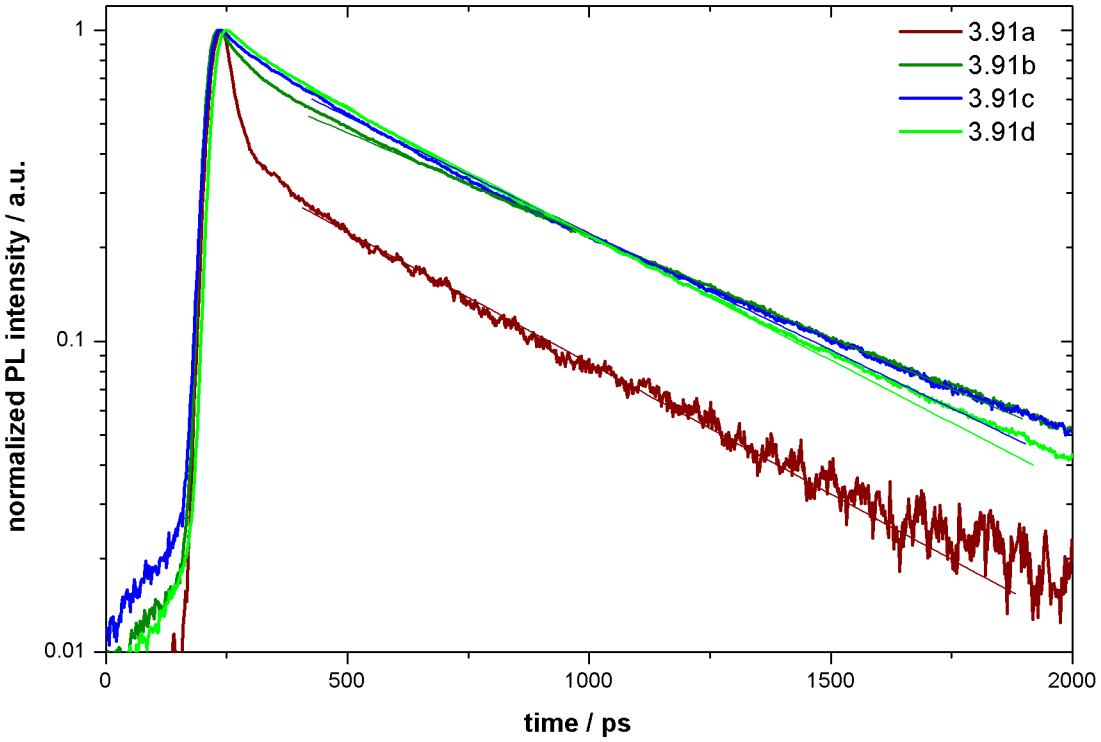

Figure 3.68: Time-resolved fluorescence spectra of **3.91a-d** in dichloromethane (1 mg/mL).

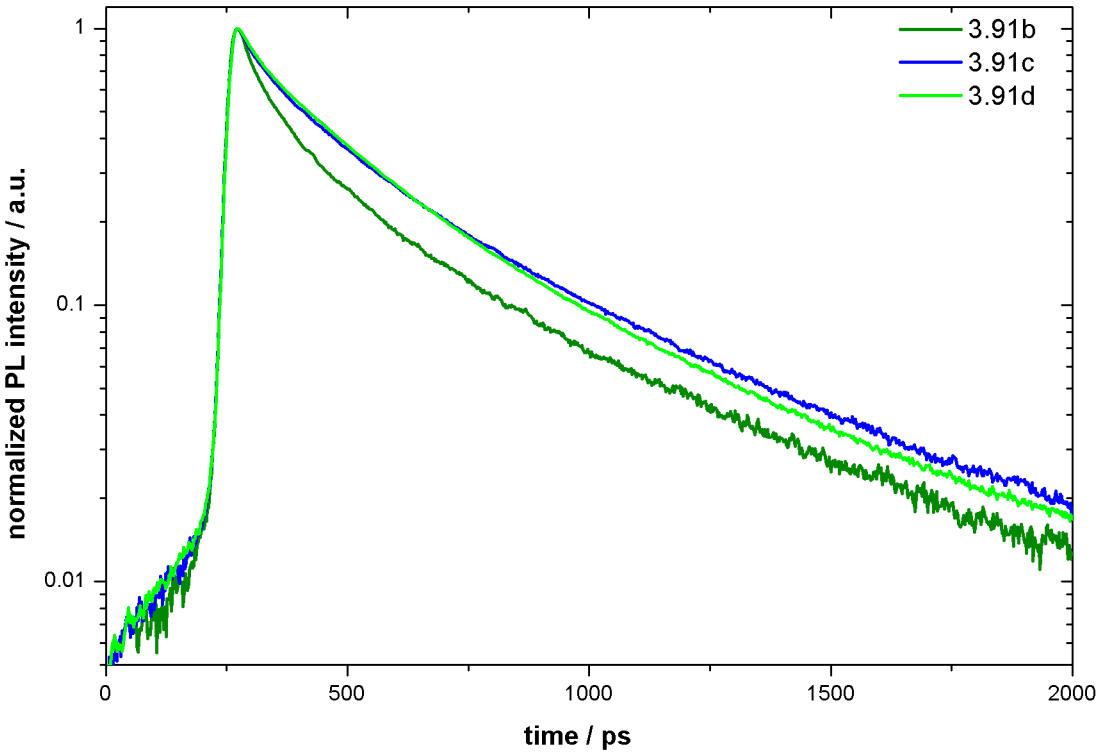

Figure 3.69: Time-resolved fluorescence spectra of **3.91b-d** in *N*,*N*-dimethylformamide (1 mg/mL).

The difference influence of an ester and a carboxylic end group in dichloromethane has been studied in the case of the trimer. Whereas the ester-terminated trimer shows an absorption maximum at 330 nm, λ_{max} for the carboxylic acid-terminated trimer is red shifted to 353 nm (Figure 3.70). This red shift indicates a decrease of the gap between the ground state and the excited state. In nonpolar solvents, like dichloromethane, carboxylic acid groups are less solvated and thus poorly stabilized, resulting in intermolecular hydrogen bonds between the carboxylic acids. In case of benzoic acid, computational and spectroscopic studies have shown, that the energy levels of the ground state as well as of the excited state, are lowered.[118] For the noted red shift, the conclusion is a stronger stabilization of the excited state compared to the ground state. In contrast to the absorption spectra of the ester and carboxylic acid terminated trimer, the fluorescence spectra show a small, but significant hypsochromic shift for the carboxylic acid terminated trimer (Figure 3.71). By exciting the molecule, the dipole is distorted and subsequently the stabilization of the dimer is changed, too. The blue shift indicates, that in this formation the level of the ground state is lowered, and consequently the blue shift appears. Time-resolves fluorescence spectroscopy of the ester and carboxylic acid are nearly identical. The *tert*-butyl ester shows a slightly higher fluorescence time (660 ps) compared to its acid (635 ps) (Figure 3.72).

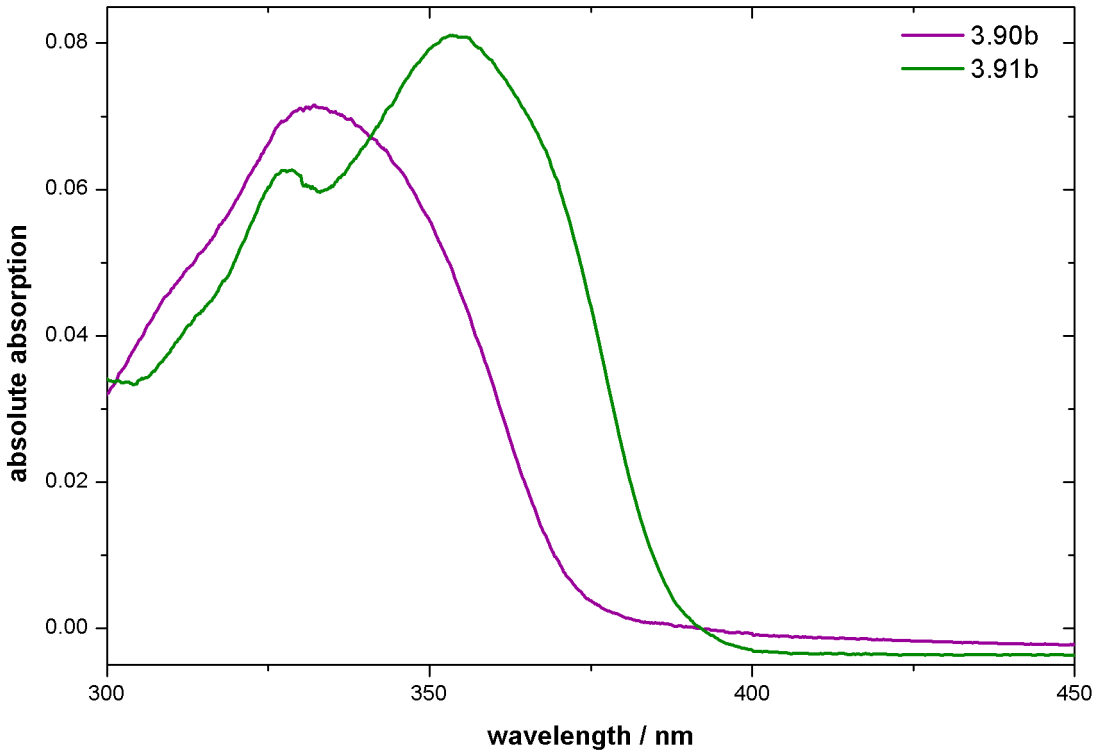

Figure 3.70: UV/vis spectra of the trimers in dichloromethane (2 x 10^{-3} mg/mL).

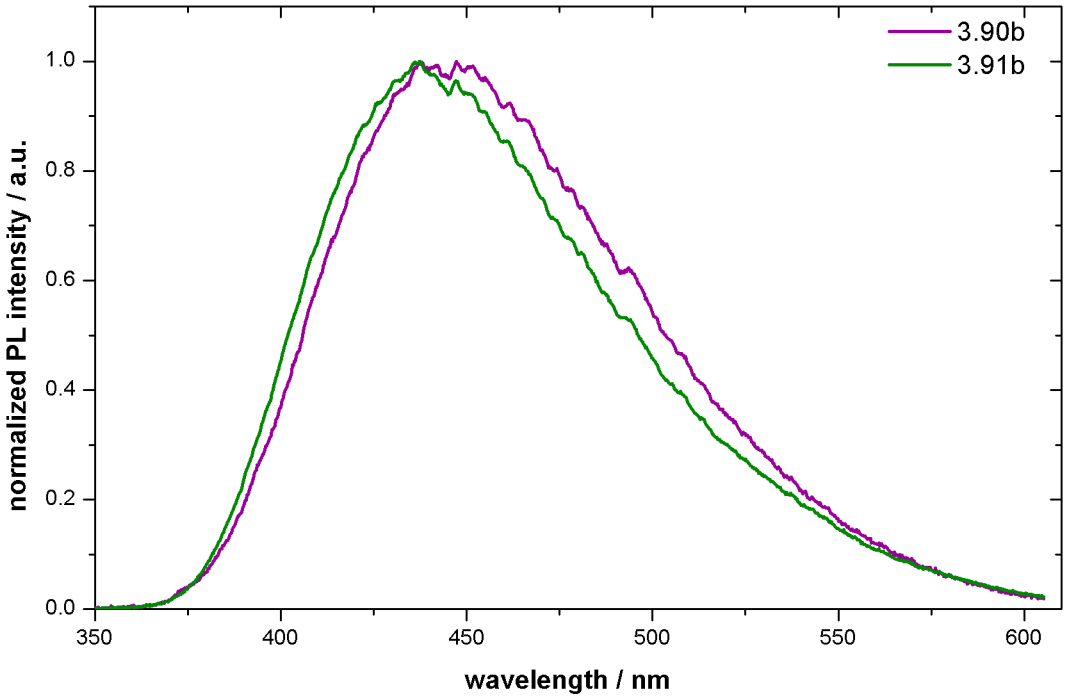

Figure 3.71: Fluorescence spectra of the trimers in dichloromethane (2 x 10^{-3} mg/mL).

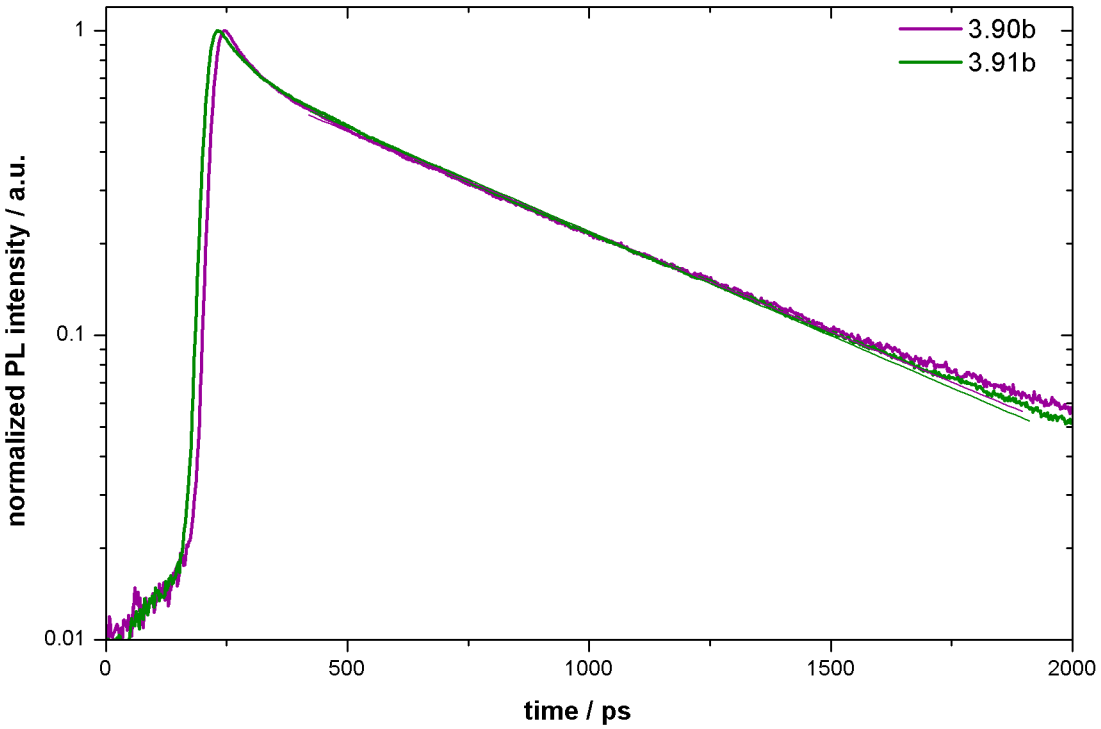

Figure 3.72: Time-resolved fluorescence spectra of the trimers in dichloromethane (1 mg/mL).

The appearance of the charge transfer band of the trimer to the pentamer **3.91b-d** in DMF was studied in detail. Concentration depending analysis of these oligomers shows a decrease of the maximum around 430 nm with increasing concentration. In all three cases the maximum at higher wavelengths gets nearly vanished at a concentration of 2.5 mg/mL (8.8 mmol/mL repeating unit) (Figure 3.73). The ratio of the absorption maxima (355 nm for **3.91b**; 337 nm for **3.91c**; 319 nm for **3.91d**) to the maximum at 430 nm is plotted against the concentration of the used oligomer (Figure 3.74). The tetramer **3.91c** shows the smallest decay compared to the trimer **3.91b** and pentamer **3.91d**. The maximum relative absorption for the tetramer is 0.47 at the lowest concentration (1/256 mg/mL) and 0.40 of the second lowest concentration (1/128 mg/mL). For the same concentration (1/128 mg/mL) the pentamer has a value of 1.07, which significant higher. The trimer shows behavior similar to the pentamer. Only the tetramer has is exceptional: Beside the lower value for the lowest concentration each value is smaller in comparison to those of the shorter respectively longer oligomer.

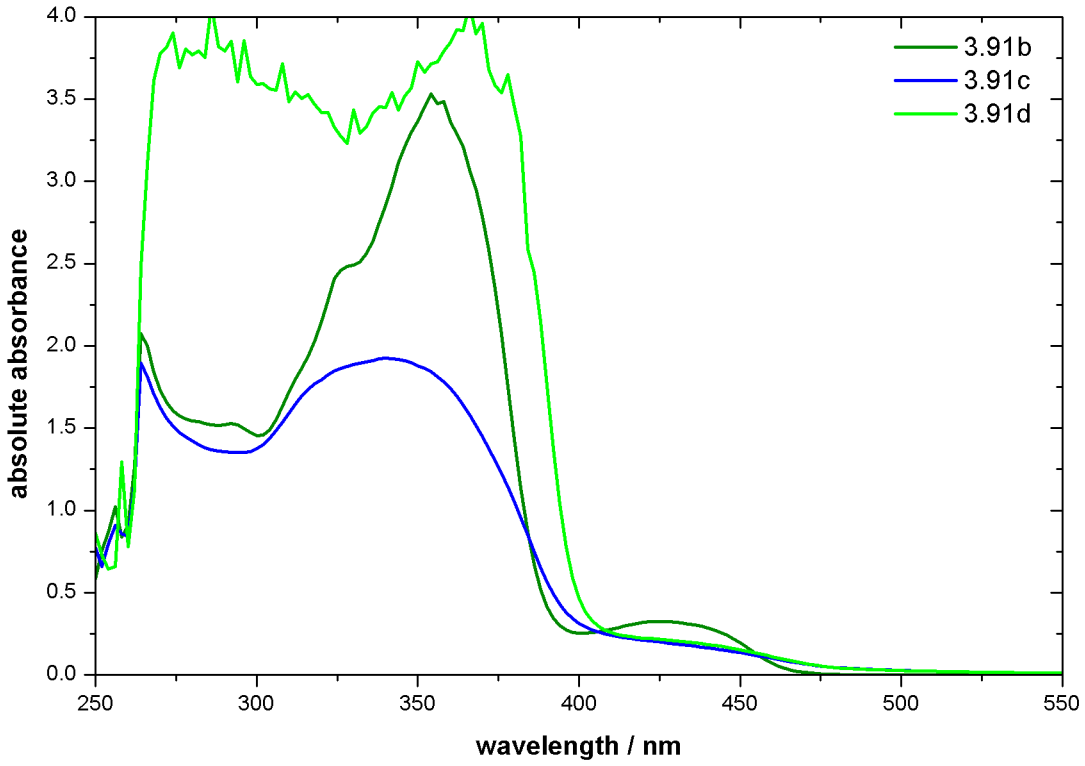

Figure 3.73: UV/vis spectra of each oligomer **3.91b-d** in DMF at 0.25 mg/mL.

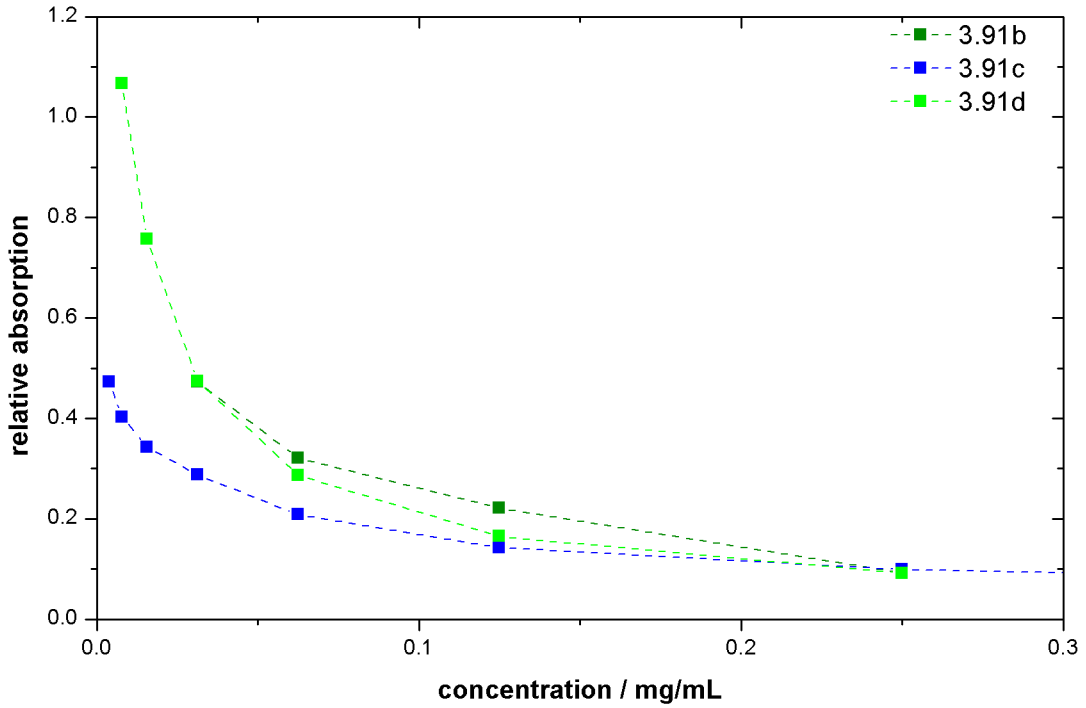

Figure 3.74: Relative absorption (peak at 430 nm compared to corresponding first maximum) for each oligomer **3.91b-d**.

The appearance of the new band with decreasing concentration let assume that aggregation is taking place. Possible explanations are: quenching of this band or the formation of *H*-aggregates at higher concentrations. In the first case, exciting the molecule to the needed state might not by possible, thus the band and 430 nm is not appearing. If the molecules form potential *H*-aggregates, the band at 430 nm is blue shifted and subsequently superimposed by λ_{max}. This phenomena was first discovered by Jelly and coworkers.[119] The so observed structures are named *J*- respectively *H*-aggregates, depending on the observed shift (hypsochromic or bathochromic). In case of a blue shift, *H*-aggregates are formed, respectively *J*-aggregates for a red shift. Due to the observed blue shift in the case of the oligo(thiophene carboxamide)s, it is clear that they form *H*-aggregates, which means a parallel stacking.

Table 3.12: Analytic data of oligo(thiophene carboxamide)s.

Compound	absorption maxima λ_{max} / nm		lg ε (in DCM)	tau / ps (in DCM)	fluorescence maxima λ_{max} / nm	
	DCM	DMF			DCM	DMF
(3.52)	308	315	4.16			
(3.91a)	332	333	4.57	515	417	475
(3.90b)	330			660	446	471
(3.91b)	353	355; 425	4.87	635	436	410; 474
(3.91c)	364	337; 431	4.65	580	428	420
(3.91d)	365 shoulder: 374	319; 429	4.74	540	427	479

Crystallographic data of the carboxylic acid terminated dimer **3.91a** show a disordered crystal structure with two independent structures. The difference between both structures is the relative position of the sulfur in the terminal thiophene rings: In one case, both sulfur atoms are directed into the same side (*syn*-conformation), whereas in the other case, both sulfur atoms are directed into different sides (*anti*-conformation) (Figure 3.75). In both cases the amide bond is fixed and the proton is orientated towards the carbonyl group of the hexyl ester forming hydrogen bonds. Further hydrogen bonds exist between two molecules. In this case, the proton next on carbon C^4 is bound to the oxygen O^{19b} (Figure 3.76). The torsion angle between both thiophene rings is smaller than 1°, which is important for a possible conjugation along the amide.

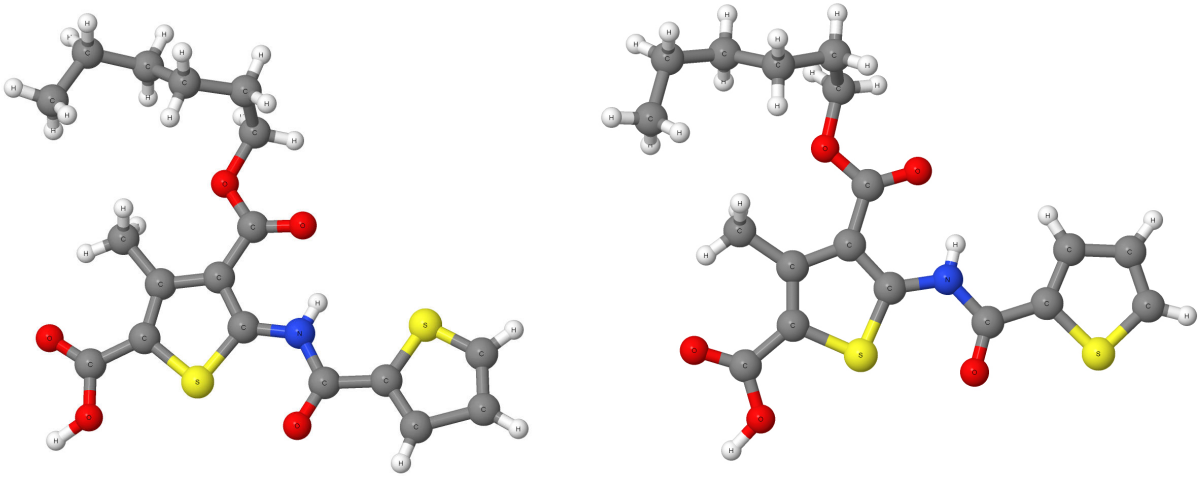

syn-conformation of **3.91a** *anti*-conformation of **3.91a**

Figure 3.75: Crystallographic data of the dimer **3.91a**.

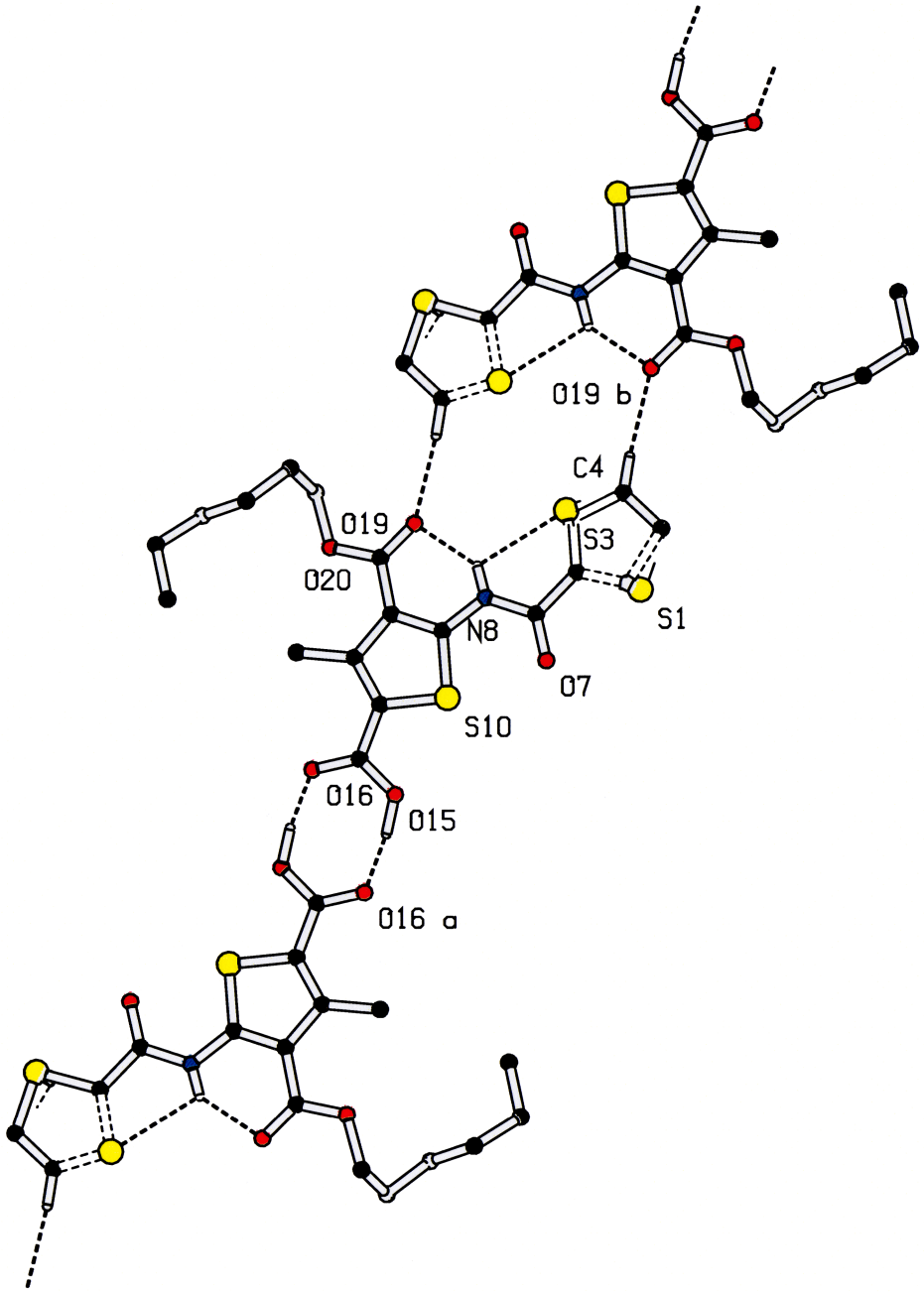

Figure 3.76: Crystallographic data of the dimer **3.91a**. Intermolecular hydrogen bonds are shown between the hydrogen on carbon C4 and the oxygen O19b.

Quantum mechanical calculations (DFT, B3LYP, 6-311+G**) of the tetra- and pentamer show clearly separated HOMO and LUMO levels for both molecules. The more interesting point is the conjugation of the electronic system over the amide bond. In the case of the tetramer, the HOMO levels reach over two aromatic thiophene unites beginning from the carboxylic group. From there the LOMO reaches till the end of the oligomer over another two thiophene units (Figure 3.77).

HOMO

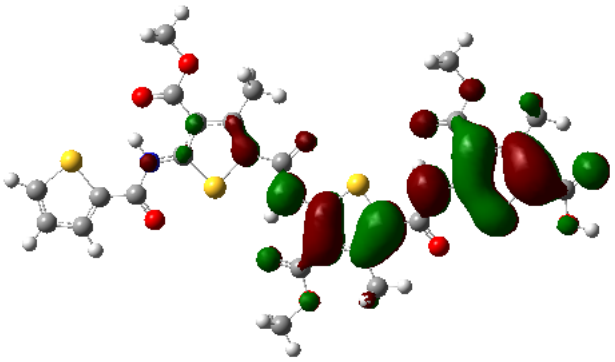

LUMO

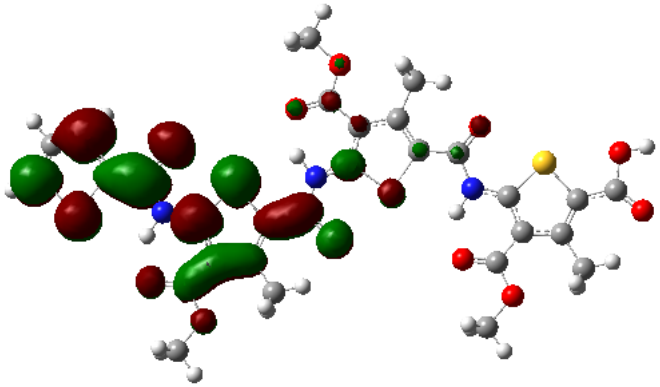

Figure 3.77: HOMO (*top*) and LUMO (*bottom*) calculations of **3.91c**.

3.4. Conclusion

A new class of fluorescent and conjugated oligomers is presented. Synthetic routes for the preparation of oligomers as well as polymers was developed and the optical properties where studied. In order to create this monomer, the synthesis of the needed aminothiophene carboxylic acid was evolved. Different synthetic approaches where tried, but only one reaction pathway led to the desired monomer: the *Gewald*-synthesis. The method allows gives access to a large variety of different aminothiophene carboxylic acids. After protecting the free amino group, the *tert*-butyl ester can be cleaved. This way both functional groups can be protected in such a way that orthogonal syntheses are possible. The first poly(thiophene carboxamide)s where synthesized using a polycondensation reaction. A molecular mass dependency of the absorbance as well as the fluorescence behavior was found for this polymer. A second peak at longer wavelength 365 nm is first increasing with the chain length, and thereafter decreasing, so showing a maximum for a specific polymer length. This phenomenon is visible in both the absorbance and fluorescence spectra. In order to understand this behavior well defined and monodisperse oligomers where synthesized. The synthetic route using a solid supported peptide synthesizer with Fmoc protected amines was unsuccessful to get the desired material. A series of monodisperse molecule were effectively synthesized in solution via acid chlorides of the oligomers and the amino group of the *tert*-butyl ester protected monomer, resulting in a new amide bond. The optical properties of the oligomers were studied in detail, revealing interesting absorption and fluorescence phenomena. With an increasing chain length, the absorption maxima are bathochromically shifted, whereas the fluorescence spectra are hypsochromically shifted. These shifts clearly indicate a conjugation along the amide bond, which has also been shown by quantum chemical calculations. A plot of the absorption energy versus the inverse chain length indicates allows predictions of the absorption wavelength for the according polymer. For a rough linear regression this value is 408 nm and not close to the found value for the polymer (365 nm). A more precise prediction gives two possible wavelengths (375 nm or 391 nm), depending on the interpretation of the pentamer's spectrum. These two values are in good agreement with the found absorption maximum of the polymer, allowing the determination of the effective conjugation length, which is reached by the pentamer having its absorption maximum at 365 nm and is the same value found for the polymer. The conjugation along the amide of the molecules is very important for their usage in optoelectronic devices. First aggregations have also been shown by the absorption spectra already for low oligomer degrees of three to five. Concentration dependency of different absorption bands where found for the tri-,

tetra- and pentamer in the polar solvent *N*,*N*-dimethylformamide. In all cases, a weak band at λ_{max}=430 nm increases in highly diluted solutions, but vanishes in higher concentrations. In case of the tetramer, this phenomenon is not as distinct.

H-aggregates are observed, which is explained by the blue shift with increasing concentration. The supramolecular structures can occur due to the hexyl chains which are not good soluble in polar solvents and therefore attend to aggregate. The stronger effect observed for the tetramer indicates that the longer oligomers may not aggregate as well as the tetramer does. A possible explanation may be a twist in the molecule, which does would not allow a perfect arrangement. Each aromatic ring might be turned for a specific angle to the rings next to it.

3.5. Further Work

The easy modification of side chains and starting molecule will lead to large variety of new chromophores. The ability of the amide bonds to build hydrogen bonds can be used in order to induce self-organization of those molecules as they do in the oligo(*p*-benzamide) system. The combination of self-organization driving groups and fully conjugation makes this class of oligomers where interesting for further studies and applications. Figure 3.78 shows the schematic synthesis of the needed thiophene monomer. By varying the different groups R^{1-3} different substitutes can be introduced. In most cases, R^1 will be the *tert* butyl ester, because this is relatively easy removed, which is needed for making linear oligomers. R^2 and R^3 are more interesting candidates for changes, because electron density as well as solubility properties can be influenced this way. The smallest R^2 group can be a hydrogen atom, which can be introduced by altering one starting molecule. By varying this molecule also longer alkyl chains can be established. Mostly, the solubility of the oligomers will be affected by those modifications. The same effect will be observed by varying R^3. In the shown oligomers, this group was a hexyl ester. This ester is very easy to be changed before the ring closure reaction shown in Figure 3.78. Though, synthetic more interesting changes can be made for that group. Instead of using an α-cyano ester, dinitrile malonate will introduce a cyano group instead of a complete ester. Knowing from the crystal structures of the dimer **(3.91a)**, this ester serves as a hydrogen bond acceptor, and thus builds a hydrogen bond with the neighboring amine. Having a different group, than that ester in that position, may lead to different aggregation behavior of the oligomers, since the amide bond is now free to perform inter-molecular instead of intra-molecular hydrogen bonds.

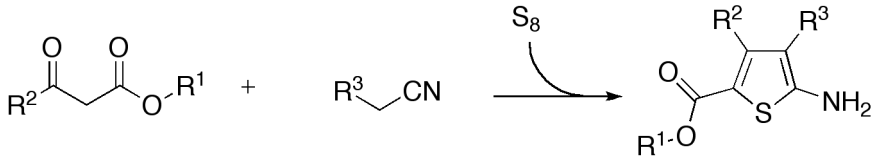

Figure 3.78: Schematic synthesis of tetra substituted thiophenes.

Different oligomers can be synthesized by introducing a *tert*-butyl ester for the rest R^3. In this case the ester can be removed, leaving a carboxylic acid or a proton when the acid is decarboxylated (Figure 3.79). In the case of the decarboxylation, linear oligomers can be created with very small or no side chains, which makes this route interesting, for studies of the plain stiff molecules and their aggregation behavior. Leaving the carboxylic acid at the molecule and the ester of rest R^1, bended oligomers can be synthesized. In this case, different conjugations over the amide bond will occur, which is very fascinating. In the case

where both carboxylic acids are useful for building oligomers, branched or dendritic systems are possible.

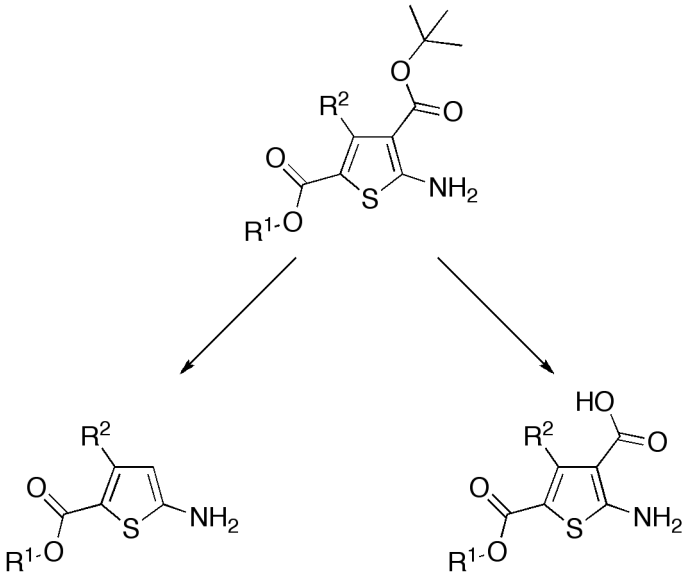

Figure 3.79: Possible thiophenes.

Figure 3.80 shows the two end groups of the oligomer **3.91d**. For both groups, electron acceptors as well as electron donors can be added, leading to different electronic properties of the molecule and shifted absorption and fluorescence spectra.

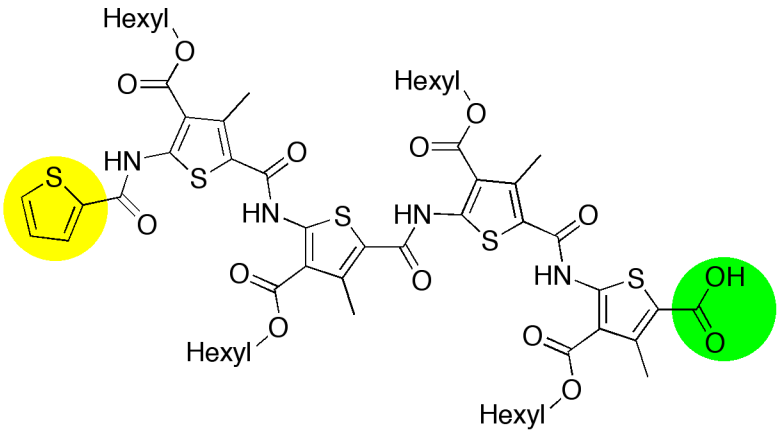

3.91d

Figure 3.80: Groups, where electron donors or acceptors can be introduced.

In all of the different synthetic possibilities, very interesting properties are achievable. Starting from different absorption and fluorescence behaviors to arrangements of supramolecular structures may be observed. The large variety of different monomers and the combination of those, will lead to a class of materials, which can be customized to the desired needs.

3.6. Experimental

Instrumentation

NMR: ^{1}H and ^{13}C nuclear magnetic resonance spectra (NMR) were recorded at a frequency of 300 MHz on a Bruker AC 300 or on a Bruker AMX 400 working at 400 MHz, respectively 100 MHZ for ^{13}C (on the Bruker AMX 400), using chloroform-*d* or benzenze-d_6 as solvent.

SEC: Size exclusion chromatography in tetrahydrofuran (THF) or chloroform was performed on an instrument consisting of a Waters 717 plus autosampler, a TSP Spectra Series P 100 pump and a set of three PSS-SDV 5 μ columns with 100, 1.000, und 10.000 Å porosity. Calibration was carried out using poly(styrene) standards provided by Polymer Standards Service and performing a 3rd order polynomial fit. The eluent was used at 30 °C and at a flow rate of 1 $mL \cdot min^{-1}$. UV absorption was detected by a SpectraSYSTEM UV2000. The specific refractive index increment(dn/dc) was measured at 30 °C on an Optilab DSP interferometric refractometer (also RI detector). For measurements in dimethylformamide (DMF) containing 1 $g \cdot L^{-1}$ of lithium bromide, an Agilent 1100 Series GPC-Setup (Gel Permeation Chromatography) was used as an integrated instrument including a PSS HEMA column ($10^6/10^5/10^4$ $g \cdot mol^{-1}$), a UV (254 nm), and RI detector. Calibration was carried out using polystyrene standards provided by Polymer Standards Service. The eluent was used at 50 °C and at a flow rate of 1 $mL \cdot min^{-1}$.

FD-MS: Field desorption mass spectra were measured on a Finnigan MAT 95.

TEM: A Philips EM 420 transmission electron microscope using a LaB_6 cathode at an acceleration voltage of 120 kV was used to obtain TEM-images. TEM grids (carbon film on copper, 300 mesh) were obtained from Electron Microscopy Sciences, Hatfield, PA, USA.

UV/vis:	UV/vis spectroscopy was performed on a JASCO V-630 UV-VIS spectrophotometer
PL:	Fluorescence was measured on a JASCO PL6200 spectrofluorometer.

Materials. All solvents and other reagents were purchased from Aldrich or Acros and used as received. Solvents were dried using standard literature methods. Deuterated chloroform-*d* (99,8%), DMSO-d_6 (99,8%), DMF-d_7 (99,5%) and pyridine-d_5 (99,5%) were purchased from Deutero GmbH and used as received.

Synthesis of hexyl cyano acetate.

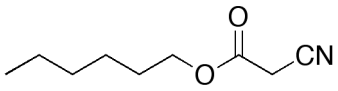

Cyanoacetic acid (51.0 g; 0.6 mol), 1-hexanol (61.0 g; 0.60 mol), *p*-toluenesulfonic acid (50 mg; 29 mmol) was refluxed under Dean-Stark conditions in toluene (250 mL) until all water was removed from the reaction mixture. The toluene was removed under reduced pressure and the product was distilled at 110 °C and 0.34 mbar to yield 92.9 g (0.55 mol; 92%) of a clear, colorless liquid.

^{1}H-NMR (300 MHz; $CDCl_3$): δ 4.19 (t, J = 6.7, 2H, $C1_{hexyl}$-*H*), 1.66 (quint, J = 7.2, 2H, $C2_{hexyl}$-*H*), 1.40-1.30 (m, 6H, C3-5_{hexyl}-*H*), 0.88 (t, J = 6.8, 3H, $C6_{hexyl}$-*H*).

Synthesis of ^{t}butyl thiophen-2-ylcarbamate (3.47).

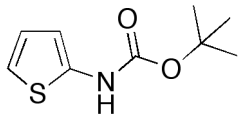

Thiophen-2-carbonyl chloride (1.0 g; 6.8 mmol) in 15 mL acetone where cooled to 0°C and NaN_3 (0.7 g; 9.6 mmol) in 5 mL water where slowly added. The mixture was stirred for one hour till the mixture was added to 40 mL ice water and extracted with 80 mL toluene. The organic phase was dried with $MgSO_4$ for 24 hours. The toluene phase is slowly added to 2 mL ^{t}butanol at 110°C. The mixture is evaporated under reduced pressure, dissolved in ether, extracted against 1 M NaOH and the organic phase is evaporated to yield 1.2 g (5.8 mmol; 85%).

^{1}H-NMR (300 MHz; DMSO-d_6): δ 10.17 (s, 1H, amide-*H*), 6.87 (dd, *J* = 5.4, 1.2 Hz, 1H, C3$_{thiophene}$-*H*), 6.80 (dd, *J* = 5.4, 3.7 Hz, 1H, C5$_{thiophene}$-*H*), 6.56 (dd, *J* = 3.6, 1.4 Hz, 1H, C4$_{thiophene}$-*H*), 3.35 (s, 9H, ^{t}Bu-*H*).

FD-MS: m/z = 199.4 [M^{+}].

Synthesis of 2-*tert*-butyl 4-hexyl 5-amino-3-methylthiophene-2,4-dicarboxylate (3.52).

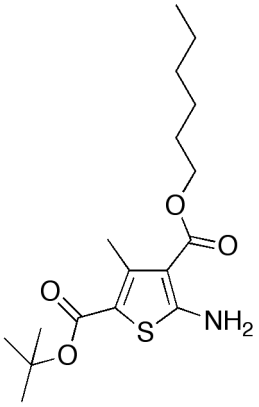

Hexyl cyanoacetate (92.9 g; 0.55 mol), sulfur (17.7 g; 0.55 mol) and *tert*-butyl acetoacetate (86.9 g; 0.55 mol) were dissolved in 400 mL hexanol and headed to 60 °C. Over a time period of about 60 minutes, morpholine (48 g; 0.55 mol) was slowly added to the reaction mixture, which turns slightly red-brown and the sulfur gets dissolved. The mixture was then heated and stirred for another 60 minutes at 60 °C. After hot filtration the mixture was allowed to cool down to room temperature and the product starts to precipitate. After recrystallization from hexanol yielding 168.2 g (0.50 mol; 90 %) of white crystals.

^{1}H-NMR (300 MHz; $CDCl_3$): δ 6.44 (s, 2H, N-*H*), 4.24 (t, *J* = 6.6 Hz, 2H, $C1_{hexyl}$-*H*), 2.66 (s, 3H, 3-Methyl-*H*), 1.73 (quintet, *J* = 7.2 Hz, 2H, $C2_{hexyl}$-*H*), 1.53 (s, 9H, ^{t}Bu-*H*), 1.42-1.30 (m, 6H, $C3,4,5_{hexyl}$-*H*), 0.89 (t, *J* = 6.9 Hz, 3H, $C6_{hexyl}$-*H*).

^{13}C-NMR (100.15 MHz; $CDCl_3$): δ(ppm): 13.94 (thiophen-CH_3); 15.97 (Ar-CH_3); 22.48 (C_4-CH_2-CH_3); 25.78 (C_3-CH_2-C-CH_3); 28.32 (O-C-(CH_3)$_3$); 28.62 (C_2-CH_2-C_2-CH_3); 31.36 (C-CH_2-C_3-CH_3); 64.21 ($COOCH_2$); 81.12 (O-*C*-(CH_3)$_3$); 108.4 (thiophene C^3); 110.21 (thiophene C^2); 146.77 (thiophene C^2); 162.31(*C*$OOCH_2$); 165.83(*C*O^{t}Bu); 166.33 (*C*-N).

FD-MS: m/z = 340.9 [M^+].

UV/vis: 308 nm (DCM), 315 nm (DMF).

Synthesis of 4-hexylthiophene-2-carboxlyic acid (3.56).

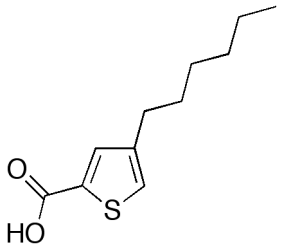

3-Hexylthiophene **(3.54)** (2.0 g; 12.0 mmol) in 20 mL THF where cooled to -78 °C and ^{t}butyl lithium (7.9 mL 1.5 M, 12.0 mmol) where slowly added. After one hour CO_2 was bubbled trough the reaction mixture. Removing the solvent under reduced pressure and column chromatography in ethyl acetate : hexanes (3:1) yielded 2.2 g (10.4 mmol; 87%).

^{1}H-NMR (300 MHz; DMSO-d_6): δ 7.04 (d, J = 1.4 Hz, 1H, $C5_{thiophene}$-*H*), 6.89 (d, J = 1.2 Hz, 1H, $C2_{thiophene}$-*H*), 1.55-1.50 (m, 2H, $C2_{hexyl}$-*H*), 1.29-1.21 (m, 6H, C3-5_{hexyl}-*H*), 0.85 (t, J = 6.7 Hz, 3H, $C6_{hexyl}$-*H*).

FD-MS: m/z = 211.9 [M^{+}].

Synthesis of 2-nitro-5-hexylthiophene-2-carboxylic acid (3.57).

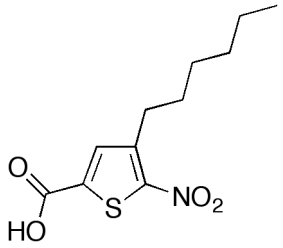

4-Hexylthiophene-2-carboxylic acid (2.0 g; 9.4 mmol) where dissolved in 10 mL acetic acid anhydride. 5 mL concentrated nitric acid in 7.8 mL acetic acid where drop wise added under ice cooling and the mixture was stirred for 24 hours. 25 mL water where added and extracted with chloroform. The organic phase was evaporated. Column chromatography in hexanes : ethyl acetate (4:1) yielded 1.1 g (4.3 mmol; 46 %).

^{1}H-NMR (300 MHz; DMSO-d_6): δ 7.70 (s, 1H,C4$_{thiophene}$-*H*), 2.98 (t, *J* = 7.7 Hz, 2H, C1$_{hexyl}$-*H*), 1.63-1.58 (m, 2H, C2$_{hexyl}$-*H*), 1.34-1.24 (m, 6H, C3-5$_{hexyl}$-*H*), 0.86 (t, *J* = 5.6 Hz, 3H, C6$_{hexyl}$-*H*).

^{13}C-NMR (75 MHz; DMSO-d_6): δ 161.74, 146.64, 137.36, 134.89, 30.89, 29.00, 28.53, 28.47, 21.96, 13.92.

FD-MS: m/z = 258.9 [M^+].

Synthesis of *tert*-butyl-thiophene-Fmoc (3.78).

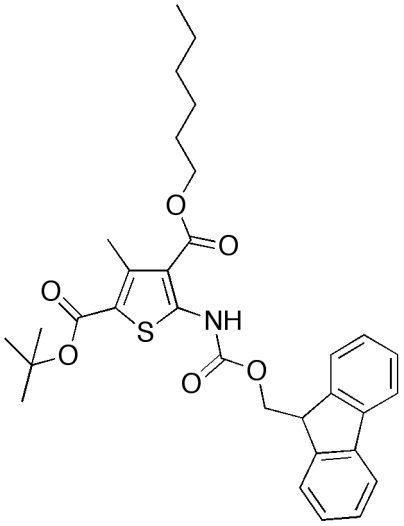

Fmoc-Cl (54.0 g; 0.20 mol) dissolved in 100 mL NMP where slowly added to **(3.52)** (50.0 g; 0.2 mol) dissolved in 100 mL NMP. The white precipitate was filtered and after recrystallization from methanol 103.7 g (0.18 mol; 92%) were obtained.

^{1}H-NMR (300 MHz; $CDCl_3$): δ 7.75 (d, *J* = 7.5 Hz, 2H), 7.60 (d, *J* = 7.4 Hz, 2H), 7.41-7.30 (m, 4H), 4.55 (d, *J* = 7.5 Hz, 2H), 4.32 (t, *J* = 7.4 Hz, 1H), 4.24 (t, *J* = 6.6 Hz, 2H, $C1_{hexyl}$-*H*), 2.80 (s, 3H, 3-Methyl-*H*), 1.69 (m, 2H, $C2_{hexyl}$-*H*), 1.51 (s, 9H, ^{t}Bu-*H*), 1.42-1.27 (m, 6H, $C3,4,5_{hexyl}$-*H*), 0.88 (t, *J* = 6.9 Hz, 3H, $C6_{hexyl}$-*H*).

FD-MS: m/z = 563.4 [M^+].

Synthesis of thiophene-Fmoc (3.79).

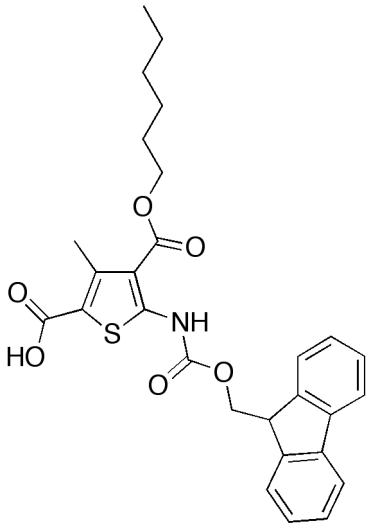

50 mL 99% aq. trifluoroacetic acid was dropwise added to **(3.78)** (100.0 g; 0.18 mol) in 5 mL water at 0°C. After 10 minutes 50 mL of 99% aq. trifluoroacetic acid were slowly added and let it react for another 15 minutes. The reaction mixture was then given to 500 mL water. After filtering and recrystallization from methanol 85.3 g(0.17 mol; 95%) were obtained.

^{1}H-NMR (300 MHz; $CDCl_3$): δ 7.75 (d, *J* = 7.5 Hz, 2H), 7.61 (d, *J* = 7.4 Hz, 2H), 7.41-7.29 (m, 4H), 4.58 (d, *J* = 7.5 Hz, 2H), 4.30 (t, *J* = 7.4 Hz, 1H), 4.25 (t, *J* = 6.6 Hz, 2H, $C1_{hexyl}$-*H*), 2.81 (s, 3H, 3-Methyl-*H*), 1.70 (m, 2H, $C2_{hexyl}$-*H*), 1.42-1.27 (m, 6H, $C3,4,5_{hexyl}$-*H*), 0.87 (t, *J* = 6.9 Hz, 3H, $C6_{hexyl}$-*H*).

FD-MS: m/z = 507.2 [M^+].

Synthesis of 5-amino-4-(hexyloxycarbonyl)-3-methylthiophene-2-carboxylic acid (3.80).

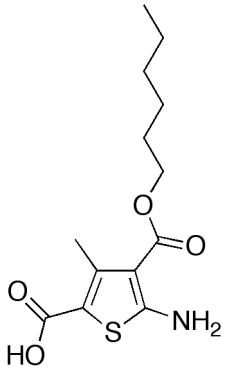

3.52 (20 g; 59 mmol) were added to 100 mL conc. hydrochloric acid and stirred for 16 hours. The reaction mixture was filtered and diluted with 100 mL water and neutralized with sodium bicarbonate. The obtained white solid was filtered and recrystallized from water to yield 11 g (39 mmol; 66%).

Synthesis of poly(4-(hexyloxycarbonyl)-3-methylthiophene amide) (3.83).

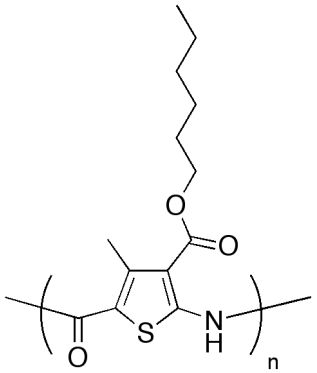

3.80 (300 mg; 1.1 mmol), DCC (300 mg; 1.5 mmol) and DMAP (200 mg; 1.6 mmol) where dissolved in 3 mL dichloromethane and stirred at room temperature for four days whereas the reaction mixtures turns from yellow to red. The crude reaction mixture was than separated by side products and divided into 60 fractions via preparative SEC. The different SEC fractions where analyzed by UV/vis-absorption and fluorescence measurements.

Synthesis of thiophene-(HT)-^{t}butyl ester (3.90a).

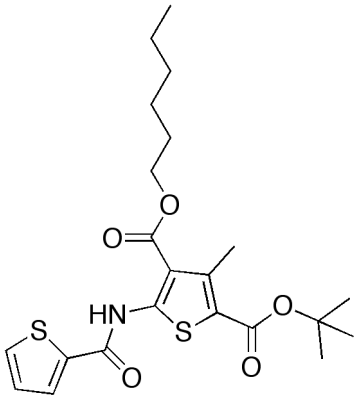

Thiophene-2-carbonyl chloride (3.9 g; 33 mmol) where dissolved in 40 mL THF and **3.52** (10.2 g; 30 mmol) in 20 mL THF and 20 mL pyridine where added and stirred at room temperature for 24 h. The reaction mixture was filtered and THF was removed under reduced pressure. The solution was precipitated into 1 M aqueous hydrochloric acid and filtered. The white solid was neutralized with 1 M sodium bicarbonate solution until the washing water was not acidic any more. Recrystallization from 1-hexanol at 100 °C yielded 10.2 g (24 mol; 80 %).

^{1}H-NMR (300 MHz; DMSO-d_6): δ 12.05 (s, 1H, amide-*H*), 8.05 (d, *J* = 4.8 Hz, 1H, C3$_{thiophene}$-*H*), 7.78 (d, *J* = 3.6 Hz, 1H, C5$_{thiophene}$-*H*), 7.30 (dd, *J* = 4.8, 4.0 Hz, 1H, C4$_{thiophene}$-*H*), 4.29 (t, *J* = 6.5 Hz, 2H, C1$_{hexyl}$-*H*), 2.62 (s, 3H, 3'-Methyl-*H*), 1.78-1.69 (m, 2H, C2$_{hexyl}$-*H*), 1.52 (s, 9H, ^{t}Bu-*H*), 1.41-1.26 (m, 6H, C3-5$_{hexyl}$-*H*), 0.85 (t, *J* = 6.9 Hz, 3H, C6$_{hexyl}$-*H*).

Synthesis of thiophene-(HT)-carboxylic acid (3.91a).

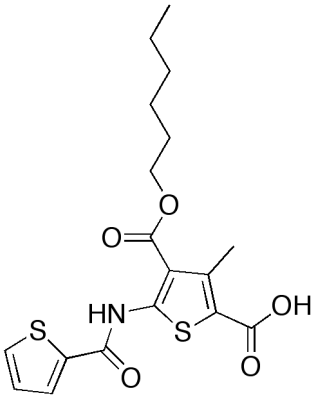

3.90a (8 g; 18.9 mmol) was added to a flask under argon atmosphere and 3 mL of water was added. The reaction vessel was cooled in a water bath, while 27 mL 98% aq. trifluoroacetic acid (TFA) were been added and stirred for 10 minutes until another 20 mL TFA were added. Crude **(3.91a)** was precipitated by adding the fivefold amount of water to the reaction mixture, and filtrated. Neutralizing the white solid was done by washing with 1 M aqueous sodium bicarbonate. Recrystallization from 1-hexanol at 100 °C yielded 5 g (13.6 mmol; 72 %).

^{1}H-NMR (300 MHz; $CDCl_3$): δ 12.55 (s, 1H, amide-*H*), 7.79 (dd, *J* = 3.8, 0.9 Hz, 1H, $C3_{thiophene}$-*H*), 7.65 (dd, *J* = 4.8, 0.8 Hz, 1H, $C5_{thiophene}$-*H*), 7.18 (dd, *J* = 4.9, 3.9 Hz, 1H, $C4_{thiophene}$-*H*), 4.38 (t, *J* = 6.6 Hz, 2H, $C1_{hexyl}$-*H*), 2.81 (s, 3H, 3'-Methyl-*H*), 1.81 (dd, *J* = 7.9, 7.0 Hz, 2H, $C2_{hexyl}$-*H*), 1.47-1.32 (m, 6H, C2-5_{hexyl}-*H*), 0.92 (t, *J* = 7.0 Hz, 3H, $C6_{hexyl}$-*H*).

^{13}C-NMR (75 MHz; $CDCl_3$): δ 167.14, 154.18, 146.91, 136.98, 132.93, 130.21, 128.93, 114.68, 65.84, 31.53, 28.68, 25.94, 22.67, 15.95, 14.15.

FD-MS: m/z = 395.28 [M^+].

UV/vis: 332 nm (DCM), 333 nm (DMF).

Synthesis of thiophene-(HT)$_2$-^{t}butyl ester (3.90b).

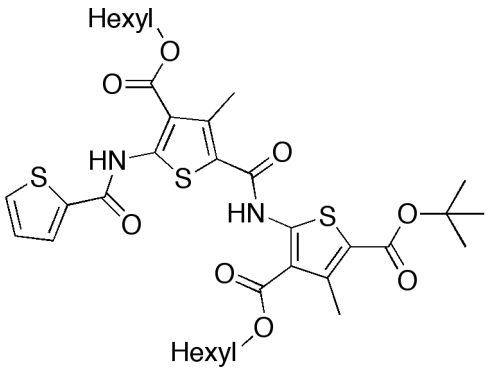

3.91a (4 g; 10.9 mmol) was added to a Schlenk flask and flushed with argon. 15 mL oxalyl chloride was added and stirred until a clear solution was obtained. After one hour of stirring oxalyl chloride was removed under reduced pressure at room temperature. The yellow solid was dissolved in 5 mL dichloromethane, which was removed under reduced pressure to remove the rest of oxalyl chloride. The yellow solid was then dissolved in 30 mL THF and **3.52** (4.1 g; 12.0 mmol) in 25 mL THF and 25 mL pyridine was added and stirred at room temperature for 24 h. The reaction mixture was filtered and THF was removed under reduced pressure. The solution was precipitated into 1 M aqueous hydrochloric acid and filtered. The solid was neutralized with 1 M sodium bicarbonate solution until the washing water was not acidic any more. Recrystallization from 1-hexanol at 100 °C yielded 6 g (8.5 mmol; 78 %).

^{1}H-NMR (300 MHz; $CDCl_3$): δ 12.52 (s, 1H, amide$_{HT\text{-}HT}$-*H*), 12.26 (s, 1H, amide$_{thiophene\text{-}HT}$-*H*), 7.79 (d, *J* = 3.6 Hz, 1H, C3$_{thiophene}$-*H*), 7.66 (d, *J* = 4.8 Hz, 1H, C5$_{thiophene}$-*H*), 7.18 (dd, *J* = 4.8, 3.9 Hz, 1H, C4$_{thiophene}$-*H*), 4.40-4.24 (m, *J* = 6.4 Hz, 4H, C1$_{hexyl}$-*H*), 2.83 (s, 3H, 3'-Methyl-*H*), 2.76 (s, 3H, 3''-Methyl-*H*), 1.86-1.74 (m, 4H, C2$_{hexyl}$-*H*), 1.57 (s, 9H, ^{t}Bu-*H*), 1.49-1.32 (m, 12H, C3-5$_{hexyl}$-*H*), 0.93-0.87 (m, 6H, C6$_{hexyl}$-*H*).

Synthesis of thiophene-(HT)$_2$-carboxylic acid (3.91b).

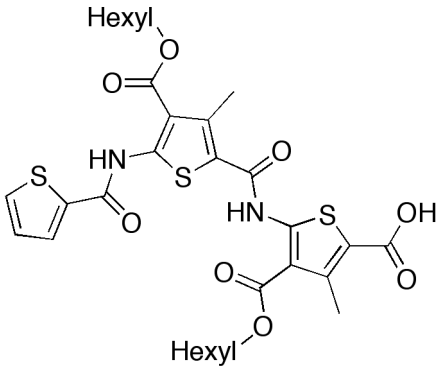

3.90 (4.0 g; 5.7 mmol) was added to a flask under argon atmosphere and 3 mL of water was added. The reaction vessel was cooled in a water bath, while 27 mL 98% aq. TFA were been added and stirred for 10 minutes until another 20 mL TFA were added. Crude **3.91b** was precipitated by adding the fivefold amount of water to the reaction mixture, and filtrated. Neutralizing the white solid was done by washing with 1 M aqueous sodium bicarbonate. Recrystallization from 1-hexanol at 100 °C yielded 3.2 g (4.8 mmol; 85 %).

^{1}H-NMR (300 MHz; $CDCl_3$): δ 12.53 (s, 1H, amide$_{HT\text{-}HT}$-*H*), 12.27 (s, 1H, amide$_{thiophene\text{-}HT}$-*H*), 7.80 (d, *J* = 3.7 Hz, 1H, C3$_{thiophene}$-*H*), 7.67 (d, *J* = 4.9 Hz, 1H, C5$_{thiophene}$-*H*), 7.19 (dd, *J* = 4.8, 4.0 Hz, 1H, C4$_{thiophene}$-*H*), 4.40-4.35 (m, 4H, C1$_{hexyl}$-*H*), 2.84 (s, 3H, 3'-Methyl-*H*), 2.80 (s, 3H, 3''-Methyl-*H*), 1.85-1.77 (m, 4H, C2$_{hexyl}$-*H*), 1.48-1.31 (m, 12H, C3-5$_{hexyl}$-*H*), 0.93-0.87 (m, 6H, C6$_{hexyl}$-*H*).

^{13}C-NMR (75 MHz; $CDCl_3$): δ 173.18, 160.48, 152.05, 149.41, 133.06, 130.20, 128.47, 114.83, 65.97, 65.81, 31.54, 31.51, 28.71, 28.77, 25.94, 25.89, 33.72, 22.68, 16.22, 14.14.

FD-MS: m/z = 649.8 [M^+].

UV/vis: 354 nm (DCM), 355 nm, 425 nm (DMF).

Synthesis of thiophene-(HT)$_3$-^{t}butyl ester (3.90c).

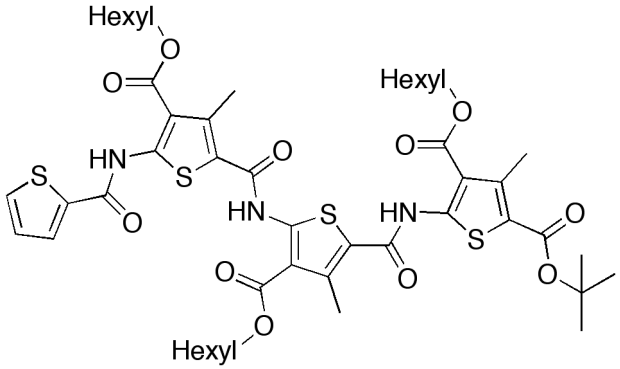

3.91 (0.50 g; 0.80 mmol) was added to a Schlenk flask and flushed with argon. 6 mL oxalyl chloride was added and stirred until a clear solution was obtained. After one hour of stirring oxalyl chloride was removed under reduced pressure at room temperature. The yellow solid was dissolved in 3 mL dichloromethane, which was removed under reduced pressure to remove the rest of oxalyl chloride. The yellow solid was then dissolved in 10 mL THF and **3.52** (0.34 g; 1 mmol) in 5 mL THF and 5 mL pyridine and was and stirred at room temperature for 24 h. The reaction mixture was filtered and THF was removed under reduced pressure. The solution was precipitated into 1 M aqueous hydrochloric acid and filtered. The solid was neutralized with 1 M sodium bicarbonate solution until the washing water was not acidic any more. Column chromatography in chloroform : ethyl acetate (95:5) yielded 0.49 g (0.49 mmol; 61 %).

^{1}H-NMR (300 MHz; $CDCl_3$): δ 12.54 (s, 1H, amide$_{\text{thiophene-HT}}$-*H*), 12.26 (s, 1H, amide$_{\text{HT-HT}}$-*H*), 12.21 (s, 1H, amide$_{\text{HT-HT}}$-*H*), 7.81 (d, *J* = 4.0 Hz, 1H, C3$_{\text{thiophene}}$-*H*), 7.67 (dd, *J* = 5.0, 0.9 Hz, 1H, C5$_{\text{thiophene}}$-*H*), 7.20 (dd, *J* = 4.9, 3.8 Hz, C4$_{\text{thiophene}}$-*H*), 4.42-4.35 (m, 4H, C2$_{\text{hexyl}}$-*H*), 4.24 (t, *J* = 6.6 Hz, 2H, C1$_{\text{hexyl}}$-*H*), 2.86 (s, 3H, 3'-Methyl-*H*), 2.84 (s, 3H, 3''-Methyl-*H*), 2.77 (s, 3H, 3'''-Methyl-*H*), 1.84-1.70 (m, 6H, C2$_{\text{hexyl}}$-*H*), 1.53 (s, 9H, ^{t}Bu-*H*), 1.37-1.30 (m, 18H, C3-5$_{\text{hexyl}}$-*H*), 0.94-0.85 (m, 9H, C6$_{\text{hexyl}}$-*H*).

Synthesis of thiophene-(HT)$_3$-carboxylic acid (3.91c).

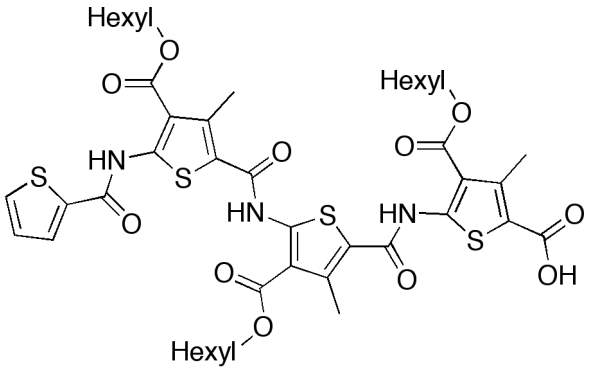

3.91b (0.40 g; 0.40 mmol) was added to a Schlenk flask and flushed with argon. 6 mL oxalyl chloride was added and stirred until a clear solution was obtained. After one hour of stirring oxalyl chloride was removed under reduced pressure at room temperature. The yellow solid was dissolved in 3 mL dichloromethane, which was removed under reduced pressure to remove the rest of oxalyl chloride. The yellow solid was then dissolved in 10 mL THF and **3.80** (0.12 g; 0.6 mmol) in 5 mL THF and 5 mL pyridine and was and stirred at room temperature for 24 h. The reaction mixture was filtered and THF was removed under reduced pressure. The solution was precipitated into 1 M aqueous hydrochloric acid and filtered. The solid was neutralized with 1 M sodium bicarbonate solution until the washing water was not acidic any more. Column chromatography in chloroform : ethyl acetate (95:5) yielded 0.22 g (0.24 mmol; 60 %).

^{1}H-NMR (300 MHz; $CDCl_3$): δ 12.54 (s, 2H, amide$_{HT\text{-}HT}$-*H*, amide$_{thiophene\text{-}HT}$-*H*), 12.30 (s, 1H, amide$_{HT\text{-}HT}$-*H*), 7.81 (d, *J* = 3.9 Hz, 1H, C3$_{thiophene}$-*H*), 7.67 (d, *J* = 5.2 Hz, 1H, C5$_{thiophene}$-*H*), 7.21-7.19 (m, 2H, C4$_{thiophene}$-*H*), 4.42-4.35 (m, 6H, C1$_{hexyl}$-*H*), 2.85 (s, 3H, 3'-Methyl-*H*), 2.81 (s, 6H, 3''-Methyl-*H*, 3'''-Methyl-*H*), 1.85-1.77 (m, 6H, C6$_{hexyl}$-*H*), 1.49-1.30 (m, 18H, C3-5$_{hexyl}$-*H*), 0.95-0.87 (m, 9H, C6$_{hexyl}$-*H*).

MALDI-ToF MS: m/z = [NaM$^+$].

UV/vis: 364 nm (DCM), 337 nm, 431 nm (DMF).

Synthesis of thiophene-(HT)$_4$-carboxylic acid (3.91d).

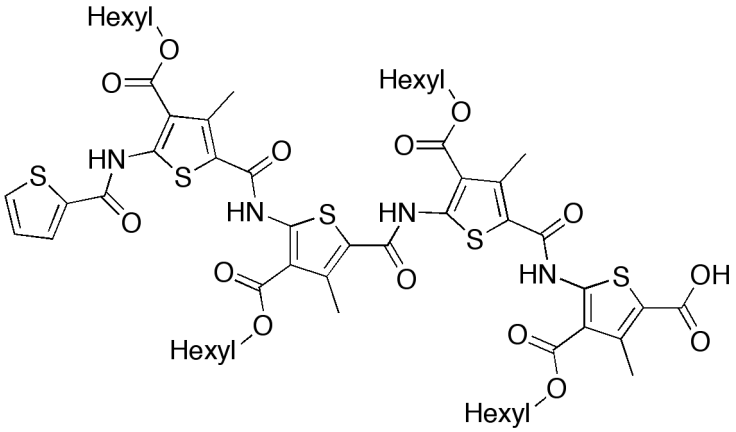

3.91c (0.10 g; 0.11 mmol) was added to a Schlenk flask and flushed with argon. 2 mL oxalyl chloride was added and stirred until a clear solution was obtained. After one hour of stirring oxalyl chloride was removed under reduced pressure at room temperature. The yellow solid was dissolved in 2 mL dichloromethane, which was removed under reduced pressure afterwards in order to remove the rest of oxalyl chloride. The yellow solid was then dissolved in 2 mL THF. **3.80** (0.030 g; 0.15 mmol) where dissolved in 5 mL THF and 5 mL pyridine and added to the solution of thiophene acid chloride and stirred at room temperature for 24 h. The reaction mixture was filtered and THF was removed under reduced pressure. The light yellow brown solution was precipitated into 1 molar aqueous hydrochloric acid and filtered. The white solid was neutralized with 1 M sodium bicarbonate solution until the washing water was not acidic any more. Column chromatography in chloroform : ethyl acetate (90:10) yielded 0.07 g (0.06 mmol; 54 %).

^{1}H-NMR (400 MHz; $CDCl_3$): δ 12.54 (s, 1H, amide$_{\text{thiophene-HT}}$-*H*), 12.32 (s, 1H, amide$_{\text{HT-HT}}$-*H*), 12.28 (s, 2H, amide$_{\text{HT-HT}}$-*H*), 7.81 (dd, *J* = 3.8, 0.6 Hz, 1H, C3$_{\text{thiophene}}$-*H*), 7.67 (dd, *J* = 4.9, 0.9 Hz, 1H, C5$_{\text{thiophene}}$-*H*), 7.20 (dd, *J* = 4.8, 4.0 Hz, 1H, C4$_{\text{thiophene}}$-*H*), 4.44-4.36 (m, 4H, C1$_{\text{hexyl}}$-*H*), 4.15-4.08 (m, 4H, C1$_{\text{hexyl}}$-*H*), 2.87 (s, 3H, 3'-Methyl-*H*), 2.86 (s, 3H, 3''-Methyl-*H*), 2.84 (s, 3H, 3'''-Methyl-*H*), 1.86-1.78 (m, 8H, C2$_{\text{hexyl}}$-*H*), 1.47-1.31 (m, 24H, C3-5$_{\text{hexyl}}$-*H*), 0.93-0.83 (m, 12H, C6$_{\text{hexyl}}$-*H*).

UV/vis: 374 nm (DCM), 319 nm, 429 nm (DMF).

3.7. Supporting Information

TGA for **3.52**

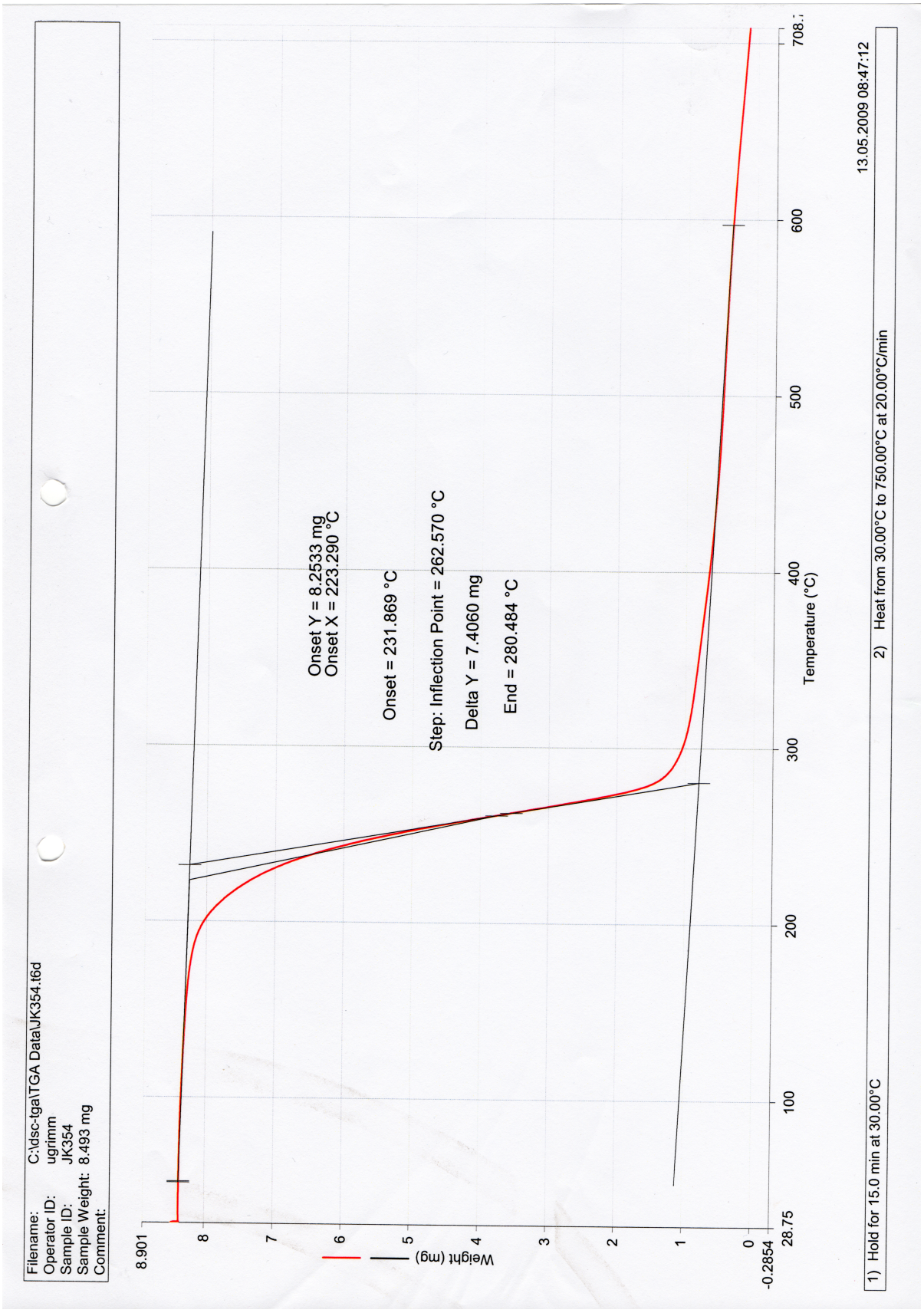

Crystallographic data for **3.91a**

Formula	$C_{18}H_{21}NO_5S_2$ molecular weight 395.48 $gmol^{-1}$ Space group P -1 (triclinic)
Absorption	$\mu = 0.32\ mm^{-1}$
Crystal size	0.04 x 0.23 x 0.44 mm^3 colorless plate
Lattice parameter	a = 7.1790(6)Å α = 93.183(2)° b = 11.5077(9)Å ß = 104.511(2)° c = 11.9069(9)Å γ = 105.898(2)° V = 907.7(2)$Å^3$ z = 2 F(000) = 416 (calculated from 6135 reflexes with 2.4° < θ < 27.8°)
Temperature	-100°C
Density	$d_{rön} = 1.447\ gcm^{-3}$
Diffractometer	SMART CCD
Radiation	Mo-K_α Graphite monochromatic
Scan – Type	ω,φ scans
Scan – Width	0.5°
Range of measurement	2° ≤ θ ≤ 28° -9 ≤ h ≤ 9 -15 ≤ k ≤ 15 -14 ≤ l ≤ 14
Reflexes	
collected	21036
independent	4353 (R_{int} = 0.0305)
observed	3555 (| F | / σ (F) > 4.0)
Corrections	Lorentz- and polarization corrections
Solution	Program: SIR-97 (direct methods)
Refinement	Program: SHELXL-97 (full matrix). 250 refined parameters, rated refinements: $w=1/[\sigma^2(F_o^2) + (0.0512*P)^2+0.53*P]$ where $P=(Max(F_o^2,0)+2*F_o^2)/3$. Hydrogen atoms inserted geometric and refined, non-hydrogen atoms refined anisotropic.
Factor of discrepancy	wR2 = 0.1069 (R1= 0.0386 for observed reflexes, 0.0509 for all reflexes)
Quality of fit	S = 1.030
Max. change of parameters	0.001 * e.s.d
Max. peak height in fourier synthesis	0.97, -0.37 $eÅ^{-3}$

End coordinates and displacement ellipsoid (Å²)

$U_{äq} = (1/3)^* \sum\sum_{ij} a_i^* a_j^* \mathbf{a}_i \mathbf{a}_j$

Atom	X	Y	Z	$U_{äq}$
S1	0.9762(2)	0.16896(8)	1.0089(1)	0.0273(3)
C2	1.0298(2)	0.3006(2)	0.9498(2)	0.0227(5)
C3	1.238(1)	0.353(1)	0.974(1)	0.038(2)
C4	1.3466(3)	0.2813(2)	1.0427(2)	0.0368(7)
C5	1.2167(3)	0.1821(2)	1.0652(2)	0.0356(7)
C1	0.997(3)	0.200(1)	1.003(2)	0.038(2)
S3	1.268(1)	0.3715(9)	0.9697(7)	0.028(1)
C6	0.8603(2)	0.3397(2)	0.8828(2)	0.0240(5)
O7	0.6845(2)	0.2825(1)	0.8695(1)	0.0350(5)
N8	0.9139(2)	0.4454(1)	0.8348(1)	0.0235(5)
C9	0.7787(2)	0.4950(2)	0.7658(1)	0.0208(5)
S10	0.52397(6)	0.42660(4)	0.72793(4)	0.0226(1)
C11	0.4857(2)	0.5426(1)	0.6461(1)	0.0205(5)
C12	0.6605(2)	0.6313(1)	0.6483(1)	0.0192(5)
C13	0.8330(2)	0.6031(1)	0.7184(1)	0.0195(5)
C14	0.2769(2)	0.5304(1)	0.5832(1)	0.0207(5)
O15	0.1469(2)	0.4332(1)	0.5982(1)	0.0316(4)
O16	0.2277(2)	0.6059(1)	0.5198(1)	0.0281(4)
C17	0.6690(3)	0.7416(2)	0.5865(2)	0.0264(6)
C18	1.0473(2)	0.6727(2)	0.7423(1)	0.0211(5)
O19	1.1840(2)	0.6415(1)	0.8039(1)	0.0290(4)
O20	1.0784(2)	0.7720(1)	0.6888(1)	0.0268(4)
C21	1.2864(2)	0.8462(2)	0.7049(2)	0.0285(6)
C22	1.3418(3)	0.9564(2)	0.7954(2)	0.0336(6)
C23	1.1904(3)	1.0288(2)	0.7781(2)	0.0404(8)
C24	1.1442(4)	1.0709(2)	0.6592(2)	0.0423(8)
C25	1.0054(3)	1.1531(2)	0.6460(2)	0.0401(8)
C26	0.7920(4)	1.0938(2)	0.6472(2)	0.0529(10)

Displacement ellipsoid

Atom	U_{11}	U_{22}	U_{33}	U_{12}	U_{13}	U_{23}
S1	0.0263(4)	0.0276(5)	0.0299(4)	0.0100(4)	0.0070(3)	0.0128(3)
C2	0.0211(7)	0.0243(8)	0.0221(8)	0.0073(6)	0.0038(6)	0.0048(6)
C3	0.041(4)	0.032(4)	0.039(3)	0.011(3)	0.007(2)	0.008(2)
C4	0.0229(9)	0.048(1)	0.034(1)	0.0114(8)	-0.0010(8)	0.0007(9)
C5	0.044(1)	0.037(1)	0.0280(10)	0.0216(9)	0.0033(8)	0.0089(8)
C1	0.041(4)	0.032(4)	0.039(3)	0.011(3)	0.007(2)	0.008(2)
S3	0.019(1)	0.030(2)	0.031(2)	0.006(1)	-0.001(1)	0.011(1)
C6	0.0203(7)	0.0279(8)	0.0239(8)	0.0087(6)	0.0042(6)	0.0061(7)
O7	0.0192(6)	0.0381(7)	0.0465(8)	0.0068(5)	0.0059(6)	0.0201(6)
N8	0.0149(6)	0.0253(7)	0.0275(7)	0.0047(5)	0.0013(5)	0.0073(6)
C9	0.0158(7)	0.0228(8)	0.0213(8)	0.0047(6)	0.0021(6)	0.0011(6)
S10	0.0148(2)	0.0224(2)	0.0272(2)	0.0035(1)	0.0017(2)	0.0065(2)
C11	0.0174(7)	0.0202(7)	0.0221(8)	0.0057(6)	0.0022(6)	0.0025(6)
C12	0.0163(7)	0.0199(7)	0.0197(7)	0.0056(6)	0.0023(6)	-0.0001(6)
C13	0.0147(7)	0.0208(8)	0.0204(8)	0.0047(6)	0.0011(6)	0.0003(6)
C14	0.0167(7)	0.0191(7)	0.0236(8)	0.0042(6)	0.0023(6)	0.0009(6)
O15	0.0154(5)	0.0267(6)	0.0450(8)	0.0010(5)	-0.0009(5)	0.0097(6)

Atom	U_{11}	U_{22}	U_{33}	U_{12}	U_{13}	U_{23}
O16	0.0185(5)	0.0274(6)	0.0341(7)	0.0070(5)	-0.0012(5)	0.0068(5)
C17	0.0194(7)	0.0246(8)	0.0336(9)	0.0063(6)	0.0035(7)	0.0088(7)
C18	0.0180(7)	0.0212(8)	0.0229(8)	0.0056(6)	0.0039(6)	0.0014(6)
O19	0.0153(5)	0.0302(7)	0.0375(7)	0.0052(5)	0.0009(5)	0.0093(5)
O20	0.0142(5)	0.0255(6)	0.0374(7)	0.0026(4)	0.0041(5)	0.0087(5)
C21	0.0154(7)	0.0295(9)	0.0377(10)	0.0007(6)	0.0082(7)	0.0082(7)
C22	0.0234(8)	0.037(1)	0.0320(10)	-0.0004(7)	0.0041(7)	0.0038(8)
C23	0.045(1)	0.036(1)	0.036(1)	0.0056(9)	0.0133(9)	-0.0003(9)
C24	0.055(1)	0.036(1)	0.041(1)	0.0125(10)	0.023(1)	0.0069(9)
C25	0.055(1)	0.0268(10)	0.041(1)	0.0105(9)	0.0173(10)	0.0069(8)
C26	0.055(1)	0.051(1)	0.057(2)	0.014(1)	0.025(1)	0.011(1)

End coordinates and displacement ellipsoid of hydrogen atoms(Å^2)

Atom	X	Y	Z	U_{iso}
H3	1.29989	0.42671	0.94833	0.045
H4	1.48924	0.30095	1.06847	0.0442
H5	1.26063	0.12413	1.11029	0.0428
H1	0.86908	0.14808	1.00496	0.045
H8	1.03598	0.48722	0.84200	0.0282
H15	0.00087	0.40676	0.54535	0.0474
H17A	0.53175	0.74189	0.54736	0.0396
H17B	0.74369	0.73978	0.52822	0.0396
H17C	0.73714	0.81520	0.64347	0.0396
H21A	1.30251	0.87329	0.62944	0.0341
H21B	1.37846	0.79662	0.73017	0.0341
H22A	1.47426	1.01127	0.79450	0.0403
H22B	1.35718	0.92900	0.87365	0.0403
H23A	1.06324	0.97767	0.79011	0.0485
H23B	1.24348	1.10111	0.83875	0.0485
H24A	1.07985	0.99845	0.59894	0.0508
H24B	1.27254	1.11602	0.64425	0.0508
H25A	1.06614	1.22211	0.71011	0.0481
H25B	1.00261	1.18750	0.57140	0.0481
H26A	0.73082	1.02317	0.58618	0.079
H26B	0.71511	1.15248	0.63230	0.079
H26C	0.79083	1.06715	0.72379	0.079

3.8. References

1. Katz, H. *J. Mater. Chem.* **1997,** 7, (3), 369-376.
2. Burroughes, J. H.; Bradley, D. D. C.; Brown, A. R.; Marks, R. N.; Mackay, K.; Friend, R. H.; Burns, P. L.; Holmes, A. B. *Nature* **1990,** 347, (6293), 539.
3. *Handbook of Conducting Polymers 2nd Edition* (Skotheim, T.; Reynolds, J.; Elsenbamer, R.) Marcel Dekker, Inc., New York, NY, USA: 1998.
4. *Handbook of Conducting Polymers* (Skotheim, T.) Marcel Dekker, Inc., New York, NY, USA: 1986.
5. *Electronic Materials: The Oligomer Approach* (Müllen, K.; Wegner, G.) John Wiley & Sons: 1998.
6. Martinez, F.; Voelkel, R.; Naegele, D.; Naarmann, H. *Mol. Cryst. Liq. Crys.* **1989**, 227-232.
7. Xu, B.; Fichou, D.; Horowitz, G.; Garnier, F. *Adv. Mater.* **1991,** 3, (3), 150-153.
8. Garnier, F.; Horowitz, G.; Peng, X.; Fichou, D. *Adv. Mater.* **1990,** 2, (12), 592-594.
9. Garnier, F.; Horowitz, G.; Fichou, D. *Synthetic Met* **1989,** 28, (1-2), 705-714.
10. Fichou, D.; Horowitz, G.; Nishikitani, Y.; Garnier, F. *Synthetic Met* **1989,** 28, (1-2), 723-727.
11. Yoshino, K. *Synthetic Met* **1989,** 28, (1-2), 669-674.
12. Yamamoto, T.; Sanechika, K.; Yamamoto, A. *J. Poly. Sci., Polym. Lett. Ed.* **1980,** 18, (1), 9-12.
13. Lin, J. W. P.; Dudek, L. P. *J. Polym. Sci., Polym. Chem. Ed.* **1980,** 18, (9), 2869-2873.
14. Yamamoto, T.; Maruyama, T.; Zhou, Z.; Miyazaki, Y.; Kanbara, T.; Sanechika, K. *Synthetic Met* **1991,** 41, (1-2), 345-348.
15. Yamamoto, T.; Morita, A.; Maruyama, T.; Zhou, Z.; Kanbara, T.; Sanechika, K. *Polym. J.* **1990,** 22, (2), 187-190.
16. Yamamoto, T.; Morita, A.; Miyazaki, Y.; Maruyama, T.; Wakayama, H.; Zhou, Z. H.; Nakamura, Y.; Kanbara, T.; Sasaki, S.; Kubota, K. *Macromolecules* **1992,** 25, (4), 1214-1223.
17. Yamamoto, T.; Osakada, K.; Wakabayashi, T.; Yamamoto, A. *Makromol. Chem., Rapid. Commun.* **1985,** 6, (10), 671-674.
18. Yamamoto, T.; Sanechika, K.; Yamamoto, A. *Bull. Chem. Soc. Jpn.* **1983,** 56, (5), 1497-1502.
19. Hotz, C. Z.; Kovacic, P.; Khoury, I. A. *J. Polym. Sci., Polym. Chem. Ed.* **1983,** 21, (9), 2617-2628.
20. Kobayashi, M.; Chen, J.; Chung, T.; Moraes, F.; Heeger, A.; Wudl, F. *Synthetic Met* **1984,** 9, (1), 77-86.
21. Colon, I.; Kwiatkowski, G. T. *J. Polym. Sci., Polym. Chem. Ed.* **1990,** 28, (2), 367-383.
22. Meyer, V. *Chem. Ber.* **1883,** 16, (1), 1465-1478.
23. Julia, L.; Davies, A. G.; Rveda, D. R.; Balta-Calleja, F. J. *Chem. Ind.* **1989**, 78.
24. Berlin, A.; Pagani, G.; Sannicol, F. *J. Chem. Soc., Chem. Commun.* **1986**, (22), 1663-1664.
25. Sugimoto, R.; Takeda, S.; Gu, H. B.; Yoshino, K. *Chem. Express* **1986,** 1, 635.
26. Jen, K. Y.; Oboodi, R.; Elsenbaumer, R. L. *Polym. Mater. Sci. Eng.* **1985,** 53, 79.
27. Elsenbaumer, R. L.; Jen, K. Y.; Oboodi, R. *Synthetic Met* **1986,** 15, (2-3), 169-174.
28. Jen, K. Y.; Miller, G.; Elsenbaumer, R. L. *J. Chem. Soc., Chem. Commun.* **1986**, (17), 1346-1347.
29. Sato, M.; Tanaka, S.; Kaeriyama, K. *J. Chem. Soc., Chem. Commun.* **1986**, (11), 873-874.
30. Hotta, S.; Rughooputh, S. D. D. V.; Heeger, A. J.; Wudl, F. *Macromolecules* **1987,** 20, (1), 212-215.
31. Chen, S. A.; Tsai, C. C. *Macromolecules* **1993,** 26, (9), 2234-2239.
32. Leclerc, M.; Diaz, F. M.; Wegner, G. *Makromol. Chem.* **1989,** 190, (12), 3105-3116.

33. Pomerantz, M.; Tseng, J. J.; Zhu, H.; Sproull, S. J.; Reynolds, J. R.; Uitz, R.; Arnott, H. J.; Haider, M. I. *Synthetic Met* **1991,** 41, (3), 825-830.
34. Sato, M.; Morii, H. *Poly. Commun.* **1991,** 32, 42.
35. Sato, M.; Morii, H. *Macromolecules* **1991,** 24, (5), 1196-1200.
36. Fichou, D., *Handbook of Oligo- and Polythiophenes* Wiley-VCH: 1999.
37. Elsenbaumer, R. L.; Yen, K. Y.; Miller, G. G.; Eckhardt, H.; Shacklette, L. W.; Jow, R., *Electronic Properties of Conjugated Polymers* (Kuzmany, H.; Mehring, M.; Roth, S.) Springer: New York, Springer Series in Solid State Sciences, 1987; Vol. 76.
38. McCullough, R. D.; Lowe, R. D. *J. Chem. Soc., Chem. Comm.* **1992**, (1), 70-72.
39. Tamao, K.; Kiso, Y.; Sumitani, K.; Kumada, M. *J. Am. Chem. Soc.* **1972,** 94, (26), 9268-9269.
40. Tamao, K.; Kodama, S.; Nakajima, I.; Kumada, M. *Tetrahedron* **1982,** 38, (22), 3347-3354.
41. Tamao, K.; Sumitani, K.; Kiso, Y.; Zembayashi, M.; Fujioka, A.; Kodama, S.; Nakajima, I.; Minato, A.; Kumada, M. *Bull. Chem. Soc. Jpn.* **1976,** 49, (7), 1958-1969.
42. Tamao, K.; Sumitani, K.; Kumada, M. *J. Am. Chem. Soc.* **1972,** 94, (12), 4374-4376.
43. Eachern, A. M.; Soucy, C.; Leitch, L. C.; Arnason, J. T.; Morand, P. *Tetrahedron* **1988,** 44, (9), 2403-2412.
44. Soucy-Breau, C.; Eachern, A. M.; Leitch, L. C.; Arnason, T.; Morand, P. *J. Heterocycl. Chem.* **1991,** 28, (2), 411-416.
45. Loewe, R. S.; Ewbank, P. C.; Liu, J.; Zhai, L.; McCullough, R. D. *Macromolecules* **2001,** 34, (13), 4324-4333.
46. Loewe, R. S.; Khersonsky, S. M.; McCullough, R. D. Journal 1999, 11, (Issue), 250-+.
47. Sheina, E. E.; Liu, J.; Iovu, M. C.; Laird, D. W.; McCullough, R. D. *Macromolecules* **2004,** 37, (10), 3526-3528.
48. Jeffries-El, M.; Sauvé, G.; McCullough, R. D. *Adv. Mater.* **2004,** 16, (12), 1017-1019.
49. Liu, J.; McCullough, R. D. *Macromolecules* **2002,** 35, (27), 9882-9889.
50. Chen, T. A.; Rieke, R. D. *J. Am. Chem. Soc.* **1992,** 114, (25), 10087-10088.
51. Chen, T. A.; Rieke, R. D. *Synthetic Met* **1993,** 60, (2), 175-177.
52. Chen, T. A.; O'Brien, R. A.; Rieke, R. D. *Macromolecules* **1993,** 26, (13), 3462-3463.
53. Chen, T. A.; Wu, X. M.; Rieke, R. D. *J. Am. Chem. Soc.* **1995,** 117, (1), 233-244.
54. Wu, X. M.; Chen, T. A.; Rieke, R. D. *Macromolecules* **1995,** 28, (6), 2101-2102.
55. Stein, P. C.; Botta, C.; Bolognesi, A.; Catellani, M. *Synthetic Met* **1995,** 69, (1-3), 305-306.
56. Maior, R. M. S.; Hinkelmann, K.; Eckert, H.; Wudl, F. *Macromolecules* **1990,** 23, (5), 1268-1279.
57. McCullough, R. D.; Lowe, R. D.; Jayaraman, M.; Anderson, D. L. *J. Org. Chem.* **1993,** 58, (4), 904-912.
58. Barbarella, G.; Bongini, A.; Zambianchi, M. *Macromolecules* **1994,** 27, (11), 3039-3045.
59. McCullough, R. D.; Lowe, R. D.; Jayaraman, M.; Ewbank, P. C.; Anderson, D. L.; Tristram-Nagle, S. *Synthetic Met* **1993,** 55, (2-3), 1198-1203.
60. Mao, H.; Xu, B.; Holdcroft, S. *Macromolecules* **1993,** 26, (5), 1163-1169.
61. McCullough, R. D.; Tristram-Nagle, S.; Williams, S. P.; Lowe, R. D.; Jayaraman, M. *J. Am. Chem. Soc.* **1993,** 115, (11), 4910-4911.
62. Stille, J. K. *Angew. Chem. Int. Edit.* **1986,** 25, (6), 508-524.
63. Zagorska, M.; Kulszewicz-Bajer, I.; Pron, A.; Firlej, L.; Bernier, P.; Galtier, M. *Synthetic Met* **1991,** 45, (3), 385-393.
64. McCullough, R. D.; Belot, J. A.; Williams, S. P., *Molecular Engineering of Advanced Materials* (Becher, J.; Schaumburg, K.) NATO Adv. Res. Workshop Series, Series C: Math. and Phys. Sci., 1995; Vol. 456, p 349.
65. McCullough, R. D.; Williams, S. P.; Tristram-Nagle, S.; Jayaraman, M.; Ewbank, P. C.; Miller, L. *Synthetic Met* **1995,** 69, (1-3), 279-282.

66. McCullough, R. D.; Williams, S. P.; Jayaraman, M.; Reddinger, J.; Miller, L.; Tristram-Nagle, S., *Eletrical, Optical, and Magnetic Properties of Organic Solid State Materials* (Dalton, L.; Lee, C.) Pittsburgh, PA, Mater. Res. Soc., 1994; Vol. 328, p 215.
67. Yue, S.; Berry, G. C.; Mccullough, R. D. *Macromolecules* **1996,** 29, (3), 933-939.
68. Prosa, T. J.; Winokur, M. J.; McCullough, R. D. *Macromolecules* **1996,** 29, (10), 3654-3656.
69. Bouman, M. M.; Meijer, E. W. *Adv. Mater.* **1995,** 7, (4), 385-387.
70. Steinkopf, W.; Köhler, W. *Lieb. Ann. Chem.* **1936,** 522, (1), 17-27.
71. Geiger, F.; Stoldt, M.; Schweizer, H.; Bäuerle, P.; Umbach, E. *Adv. Mater.* **1993,** 5, (12), 922-925.
72. Gronowitz, S.; Karlsson, H. *Arkiv. Kemi.* **1960,** 17, 89.
73. Rossi, R.; Carpita, A.; Ciofalo, M.; Houben, J. L. *Gazz. Chim. Ital.* **1990,** 120, 793.
74. Kauffmann, T. *Angew. Chem.* **1974,** 86, (9), 321-335.
75. Kagan, J.; K. Arora, S. *Heterocycles* **1983,** 20, (10), 1937-1940.
76. Wynberg, H.; Logothetis, A. *J. Am. Chem. Soc.* **1956,** 78, (9), 1958-1961.
77. Atkinson, R.; Curtis, R.; Phillips, G. *J. Chem. Soc., C* **1967**, 2011-2015.
78. Nilsson, M.; Ullenius, C. *Acta Chem. Scand.* **1970,** 24, 2379.
79. Fanta, P. E. *Synthesis* **1974**, 9.
80. Corriu, R. J. P.; Masse, J. P. *J. Chem. Soc., Chem. Commun.* **1972,** 3, 144.
81. Kumada, M. *Pure Appl. Chem.* **1980,** 52, (3), 669-679.
82. Carpita, A.; Rossi, R.; Veracini, C. A. *Tetrahedron* **1985,** 41, (10), 1919-1929.
83. Kalinin, V. *Synthesis* **1992,** 1992, (05), 413-432.
84. Azizian, H.; Eaborn, C.; Pidcock, A. *J. Organomet. Chem.* **1981,** 215, (1), 49-58.
85. Kashin, A. N.; Bumagina, I. G.; Bumagin, N. A.; Bakunin, V. A. *J. Org. Chem., USSR* **1981,** 17, 789.
86. Crisp, G. T. *Synth. Commun.* **1989,** 19, (1&2), 307-316.
87. Yui, K.; Aso, Y.; Otsubo, T.; Ogura, F. *Bull. Chem. Soc. Jpn.* **1989,** 62, (1539).
88. Miyaura, N.; Yanagi, T.; Suzuki, A. *Synth. Commun.* **1981,** 11, (7), 513-519.
89. Miller, R. B.; Dugar, S. *Organometallics* **1984,** 3, (8), 1261-1263.
90. Gronowitz, S.; Peters, D. *Heterocycles* **1990,** 30, 645.
91. Gronowitz, S.; Lawitz, K. *Chem. Scr.* **1983,** 22, 265.
92. Pham, C. V.; Burkhardt, A.; Shabana, R.; Cunningham, D. D.; Jr, H. B. M.; Zimmer, H. *Phosph. Sulf. Silic.* **1989,** 46, (3&4), 153-168.
93. Becker, R. S.; de Melo, J. S.; Macanita, A. L.; Elisei, F. *Pure & Appl. Chem.* **1995,** 67, 9.
94. Abbel, R.; Frey, H.; Schollmeyer, D.; Kilbinger, A. F. M. *Chem. Eur. J.* **2005,** 11, 2170-2176.
95. Abbel, R.; Schleuss, T. W.; Frey, H.; Kilbinger, A. F. M. *Macromol. Chem. Physic.* **2005,** 206, (20), 2067-2074.
96. Pope, M.; Swenberg, C. E., *Electronic Processes in Organic Crystals and Polymers* 2nd Edition; Oxford University Press: Oxford, 1999.
97. "Lumineszenz", Microsoft Encarta Online-Enzyklopädie **2008**, http://de.encarta.msn.com
98. Winter, R.; Noll, F., Methoden der Biophysikalischen Chemie. In B:G: Teubner: 1998.
99. Nigam, S.; Rutan, S. *Appl. Spectroscopy* **2001,** 55, (11), 362-370.
100. Reichardt, C., In *Solvents and Solvent Effect in Organic Chemistry, 3rd Edition*, Wiley-VCH: Weinheim, 2002; pp 329-359.
101. Gewald, K. *Chem. Ber.* **1965,** 98, (11), 3571-3577.
102. Gewald, K.; Schinke, E.; Böttcher, H. *Chem. Ber.* **1966,** 99, (1), 94-100.
103. *Organikum* (Becker, H. G. O.; Beckert, R.; Domschke, G.; Fanghändel, E.; Habicher, W. D.; Metz, P.; Pavel, D.; Schwetlick, K.) 21.; Wiley-VCH: Weinheim, Germany, 2001.
104. Valencic, M. *Tetrahedron letters* **1998,** 39, (12), 1625-1628.

105. Marcantoni, E.; Massimo Massaccesi, a.; Torregiani, E.; Bartoli, G.; Bosco, M.; Sambri, L. *J. Org. Chem* **2001,** 88, (12), 4430-4432.
106. Klemm, L. H.; Antoniades, E. P.; Lind, C. D. *J. Org. Chem.* **1962,** 27, (2), 519-526.
107. Lampe, J. W.; Hughes, P. F.; Biggers, C. K.; Smith, S. H.; Hu, H. *J. Org. Chem.* **1996,** 61, (14), 4572-4581.
108. Pyne, S. G. *Tetrahedron Lett.* **1987,** 28, (40), 4737-4740.
109. Bergeron, R. J.; Mcmanis, J. S. *J. Org. Chem.* **1988,** 53, (13), 3108-3111.
110. Schwartz, M. A.; Rose, B. F.; Vishnuvajjala, B. *J. Am. Chem. Soc.* **1973,** 95, (2), 612-613.
111. Rao, T. S.; Nampalli, S.; Sekher, P.; Kumar, S. *Tetrahedron Lett.* **2002,** 43, (43), 7793-7795.
112. Katritzky, A. R.; Hai-Ying He, a.; Suzuki, K. *J. Org. Chem.* **2000,** 65, (24), 8210-8213.
113. Newman, H. *J. Org. Chem.* **1965,** 30, (4), 1287-1288.
114. Quick, J.; Meltz, C. *J. Org. Chem.* **1979,** 44, (4), 573-578.
115. Baker, R.; Castro, J. L. *J. Chem. Soc., Perkin Trans. 1* **1990**, 47-65.
116. Albanese, D.; Corcella, F.; Landini, D.; Maia, A.; Penso, M. *J. Chem. Soc., Perkin Trans. 1* **1997**, (3), 247-250.
117. Meier, H.; Stalmach, U.; Kolshorn, H. *Acta Polymer.* **1997,** 48, (9), 379-384.
118. Lourderaj, U.; Giri, K.; Sathyamurthy, N. *J. Phys. Chem. A* **2006,** 110, (8), 2709-2717.
119. Jelly, E. E. *Nature* **1936,** 128, 1009.

Chapter 4. Supplements: Reactions in micro structured reactors

4.1. Ionic Liquids on Demand in Continuous Flow

Daniel Wilms, Johannes Klos, Andreas F. M. Kilbinger, Holger Löwe*, and Holger Frey*

Published in: "Ionic Liquids on Demand in Continuous Flow." D. Wilms; J. Klos; A.F.M. Kilbinger; H. Lowe; H. Frey; *Org. Process Res. Dev.* **2009** , 13 (5), 961-964.

4.1.1. Abstract

We report on the development of an alternative protocol for the facile solvent-free synthesis of various novel imidazolium-based ionic liquids (ILs) that affords highly pure products without the necessity of subsequent purification steps. The continuous approach is based on the combination of HPLC pumps with a micromixer and a capillary residence tube. Our system provides a high degree of control over the alkylation reactions due to a high surface-to-volume ratio and superior heat- and mass transport. Within the scope of our studies, we focused on ionic liquids containing differently substituted phenyl rings and characterized these compounds with respect to further use for direct application or subsequent reaction sequences. Scale-up can conveniently be achieved by operating several reactors with high continuous throughput in parallel.

4.1.2. Introduction

Ionic liquids are generally understood as fluids that solely consist of ions, yet differ from conventional molten salts in a variety of properties.[1] While the latter mostly exhibit high melting points, viscosity and corrosiveness, the former species are usually liquid below 100°C, non-volatile and possess an almost negligible vapor pressure. Numerous ionic liquids have been synthesized in the past,[2-5] however this class of compounds only attracted broad attention when hydrolysis-stable compounds with strongly expanded potential for practical applications were introduced in the early 1990s.[6] Within the last 15 years, a wide variety of ionic liquids have been prepared, characterized with respect to both physical and chemical properties and increasingly used as an alternative to classic organic solvents, as they often show high dissolving power for otherwise sparingly soluble compounds.[1, 7, 8] The first step in the synthesis of ionic liquids usually involves formation of the cation by quarternization of an amine or phosphane. Variation of the alkylating agent leads to salts with different anions, typically halide ions. The demand for ionic liquids for a variety of synthetic and analytical purposes has been steadily growing in recent years. Due to their inherent non-volatility, ionic liquids can not be conveniently distilled prior to use as solvents or reactants. However, very high purity of these compounds is essential for their practical use, which often requires tedious subsequent purification steps, leading to high cost and limited potential for industrial application.

Microstructured reactors have recently attracted increasing interest due to significant benefits originating in very short diffusion pathways and large interfacial contact areas per unit volume (10,000 – 50,000 m^2/m^3)[9] that result in superior heat and mass transfer compared to conventional lab reactors. Consequently, higher yields and selectivities as well as improved product qualities have been achieved by transferring chemical reactions (especially those that are highly exothermic or endothermic) from classical batch reactors to microstructured devices.[9-14] Higher throughput of products is often conveniently accessible by running several microreactors in a parallel set-up. Thus continuous reaction platforms based on micromixing of reactants offer intriguing potential for the preparation of ionic liquids. Waterkamp et al. described the preparation of 1-butyl-3-methylimidazolium bromide in a microstructured reactor and carried out an elegant process intensification study.[15] In another interesting study, Renken et al. reported on the high reactor performance of a microstructured device in the case of a continuously synthesized imidazolium ethylsulfate.[16] Here we present the development of a simple but highly

versatile approach for the synthesis of a variety of high purity ionic liquids in a continuous flow reactor equipped with a micromixer, circumventing any additional purification steps.

4.1.3. Experimental

Materials: All chemicals were purchased from Acros Organics and used as received. Deuterated DMSO-d_6 was purchased from Deutero GmbH and used as received.

Instrumentation: ^{1}H-NMR- and ^{13}C-NMR- spectra were recorded at 300 MHz and 75 MHz respectively on a Bruker AC and are referenced internally to residual proton signals of the deuterated solvent.

DSC curves were recorded on a Perkin Elmer DSC 7 and a Perkin Elmer Thermal Analysis Controller TAC 7/DX.

X-Ray structure determination was collected on a Bruker AXS Smart CCD diffractometer with graphite monochromated Mo-K_α radiation (λ = 0.71069 Å).

Synthesis of ionic liquids in batch: In a typical experiment, a 100 mL two-necked glass flask equipped with a a mechanical stirrer was charged with 17.78 mL (20.8 g, 0.126 mol) 1-bromohexane and 10 mL (10.35 g, 0.126 mol) 1-methylimidazole and immediately immersed into an oil bath pre-tempered to the desired temperature. After stirring for 10 min, small samples were removed, cooled down to 0°C and dissolved in DMSO-d_6 for NMR characterization.

Synthesis of ionic liquids in continuous flow: All reactions were carried out in a continuous flow reaction set-up provided by the Institut für Mikrotechnik Mainz (IMM). It consists of a tempered oil bath hosting the micromixing device (stainless steel interdigital SIMM-V2 mixer with an internal volume of 8 μL and channel widths of 45 μm) that is equipped with two reactant inlets and one outlet. In a typical experiment, alkyl bromide and imidazole were separately pumped into the mixing chamber. After mixing, the reaction mixture is directly guided into the respective capillary residence tube with a diameter of 500 μm (Volume = 10mL or 30 mL). The rear end of the tubular delay tube leads to the reactor outlet. Flow rates are controlled via HPLC pumps (Knauer WellChrom K-501, inert 10mL pump heads with ceramic inlays).

4.1.4. Results and Discussion

All syntheses presented in this paper were carried out in a reactor equipped with a stainless steel slit-interdigital mixer provided by the *Institut für Mikrotechnik Mainz* (IMM). The layout of the micromixer allows mixing processes to take place within milliseconds due to the combination of the regular flow pattern created by multi-lamination with geometric focusing (Figure 4.1).

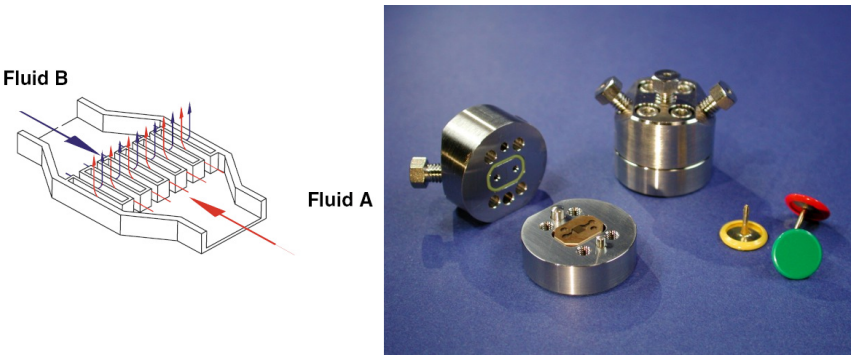

Figure 4.1: Mixing principle and set-up of the slit-interdigital mixer. The inner volume of the micromixer is 8 µL. Mixing takes place by very fast diffusion between the thin reactant layers formed by the parallel microchannel alignment.

Residence times are very short as the inner volume of the mixer is extremely small (approximately 8µL). High pressure stability of the set-up (up to 100 bar) permits continuous flow at viscosities of up to 10,000 mPas. In order to determine the applicability of the continuous reactor set-up for the intended synthesis of ionic liquids, a compound well established in conventional batch synthesis (3-hexyl-1-methylimidazolium bromide **IL-1**) was targeted. It can be obtained from alkylation of 1-methylimdidazole with 1-bromohexane and exhibits very low viscosity at elevated temperatures. Hence, it was considered a suitable reaction product for an initial test-run of the applied set-up, which included two HPLC pumps separately introducing the liquid reactants to the preheated micromixer. There, the fluids are combined to form a homogeneous solution that is passed through a residence tube of variable length before the reaction product is recovered at the outlet of the device (Figure 4.2).

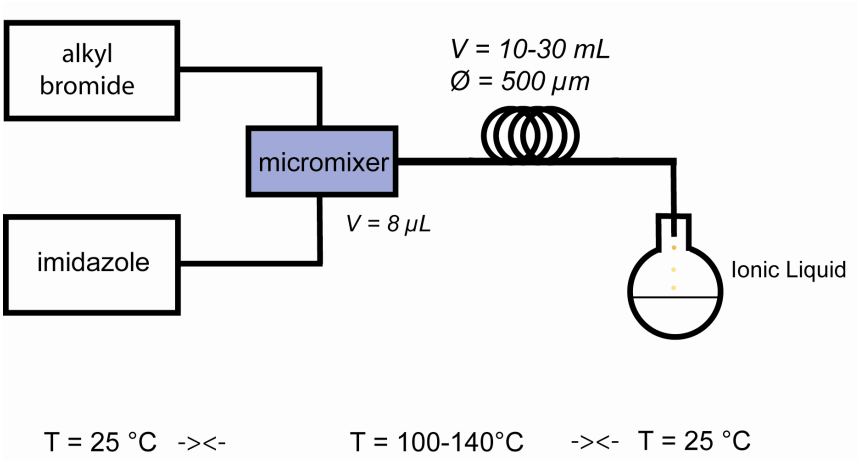

Figure 4.2: Illustration of the experimental set-up for the synthesis of ionic liquids in continuous flow.

The reaction time can be varied by simply adjusting the flow rate and/or elongation or shortening of the residence tube. Compound **IL-1** was obtained as a slightly yellow liquid. The highly efficient mixing process permits working at a temperature of 140°C without noticeable hotspot formation. These reaction conditions accounted for very short reaction times of 5 – 10 min, depending on the specific system and the flow rates. The ^{1}H-NMR spectrum of **IL-1** is shown in Figure 4.3. It indicates a remarkably high quality of the crude ionic liquid recovered directly from the outlet of the microreactor set-up without the necessity for further purification steps.

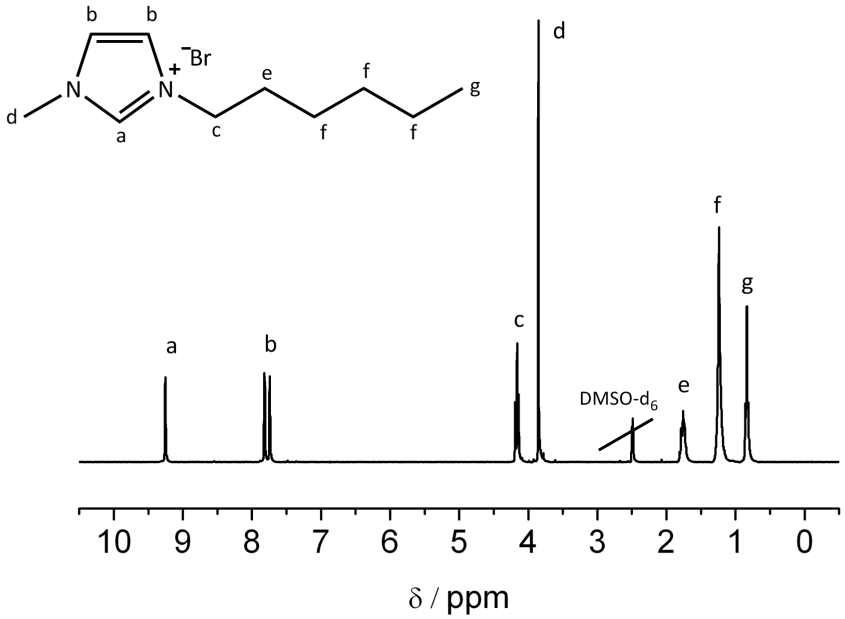

Figure 4.3 ^{1}H-NMR spectrum of 3-hexyl-1-methylimidazolium bromide (IL-1).

In addition, analysis by HPLC showed less than 1% of impurities (mostly unreacted starting materials). In the conventional batch synthesis, the reaction proceeds explosively at temperatures higher than 100°C and thus has to be carried out at milder conditions. Lower temperatures however involve the drawback of significantly slower kinetics. High conversions cannot be achieved within reaction times in a range comparable to the continuous flow approach. For instance, after 10 min at 60°C, a conversion of only 5% was observed in the batch experiment, whereas the continuous flow set-up permits to work safely at high temperatures without thermal overrun and subsequent loss of control over the reaction. NMR spectra and conversion data for the samples obtained by the standard batch approach can be found in the Supporting Information. Encouraged by the promising initial results obtained by applying the continuous set-up we directed our efforts towards the synthesis of entirely new ionic liquids that had not been reported previously. These were prepared by alkylation of alkylimidazoles with phenylalkyl bromides in the microstructured reactor. The novel compounds represented an interesting class of ILs for probing and establishing the versatility of our continuous flow process. Figure 4.4 depicts the pathway to four different novel ionic liquids that we prepared in the microstructured reaction device described above.

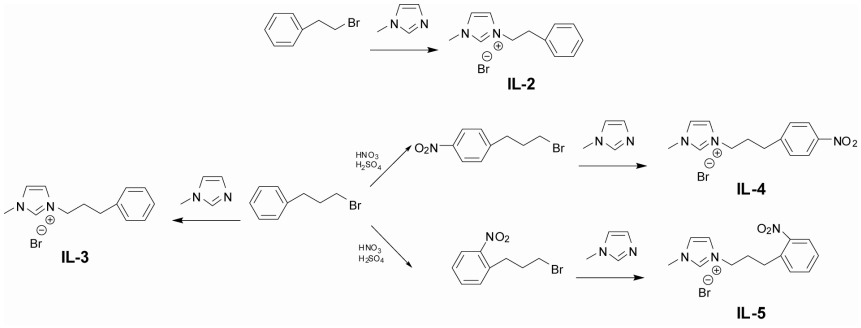

Figure 4.4: Synthesis of phenylalkyl imidazolium bromides.

All compounds were obtained as slightly yellow or orange liquids at high throughputs between 100 and 200 ml/h at analogous conditions to the preparation of **IL-1**. The respective ^{1}H-NMR spectra of compounds **IL-2 – IL-5**, measured directly after recovery from the continuous reaction device (see Figure 4.5) indicate complete reactant conversion as well as the absence of any undesired side products, which are frequently observed in conventional batch syntheses for ionic liquids.

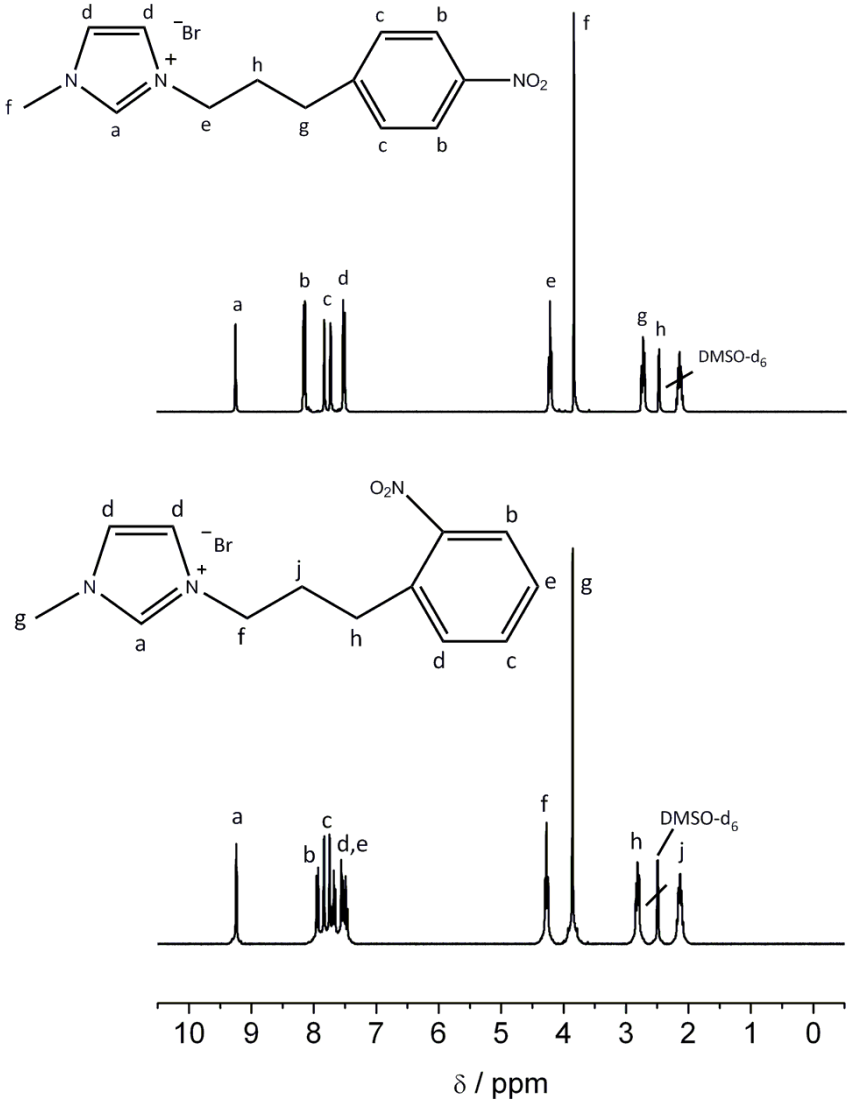

Figure 4.5: ^{1}H-NMR spectra of novel nitrophenyl substituted ionic liquids IL-4 (top) and IL-5 (bottom).

It should be noted that compound **IL-2** differs from the ionic liquid **IL-3** by just one methylene group. However, **IL-2** does not remain liquid at room temperature, but turns into a tough yellow solid after several hours that can be recrystallized from acetone to form colorless needles. The crystal structure of recrystallized **IL-2** was characterized by X-ray crystallography and is shown in Figure 4.6.

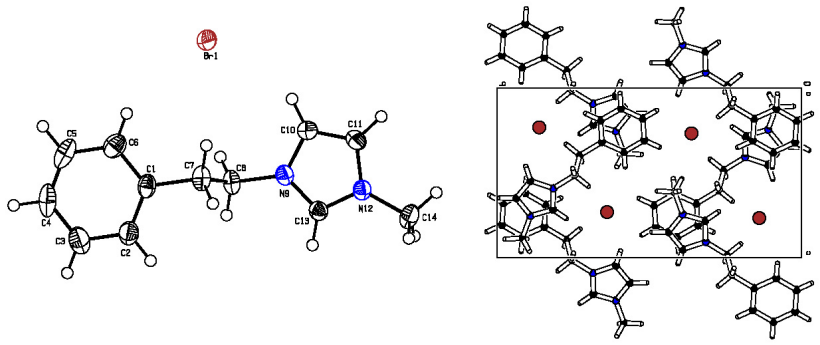

Figure 4.6: Single crystal X-ray structure of 1-methyl-3-phenethyl-imidazolium bromide **IL-2**.

The additional methylene group incorporated into compound **IL-3** is sufficient to prevent formation of a highly ordered crystal lattice at room temperature. The ionic liquids possessing a nitro group on the phenyl substituent remained liquid at room temperature for prolonged periods, but started crystallizing after several weeks. Nitro groups introduce an additional polar moiety capable of intermolecular interaction that apparently promotes slow crystallization, a behavior that is not observed for the non-substituted derivative **IL-3**. Thermal analysis (DSC) of the ionic liquids obtained from the microreactor showed generally low glass transition temperatures below 0°C and a clear trend in the phenyl-substituted series **IL-2 – IL-5**. The presence of an additional nitro group leads to a strong increase of the T_g. Compound **IL-1** exhibits the lowest transition temperature, attributed to the disorder associated with the flexible alkyl substituent. While **IL-3** is liquid at room temperature, all other species, exhibiting the typical characteristics of ionic liquids, should be employed at temperatures above 50°C where they form viscous liquids.

Ionic liquids **IL-1 – IL-5** represent typical examples for expedient, easily accessible ionic liquids that exhibit high dissolving power for polar organic compounds. Another interesting ionic liquid prepared within the scope of our initial investigations was a structure containing a vinyl instead of a methyl group (Figure 4.7). This was achieved by reaction of vinyl imidazole with 1-bromohexane.

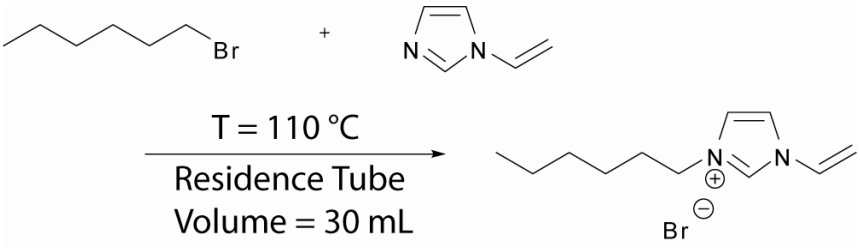

Figure 4.7: Synthesis of 3-hexyl-1-vinylimidazolium bromide.

In order to prevent thermal polymerization of the vinyl function, this compound was prepared at a reduced temperature of 110°C using a delay loop with an increased inner volume of 30 mL. Incorporation of a vinyl group into an ionic liquid offers great potential for structural diversification, as the respective compounds can be derivatized by subsequent reaction sequences such as olefin cross metathesis, radical polymerization, hydrosilylation and other olefin addition reactions. It is important to point out the versatility of the process described. Reaction temperatures and residence times can be individually chosen without having to change the experimental set-up. A crucial advantage of the described approach is the possibility to prepare large product amounts under little experimental effort. Scale-up can be achieved by simply operating several continuous flow reactors in parallel. While in a typical experiment using a single microstructured reactor, up to 200 mL of high purity ionic liquid can be prepared, the employment of additional similar devices and parallel operation provides convenient access to multi-kilogram per hour scales without having to resort to a more complex system.

Table 4.1. Glass temperatures of ionic liquids synthesized in the microstructured reaction device.

Ionic liquid	**IL-1**	**IL-2**	**IL-3**	**IL-4**	**IL-5**	**IL-6**
T_g / °C	- 68.6	- 47.3	- 39.1	- 8.9	- 6.3	- 65.6
Crystallization at room temperature	No	Yes	No	Yes	Yes	No

4.1.5. Conclusion

In conclusion, we have developed a quick and facile continuous flow process for the synthesis of ionic liquids in a microstructured reactor. The remarkably versatile approach based on micromixing of the reactants permitted the first preparation of imidazolium-type ILs bearing additional aromatic units. A wide variety of further novel ionic liquids are conveniently accessible by this procedure under facile control of the reaction parameters. Our approach avoids time consuming purification steps while meeting the strict demands for highly pure reaction products and simultaneously bearing the possibility to prepare large scales of the desired compounds "on demand". Further work will involve counter ion variation as well as detailed kinetic studies. This will finally lead to the rapid synthesis of tailor-made products for a steadily growing demand for ionic liquids.

4.1.6. References

1. Wasserscheid, P.; Keim, W. *Angew. Chem. Int. Ed.* **2000,** 39, 3773.
2. Wasserscheid, P.; Welton, T., *Ionic Liquids in Synthesis*. Wiley-VCH: Weinheim, 2003.
3. Sugden, S.; Wilkins, H. *J. Chem. Soc.* **1929**, 1291.
4. Chum, H. L.; Koch, V. R.; Miller, L. L.; Osteryoung, R. A. *J. Am. Chem. Soc.* **1975,** 97, 3264.
5. Wilkes, J. S.; Levisky, J. A.; Wilson, R. A.; Hussey, C. L. *Inorg. Chem.* **1982**, 1263.
6. Wilkes, J. S.; Zaworotko, M. J. *J. Chem. Soc. Chem. Commun.* **1992**, 965.
7. Welton, T. *Chem. Rev.* **1999,** 99, 2071.
8. Holbrey, J. D.; Seddon, K. R. *Clean Products and Processes* **1999,** 1, 223.
9. Hessel, V.; Löwe, H.; Müller, A.; Kolb, G., *Chemical Micro Process Engineering*. Wiley-VCH: Weinheim, 2005.
10. Ehrfeld, W.; Hessel, V.; Löwe, H., *Microreactors: New Technology for Modern Chemistry*. Wiley-VCH: Weinheim, 2000.
11. Thayer, A. M. *Chem. Eng. News* **2005,** 83, 43.
12. Geyer, K.; Codée, J. D. C.; Seeberger, P. H. *Chem. Eur. J.* **2006,** 12, 8434.
13. Jähnisch, K.; Hessel, V.; Löwe, H.; Baerns, M. *Angew. Chem. Int. Ed.* **2004,** 43, 406.
14. Kockmann, N.; Brand, O.; Fedder, G. K., *Micro Process Engineering*. Wiley-VCH: Weinheim, 2006.
15. Waterkamp, D. A.; Heiland, M.; Schlüter, M.; Sauvageau, J. C.; Beyersdorff, T.; Thöming, J. *Green Chem.* **2007,** 9, 1084.
16. Renken, A.; Hessel, V.; Löb, P.; Miszczuk, R.; Uerdingen, M.; Kiwi-Minsker, L. *Chem. Eng. Proc.* **2007,** 46, 840.

4.2. Synthesis of Hyperbranched Polyglycerol in a Continuous Flow Microreactor

Daniel Wilms[1], Jörg Nieberle[1], Johannes Klos[1], Holger Löwe[1,2*] and Holger Frey[1*]

Published in: "Synthesis of Hyperbranched Polyglycerol in a Continuous Flow Microreactor" D. Wilms, J. Nieberle, J. Klos, H. Löwe, H. Frey, *Chem. Eng. Technol.* **2007**, 30(11), 1519-1524.

4.2.1. Abstract

Hyperbranched polymers have been synthesized in a microreactor for the first time, employing the known ring-opening multibranching polymerization of glycidol. Microreactors are well-recognized to be beneficial for highly exothermic reactions because of their capability to enhance mass and heat transfer due to short diffusion pathways and large interfacial areas per volume. The characteristics of the microstructured reaction system were utilized to engineer a continuous flow process for the preparation of well-defined hyperbranched polyglycerols with molecular weights up to 1,000 g/mol. Increased flow rates, as well as the use of highly polar solvents, led to the partial formation of very narrowly distributed (M_w/M_n = 1.05 – 1.15) high molecular weight fractions (M_n up to 150,000 g/mol). NMR- and MALDI-ToF spectra confirmed incorporation of the multifunctional initiator core into the hyperbranched polymer structure.

[1] Johannes Gutenberg University Mainz, Institute of Organic Chemistry, Mainz, Germany

[2] Institut für Mikrotechnik Mainz GmbH, Mainz, Germany

4.2.2. Introduction

In recent years, organic synthesis in microreactors has attracted increasing interest due to their inherent characteristics like excellent heat and mass transfer, originating in very short diffusion pathways and large interfacial contact areas per unit volume (10,000 – 50,000 m^2/m^3).[1] Oftentimes higher yields and selectivities as well as improved product qualities can be achieved by transferring chemical reactions from classical batch set-ups to microreactors, particularly when they proceed highly exothermic or endothermic. Furthermore, convenient access to large scales of products have rendered microreactors superior to conventional lab-scale reactors in a variety of reactions.[1-11]

Microreactor-based processes offer intriguing potential also with respect to polymerizations (particularly ring-opening polymerizations), since they usually proceed strongly exothermic and are diffusion-limited due to their fast kinetics. Nevertheless, only few efforts have been reported to date towards the preparation of polymers in such microdimensional devices. This is due to the high viscosity of polymer solutions or melts, which represents an often insuperable obstacle for the microchannels and consequently for the continuous nature of the processes.[12] The works recently published in this context include free radical[13] and anionic[14] polymerizations in capillary reactors as well as the synthesis of block copolymers[15] and a recent, elegant and rapid pathway leading to PAMAM dendrimers.[16] To the best of our knowledge, the preparation of hyperbranched polymers in a microstructured reactor has not been reported to date. However, since branched polymers generally possess lower viscosity than their linear counterparts both in solution and in the melt, we considered it a worthwhile challenge to realize a hyperbranching polymerization in a microreactor set-up. On the other hand, ring-opening of highly strained epoxides is a fast and exothermic reaction that qualifies for syntheses in a microreactor.

Hyperbranched polyglycerols exhibit several benefits, e.g., a high number of hydroxyl groups as a versatile functionality, excellent biocompatibility[17] and offer the possibility to tailor architecture, functionality and solubility. At elevated temperatures exceeding 80°C, low molecular weight hyperbranched polyglycerols exhibit low viscosity, whereas under ambient conditions they are honey-like. For the microreactor set-up, low product viscosities are essential to avoid clogging of the channels within the microstructured device.

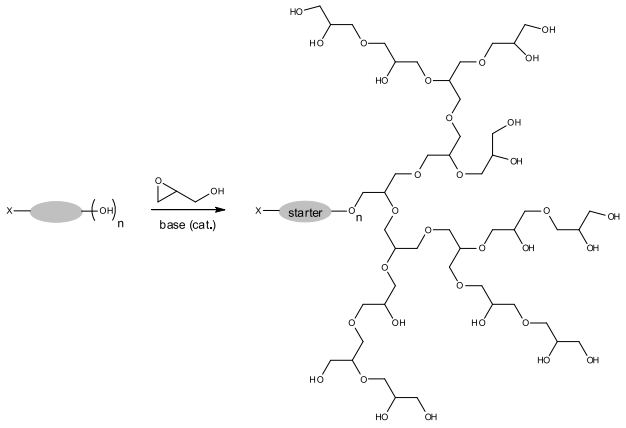

Figure 4.8: Synthetic procedure for the anionic polymerization of glycidol.

Controlled polymerization of glycidol (Figure 4.8) is classically carried out by starting the reaction with a partially deprotonated multifunctional initiator (e.g., trimethylol propane, TMP) and subsequent slow addition of the monomer to the reaction in the course of several hours.[18,19] This approach permits control over molecular weights, leading to well-defined polymers, but it is also time-consuming and involves a rather intricate set-up. Taking the advantageous characteristics of microstructured devices into account, the development of a quick and versatile continuous synthesis process marks a significant advance in the production of the hyperbranched materials.

4.2.3. Experimental Setup

We used an organic synthesis bench scale plant (provided by the *Institut für Mikrotechnik Mainz*) that consists of a stainless steel micromixing device in combination with interdigital microchannels. This setup comprises two preheating loops as well as four delay loops of different length. Preheating loops, micromixer and delay loops are immersed into a tempered oil bath providing direct temperature control. The mixing element is embedded in a stainless steel container fitted with two inlets (connected to the preheating loops) and one outlet (leading to the delay loop). It combines the regular flow pattern created by multi-lamination with geometric focusing, which speeds up liquid mixing (Figure 4.9). The microchannel dimensions are 45 x 200 μm. Both reactant streams are introduced into the microchannels by means of two programmable HPLC pumps that permit direct control over the respective flow rates. Upon entry to the mixing device, each reactant stream is divided into several lamellas. When they pass through the slit (perpendicular to the entering streams), the lamellas are hydrodynamically focused. Mixing hence relies solely on fast diffusion between the thin reactant layers. Undesired turbulences thus can be efficiently suppressed. The inner volume of the mixer is approximately 8 μL and residence times are between 14 and 720 ms, depending on the flow rates. It shows a pressure stability of up to 100 bar, allowing continuous flow at viscosities of up to 10,000 mPas.

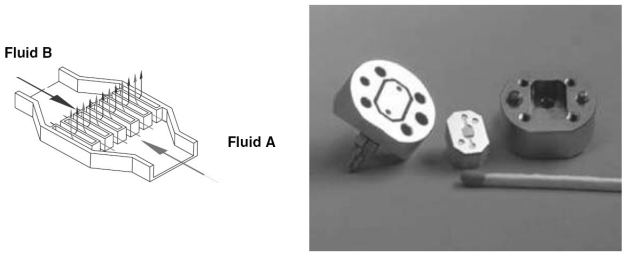

Figure 4.9: Mixing principle and set-up of the slit-interdigital micromixer.

4.2.4. Materials and Methods

4.2.4.1. Materials

All chemicals were purchased from Acros Organics and used as received unless otherwise stated. Diglyme and NMP were distilled over CaH_2 prior to use. DMF was dried over P_2O_5. Purification of glycidol was carried out by vacuum distillation over CaH_2.

4.2.4.2. Synthesis of Hyperbranched Polyglycerols

Before each reaction, methanol was pumped through the microreactor setup for 30-60 minutes at 1 ml/min via both HPLC pumps, followed by freshly distilled solvent (Diglyme, DMF or NMP) for 10 min at 1 ml/min. Purified glycidol was kept under argon atmosphere in a flask covered with a septum. TMP and the amount of potassium methylate necessary to deprotonate 10% of the hydroxyl groups were combined in a one-necked flask and melted at 70°C under reduced pressure on a rotary evaporator. Residual methanol was removed under high vacuum conditions. The initiator was dissolved in the respective solvent under argon atmosphere. Both reactant flasks were connected to the HPLC pumps via PTFE tubes transfixed through the septa and the oil bath was tempered to the desired temperature (usually 120°C). For all experiments covered in this paper, a delay loop with an inner volume of 10 ml was used. Flow rates were adjusted via the control elements of the HPLC pumps. Mixing of the reactants in the microreactor took place within several milliseconds, whereupon the solution was passed through the delay loop, before the product was recovered at the outlet of the device and immediately quenched with methanol. The time scale available for the polymerization hence can be varied by flow rate adjustment or modification of the delay loop. It is obvious that the respective flow rates determine the ratio of monomer and initiator present in the micromixer. Methanolic solutions of the products were stirred with a cation exchange resin (Lewatit K 1131) at room temperature until neutral. After filtration, the product was redissolved in methanol, precipitated twice in cold acetone and dried in vacuum at 80°C for 12 h.

4.2.4.3. Characterization

NMR spectra were recorded on a Bruker AC 300 nuclear magnetic resonance spectrometer at a frequency of 300 MHz (^{1}H) and 75 MHz (^{13}C) respectively. Deuterated methanol (methanol-d_4) was used as solvent. SEC measurements were carried out in DMF, using an Agilent 1100 Series with PSS Gram column, RI- and UV-detector. All SEC diagrams show the RI detector signal and the molecular weights refer to linear polystyrene (PS) standards. MALDI-ToF spectra were recorded in reflection mode on a Shimadzu Axima CFR mass spectrometer using a CCA matrix.

4.2.5. Results

In order to keep the product viscosity low and hence to ensure continuous flow through the microchannels, a molecular weight of 1,000 g/mol was targeted initially. ^{1}H-NMR analysis of the polymer obtained showed the characteristic resonances of the TMP core at 0.9 and 1.4 ppm (Figure 4.10 a). The molecular weight can be calculated from a comparison of the integrals of the different polymer repeat units and the initiator core. A value of M_n = 1,100 g/mol was obtained for this sample, which represents an average degree of polymerization of 13 and thus polyether polyols with 15 hydroxyl end groups.

The formation of a hyperbranched structure during the polymerization of glycidol strongly relies on a proton exchange equilibrium that permits reaction of both primary and secondary alkoxide end groups. It was an intriguing issue whether this mechanism would also be effective in the case of the short reaction times of the microreactor. ^{13}C-NMR spectra of PG were first interpreted by Vandenberg[20] and later this work was extended by Dworak and Penczek,[21,22] before in the late 1990ies a detailed assignment of the different ^{13}C-NMR signals of hyperbranched polyglycerol was carried out (Figure 4.10 b).[18]

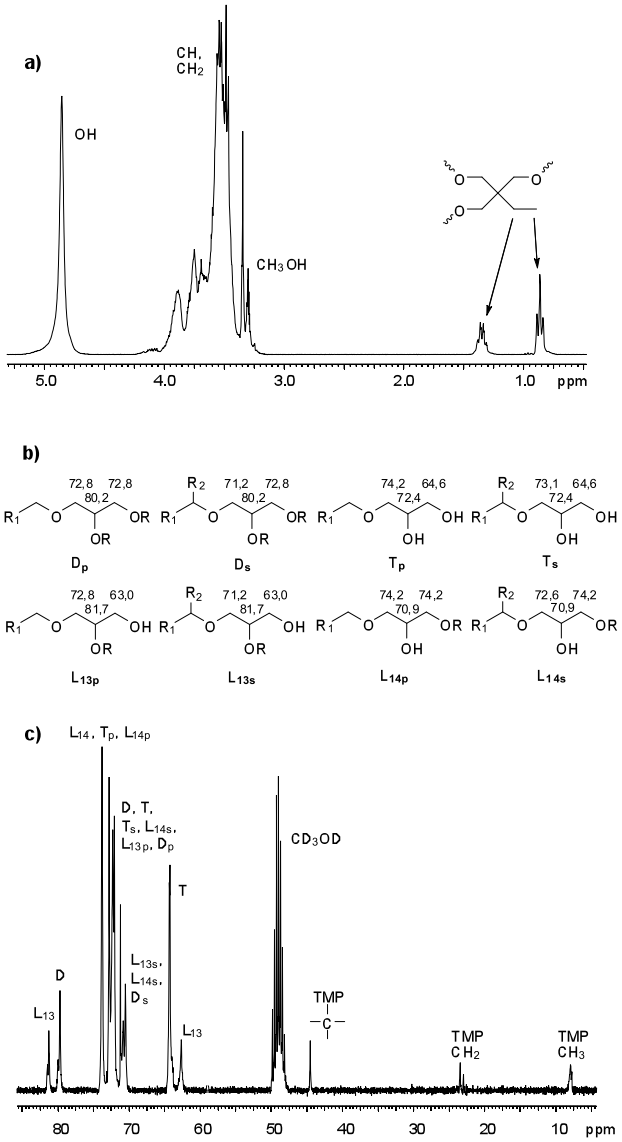

Figure 4.10: (a) ^{1}H-NMR spectrum of microreactor-based PG_{1000} with TMP core; (b) assignment of ^{13}C-NMR shifts to the different structural units of hyperbranched polyglycerol. (c) ^{13}C-NMR spectrum of PG_{1000} with TMP core.

The polyglycerol samples synthesized in the microreactor show all resonances typical for the dendritic, linear and terminal units as well as the signals of the TMP core (Figure 4.10 c), confirming the hyperbranched structure. The SEC trace of the same hyperbranched polyglycerol sample is shown in Figure 4.11. The molecular weight was determined to be 700 g/mol (PS standards), lower than the molar mass obtained from NMR spectroscopy. Using linear PEG standards for SEC calibration led to a similar value. The slight underestimation is typical for a hyperbranched structure.

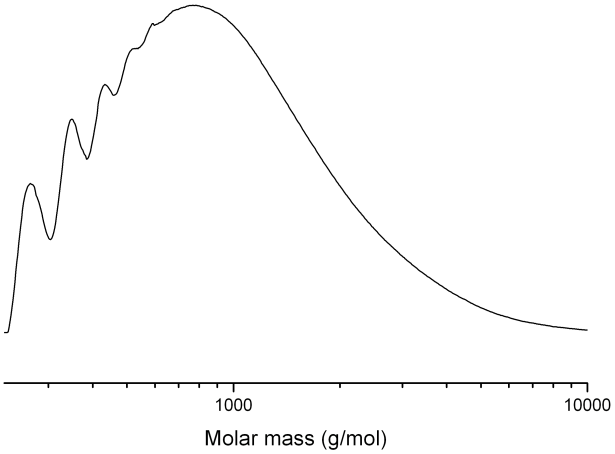

Figure 4.11: SEC diagram of PG_{1000}.

Since the short reaction times in the microreactor do not permit to realize slow monomer addition conditions like in the established batch process,[18] it was an important question, whether incorporation of the initiator-core into the hyperbranched structure can be achieved. The respective MALDI-ToF spectrum showed the presence of a small fraction of polymer based on a methoxy-core and almost exclusively the desired PG with a TMP core. This observation is common in the base-initiated polymerization of glycidol. Complete removal of residual methanol from the initiator solution is challenging, since this requires stringent conditions that may also lead to evaporation of TMP and therefore a change of the targeted stoichiometry.

Further optimization of the reaction conditions included an investigation of the necessary residence time of the reactants in the microchannels. In a series of experiments the flow rates of initiator solution and monomer were gradually increased, followed by characterization of the products by NMR spectroscopy and SEC. Table 4.2 gives the respective flow rates as well as molecular weights calculated from ^{1}H-NMR spectra. Obviously, increased flow rates led to higher molecular weights. At first glimpse this is surprising, considering that reduced reaction times may be expected to result in a lower degree of polymerization. SEC diagrams of the polymers obtained at increased flow rates (Figure 4.12 a) exhibit a major fraction of low molecular weight (M_n ~ 700 g/mol) as well as a minor, narrow polydispersity fraction of high molecular weight. Isolation of the high molecular weight fractions by dialysis in methanol gave almost solid hyperbranched polyglycerols (M_n ~ 140,000 g/mol, PS standards) with surprisingly narrow polydispersity of ca. 1.1-1.2. Interestingly, Brooks et al. observed the formation of similarly narrow dispersed high molecular weight polyglycerols when they used dioxane instead of diglyme

as solvent for the conventional batch synthesis.[23] The SEC-diagram of the high-molecular fraction isolated from sample PG-3 is shown in Figure 4.12 b. At this point the reason for the formation of the high molecular weight side product remains unclear. Most probably, at increased flow rates, a mixing process solely based on diffusion is possibly impeded by occurring turbulences, resulting in the formation of "hot spots" where the polymerization proceeds much faster than in other parts of the reaction mixture. Another generally observed consequence of increasing the flow rates in the synthesis of polyglycerol is the formation of a much more intensely colored product.

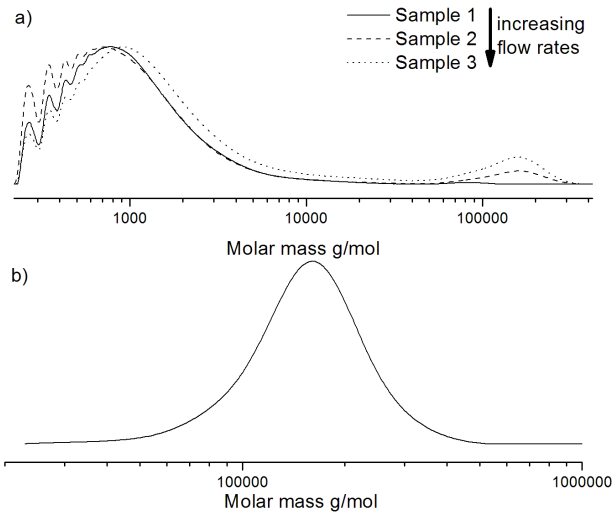

Figure 4.12: (a) SEC diagrams of polyglycerols obtained at different flow rates. (b) SEC diagram of the high molecular weight fraction of sample 3 (isolated by dialysis in methanol).

Increasing the monomer to initiator ratio by flow rate adjustment led to flow discontinuities, which were due to an increase of the viscosity of the formed polymer. Subsequent partial clogging of the microchannels promoted additional hot spot formation. A modified reactor design with wider microchannels and an alternative mixer design will be tested for the controlled continuous synthesis of higher molecular weight polyglycerols in the future.

Replacing the partially deprotonated TMP core with a simple monofunctional base initiator (potassium-*t*-butylate) led to broader molecular weight distributions and a loss of control over the reaction, as expected.[24] This outlines the significance of the multifunctional initiator core for the synthesis of well-defined polyglycerols, even though slow monomer addition conditions were not applied in this approach.

Further studies involved variation of the solvent used for the initiator solution. Compared to diglyme, DMF and NMP are more polar solvents that show much better dissolving power for the potassium salts of TMP. Their high boiling points allow working at the same temperature like in the previous experiments (> 100°C). In both solvents, a significant fraction of the narrowly dispersed and less soluble high molecular weight fractions was observed. Apparently high solvent polarity promotes faster, but also less diffusion-controlled mixing of the reactants. The TMP-core was completely incorporated into the polymers, which is evidenced by the MALDI-ToF spectrum obtained from the lower molecular weight fraction (M_n ~ 1,000 g/mol) of the polyglycerol synthesized in DMF (Figure 4.13).

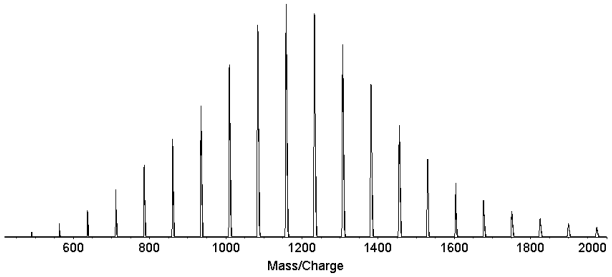

Figure 4.13: MALDI-ToF spectrum of a polyglycerol sample synthesized in the microreactor using DMF as a solvent. Each peak corresponds to the added masses of the TMP core, a certain number of glycidol units and one Li^+ ion.

Table 4.2: Molecular weights calculated from NMR data for polyglycerols obtained at different flow rates.

Sample No.	Target M_n (g/mol)	Flow Rate Monomer	Flow Rate Initiator	Molar Ratio Initiator/Monomer	M_n (^{1}H-NMR)
PG-1	1,000	0.81 ml/min 12.21 mmol/min	1 ml /min 1.04 mmol/min	1 : 11.7	1,100
PG-2	1,000	1.62 ml/min 24.43 mmol/min	2 ml/min 2.09 mmol/min	1 : 11.7	1,300
PG-3	1,000	2.05 ml/min 30.91 mmol/min	2.5 ml/min 2.64 mmol/min	1 : 11.7	1,600

4.2.6. Summary and Outlook

In conclusion, to the best of our knowledge this represents the first report on a continuous process for the preparation of a hyperbranched polymer in a microstructured reactor. The highly efficient heat and mass transport in microreactors affords a quick pathway to these materials, without having to resort to time-consuming conventional methods. Reaction times and experimental effort were significantly reduced compared to the classical batch methods. The polymer structure was investigated in detail by NMR spectroscopy, confirming the hyperbranched topology and indicating incorporation of the trifunctional initiator core into the polymers. MALDI-ToF spectra confirmed this result. SEC analysis of the polymers prepared at different flow rates and in various solvents showed formation of remarkably narrowly dispersed high molecular weight fractions, when flow rates were increased or upon usage of highly polar solvents. As glycidol, like several other epoxide monomers, is a highly toxic compound, the reaction can be carried out in the safer environment of the contained microreactor devices. We are convinced that this example of transferring a well-established but tedious synthesis procedure to a microdimensional device will motivate further studies, particularly in the area of hyperbranched polymers, to realize polymerizations in microreactor systems rather than in traditional set-ups.

4.2.7. References

1. V. Hessel; H. Löwe; A. Müller; G. Kolb, in Chemical Micro Process Engineering 1+2. Fundamentals, Modelling and Reactions/Processes and Plants, Wiley-VCH, Weinheim **2005**.
2. W. Ehrfeld; V. Hessel; H. Löwe, in Microreactors: New Technology for Modern Chemistry, Wiley-VCH, Weinheim **2000**.
3. A. M. Thayer Chem. Eng. News **2005**, 83 (22), 43.
4. S. H. DeWitt Curr. Opin. Chem. Biol. **1999**, 3 (3), 350. DOI: 10.1016/S1367-5931(99)80052-0
5. K. Jähnisch; V. Hessel; H. Löwe; M. Baerns Angew. Chem. Int. Ed. **2004**, 43 (4), 406. DOI: 10.1002/anie.200300577.
6. P. Watts; S. J. Haswell Chem. Soc. Rev. **2005**, 34 (3), 235. DOI: 10.1039/b313866f.
7. H. Pennemann; P. Watts; S. J. Haswell; V. Hessel; H. Löwe Org. Process Res. Dev. **2004**, 8 (3), 422. DOI: 10.1021/op0341770.
8. K. F. Jensen Chem. Eng. Sci. **2001**, 56 (2), 293. DOI: 10.1016/S0009-2509(00)00230-X.
9. L. Kiwi-Minsker; A. Renken Catal. Today **2005**, 110 (1-2), 2. DOI:10.1016/j.cattod.2005.09.011
10. V. Hessel; G. Kolb; C. de Bellefon Catal. Today **2005**, 110 (1-2), 1. DOI: 10.1016/S0920-5861(05)00744-3
11. N. Kockmann; O. Brand; G. K. Fedder, in Micro Process Engineering, Wiley-VCH, Weinheim **2006**.
12. V. Hessel; C. Serra; H. Löwe; G. Hadziioannou Chem. Ing. Tech. **2005**, 77 (11), 1693. DOI: 10.1002/cite.200500142
13. T. Iwasaki; J. Yoshida Macromolecules **2005**, 38 (4), 1159. DOI: 10.1021/ma048369m.
14. T. Honda; M. Miyazaki; N. Nakamura; H. Maeda Lab Chip **2005**, 5 (8), 812. DOI: 10.1039/b505137a
15. T. Wu; Y. Mei; C. Xu; H. C. M. Byrd; K. L. Beers Macromol. Rapid Commun. **2005**, 26 (13), 1037. DOI: 10.1002/marc.200500214.
16. S. H. Liu; C. H. Chang Chem. Eng. Technol. **2007**, 30 (3), 334. DOI: 10.1002/ceat.200600353.
17. R. K. Kainthan; J. Janzen; E. Levin; D. V. Devine; D. E. Brooks Biomacromolecules **2006**, 7 (3), 703. DOI: 10.1021/bm0504882.
18. A. Sunder; R. Hanselmann; H. Frey; R. Mülhaupt Macromolecules **1999**, 32 (13), 4240. DOI: 10.1021/ma990090w.
19. A. Sunder; H. Frey; R. Mülhaupt Macromol. Symp. **2000**, 153 (1), 187. DOI: 10.1002/1521-3900(200003)153:1.
20. E. J. Vandenberg J. Polym. Sci., Part a: Polym. Chem. **1985**, 23 (4), 915. DOI: 10.1002/pol.1985.170230401.
21. R. Tokar; P. Kubisa; S. Penczek; A. Dworak Macromolecules **1994**, 27 (2), 320. DOI: 10.121/ma00080a002.
22. A. Dworak; W. Walach; B. Trzebicka Macromol. Chem. Phys. **1995**, 196 (6), 1963. DOI: 10.1002/macp.1995.021960616.
23. R. K. Kainthan; E. B. Muliawan; S. G. Hatzikiriakos; D. E. Brooks Macromolecules **2006**, 39 (22), 7708. DOI: 10.1021/ma0613483.
24.] R. Hanselmann; D. Hölter; H. Frey Macromolecules **1998**, 31 (12), 3790. DOI: 1998. ma971197r.

4.3. Carbanions on Tap – Living Anionic Polymerization in a Microstructured Reactor

Frederik Wurm[1], Daniel Wilms[1], Johannes Klos[1], Holger Löwe*[1] and Holger Frey*[1]

Published in: "Carbanions on Tap - Living Anionic Polymerization in a Microstructured Reactor" F. Wurm, D. Wilms, J. Klos, H. Löwe and H. Frey, *Macromol. Chem. Phys.* **2008**, 209 (11), 1106-1114.

4.3.1. Abstract

The paper describes the living anionic polymerization of styrenes to homo- and diblock copolymers in continuous flow, using a microstructured mixing set-up ("microreactor"). Reaction times and experimental effort are significantly reduced compared to classical batch methods that require stringent reaction conditions and strict drying of the apparatus by "break-seal" and "high vacuum" techniques. In continuous flow, residual impurities can be removed by purging the reactor with monomer and initiator solution before polymer samples are collected at the device outlet on a scale of up to 200 g/h. Facile molecular weight adjustment is achieved by variation of the flow rates of initiator or monomer solutions. The polymerization of styrene in THF and cyclohexane was studied with respect to control of molecular weight and polydispersity. Furthermore, diblock copolymers, with different block lengths and low polydispersities, consisting of styrene- and 4-*tert*-butoxystyrene blocks were synthesized, employing a second micromixer for a delayed introduction of the additional monomer. All materials were investigated by NMR-spectroscopy, SEC/MALLS and MALDI-ToF mass spectrometry, confirming narrow molecular weight distributions (M_w/M_n 1.09 to 1.25), molecular weights in the range of 500 to 70,000 g/mol and complete end-functionalization. No dimerization due to side reactions that would occur in the presence of oxygen was observed, evidencing efficient shielding of the apparatus from environmental influences.

4.3.2. Introduction

Organic syntheses in microreactors have attracted increasing attention in recent years due to characteristic advantages arising from typical features like excellent heat and mass transfer as well as precise control of residence times. Highly efficient mixing and heat dissipation, originating in very short diffusion pathways and large interfacial contact areas per unit volume (10,000 – 50,000 m^2/m^3)[1] have been shown to improve yields, selectivities and product qualities in numerous comparative studies of established organic synthesis procedures. Due to their inherent supremacy in heat transfer, microstructured reactors offer particular potential for transformations that proceed highly exothermic or endothermic. Furthermore, convenient access to large scales of products by operating several set-ups in parallel has rendered microreactors superior to conventional lab-scale reactors in a variety of organic reactions.[2]

Continuous flow processes involving micromixers offer intriguing potential also with respect to various types of controlled polymerizations, since they usually proceed strongly exothermic and exhibit fast kinetics. Nevertheless, only limited efforts have been reported to date towards the actual preparation of polymers in such microdimensional devices. This may be ascribed to the high viscosity of polymer solutions or melts, which represents a common and in many cases insuperable obstacle for the continuous nature of the processes due to clogging of the microchannels, especially at high degrees of polymerization.[3] Only within recent years, vital progress in this field has been made by several research groups who carried out free radical,[4] controlled radical,[5] anionic[6] and cationic polymerizations[7] using different microreactor designs. The fascinating potential of polymer chemistry in continuous flow has also been pointed out by recent studies focusing on the synthesis of dendrimers[8] and block copolymers[9] in microfluidic devices. Very recently, our group reported the first preparation of hyperbranched polyglycerol via anionic ring-opening multibranching polymerization in a microstructured reactor.[10] The microstructured environment proved to be particularly promising for control of the ring-opening of highly strained epoxides, because these reactions typically proceed very fast and highly exothermic. A very recent overview article by summarizes numerous modern approaches developed in this area.[11]

Since Michael Szwarc's seminal report on living polymerization in the 1950ies,[12] the principles of this type of polymerization have received tremendous attention by a large scientific community and have become a fundamental subject matter for collegian education. A comprehensive review can be found in the very recent literature.[13]

Only a few years after the first report on living polymers, pioneering work involving anionic polymerization in continuous flow was accomplished by M. Szwarc et al.[14] and G. V. Schulz et al.[15] At that time these authors focused on the study of anionic polymerization kinetics in a macroscopic glass tube, using a rapid turbulent mixing technique based on a four-way jet device. The same mixing principle was used in 1982 by Lochmann et al. who reported on oligomerization of acrylates using a continuous flow technique and steel capillaries.[16] The continuous flow approach was later extended by A. Müller et al. in elegant work, using a flow-tube reactor for a detailed kinetic investigation of the anionic polymerization of methyl methacrylate and for the preparation of block copolymers,[17] obtaining impressively low polydispersities M_w/M_n in the range of 1.1 – 1.2. Various patents by Elf-Atochem (later: Atofina, now: Arkema)[18] describe the industrial application using continuously operating pumps.

Herein we report the use of a microstructured mixer under continuous flow conditions for the living carbanionic polymerization. The crucial issues in the context of this work are (i) does the microstructured mixing device represent a useful synthesis tool for the carbanionic polymerization to functional polymers from the analytical to the multigram scale? (ii) How does the quality of the polymers compare to well-established anionic batch methods on the one hand and to flow-tube based processes used for kinetical investigation on the other hand? (iii) Does the polymerization primarily take place in the micromixing device itself or in the ensuing delay tube?[19] (iv) Can the method be exploited for the synthesis of more complex macromolecular architectures, such as block copolymers?

To answer these questions we considered styrene-based monomers to be suitable candidates for a study of continuous carbanionic polymerization in a microstructured device. Figure 4.14 shows the schematic layout of the employed reaction set-up.

Figure 4.14: Schematic layout of anionic styrene polymerization in a microstructured reaction set-up in continuous flow.

4.3.3. Experimental

Materials: Cyclohexane and tetrahydrofuran (THF) (Acros) for polymerizations were dried by cryo-transfer from a dark-red colored living polystyrene (PS) solution just prior to use. Styrene and 4-*tert*-Butoxystyrene (Acros) were stored over CaH_2 and freshly distilled prior to use. Methanol, chloroform and other solvents and reagents were purchased from Acros and used as received. *sec*-Butyllithium (*sec*-BuLi, 1.3M, Acros) was used as received. The concentration of the initiator was determined by the Gilman double titration method.[20] Chlorodimethylsilane (Acros) was dried over CaH_2, cryo-transferred into an ampoule and stored until used. CaH_2 was purchased from Fluka and used as received. All degassing and cryo-transfer procedures were carried out using a vacuum line and liquid nitrogen as cooling agent. Deuterated chloroform-*d* was purchased from Deutero GmbH and used as received.

Instrumentation: ^{1}H-NMR- and ^{13}C-NMR- spectra were recorded at 300 MHz on a Bruker AC and are referenced internally to residual proton signals of the deuterated solvent. Size exclusion chromatography (SEC) was performed on an instrument consisting of a Waters 717 plus autosampler, a TSP Spectra Series P 100 pump and a set of three PSS-SDV 5m columns with 100, 1,000, and 10,000Å porosity. THF was used as an eluent at 30°C and at a flow rate of 1 mL/min. UV absorptions were detected by a SpectraSYSTEM UV2000. Multi-angle laser light scattering (MALLS-detection) was carried out on a Wyatt Dawn 18 angle online light scattering detector. Matrix-assisted laser desorption ionization mass spectrometry (MALDI-MS) spectra were recorded in reflection mode on a Shimadzu Axima CFR mass spectrometer using a pencil lead matrix.[21]

Micromixer device: All polymerizations were carried out in a microstructured reaction set-up provided by the *Institut für Mikrotechnik Mainz (IMM).* It consists of a tempered oil or water bath hosting the mixing devices (stainless steel interdigital SIMM-V2 mixer with an internal volume of 8 μL) that is equipped with two reactant inlets and one outlet. After mixing, the reaction mixture is directly guided into the respective delay tube (60μL or 2 mL). The rear end of the delay tube is immersed in the degassed quenching agent.. Flow rates are controlled via HPLC pumps (Knauer WellChrom K-501, inert 10mL pump heads with ceramic inlays).

Synthesis of polystyrene. Before each reaction the solvent (p.A. grade cyclohexane or THF) was pumped through the microstructured reactor set-up for approximately 15

minutes at 0.5 ml/min via both HPLC pumps, followed by freshly distilled dry and degassed solvent for an additional 10 min at 0.5 ml/min. Purified styrene was kept under argon atmosphere in a flask covered with a septum as a 10-20 weight% solution in dry cyclohexane or THF. In a second flask the desired solvent and the required amount of initiator (*sec*-BuLi) were combined by cryo-transfer of the solvent and injection of the initiator solution via syringe. Both reactant flasks were connected to the HPLC pumps via PTFE tubes transfixed through the septa and the water/oil bath of the reactor plant was tempered to the desired temperature (25°C or 80°C respectively). For all experiments carried out in cyclohexane, a delay tube with an internal volume of 2 ml was used (250 cm length and 1000 μm diameter). For reactions in THF, the polymers were recovered directly behind a short tube (30 cm length and 500 μm diameter, volume approx. 60 μL) connected to the micromixer. Flow rates were adjusted via the control elements of the HPLC pumps. When cyclohexane was used as a solvent, mixing of the reactants in the microreactor took place within several milliseconds, whereupon the solution was passed through the delay tube to complete polymerization, before the product was recovered at the outlet of the device and immediately quenched with degassed methanol or dimethylchlorosilane. The time scale available for the polymerization can either be varied by flow rate adjustment or modification of the delay loop. It is obvious that the respective flow rates determine the ratio of monomer to initiator present in the micromixer. Due to the significantly faster kinetics of anionic polymerization in polar solvents, e.g. THF, the delay tube was removed and the polymers were directly recovered behind a short outlet connected to the mixer and a vessel for product recovery. Polystyrene samples were subsequently dried in vacuum at 40°C for 12 h.

Block Copolymer Synthesis For the synthesis of block copolymers THF was used as the solvent. A second micromixing device was installed after the living polystyrene anions passed a delay tube of 35 cm length and 500 μm diameter. Following the second mixer the above mentioned outlet tube wit 30 cm length and 500 μm diameter was installed. The second monomer (4-tert-butoxystyrene) was pumped into the second micromixer via a third HPLC-pump with different flow rates. When the flow of styrene was stopped completely, a homopolymer of 4-tert-butoxystyrene could be synthesized. By variation of the flow rates of both monomers, different diblock copolymers with varying block lengths could be synthesized. Polymers were recovered after precipitation into degassed methanol and drying in vacuo at 40°C for 12 h.

4.3.4. Results and Discussion

Polystyrene - Homopolymerization and influence of solvent. We investigated the anionic polymerization of styrene in two representative solvents of different polarity, THF as a typical polar and cyclohexane as a nonpolar solvent. The geometry of the employed micromixer allows mixing processes to take place within less than a millisecond due to the combination of the regular flow pattern created by multi-lamination with geometric and hydrodynamic focusing (Figure 4.15). Residence times in the mixing device are very short due to the extremely small inner volume of the interdigital mixer. High pressure stability of the set-up (up to 100 bar) permits continuous flow at viscosities of up to 10,000 mPas. An important motivation for us was the fact that continuous radical solution polymerization of styrene is one of the most important methods for the commercial production of polystyrene although suspension polymerization is also widely used.[22] On an industrial scale, continuous anionic polymerization is carried out by Arkema,[18] however, no reports focusing on the use of microstructured continuous reaction devices for the living anionic polymerization of vinyl monomers on larger synthetic scales can be found in the literature.

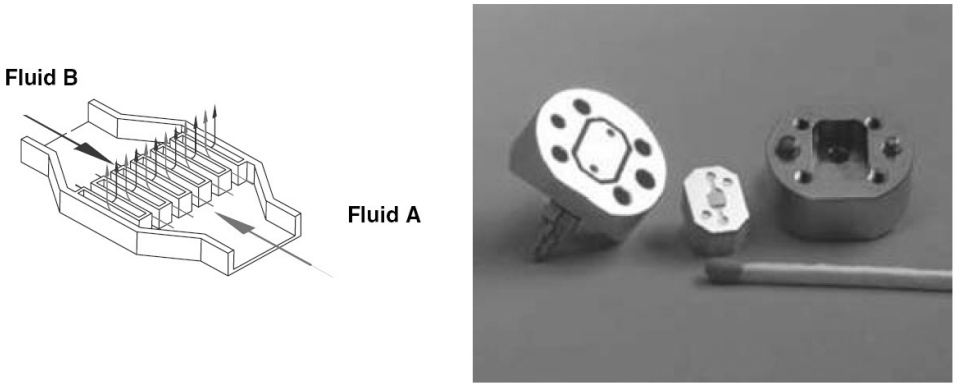

Figure 4.15: Mixing principle and set-up of the slit-interdigital mixer. The inner volume of the micromixer is 8 µL. Mixing takes place by very fast diffusion between the thin reactant layers formed by the parallel microchannel alignment

The characteristics of the microreactor set-up permitted a significant reduction of reaction times and experimental effort compared to classical batch methods that are often conducted in individually crafted glass-reactors for each reaction by tedious “break-seal” and “high vacuum” techniques for anionic polymerization.[23] The main advantage of the microstructured reaction set-up is a significant improvement of control over very fast reactions. Additionally, the experimental effort is considerably reduced compared to the

abovementioned flow-tube reactions carried out in the past. The microstructured reaction device as well as the attached delay tubes can be cleansed in a simple manner from any residual impurities by purging with both monomer and initiator solution prior to the collection of polymer at the device outlet. Products can be obtained on large scales due to the stable operating conditions.

Before our initial experiments, we believed the polymerization of styrene in THF to be a suitable candidate for synthesis in a microreactor due to the very fast kinetics.[14,15,24] Propagation rate constants in anionic polymerizations are dramatically affected by the nature of the reaction medium. The apparent reaction rate constant, which depends on the solvent, temperature and concentration, is increased by two orders of magnitude in polar solvents like THF compared to the rate constants in nonpolar solvents like cyclohexane or benzene.[25] These considerable differences in reaction kinetics can be attributed to aggregation of the living chains in nonpolar solvents, slowing down the propagation rate. A polar solvent like THF acts as a solvating agent for the lithium counter ion and partially leads to solvent-separated ion pairs, resulting in free ions depending on the concentration; thus, kinetic constants are significantly increased.

We used different delay tubes for accomplishment of the polymerization reaction: For polymerizations carried out in cyclohexane, a relatively long delay tube (250 cm length and 1000 μm diameter, volume approx. 2 mL) was used, while the direct outlet following the micromixer (30 cm length and 500 μm diameter, volume approx. 60 μL) proved sufficient for polymerizations in THF. The living polystyryl anions recovered at the reactor outlet were immediately quenched under argon atmosphere to prevent dimerization and other known side reactions due to the presence of oxygen.

Aiming at precise molecular weight control and narrow molecular weight distributions, anionic batch polymerizations in polar solvents are usually carried out at very low temperatures (-78°C) in order to maintain control over the reaction. It was one of the primary objectives of this work to take advantage of the microstructured reaction set-up to carry out the polymerization of styrene in THF at room temperature. For this purpose the micromixer was immersed into a water bath at 25°C. Under these conditions, dissipation of the reaction heat cannot be achieved in a conventional reaction flask, preventing any control over the polymerization, which may lead to an explosion.

The products were recovered by precipitation into degassed methanol directly after passing the micromixer device and the attached outlet tube (V = 60 μL). A scheme of the reaction set-up employed is shown in Figure 4.16.

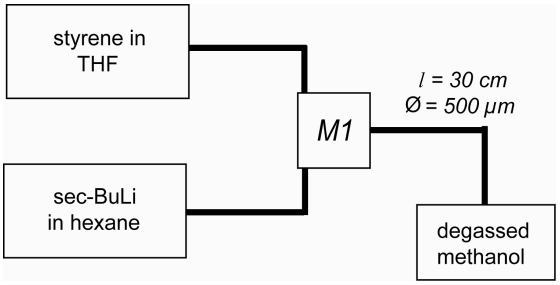

Figure 4.16: Schematic reactor set-up for homopolymerization of styrene in tetrahydrofuran. M1= stainless steel micromixer with 8μL volume.

For all polymers, the residence time of the reaction mixture in the set-up (mixer & delay tube) before quenching was kept below 10 seconds. The time of residence was estimated to be in the range of 10 half-lifes of the polymerization reaction in order to ensure that complete conversion in the continuous flow capillary is guaranteed. With an approximate initiator concentration of 1 mM in the mixture, one can estimate a rate constant of more than 1,000 L/mol s from the data given by Szwarc et al. [14] and thus a half-life of $t_{1/2} < 0.5$ s. Therefore, the reaction can be completed within several seconds even for very high molecular weights. Convenient adjustment of the degrees of polymerization was achieved by simple variation of the ratio between monomer and initiator solution flow rates. Hence, polystyrenes in a broad range of molecular weights (from 1,700 to 70,000 g/mol) with moderate to narrow molecular weight distributions were obtained in all cases (Table 4.3) within several seconds.

Table 4.3: Characterization data of polystyrene samples prepared by anionic polymerization in a microstructured reaction set-up using THF as solvent.

Sample	M_n [a]	M_n [b]	M_w/M_n [b]
PS-1	2,000	1,700	1.28
PS-2	3,000	2,300	1.14
PS-3	4,000	3,600	1.11
PS-4	5,000	6,400	1.10
PS-5	6,000	6,900	1.09
PS-6	10,000	10,500	1.14
PS-7	12,000	11,300	1.09
PS-8	15,000	17,000	1.10
PS-9	40,000	42,200	1.24
PS-9[c)]*	*40,000*	*53,000*	*1.41*
PS-10	60,000	71,000	1.25

[a]) theoretical value of the number average of the molecular weight distribution in g/mol.
[b]) number average of the molecular weight distribution in g/mol and molecular weight distribution determined by size exclusion chromatography in tetrahydrofuran.
[c]) quenched in an open beaker (side reactions with oxygen occur).

Characterization results (^{1}H-NMR-spectra and SEC-elugrams) showed full conversion of styrene. Within the scope of these experiments, the initiator was either dissolved in THF or hexane. It has to be pointed out that THF solutions of *sec*-BuLi have to be cooled prior to pumping them into the reactor to prevent decomposition of the carbanions by nucleophilic displacement at the carbon-oxygen bond of the ether. The decomposition rate of carbanions in THF at 20°C has been reported to amount to a few percent per minute. However, it can be significantly decreased by working at temperatures below 0°C. [26] The use of hexane solutions of *sec*-BuLi was shown to be more convenient, as cooling is not necessary. However, the previously established polymerization conditions in pure THF remain suitable for quantitative conversion of the monomer, despite the presence of a mixture of polar and non-polar solvent in the reaction zone. Figure 4.17 shows the SEC-traces of the polystyrene homopolymer sample synthesized in THF at 25°C; all samples exhibit a narrow molecular weight distribution (MWD) even up to high molecular masses. Interestingly, reasonably narrow MWD (cf. Table 4.3 **PS-9***) can be obtained even when the reaction is quenched in an open beaker, leading to partial reaction of the living chains with oxygen leading to partial coupling of the chains (see SEC-diagram supporting information).

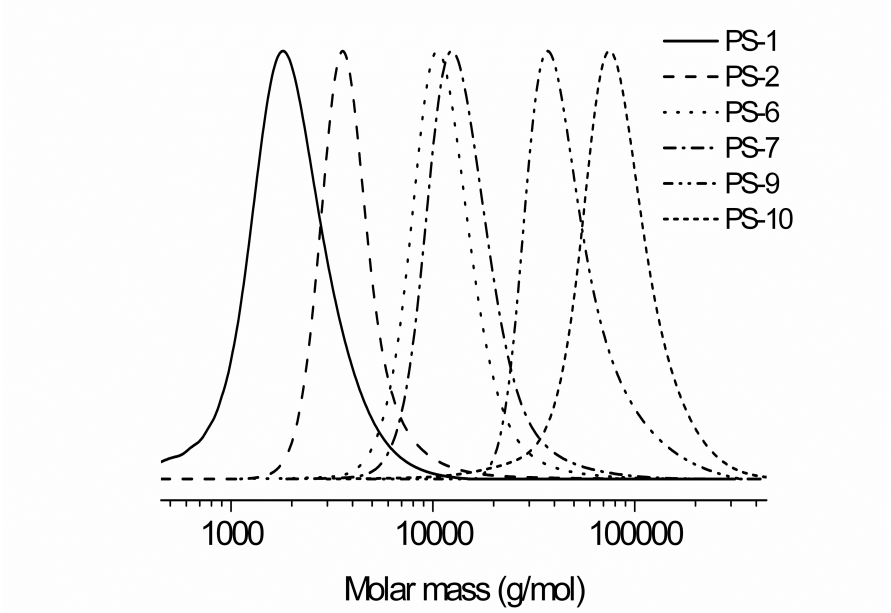

Figure 4.17: Molecular weight distributions determined via size exclusion chromatography (THF) of selected polystyrene samples prepared in the microstructured reaction set-up using tetrahydrofuran as the reaction media.

In the following experiments we investigated the anionic polymerization of styrene in cyclohexane as a nonpolar solvent.

As expected, no polymerization was observed at room temperature, when the reaction mixture was recovered behind the 60 μL outlet tube connected to the micromixer. In order to achieve quantitative conversion, we installed a delay tube of 250 cm length and 1000 μm diameter (V = 2 mL) behind the micromixer. Under ambient conditions, however, polymerization of styrene in cyclohexane still resulted in poor conversion and produced only oligomers in low yield. After increasing the bath temperature to 80°C, narrowly dispersed polystyrene samples showing moderate agreement with the targeted molecular weights were obtained in quantitative yields. Figure 4.18 depicts the respective SEC-curves obtained from several polystyrene samples prepared at different flow rate ratios in one single experimental set-up.

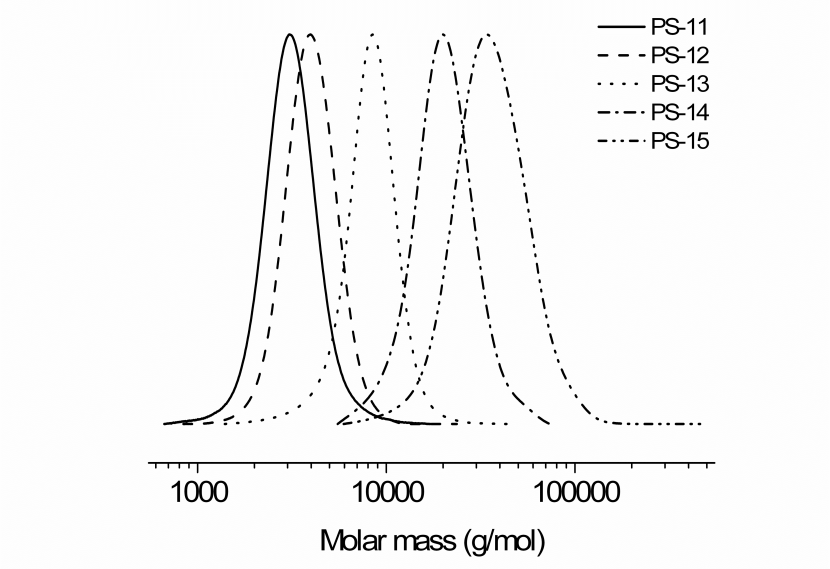

Figure 4.18. Molecular weight distributions determined via size exclusion chromatography in tetrahydrofuran of polystyrene samples prepared in the microstructured reaction set-up with cyclohexane as the reaction medium.

NMR spectroscopy showed full monomer conversion up to a molecular weight of approximately 20,000 g/mol. Higher degrees of polymerization could not be achieved in cyclohexane under these conditions. It is important to point out that conventional batch polymerization of styrene in cyclohexane is conducted at considerably lower temperatures (usually at room temperature) and thus requires several hours to completion. Therefore, using the presented continuous flow approach involving a micromixer, the reaction time required for quantitative monomer conversion can be drastically reduced. Living polystyrene-carbanions can be collected at the outlet for subsequent reaction and functionalization sequences. In cyclohexane, the residence times of the solutions for passing the micromixer and the subsequent delay tube vary between less than one and five minutes, depending on the flow rates.

Both proton terminated polystyrene as well as functional polystyrene samples (terminated with chlorodimethylsilane) were successfully prepared in continuous flow (Table 4.4). The respective MALDI-ToF characterization of sample PS-11 showed only one single distribution mode proving quantitative incorporation of the functional silane group and complete absence of unfunctionalized polymer that would result in a second distribution mode (Figure 4.19).

Applying the respective reaction conditions for both solvent systems, the production of large amounts of series of low polydispersity polystyrenes with varied molecular weights can be conveniently realized in one single experiment, i.e., within only a few hours, by simple variation of the ratio between the corresponding flow rates. Reviewing the results discussed above, we chose THF as the more suitable solvent for further experiments, particularly for the polymerization of a second monomer onto the living polystyrene chains. In this case, additional heating is not necessary and quantitative conversion can be achieved up to high molecular masses.

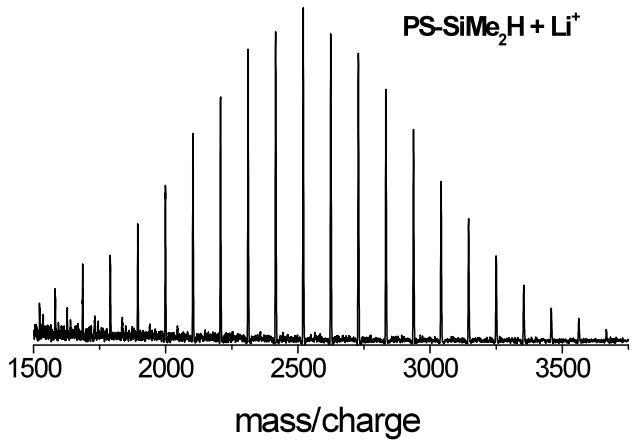

Figure 4.19: MALDI-ToF spectrum of $SiMe_2H$-terminated polystyrene (PS-11) measured with pencil lead as a matrix and lithium trifluoroacetate as additive, supporting the living nature of the polymerization.

Considering our promising initial results, it has to be noted that there are still at least two factors accruing from the use of the microstructured device for living anionic polymerization that have to be critically evaluated: (i) MWDs obtained from the polymers prepared in the continuous reactor are almost entirely in the range of 1.1 while batch reactors can produce even lower polydispersities. This may be ascribed to the use of HPLC-pumps equipped with only a single pump head that generates imperfect flow rate continuity and hence broadened MWDs in our set-up. (ii) Fast and highly efficient mixing of monomer and initiator is a crucial aspect, which necessitates the evaluation of the mixing pattern in microstructured continuous flow devices. [27] The interdigital micromixer employed for our reaction set-up gives rise to perfect lamellar mixing[28] which has a strong influence on the polymerization behavior in continuous flow (an illustration of the

respective mixing profile can be found in the supporting information). Flow rates are generally in the range between 0.2 mL/min and 5 mL/min. Early works by G. Taylor[29] regarding matter in turbulent flow and later on polymerization kinetics deal with a hydrodynamic polydispersity that broadens the molecular weight distribution for polymerizations in continuous flow reactors (in addition to the kinetic polydispersity). It is well-known for conventional flow tube reactors that turbulent flow ensures a lower polydispersity than a laminar flow pattern. [30] The micromixing device we have been using protrudes by high stability and fast mixing based on diffusion. An extremely low surface-to-volume ratio assures efficient heat dissipation from the mixing zone. However, laminar flow through the delay tube at higher molecular weights, i.e. higher viscosities may be leading to a broadening in molecular weight distributions. The effect of using alternative mixer geometries, e.g., T-shaped mixers generating turbulent flow will be part of our future investigations.

Table 4.4: Characterization data for polystyrene samples prepared by anionic polymerization in a microstructured reactor set-up, using cyclohexane as a solvent at 80°C.

Sample	M_n [a]	M_n [b]	M_w/M_n [b]
PS-10	500	570	1.25
PS-11	2,000	3,000	1.09
PS-12	3,000	3,300	1.10
PS-13	6,000	8,000	1.08
PS-14	20,000	24,000	1.11
PS-15	30,000	32,000	1.21

[a]) theoretical value of the number average molecular weight in g/mol.

[b]) number average molecular weight in g/mol and molecular weight distribution determined by size exclusion chromatography in tetrahydrofuran.

Block Copolymer Synthesis

Precise assembly of block-copolymers[31] and more complex macromolecular architectures[32] represents one of the most impressive advantages of living polymerization. Following the related kinetic studies, block copolymer synthesis in a flow tube reactor was carried out in the late 1990ies by Müller et al.[33] Our next efforts were dedicated to the preparation of well-defined block copolymers in the continuous flow set-up. Hence, we

investigated the synthesis of block copolymers using a second, commercially available styrene-based monomer, 4-*tert*-butoxystyrene. Figure 4.20 illustrates the modified experimental set-up for block copolymerization.

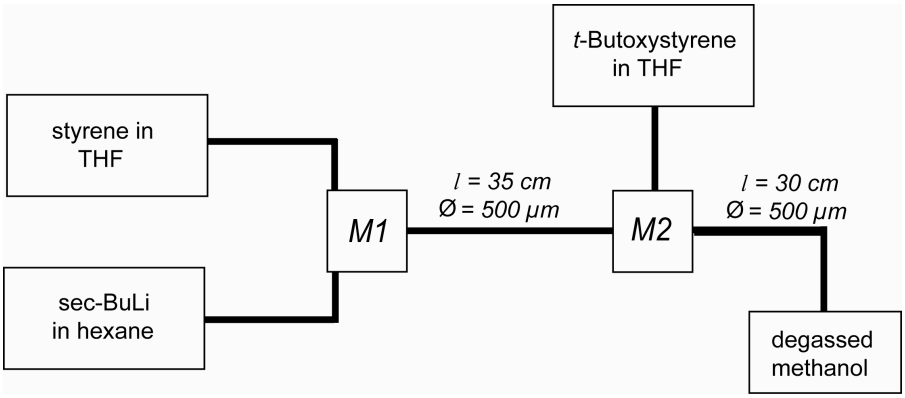

Figure 4.20: Schematic reactor set-up for diblock copolymer synthesis using styrene and 4-*tert*-butoxystyrene in tetrahydrofuran. M1 / M2= micromixers with 8μL volume each.

THF was chosen as reaction solvent and styrene as the monomer for the first block. As in the preceding experiments different block lengths and molecular weights were obtained by variation of the flow rates. Molecular weight distributions of the block copolymers were determined by SEC and proven to be similarly narrow as for the homopolymers, indicating complete block transfer and absence of termination reactions. Figure 4.21 shows the SEC-traces of the poly(styrene-*b*-4-*tert*-butoxystyrene) diblock copolymers.

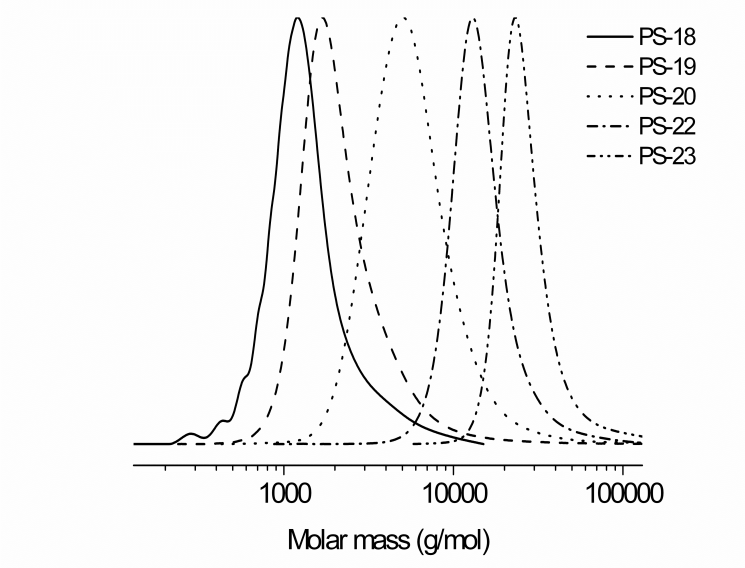

Figure 4.21: Molecular weight distributions determined via size exclusion chroma-tography of poly(styrene-*b*-4-*tert*-butoxystyrene) samples prepared in THF

It can be seen from the block copolymer data summarized in Table 4.5 (NMR-spectra of the polymers are given in the supporting information) that conversion of the monomers is quantitative after passing the micromixers and two short delay tubes (l_1=35 cm, Ø=500 μm and l_2=30 cm, Ø=500 μm). Furthermore NMR and SEC characterization showed full monomer conversion. Variation of the corresponding flow rates allowed a precise adjustment of the block ratios which range from pure poly(4-*tert*-butoxystyrene) homopolymer to several other ratios of incorporated styrene blocks. In all cases remarkably low polydispersities in the range of 1.1-1.2 were obtained. It has to be mentioned that the achieved polydispersities are not as narrow as they are usually attained in conventional batch reactions, but they are still suitable for the most relevant uses of block copolymers reported in the pertinent literature[24,31,32] and the materials can be synthesized in a convenient procedure.

These results hint at the intriguing potential of the continuous flow approach in combination with fast and efficient mixing for the preparation of block copolymers and further complex polymer architectures via anionic polymerization.

Table 4.5: Characterization data of polystyrene-*b*-poly(4-tert-butoxystyrene) samples prepared by anionic polymerization in a microstructured reaction set-up using THF as solvent.

Sample	S:*t*-BuOS[a)]	M_n[b]	M_n[c]	M_n[d]	M_w/M_n[e]
PS-17	0:35	3,600	3,700	4,200	1.21
PS-18	5:5	1,400	1,300	1,500	1,18
PS-19	10:5	1,900	1,900	2,100	1,22
PS-20	22:12	4,400	4,800	4,700	1,17
PS-21	80:30	13,600	13,100	13,600	1,15
PS-22	200:25	25,300	24,700	25,600	1,14

[a]) Block ratio styrene (S) : 4-*t*-butoxystyrene (*t*-BuOS) adjusted by flow rates.

[b]) theoretical value of the number average molecular weight distribution in g/mol.

[c]) number average of the molecular weight distribution in g/mol determined by size exclusion chromatography in tetrahydrofuran.

[d]) number average of the molecular weight distribution in g/mol determined by multi-angle light scattering (MALLS) in tetrahydrofuran.

[e]) polydispersity index determined by MALLS detection in tetrahydrofuran.

4.3.5. Conclusion and Outlook

In summary, we have presented a versatile process for living carbanionic polymerization with subsequent functional termination and diblock copolymer synthesis, using a continuous flow reactor set-up equipped with a micromixing device. The inherent characteristics of the microfluidic device, particularly efficient heat and mass transport, open a rapid pathway to well-defined polymers, avoiding time-consuming and laborious conventional methods that involve individual reactor crafting and prolonged reaction times.

Two different solvents (THF and cyclohexane) were studied as typical examples for polar and nonpolar reaction media, respectively. In THF, the very fast kinetics is apparent (over 1,000 L/mol s), while in cyclohexane propagation is considerably slower. In both cases narrowly distributed polystyrene homopolymers were continuously collected at the outlet and quenched with either methanol or a chlorosilane for the introduction of a functional end group. Variation of molecular weights was conveniently realized by adjustment of the flow-rate parameters. Consequently it is also possible to obtain a broad variety of different molecular weight samples in one single experimental set-up within several minutes to hours, depending on the desired product scale. In THF, the polymerization is very fast, and at room temperature full conversion is achieved after passing of a volume of less than 100 μL. Cyclohexane, however, is not capable of solvating the lithium counter ions, leading to multiple chain aggregation and thus significantly slower propagation rates. Increased temperatures and/or longer residence times are required for quantitative monomer consumption.

Moreover, the synthesis of block copolymers with low polydispersity has been accomplished by subsequent addition of a further monomer via a second micromixer. While the molecular weight distribution of these compounds is not as narrow as those obtained via the classical break seal- and high vacuum-techniques, they are still suitable for most relevant purposes of block copolymers reported in the pertinent literature.

We are convinced that this example of transferring a well-established polymer synthesis procedure to a microdimensional device will motivate further studies, involving the modification of polymer architectures by further variation of the reactor design and the monomers employed.

4.3.6. References

1. V. Hessel, H. Löwe, A. Müller, G. Kolb Chemical Micro Process Engineering 1+2. Fundamentals, Modelling and Reactions/Processes and Plants, Wiley-VCH, Weinheim **2005**.
2. a) W. Ehrfeld, V. Hessel, H. Löwe Microreactors: New Technology for Modern Chemistry, Wiley-VCH, Weinheim **2000**. b) A. M. Thayer Chem. Eng. News **2005**, 83, 43. c) S. H. DeWitt Curr. Opin. Chem. Biol. **1999**, 3, 350. d) K. Jähnisch, V. Hessel, H. Löwe, M. Baerns Angew. Chem. Int. Ed. **2004**, 43 (4), 406. e) P. Watts, S. J. Haswell Chem. Soc. Rev. **2005**, 34, 235. f) H. Pennemann, P. Watts, S. J. Haswell, V. Hessel, H. Löwe Org. Process Res. Dev. **2004**, 8, 422. g) K. F. Jensen Chem. Eng. Sci. **2001**, 56, 293. h) L. Kiwi-Minsker, A. Renken Catal. Today **2005**, 110, 2. i) V. Hessel, G. Kolb, C. de Bellefon Catal. Today **2005**, 110, 1. j) N. Kockmann, O. Brand, G. K. Fedder, Micro Process Engineering, Wiley-VCH, Weinheim **2006**.
3. V.. Hessel, C. Serra, H. Löwe, G. Hadziioannou Chem. Ing. Tech. **2005**, 77, 1693.
4. T. Iwasaki, J. Yoshida Macromolecules **2005**, 38, 1159.
5. a) T. Wu, Y. Mei, J. T. Cabral, C. Xu, K. L. Beers J. Am. Chem. Soc. **2004**, 126, 9880. b) C. Rosenfeld, C. Serra, C. Brochon, G. Hadziioannou, Chem. Eng. Sci. **2007**, 62, 5245-5250.
6. a) T. Honda, M. Miyazaki, N. Nakamura, H. Maeda Lab Chip **2005**, 5, 812. b) M. Miyazaki, T. Honda, H. Nakamura, H. Maeda Chem. Eng. Technol. **2007**, 30, 300.
7. a) A. Nagaki, K. Kawamura, S. Suga, T. Ando, M. Sawamoto, J. Yoshida, J. Am. Chem. Soc. **2004**, 126, 14702. b) T. Iwasaki, A. Nagaki, J. I. Yoshida, Chem. Commun. **2007**, 12,1263. c) T. Iwasaki, J. Yoshida, Macroml. Rapid Commun. **2007**, 28, 1219. d) M. Ouchi, N. Inagaki, T. Ando, M. Sawamoto, Polym. Prepr. (Am. Chem. Soc., Div. Polym. Chem.) **2005**, 46, 939.
8. S. H. Liu, C. H. Chang Chem. Eng. Technol. **2007**, 30 (3), 334.
9. a) T. Wu, Y. Mei, C. Xu, H. C. M. Byrd, K. L. Beers Macromol. Rapid Commun. **2005**, 26, 1037. b) C. Rosenfeld, C. Serra, C. Brochon, V. Hessel, G. Hadziioannou Chem. Eng. J. **2008** 15, 242-246. c) C. Rosenfeld, C. Serra, S. O. Donohue, G. Hadziioannou Macromol. React. Eng. **2007**, 1, 547-552.
10. D. Wilms, J. Nieberle, J. Klos, H. Löwe, H. Frey Chem. Eng. Technol. **2007**, 30, 1519.
11. D. Wilms, J. Klos, H. Frey Macromol. Chem. Phys. **2008**, 209, 343.
12. M. Szwarc, Nature **1956**, 178, 1168.
13. D. Baskaran, A. H. E. Müller Progr. Polym. Sci. **2007**, 32, 173
14. C. Geacintov, J. Smid, M. Szwarc J. Am. Chem. Soc. **1962**, 84, 2508. b) D. N. Bhattacharyya, C. L. Lee, J. Smid, M. Szwarc J. Am. Chem. Soc. **1963**, 85, 533. c) D. N. Bhattacharyya, C. L. Lee, J. Smid, M. Szwarc J. Phys. Chem. **1965**, 69, 612.
15. a) H. Hostalka, R. V. Figini, G. V. Schulz Makromol. Chem. **1964**, 71, 198. b) G. Löhr, G. V. Schulz Makromol. Chem. **1964**, 77, 240. c) H. Hostalka, G. V. Schulz Z. Phys. Chem. **1965**, 45, 305. d) H. Hostalka, G. V. Schulz Z. Phys. Chem. **1965**, 45, 286. e) L. L. Böhm, G. V. Schulz Makromol. Chem. **1972**, 153, 5. f) G. Löhr, B. J. Schmitt, G. V. Schulz Z. Phys. Chem. **1972**, 78, 177.
16. H. J. Adler, L. Lochmann, S. Pokorny, W. Berger, J. Trekoval Macromol. Chem. Phys. **1982**, *183*, 2901.
17. a) D. Baskaran, A. H. E. Müller Macromolecules **1997**, 30, 1869. b) D. Baskaran, A. H. E. Müller, S. Sivaram Macromolecules, **1999**, 32, 1356. c) D. Baskaran, A. H. E. Müller, S. Sivaram Macromol. Chem. Phys. **2000**, 101, 1901. d) H. Königsmann, S. Jüngling, A. H. E. Müller Macromol. Rapid Commun. **2000**, 21, 758. e) X. Marcarian, L. Falk, A.H.E. Müller, F. Pla, J. Villermaux DECHEMA Monographs **1988**, 134, 577.
18. a) X. Marcarian; C. Navarro; L. Falk; F. Pla, EP0913187, **1999**, to Elf-Atochem. b) X. Marcarian; C. Navarro; L. Falk; F. Pla, US2002128416, **2002**, to Atofina.

19. Note: It should be distinguished between the set-up in this work and the classical flow tubes used by other authors, e.g. references 13,14,15. We use the term "delay tube" for the capillary (500 μm or 1000 μm diameter) that is directly attached to the micro mixer. The term "flow tube" is attributed to the classical macroscopic continuous reactors.
20. H. Gilman; A. H. Haubein J. Am. Chem. Soc. **1944**, 66, 1515.
21. E. Berger-Nicoletti, F. Wurm; A. Kilbinger; H. Frey Macromolecules **2007**, 40, 746.
22. E. R. Moore, Ed., „Styrene Polymers," pp. 1-246 in Encyclopedia of Polymer Science and Engineering, 2nd ed., Vol. 16, Wiley-Interscience, New York **1989**.
23. N. Hadjichristidis; H. Iatrou; S. Pispas ; M. Pitsikalis J. Polym. Sci. Part A: Polym. Chem. **2000**, 38, 3211.
24. M. Morton "Anionic Polymerization: Principles & Practice", Academic Press Inc. **1983**
25. M. Szwarc, J. Smid, „The Kinetics of Propagation of Anionic Polymerization and Copolymerization", Chap. 5 in Progress in Reaction Kinetics, Vol. 2, G. Porter, ed., Pergamon Press, Oxford, 1964
26. R. P. Quirk in Encyclopedia of Polymer Science and Technology (online version), Wiley-VCH, New York, **2002**.
27. V. Hessel, H. Löwe, F. Schönfeld Chem. Eng. Sci. **2005**, 60, 2479.
28. V. Hessel, S. Hardt, H. Löwe, F. Schönfeld AIChE J. **2003**, 49, 566.
29. G. Taylor Proc. Roy. Soc. Ser. A **1954**, 223, 446
30. G. Löhr, G. V. Schulz Z. Phys. Chem. **1969**, 65, 170.
31. N. Hadjichristidis, S. Pispas, G. Floudas "Block Copolymers: Synthetic Strategies, Physical Properties, and Applications", Wiley-Interscience, New York **2003**.
32. N. Hadjichristidis, M. Pitsikalis, S. Pispas, H. Iatrou *Chem. Rev.* **2001**, *101*, 3747.
33. T. Hofe, A. Maurer, A. H. E. Müller, GIT Labor Fachz. **1998**, 42, 1127.

Chapter 5. Appendix

5.1. List of Abbreviations

acac	acetylacetonate
bipy	2,2′-bipyridine
CH	cyclohexane
cod	1,5-cyclooctadiene
conc	concentrated
dba	dibenzylideneacetone
DCB	2,6-dichlorobenzoyl chloride
DCC	*N*,*N*′-dicyclohexylcarbodiimide
DCM	dichloromethane
DMAc	dimethylacetamide
DMAP	4-dimethylaminopyridine
DME	dimethyl ether
DMF	dimethylformamide
dppe	1,2-bis(diphenylphosphino)ethane
dppf	1,1′-bis(diphenylphosphino)ferrocene
dppp	1,3-bis(diphenylphosphino)propane
EDOT	3,4-ethylendioxythiophene
Fmoc	9-Fluorenylmethyloxy carbonyl
Fmoc-Cl	9-Fluorenylmethyloxy carbonyl chloride
Fmoc-*O*Su	9-Fluorenylmethyloxy carbonyl *O*-succinimide
GRIM	Grignard metathesis
HH	head-to-head
HOMO	highest occupied molecular orbital
HT	head-to-tail
IL	ionic liquid
LDA	lithium diisopropylamide

LED	light emitting device
LUMO	lowest unoccupied molecular orbital
NBS	*N*-bromosuccinimide
NMP	*N*-methyl-2-pyrrolidone
NMR	nuclear magnetic resonance
OPBA	oligo-(*p*-benzamide)
PAT	poly(alkylthiophene)
PHT	poly(hexylthiophene)
PLED	polymer light emitting device
RT	room temperature
SEC	size exclusion chromatography
^{t}Boc	*tert*-butyloxycarbonyl
PBA	*p*-benzamide
PT	poly(thiophene)
SEM	scanning electron microscopy
TEM	transmission electron microscopy
TFA	trifluoroacetic acid
TGA	thermogravimetric analysis
THF	tetrahydrofuran
THP	tetrahydropyranyl
TMEDA	tetramethylethylenediamine
TT	tail-to-tail
UV/vis	ultraviolet-visible spectroscopy

5.2. List of Publications

Articles

- "Synthesis of hyperbranched polyglycerol in a continuous flow microreactor" Wilms, D.; Nieberle, J.; Klos, J.; Loewe, H.; Frey, H. *Chem. Eng. Tech.* **2007**, *30*, 1519-1524.
- "Automated Large-Scale Synthesis of Supramolecular Oligo(p-benzamide) Block Copolymers" Klos, J.; Wurm, F.; König, H. M.; Kilbinger, A. F. M. *Macromolecules* **2007**, *40*, 7827-7833.
- "Synthesis of hyperbranched polyglycerol via ring-opening polymerization of glycidol in a microstructured reactor" Wilms, D.; Nieberle, J.; Klos, J.; Loewe, H.; Frey, H. *PMSE Prepr.* **2007**, *97*, 101-102.
- "Synthesis of hyperbanched polyglycerol via ring-opening polymerization of glycidol in a microstructured reactor" Wilms, D.; Nieberle, J.; Klos, J.; Lowe, H.; Frey, H. *Abstracts of Papers, 234th ACS National Meeting, Boston, MA, United States, August 19-23, 2007* **2007**, PMSE-054.
- "Well-defined supramolecular oligo(p-benzamide) block copolymers in a facile one-pot reaction" Klos, J.; Wurm, F.; Kilbinger, A. F. M. *Abstracts of Papers, 235th ACS National Meeting, New Orleans, LA, United States, April 6-10, 2008* **2008**, PMSE-493.
- "Microstructured reactors for polymer synthesis: A renaissance of continuous flow processes for tailor-made macromolecules?" Wilms, D.; Klos, J.; Frey, H. *Macromol. Chem. Physic.* **2008**, *209*, 343-356.
- "Well-defined hyperbranched and linear polymers by anionic polymerization in continuous flow" Wilms, D.; Klos, J.; Wurm, F.; Loewe, H.; Frey, H. *PMSE Prepr.* **2008**, *98*, 642-643.
- "Well-defined hyperbranched and linear polymers by anionic polymerization in continuous flow" Wilms, D.; Klos, J.; Wurm, F.; Lowe, H.; Frey, H. *Abstracts of Papers, 235th ACS National Meeting, New Orleans, LA, United States, April 6-10, 2008* **2008**, PMSE-363.
- "Ionic polymerizations in microstructured reactors" Wilms, D.; Wurm, F.; Klos, J.; Loewe, H.; Frey, H. *Chim. Oggi.* **2008**, *26*, 32-36.
- "Carbanions on tap - Living anionic polymerization in a microstructured reactor" Wurm, F.; Wilms, D.; Klos, J.; Loewe, H.; Frey, H. *Macromol. Chem. Physic.* **2008**, *209*, 1106-1114.

- "Oligo(thiopheneamide) graft-copolymers by ROMP" Hilf, S.; Klos, J.; Kilbinger, A. F. M. *Polym. Prepr. (Am. Chem. Soc., Div. Polym. Chem.)* **2009**, *50*
- "Polymerizable Well-Defined Oligo(thiophene amide)s and their ROMP Block Copolymers" Hilf, S.; Klos, J.; Char, K.; Woo, H.; Kilbinger, A. F. M. *Macromol. Chem. Physic.* **2009**, *30*, 1249-1257.
- "Poly(thiopheneamide)s: A new class of photoactive and conjugated polymers" Klos, J.; Hilf, S.; Kilbinger, A. F. M. *Abstracts of Papers, 237th ACS National Meeting, Salt Lake City, UT, United States, March 22-26, 2009* **2009**, POLY-325.
- "Ionic Liquids on Demand in Continuous Flow" Wilms, D.; Klos, J.; Kilbinger, A. F. M.; Lowe, H.; Frey, H. *Org. Process Res. Dev.* **2009**, *13*, 961-964.
- "Synthesis and Noncovalent Protein Conjugation of Linear-Hyperbranched PEG-Poly(glycerol) α,ω-Telechelics" Wurm, F.; Klos, J.; Rader, H. J.; Frey, H. *J. Am. Chem. Soc* **2009**, *131*, 7954-7955.
- "Oligo(thiophene amide)s", Klos, J.; Hilf, S.; Kamm, V.; Andrienko, D.; Laquai, F.; Kilbinger, A.F.M., *submitted*
- "Aggregation behaviuor of oligo(*p*-benzamide)s", Klos, J.; Woo, H.; Char, K.; Kilbinger, A.F.M., *in preperation*

Presentations

- „Well-defined supramolecular oligo(*p*-benzamide) block copolymers in a facile one-pot reaction" **235th ACS National Meeting**, April 2008, New Orleans, LA, USA
- „Ionic Liquids in Continuous Flow Microreactors" **2008 AIChE Spring National Meeting**, April 2008, New Orleans, LA, USA
- „Poly(thiopheneamide)s: A new Class of Photoactive and Conjugated Polymers" **237th ACS National Meeting**, March 2009, Salt Lake City, UT, USA

Posters

- „Automated Large-Scale Synthesis of PEG-oligoaramide-block-copolymers" **GdCh Fachgruppentagung „Polymers and Coatings"**, Sept. 2006 Mainz, Germany
- „Large scale synthesis of well-defnied oligo(*p*-benzamide) block copolymers" **3rd STIPOMAT Conference,** Ocotober 2007 Les Diableres, Switzerland
- „Living Polymers on Tap: Anionic Polymerization in Continuous Flow" **Hannover Messe 2008**, April 2008 Hannover, Germany

- „Well-defined oligo(*p*-benzamide) block copolymers synthesized in a one-pot reaction“ **42nd IUPAC World Polymer Congress MACRO 2008**, July 2008 Taipei, Taiwan

5.3. Danksagung

5.4. Curriculum Vitae

Johannes Klos

Bouguenais-Allee 16, 65462 Ginsheim-Gustavsburg, Germany
Telefon: +49-6144-335253 E-Mail: johannes.klos@gmx.de
Date and Place of Birth: May 28th, 1981, Neunkirchen/Saar, Germany

Employment Experience

anjo Oberflächentechnik GmbH, Trebur, Germany **since July 2009**

Deutsches Rotes Kreuz, Trebur, Germany **August 2000 – September 2001**
Community Service

Education

Ph.D. Student at the University of Mainz, Germany **October 2006 – June 2009**
Theme: "Synthesis and Characterization of Oligo(thiophene carboxamide)s" in the group of PD. Dr. Andreas F.M. Kilbinger

Diploma Student at the University of Mainz, Germany **January 2006 – September 2009**
Theme: „Entwicklung und Automatisierung eines Syntheseverfahrens zur Herstellung von Polyethylenglycol-*block*-oligo-*p*-benzamiden" in the group of Prof. Dr. Holger Frey

Studies of Chemistry at the University of Mainz, Germany **October 2001 – December 2005**
Obtained Degree: Diploma in Chemistry

St. Katharinen Gymnasium zu Oppenheim, Germany **August 1991 – June 2000**
Obtained Degree: Abitur

Grundschule Geinsheim, Germany **August 1987 – July 1991**

International Experience

Seoul National University, South Korean **June 2008 – December 2008**
Theme: "Studies of the aggregation behavior of oligo(p-benzamide)s" in the group of Prof. Kookheon Char

University of Toronto, Canada **September 2004 – February 2005**
Theme: "Enantioselective Hydrogenation of Ketones and Imines with Newly Synthesized Ruthenium-based Catalysts" in the group of Prof. Bob Morris

Skills

Languages:	german (native)
	english (fluent)
Computer literacy:	Windows, MacOS
	MS Office
	MS Visual Studio, Embarcadero RAD Studio